Universiteit Gent
Faculteit Ingenieurswetenschappen
en Architectuur
Vakgroep Wiskundige Analyse

# Numerical Methods for Flow and Transport in Textile Materials

## Numerieke methoden voor stroming en transport in textiel

Tineke Goessens

Promotor: Prof. Dr. D. Constales
Co-promotors: Dr. B. Malengier, Dr. R. De Staelen

Proefschrift ingediend tot het bekomen
van de academische graad van
Doctor in de Ingenieurswetenschappen:
Wiskundige Ingenieurstechnieken
Academiejaar 2015-2016


Ghent University
Faculty of Engineering and Architecture
Department of Mathematical Analysis

**Supervisor:**
prof. dr. Denis Constales

Research Group Numerical Analysis and Mathematical Modelling
Department of Mathematical Analysis
Faculty of Engineering and Architecture
Ghent University
Galglaan 2 - S22
B-9000 Ghent, Belgium
http://www.nam2.ugent.be


**Members of the examination board:**

| | |
|---|---|
| prof. dr. Rik Van de Walle (chairman) | Ghent University, Belgium |
| prof. dr. Lieva Van Langenhove (secretary) | Ghent University, Belgium |
| prof. dr. Marnix Van Daele | Ghent University, Belgium |
| prof. dr. Denis Constales (supervisor) | Ghent University, Belgium |
| dr. Benny Malengier (co-supervisor) | Ghent University, Belgium |
| dr. Rob De Staelen (co-supervisor) | Ghent University, Belgium |
| prof. RNdr. ir. Jozef Kačur | Comenius University, Slovakia |
| prof. dr. Grigoriy Yablonsky | Saint Louis University, USA |

**Fundation:**
Authors gratefully acknowledge the support of the European Commission, FP7, NO BUG, project number 228639

Dissertation to obtain the degree of
Doctor of Mathematical Engineering
Academic year 2015-2016

# Dankwoord

Het is ondertussen bijna 7 jaar geleden dat ik de kans kreeg om te beginnen werken aan dit doctoraat waarvan deze thesis het resultaat is. Na mijn masterproef in toegepaste wiskunde leek het mij een heerlijke uitdaging om van start te gaan binnen de onderzoeksgroep Numerical Analysis and Mathematical Modeling van de vakgroep Wiskundige Analyse. Zeker omdat dit kon als assistent aan de vakgroep. In mijn laatste masterjaar maakte ik namelijk mijn lerarenopleiding af met op dat moment als doel ooit in het onderwijs terecht te komen. Wat uiteindelijk ook het doel was waarmee ik mijn opleiding Wiskunde startte. En daar komen mijn ouders ter sprake, die ik dan ook als eerste wil bedanken. De interesse voor het onderwijs, naast die voor onderzoek, kwam blijkbaar mee met de genen. Ze gaven mij ook altijd de kans om vrij mijn eigen leven uit te stippelen. Toen iedereen mij aanraadde om Latijn te gaan studeren in het middelbaar, lieten zij mij de keuze om dat niet te doen, wat resulteerde in een studierichting in het 5de jaar waar ik ten volle in geïnteresseerd was (Wetenschappen-Wiskunde). Mijn passie voor die 2 domeinen was toen al groot, zo groot dat ik niet kon kiezen wat ik daarna zou gaan doen. Mama en papa schuimden met mij alle opendeurdagen van alle mogelijke studies af, en hielpen mij om door het bos de bomen te blijven zien, wat, alle inspanningen ten spijt, grandioos mislukte. Tot papa opperde dat ik misschien "gewoon" wiskunde kon gaan studeren. Dat was toch mijn lievelingsvak? Een keuze die ik zeker opnieuw zou maken! Ook toen ik afstudeerde kwamen ze met suggesties aandraven, altijd stonden ze dus klaar voor mij met vrijblijvende ideeën en onvoorwaardelijke steun. Ze leerden mij om er ten volle voor te gaan en altijd mijn eigen doelen te blijven nastreven.
De keuze viel toen dus op de start als assistent gecombineerd met een doctoraatsonderzoek, met dank aan mijn toenmalige promotor Prof. Dr. em. Roger Van Keer.
Om deze thesis tot stand te brengen, mag ik zeker niet vergeten om mijn huidige promotor en co-promotoren te bedanken, Prof. Dr. Denis Constales voor de uitermate informatieve, interessante, en bij momenten overdonderende inzichten, en Dr. Benny Malengier voor de professionele begeleiding, debuggen van mijn programmeerblunders, het samen ontdekken van de Marokkaanse Medina in Rabat en de administratieve en wetenschappelijke ondersteuning

bij het NO BUG project tijdens de eerste vier jaar van mijn doctoraat.
Daarnaast wil ik ook al mijn collega's bedanken voor de leuke tijd samen, Hilde, Lander, Michael, Tim, Marijke, Karel en in het bijzonder Rob, mijn bureaugenoot en tevens co-promotor. De carnavalsmuziek van Ajoin Music, de quotes uit Het Eiland aan de muur, vrij associëren tijdens de lunch, gevolgd door een heerlijke koffie, espresso natuurlijk, waren welkome ontspanningsmomenten. Mijn vrienden mag ik zeker ook niet vergeten bedanken voor de boeiende, swingende, prettig gestoorde feestjes en langgerekte avonden op de Vlasmarkt en hun steun en de babbels tussendoor. Ook mijn ontspannende vrijdagavonden horen in dit lijstje, met dank aan iedereen van Harmonie Con Animo, waar ik er steeds in slaag mijn week met culturele schoonheid (of toch alleszins een poging tot...) af te sluiten.
En last but not least, wil ik een heel grote dankjewel zeggen aan mijn steun en toeverlaat, Sven, die een medaille voor moed en zelfopoffering verdient voor zijn eeuwige geduld en luisterend oor. Om altijd een schitterende papa te zijn voor onze twee kleine schatten, en klaar te staan voor mij, zowel als man als als vriend. Om mij met mijn voetjes op de grond te houden. Om mij altijd, ja, echt altijd, te kunnen doen lachen. Ik draag dit werk dan ook graag op aan hem en onze twee kaboutertjes, Kobe en Nina, die mijn leven compleet maken en het met trots en plezier vullen.

Tineke
Gent, 1 januari 2016

# Contents

# List of Symbols

| Symbol | Definition | Unit |
|---|---|---|
| A | Exchange matrix | |
| $A^i_{f,j}$ | The $i$th type of fiber's area in the $j$th ring zone | $\mathrm{m}^2$ |
| $A^i_{f,\Omega}$ | Area of the $i$th type of fibers' cross-section in the considered zone $\Omega$ | $\mathrm{m}^2$ |
| $\mathcal{B}_n(x,y)$ | A combination of the Bessel functions of first and second kind of order $n$ | |
| $C^*(\mathrm{T})$ | Equilibrium or saturation concentration at temperature T | $\mu\mathrm{g}\cdot\mathrm{mm}^{-3}$ |
| $C_a$ | Air concentration in the inter-fiber void space | $\mathrm{kg}\cdot\mathrm{m}^{-3}$ |
| $C^*_\mathrm{a}$ | Saturated concentration in air | $\mu\mathrm{g}\cdot\mathrm{mm}^{-3}$ |
| $C_{a,B}$ | Concentration of the component in the air at the boundary | $\mu\mathrm{g}\cdot\mathrm{mm}^{-3}$ |
| $C_B(t)$ | Concentration at the boundary | $\mu\mathrm{g}\cdot\mathrm{mm}^{-3}$ |
| $C_b$ | Concentration bound to the fiber that cannot be released | $\mu\mathrm{g}\cdot\mathrm{mm}^{-3}$ |
| $C_f$ | Concentration of active ingredient in the fiber/ fiber coating | $\mu\mathrm{g}\cdot\mathrm{mm}^{-3}$ |
| $C_{f_i}$ | Concentration of active ingredient in fiber coating of layer $i$ | $\mu\mathrm{g}\cdot\mathrm{mm}^{-3}$ |
| $C_{f_s}$ | Concentration of the volatile at the outside-surface of the fiber | $\mu\mathrm{g}\cdot\mathrm{mm}^{-3}$ |
| $\bar{C}_i$ | Mean concentration of AI in domain $i$ | $\mu\mathrm{g}\cdot\mathrm{mm}^{-3}$ |
| $\overline{\overline{C_i}}$ | Average concentration of AI over the complete domain, with $i = f,y,r$ | $\mu\mathrm{g}\cdot\mathrm{mm}^{-3}$ |
| $c_{n,X}$ | $n$'th cumulant for $X$ = fiber, yarn or room | |
| $C_0$ | Initial concentration of AI in the fiber coating | $\mu\mathrm{g}\cdot\mathrm{mm}^{-3}$ |
| $C_\mathrm{out}$ | Concentration of AI in the air surrounding the yarn at distance $d_\mathrm{out}$ | $\mu\mathrm{g}\cdot\mathrm{mm}^{-3}$ |
| $c_{\nu a}$ | Volumetric heat capacity of the air | $\mathrm{kJ}\,.\,\mathrm{m}^{-3}\cdot\mathrm{K}^{-1}$ |
| $c_\nu$ | Dynamic volumetric specific heat of the fabric | $\mathrm{J}\cdot\mathrm{m}^{-3}$ |
| $c_n$ | $n$'th cumulant of the distribution | |
| $C_v$ | Water vapor concentration in the air filling the inter-fiber void space | $\mathrm{kg}\cdot\mathrm{m}^{-3}$ |
| $C_X(t)$ | Cumulant-generating function | |
| $C_y$ | Concentration of active ingredient in the yarn void space | $\mu\mathrm{g}\cdot\mathrm{mm}^{-3}$ |

| Symbol | Definition | Unit |
|---|---|---|
| $d$ | Density of a liquid chemical | $\mathrm{g \cdot cm^{-3}}$ |
| $D$ | Diffusion coefficient of the AI in the room | $\mathrm{mm^2 \cdot s^{-1}}$ |
| $D_c^m$ | Distance between $m$th fiber center and the yarn center | $\mathrm{m}$ |
| $D_{f_s}$ | Diffusion coefficient at the fiber's surface | $\mathrm{mm^2 \cdot s^{-1}}$ |
| $D_f$ | Diffusion coefficient of the AI in the fiber coating | $\mathrm{mm^2 \cdot s^{-1}}$ |
| $D_g$ | Diffusion coefficient of water vapor in the air of the fabric | $\mathrm{m^2 \cdot s^{-1}}$ |
| $D_l(\epsilon_l)$ | Diffusion coefficient of liquid water in the fabric | $\mathrm{m^2 \cdot s^{-1}}$ |
| $D_{mn}^{\text{req}}$ | Required distance between fibers $m$ and $n$ | $\mathrm{m}$ |
| $D_{mn}$ | Distance between fibers $m$ and $n$ | $\mathrm{m}$ |
| $D_{p,q}$ | Diffusion coefficient for AI $p$ in layer coating $q$ | $\mathrm{mm^2 \cdot s^{-1}}$ |
| $D_y$ | Diffusion coefficient of the AI in the yarn void space | $\mathrm{mm^2 \cdot s^{-1}}$ |
| $\Delta D_{mn}$ | Difference between the required distance and the real distance for fibers $m$ and $n$ | $\mathrm{m}$ |
| $\Delta D_{y/f}^m$ | Distance needed to move fiber $m$ back to the yarn domain | $\mathrm{m}$ |
| $\ell$ | Length of a fiber | $\mathrm{mm}$ |
| $F(x)$ | Cumulative distribution function of random variable $X$ | |
| $f_A(r)$, $f_A(r,\theta)$ | Area fraction function in polar coordinates. Indicates the fraction of the area that is a fiber at the point ($r$,$\theta$) | |
| $\bar{f}_{A_m}$ | Area fraction between the fibers' area in the $m$th ring zone and the area of the $m$th ring zone | |
| $F_L$ | Total thermal radiation incident inside the clothing traveling to the left | $\mathrm{W \,.\, m^{-2}}$ |
| $F_R$ | Total thermal radiation incident inside the clothing traveling to the right | $\mathrm{W \,.\, m^{-2}}$ |
| $F_T(t)$ | Diffusive flux, i.e. probability distrubution of all the possible moments in time $T$ when a particle passes a ce | |
| $f_X(x)$ | Probability density function of random variable $X$ | |
| $G$ | Weight of a piece of fabric of a certain area | $\mathrm{g \cdot cm^{-1}}$ |
| $h$ | Width of each ring zone @ | $\mathrm{m}$ |
| $H$ | Height of the fabric | $\mathrm{mm}$ |
| $h_{b\to f}$ | mass transfer coefficient for the AI from bounded to free material | |
| $h_{lg}$ | Mass transfer coefficient for evaporation and condensation | |
| $\mathcal{I}_i$ | The modified Bessel functions of the first kind of order $i$ | |
| $k$ | Constant of proportionality corresponding to the rate of exchange between two levels | |
| $\tilde{k}_{\text{evap}}$ | evaporation proportionality constant | |
| $k_{\text{evap}}$ | Evaporation speed | $\mathrm{mm \cdot s^{-1}}$ |
| $\mathcal{K}_i$ | The modified Bessel functions of the second kind of order $i$ | |
| $K_{\text{mix}}$ | Effective thermal conductivity of the fabric | $\mathrm{W \,.\, m^{-1} \cdot K^{-1}}$ |
| $\mathcal{L}$ | Laplace transform | |
| $M$ | Molecular weight of the chemical | $\mathrm{g \cdot mol^{-1}}$ |
| $M_0$, $M_j$ | VL number in the $j$th ring zone; 0 means the central zone | |

| Symbol | Definition | Unit |
|---|---|---|
| $M_f^{i,j}$ | Average fiber mass for fibers at yarn position $[r_i, r_{i+1}]$ at time $t$ | $\mu\mathrm{g} \cdot \mathrm{mm}^{-1}$ |
| $m_n^s$ | Standardized $n$'th moment of the distribution | |
| $m_n$ | $n$'th moment of the distribution | |
| $M_{n,X}$ | $n$'th moment for $X$ = fiber, yarn or room | |
| $M_X(t)$ | Moment-generating function of random variable $X$ | |
| $n$ | Number of fibers in a shell of the yarn discretization | |
| $n_{\text{horyarns}}$ | Number of horizontal yarns in the fabric | |
| $N_f^i$ | Total number of fibers of type $i$ | |
| $N_f$ | Total number of fibers in a yarn cross-section | |
| $n_f$ | Number of intervals for the numerical model of the fiber | |
| $n_r$ | Number of intervals for the numerical model of the room | |
| $n_{r_o}$ | Number of discretization intervals in the overlap zone of the room | |
| $N_t$ | Number of fiber types in a blend | |
| $n_{\text{vertyarns}}$ | Number of vertical yarns in the fabric | |
| $n_y$ | Number of intervals for the numerical model of the yarn | |
| $n_{y_o}$ | Number of discretization intervals in the overlap zone of the yarn | |
| $P^\star(T)$ | Saturation vapo pressure | Pa |
| $p_f$ | Peclet number of the fiber equation | |
| $P_f^i$ | Percentage of fiber type $i$ in a blend | % |
| $P_h$ | Ambient pressure | mmHg |
| $P_v$ | Vapor pressure | mmHg |
| $p_{\text{VL}}(r)$, $p_{\text{VL}}(r,\theta)$ | VL fiber-distribution probability in polar coordinates. Indicates the probability that a VL contains a fiber | |
| $p_x$ | Peclet number of the room equation | |
| $p_y$ | Peclet number of the yarn equation | |
| $q$ | Constant of proportionality corresponding to the rate of exchange between two levels | |
| $R$ | Fiber radius | mm |
| $R_f$ | Coated fiber radius | mm |
| $R_f^i$ | Average fiber radius for fiber of type $i$ | m |
| $R_f^{\text{av}}$ | Average value of the fiber radius | m |
| $R_f^{\max}$, $R_f^{\min}$ | Maximum and minimum value of the fiber radius | m |
| $R_{i\ell}$ | Left boundary of the overlap zone in the domain of level $i$ | |
| $R_{ir}$ | Right boundary of the overlap zone in the domain of level $i$ | |
| $R_j$ | Outer radii of the $j$th ring zone | m |
| $R_{\text{wv}}$ | Individual gas constant of water vapor | |
| $R_{\text{VL}}$ | VL radius | m |
| $R_{y_o}$ | Radius of the yarn corresponding to the beginning of the overlap zone | |
| $R_y$ | Radius of yarn (indicated by $y$) | m |
| $S$ | Effective area fraction | $\mathrm{mm}^{-1}$ |

| Symbol | Definition | Unit |
|---|---|---|
| $S_{\text{fab}}$ | Total fabric surface | $\text{mm}^2$ |
| $S_{\text{fib}}$ | Total fiber surface | $\text{mm}^2$ |
| $S_{\text{horfib}}$ | Surface of a horizontal fiber | $\text{mm}^2$ |
| $S_f^i$ | Area of the fiber cross-section for type $i$ with average radius | $\text{m}^2$ |
| $S_f$ | Surface/volume ratio of the fiber | $\text{mm}^{-1}$ |
| $S_{\text{vertfib}}$ | Surface of a vertical fiber | $\text{mm}^2$ |
| $T$ | Temperature of the fabric | K |
| $t_f$ | Characteristic time of the fiber equation | s |
| $t_x$ | Characteristic time of the room equation | s |
| $t_y$ | Characteristic time of the yarn equation | s |
| $\mathbf{u}_m, \mathbf{u}_n$ | Vector position of fibers $m$ and $n$ | |
| $\mathbf{u}_m^{'}$ | New position for the fiber $m$ | |
| $\|\mathbf{u}_{mn}\|$ | Norm of the vector $\mathbf{u}_{mn}$ | |
| $u_g$ | Velocity of the gaseous phase, i.e. water vapor and air | $\text{m} \cdot \text{s}^{-1}$ |
| $u_p$ | Concentration of AI $p$ | $\mu\text{g} \cdot \text{mm}^{-3}$ |
| $\Delta\mathbf{u}_m^n, \Delta\mathbf{u}_n$ | Movements for fiber $m$ and $n$ | |
| $\Delta\mathbf{u}_{mn}$ | Movement for overlapping fibers $m$ and $n$ | |
| $\Delta\mathbf{u}_m^y$ | Movement of the fiber $m$ back to the yarn domain | |
| $V$ | Volume of the fibers per $\text{cm}^2$ | $\text{mm}^3 \cdot \text{cm}^{-1}$ |
| $\text{V}_c$ | Volume of the coating on the fiber | $\text{mm}^3$ |
| $v_f$ | Evaporation speed of the AI in the fiber | $\text{mm} \cdot \text{s}^{-1}$ |
| $\text{V}_f$ | Volume of one fiber | $\text{mm}^3$ |
| $v_{\text{fiya}}$ | Evaporation speed of the AI from the fiber to the yarn | $\text{mm} \cdot \text{s}^{-1}$ |
| $V_{d_i}$ | Volume of overlap zone of level $i$ with dimension $d_i$ | |
| $v_x$ | Evaporation speed of the AI in the room | $\text{mm} \cdot \text{s}^{-1}$ |
| $v_y$ | Evaporation speed of the AI in the yarn | $\text{mm} \cdot \text{s}^{-1}$ |
| $v_{\text{yaro}}$ | Evaporation speed of the AI from the yarn to the room | $\text{mm} \cdot \text{s}^{-1}$ |
| $W$ | Width of the fabric | mm |
| $W_{d_i}$ | Codimension of overlap zone of level $i$ with dimension $d_i$ such that the total volume is that of the unit ball | |
| $W_s$ | Liquid water content on the fiber surface | % |

| Symbol | Definition | Unit |
|---|---|---|
| $\alpha$ | Proportional value for moving two overlapping fibers | |
| $\alpha$ | Proportionality constant | |
| $\alpha_{fy}$ | Surface/volume ratio of the fiber to the yarn | $\mathrm{mm}^{-1}$ |
| $\alpha_{ry}$ | Surface/volume ratio of the yarn to the room | $\mathrm{mm}^{-1}$ |
| $\epsilon$ | Coefficient to avoid repetitive oscillation in the fibers movement | |
| $\varepsilon$ | Relative error to evaluate $\alpha$ value's effect | |
| $\epsilon_f$ | Volumetric fraction of fibers in the textile | |
| $\epsilon_g$ | Porosity of the textile, i.e. the volumetric fraction of the gaseous phase (water vapor and air) | |
| $\gamma$ | Shifting coefficient | |
| $\Gamma_f$ | Effective sorption rate of moisture of the fibers | $\mathrm{kg} \cdot \mathrm{m}^{-3} \cdot \mathrm{s}^{-1}$ |
| $\Gamma_{\text{in}}$ | Source term that describes the amount of AI coming out of a fiber cross-section per time unit | $\mu\mathrm{g} \cdot \mathrm{mm}^{-3} \cdot \mathrm{s}^{-1}$ |
| $\Gamma_{lg}$ | Evaporation/condensation rate of liquid/vapor | $\mathrm{kg} \cdot \mathrm{m}^{-3} \cdot \mathrm{s}^{-1}$ |
| $\Gamma_{\text{out}}$ | Sink term that describes the amount of AI leaving the yarn per time unit | $\mu\mathrm{g} \cdot \mathrm{mm}^{-3} \cdot \mathrm{s}^{-1}$ |
| $\lambda_l$ | Heat of sorption or desorption of liquid water by fibers | $\mathrm{kJ} \cdot \mathrm{kg}^{-1}$ |
| $\lambda_{lg}$ | Heat of evaporation/condensation of liquid/vapor | $\mathrm{kJ} \cdot \mathrm{kg}^{-1}$ |
| $\lambda_\nu$ | Heat of sorption or desorption of vapor by fibers | $\mathrm{kJ} \cdot \mathrm{kg}^{-1}$ |
| $\rho_{\max}$ | Fiber radius with coating | $\mathrm{mm}$ |
| $\rho_{\min}$ | Fiber radius without coating | $\mathrm{mm}$ |
| $\rho_f$ | Density of the fiber | $\mathrm{kg} \cdot \mathrm{m}^{-3}$ |
| $\rho_f$ | Linear density of a fiber | $\mathrm{g} \cdot \mathrm{m}^{-1}$ |
| $\rho_l$ | Density of the liquid water | $\mathrm{kg} \cdot \mathrm{m}^{-3}$ |
| $\sigma$ | Variance of the distribution | |
| $\sigma_f$ | Mean deviation of the fiber diameter | |
| $\tau_g$ | Effective tortuosity of the fabric for water vapor and air diffusion | |
| $\tau_l$ | Effective tortuosity of the fabric for liquid water diffusion | |
| $\tau_y$ | Tortuosity of the yarn | |
| $\varnothing_f$ | Diameter of the fibers | $\mathrm{cm}$ |
| $\xi_n$ | Proportions of moisture sorption at fiber surface covered by air and water vapor (n=1) and liquid water (n=2) | |

# English Summary

Protective measures against mosquito born diseases constitute an important market, not only for application in tropical areas where diseases like malaria and dengue are frequent, but also in Europe where mosquitoes are considered irritating beggars. This research is focusing in particular on treated mosquito bed nets, but can also be used for textile garments.

The first part of the research in this thesis is part of the 'Novel release system and bio-based utilities for insect repellent textiles and garments' (NO BUG)-project, a European consortium consisting of various research partners, universities and textile companies. The mathematical engineering part of this research consists of the mathematical modeling of these garments and simulating the life time of the modeled treated textile. A computer toolbox, named STICK, or Sophisticated Textile Information Computing Kit, was developed that incorporates all possible setups of the textile and the chemical treatment of the bed net and calculates the efficiency of the garment. It was built using the programming language Python and utilizes the finite volume method which has been implemented with the FiPy package.
Therefore a new three scale approach for mathematical textile models is suggested including three levels of the textile garment. A textile fabric is built up out of little fibers, which are twisted and knotted to make a yarn or thread. These yarns are then woven or knitted into a piece of fabric. Each of these three levels of a textile cloth is studied as a level in the mathematical model. The first level is the micro-level describing diffusion of a chemical substance, the *active ingredient* (AI) in void space between the fibers. The second level is that of the yarn, i.e. the meso-level, which is included because for loose textile substrates the saturation vapor pressure of the AI will influence the release rate from the fibers, and its value will vary over the yarn cross section. The third and final model is the macro-level that describes the diffusion of the AI out of the yarns to the total fabric and its environment.

In this work we present two upscaling techniques for the three step multiscale model. The active component is tracked in the fiber, the yarn, and finally

at the fabric level. At the fiber level a one-dimensional reduction to a non-linear diffusion equation (with concentration dependent diffusion coefficient) is performed and solved using the method of lines. The outcome is upscaled via the *volume averaging method* and used as an input for the yarn level. At this level a one-dimensional model can be applied to calculate the concentration of the AI, which on its turn is upscaled using *overlapping domain decomposition* as input for the fabric level model.

It was decided to concentrate only on multilayer finishes of open structures, e.g. lattices like nets and simple fabrics. Hence, there is a full coupling between three levels of modeling. This approach gives the possibility to optimize for fiber-yarn layouts, to obtain a better understanding of the life cycle of the textile and eventually the ability to consider some additional mechanisms to provide toxicity/repellency: micro-capsules or bio-repellents. It was decided not to consider the effects of water and heat, as these don't play a major role in the use-scenario's of the finished fabrics.

Next to the one-dimensional yarn model it is also possible to use a two dimensional model and solve this with the finite element method. To be able to model the meso-level in two dimensions a layout construction algorithm is presented to provide for a realistic representation of the yarn cross section. The developed *extended virtual location method* exhibits less regularity than existing methods and can handle blends of different types of fibers in one fabric piece.

In collaboration with the Department of Organic Chemistry of Ghent University some experimental tests were performed in order to be able to validate the developed mathematical model and corresponding toolbox. This resulted in a bioassay on the effectiveness of a textile *slow release* system for mosquito control. As a conclusion of this analysis we found excellent correspondence between the model and the known results of the AI DEET. The mathematical modeling can help in identifying optimal use conditions. In field test however the slow-release system bed nets performed better than the model predicted. This was assumed to be caused by a lack of knowledge about the type of textile together with its specific properties used in the field testing. Also in future work the room's geometry could be altered and the effect of air movement should be analysed further.

The second part of this research consists of a more purely mathematical view of the problem setting of the NO BUG-project. The textile model is further analyzed at equilibrium points, where concentration is moving from one level to the next and the model is in a equilibrium state, i.e. the *characteristic times* of the system. These are studied for both upscaling techniques used in the first part of the research as presented in the latest three A1 articles included in this work.

# Outline

This dissertation comprises a summary of the research of the author, together with the peer reviewed articles, published/accepted for publication to this date.

**Chapter 1** gives the reader a brief introduction on the purpose of this research, the diffusion model, the literature which this research is based upon, some chemical background about one of the used volatile active ingredients DEET and the theory of two upscaling methods, volume averaging method and overlapping domain decomposition technique.

**Chapter 2** gives the three scale model that is used in this research, explaining each of the three levels in the model and how the calculations and simulations were made using the STICK-toolbox. This chapter contains the elaboration of the article 'A Volume averaging and overlapping domain decomposition technique to model mass transfer in textiles', published in Journal of Computational an Applied Mathematics, by Elsevier in 2014. Furthermore, the theory of the extended virtual location method to create a suitable and realistic representation of the yarn cross-section is given.

**Chapter 3** contains the calculation of the needed input variables for the model under consideration in Chapter 2 and the matching of these variables with experimental values. In this chapter one can also find the exact reproduction of the article 'Model based determination of the influence of textile fabric on bioassay analysis and the effectiveness of a textile slow release system of DEET in mosquito control', published in Pest Management Science, by John Wiley & Sons, Ltd. in 2015.

**Chapter 4** comprises the theory of characteristic times followed by the exact reproduction of three articles:

1. 'Characteristic times for multiscale diffusion of active ingredients in coated textiles', published in Journal of Computational an Applied Mathematics, by Elsevier in 2015.

2. 'Characteristic times and inverse problems for diffusion in coated textiles', published in Applied Mathematics and Information Sciences, by NSP in 2015.

3. ‘Characteristic times in a three scale model with overlapping domain decomposition’, accepted for publication in Journal of Computational an Applied Mathematics, by Elsevier in 2016.

# Nederlandstalige Samenvatting

Beschermende maatregelen tegen ziektes overgebracht door muggen vormen een belangrijke markt, niet alleen voor toepassing in tropische gebieden waar ziektes als malaria en dengue frequent voorkomen, maar ook in Europa, waar de muggen als uitermate irritant worden beschouwd. Dit onderzoek richt zich in het bijzonder op behandelde muskietennetten, maar kan ook gebruikt worden voor kledingstukken.

Het eerste deel van het onderzoek in dit proefschrift is onderdeel van het 'Novel release system and bio-based utilities for insect repellent textiles and garments' (NO BUG) -project, een Europees consortium bestaande uit diverse onderzoekspartners, universiteiten en bedrijven in de textielindustrie.

Het ingenieurs-technische deel van dit onderzoek bestaat uit de wiskundige modellering van deze kledingstukken en het simuleren van de levensduur van het gemodelleerde behandelde textiel. Er werd een computer toolbox, genaamd STICK, of Sophisticated Textile Information Computing Kit, ontwikkeld die alle mogelijke samenstellingen van het textiel en de chemische behandeling van het bed net gebruikt als input en de efficiëntie van het kledingstuk berekent. Deze toolbox werd geïmplementeerd met behulp van de programmeertaal Python en maakt gebruik van de eindige volume methode via het FiPy pakket.
Er wordt een nieuwe aanpak voor wiskundige textielmodellen, gebruik makend van drie schalen, voorgesteld overeenkomstig met de drie niveaus van een textiel product. Een textielweefsel is opgebouwd uit kleine vezels, die gedraaid en geknoopt worden om een garen of draad te maken. Deze garens worden vervolgens geweven of gebreid in een stuk stof. Elk van deze drie niveaus van een stuk stof wordt bestudeerd als een niveau in het wiskundig model. Het eerste niveau is het microniveau en beschrijft diffusie van een chemische substantie, de *werkzame stof* (WS), in de lege ruimten tussen de vezels. Het tweede niveau is dat van het garen, ook het meso-niveau genoemd, dat eveneens in dit onderzoek werd opgenomen. Dit omdat voor los geweven stoffen de verzadigde dampdruk van de WS een invloed zal hebben op de snelheid waarmee deze WS wordt afgegeven door de vezels en de waarde

ervan zal variëren over de doorsnede van de draad. Het derde en laatste model is dat voor het macroniveau dat de verspreiding van de WS beschrijft van de garens naar het totale materiaal en zijn omgeving.

In dit werk presenteren we twee upscaling technieken voor het drieschalenmodel. De actieve component wordt gevolgd in de vezel, het garen, en tenslotte op stofniveau. Op het vezelniveau wordt een ééndimensionale reductie tot een niet-lineaire diffusievergelijking uitgevoerd en opgelost met behulp van de lijnmethode. Het resultaat wordt herschaald via de *volume-uitmiddelingsmethode* en gebruikt als input voor het garenniveau. Op dit niveau kan een ééndimensionaal model worden toegepast om de concentratie van de WS te berekenen, die dan opnieuw herschaald wordt via *overlapping domain-decompositie* en als input voor het stofniveau dient.

Er werd beslist om ons specifiek te concentreren op meerlagige afwerkingen van open structuren, bv. netten met een roosterstructuur en eenvoudige stoffen. Voor deze structuren zijn de drie gemodelleerde niveaus volledig aan elkaar gekoppeld. Deze aanpak maakt het mogelijk om de layout van de vezel-draadstructuur te optimaliseren, om een beter inzicht te krijgen in de levensduur van het textiel en uiteindelijk ook in de staat te zijn om andere mechanismen te beschouwen die een stof giftig of afstotelijk maken voor muggen: microcapsules of afweermiddelen van biologische afkomst.

Naast het ééndimensionale model voor het draadniveau is het ook mogelijk om gebruik te maken van een tweedimensionaal model dat kan worden opgelost met de eindige elementenmethode. Om dit meso-niveau te kunnen modelleren in twee dimensies wordt een constructie algoritme voorgesteld dat een realistische voorstelling van een draaddoorsnede verschaft. De ontwikkelde *extended virtual location methode* vertoont minder regelmaat dan de bestaande methodes en is in staat om een representatie te geven van een stof bestaande uit een mix van verschillende types van vezels.

In samenwerking met de vakgroep Organische Chemie van de Universiteit Gent werden experimenten uitgevoerd om het wiskundige model en de bijhorende toolbox te valideren. Dit resulteerde in een bio-analyse van de effectiviteit van een *slow release*-systeem voor muggenbestrijding. Als conclusie van deze analyse werd een uitstekende overeenkomst tussen het model en de gekende resultaten van de WS DEET gevonden. Bij veldtesten presteerden de slow release-bednetten echter beter dan het model voorspelde. We veronderstellen dat de oorzaak hiervoor ligt bij een gebrek aan kennis over het gebruikte type textiel en zijn specifieke eigenschappen. Daarnaast zou de geometrie van de kamer verder uitgewerkt moeten worden en het effect van de luchtstroming in acht moeten genomen worden bij toekomstig onderzoek.

Het tweede gedeelte van dit proefschrift bestaat uit een meer zuiver wis-

kundige kijk op de probleemstelling van het NO BUG-project. Het textielmodel wordt verder geanalyseerd in die punten waar het model in evenwicht blijkt te zijn, daar waar de concentratie van de WS van het ene naar het volgende niveau overgaat, i.e. de *karakteristieke tijden* van het systeem. Deze worden bestudeerd voor beide upscaling technieken uit het eerste gedeelte van dit onderzoek en voorgesteld aan de hand van de drie laatst gepubliceerde A1 artikels, eveneens opgenomen in dit werk.

## Overzicht

Deze verhandeling beslaat een samenvatting van het onderzoek van de auteur, samen met de peer reviewed artikels, gepubliceerd/geaccepteerd voor publicatie tot op heden.

**Hoofdstuk 1** geeft de lezer een korte inleiding over het doel van dit onderzoek, het diffusiemodel, de literatuur waar deze studie op gebaseerd werd, chemische achtergrondinformatie over de gebruikte vluchtige werkzame stof DEET en de theorie achter de twee upscaling methoden, de volume-uitmiddelingsmethode en de overlapping domain-decompositie.

**Hoofdstuk 2** omschrijft het drieschalen model dat gebruikt wordt in dit onderzoek met een verdere uitdieping omtrent elk van de drie niveaus en de berekeningen en simulaties die met de STICK-toolbox werden gemaakt. Dit hoofdstuk bevat de verder uitwerking van het artikel 'A Volume averaging and overlapping domain decomposition technique to model mass transfer in textiles', gepubliceerd in Journal of Computational an Applied Mathematics, door Elsevier in 2014. Tenslotte wordt de theorie van de extended virtual location methode gepresenteerd om een passende en realistische voorstelling van een draaddoorsnede te maken.

**Hoofdstuk 3** bevat de berekening van de benodigde input-variabelen voor het model uit Hoofdstuk 2 en de validatie van deze variabelen aan de hand van experimentele waarden. In dit hoofdstuk kan men eveneens de exacte reproductie vinden van het artikel 'Model based determination of the influence of textile fabric on bioassay analysis and the effectiveness of a textile slow release system of DEET in mosquito control', gepubliceerd in Pest Management Science, door John Wiley & Sons, Ltd. in 2015.

**Hoofdstuk 4** omvat de theorie van de karakteristieke tijden gevolgd door de exacte weergave van de drie artikels:

1. 'Characteristic times for multiscale diffusion of active ingredients in coated textiles', gepubliceerd in Journal of Computational an Applied Mathematics, door Elsevier in 2015.

2. 'Characteristic times and inverse problems for diffusion in coated textiles', gepubliceerd in Applied Mathematics and Information Sciences, door NSP in 2015.

3. 'Characteristic times in a three scale model with overlapping domain decomposition', geaccepteerd voor publicatie in Journal of Computational an Applied Mathematics, door Elsevier in 2016.

CHAPTER 1

# Diffusion background information, Two scale modeling and Literature study

## 1.1 Motivation of the research

Imagine. It is midnight, you are sleeping. A nice slender female of the Anopheles gambiae mosquito comes merrily floating around your ears. After dodging your hand sweeping around to end the annoying buzz, she seeks a part of bare ankle that comes out from under the sheets. Then she throws her greedy stiletto's, two sharp serrated daggers, in the attack. The result can be a little red itchy bump, but for an estimated 250 million people per year the outcome is much worse. For one million of them this nightmare ends up even fatal. Every 30 seconds one person dies due to malaria.

Protective measures against this insect constitute therefore an important market, not only for application in tropical areas where diseases like malaria and dengue are frequent, but also in Europe where mosquitoes are considered irritating beggars. Two of these protective measures belong to the research field of intelligent textiles. The first is the protective clothing for professional volunteers, researchers in the field, missionaries, traveling business people, and so on. The second protective measure one can take is using a treated mosquito bed nets. This research will focus on the second one in particular.

However, these protective garments are subject to two major problems. The first issue has to do with the currently used chemical constituents. If used

incorrectly they can be harmful for a person's health. This issue was already mentioned several times in both scientific articles and popular media. When applying the chemical constituents, permethrin and DEET, to the textile a protective mask should always be used, which isn't always available. Secondly wastewater of the treating process must be purified the correct way so the chemicals are prohibited to enter the eco system. Additionally, mosquitoes become increasingly resistant to the chemical components nowadays still used in the protective garments. The second problem is the life time of the treated fabric. After a standard number of washes a treated T-shirt or bednet must be still repelling enough to avert mosquitoes, so no additional costs should be made to replace or retreat the existing mosquito protection.

The first part of the research in this thesis is part of the 'Novel release system and bio-based utilities for insect repellent textiles and garments' (NO BUG) -project, a European consortium consisting of various research partners, universities and textile companies.
The two main goals of this project in the framework of the European Commission program FP7, consist of scientifically bypassing the aforementioned problems. In particular these goals were the improvement of the treated garments and the construction of garments with natural, biological and biodegradable repellents which are not harmful for a person's health and the environment. The improvement should be realized by developing new slow-release systems resulting in a more sustainable textile garment that can be washed without losing its effect and can be used throughout the whole mosquito season.
The mathematical/engineering part of this research consists of the mathematical modeling of these garments and simulating the life time of the modeled treated textile. The production of expensive, both in time as money, prototypes can be avoided by constructing a computer toolbox that incorporates all possible compositions of the textile and its chemical treatment and calculates the efficiency of the garment. An estimation can be made of the life time and the concentration of the active ingredient in the air surrounding the textile and the inverse problem of which factors should be changed and have the most influence, to improve the protective textile, can be solved.

We focus on the mathematical modeling of multi-layer textile garments, in particular the emphasis is on the diffusion of a substance to the outer boundary of textiles that are coated with a polymer solution of an active ingredient (AI), e.g. a insect repellent, a perfume or a healing substance. This substance can easily be replaced by other volatiles which have a repellent effect or other substances under consideration. Based on the results of this study an inverse problem is encountered and once solved it can answer the question of how much of the AI has to be present on the textile fiber, so the concentration at the outer boundary of the textile stays high enough for as long as possible to be

effective (e.g. repel or even kill mosquitoes, have a noticeable odor for humans, a healing effect, etc. ).

NO BUG results could play an important role in reducing the number of deadly malaria and dengue fever cases in health workers and the general population. Furthermore, bio-repellents offer an eco-friendly alternative to currently used hazardous chemicals.

The second part of this research consists of a more purely mathematical view of the problem setting of the NO BUG project.
The textile model is analyzed further at equilibrium points, where concentration is moving from one level to the next and the model is in a equilibrium state, i.e. the characteristic times of the system.

The model itself is based upon the diffusion equation. It is build up out of three governing equations describing the three levels of a textile fabric, the fiber level, the yarn level and the total fabric itself. The concentration is tracked from fiber to the air surrounding the fabric using upscaling from one level to another.

## 1.2 Diffusion of moisture in textiles

*Diffusion* is the process by witch matter is transported from one part of a system to another as a result of random molecular motions from a region of high concentration to a region of low concentration, [5, 56].

It differs from a fluid's *bulk flow* or *bulk motion*, where a pressure gradient or, as a result, the movement of the fluid itself is responsible for the motion of the molecules. A fluid mechanism due to bulk motion is advection, where a fluid transports some conserved quantity or material mathematically described by a vector field. One easily visualized example of advection is the transport of ink dumped into a river. As the river flows, ink will move downstream via advection, as the water's movement itself transports the ink. If added to a lake without significant bulk water flow, the ink would simply disperse outwards from its source in a diffusive manner, which is not advection. Note that as it moves downstream, the "pulse" of ink will also spread via diffusion. The sum of these processes is called *convection*.

There are two ways to introduce the notion of diffusion: either a phenomenological approach starting with Fick's laws of diffusion and their mathematical consequences, or a physical and atomistic one, by considering the random walk of the diffusing particles.

In the phenomenological approach, diffusion is the net movement of a substance from a region of high concentration to a region of lower concentration without bulk motion. This is also referred to as the movement of a substance down a concentration gradient. According to Fick's laws, the diffusion flux, i.e. the rate of transfer of a diffusion substance through a unit area of a section is proportional to the negative gradient of concentrations measured normal to the section. Some various generalizations of Fick's laws were developed in the frame of thermodynamics and non-equilibrium thermodynamics.
Diffusion results in mixing of the substance in a fluid or mass transport of this substance, without requiring bulk motion (bulk flow). Thus, as mentioned above, diffusion should not be confused with convection, or advection, which are other transport phenomena that utilize bulk motion to move particles from one place to another.

From the atomistic point of view, diffusion is considered as a result of the random walk of the diffusing particles, i.e. molecules or atoms of a substance. In molecular diffusion, the moving molecules are self-propelled by thermal energy. Random walk of small particles in suspension in a fluid was discovered in 1827 by Robert Brown and further developed by Rayleigh in 1880, who solved a more general form of this problem in the context of sound waves in heterogeneous materials, and Bachelier in 1900, who further developed the connection between discrete random walks and the continuous diffusion or heat equation. The theory of the Brownian motion and the atomistic backgrounds of diffusion were analyzed further by Albert Einstein. This concept of diffusion is typically applied to any subject matter involving random walks in ensembles of individuals, [56, 30].

In this research the first approach will be used for the first, more physical, part of this thesis (Chapters 2, 3 and 4) corresponding to Fick's first law of Diffusion. In the second, somewhat more mathematical, part of this thesis (Chapter 5) the atomistic point of view will be used to be able to calculate the characteristic times of the system when diffusion flux is considered as being the probability density function of all possible moments in time when a particle passes a certain point in space. Further notice on this topic will be given in Chapter 5.

Fick's first law of diffusion is described as

$$F = -D\frac{\partial C}{\partial x}, \tag{1.1}$$

with $F$ the rate of transfer per unit area of section, $C$ the concentration of the diffusing substance, $x$ the space coordinate measured normal to the section,

and $D$ the diffusion coefficient. This diffusion coefficient can be a constant, but also can vary with concentration or time. The unit of $D$ is area per unit time, e.g. $\mathrm{cm}^2 \,/\, \mathrm{s}$, depending on the unit of $F$ and $C$, which should be the same. The negative sign in eq. (1.1) arises because diffusion occurs in the direction opposite to that of increasing concentration. It is important to notice that the latter equation is only valid for an isotropic medium, whose structure and diffusion properties in the neighborhood of any point are the same relative to all directions, meaning that there is a symmetry resulting in a flow at any point along the normal to the surface of constant concentration through the point.

To derive the partial differential equation of diffusion in an isotropic medium (i.e. a medium without directional preference) we use the procedure of [5]. Consider a rectangular parallelepiped with sides parallel to the axes of coordinates and of lengths $2\,\mathrm{d}x$, $2\,\mathrm{d}y$ and $2\,\mathrm{d}z$. Let the centre of the element be at $P(x,y,z)$ where the concentration of the diffusing substance is $C$, and $F_x$ is the rate of transfer through a unit area of the plane perpendicular to the axis of $x$ through $P$. Let $ABCD$ and $A'B'C'D'$ be the faces perpendicular to the axis of $x$. Then

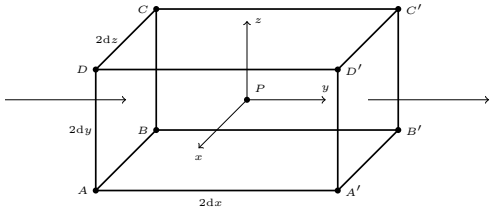


Figure 1.1: Rectangular parallelepiped

the rate at which the substance enters the parallelepiped through face $ABCD$ with area $A_{ABCD}$ in the plane at $x - \mathrm{d}x$ is given by

$$A_{ABCD}F_{x-\mathrm{d}x} = 4\,\mathrm{d}y\,\mathrm{d}z F_{x-\mathrm{d}x} = 4\,\mathrm{d}y\,\mathrm{d}z\left(F_x - \frac{\partial F_x}{\partial x}\,\mathrm{d}x\right).$$

Similarly the rate of loss of the diffusing substance through face $A'B'C'D'$ is

$$4\,\mathrm{d}y\,\mathrm{d}z\left(F_x + \frac{\partial F_x}{\partial x}\,\mathrm{d}x\right).$$

From these two faces we achieve the contribution to the rate of increase of diffusing substance in the element along the $x$ axis

$$4\,\mathrm{d}y\,\mathrm{d}z\left(F_x - \frac{\partial F_x}{\partial x}\,\mathrm{d}x\right) - 4\,\mathrm{d}y\,\mathrm{d}z\left(F_x + \frac{\partial F_x}{\partial x}\,\mathrm{d}x\right) = -8\,\mathrm{d}x\,\mathrm{d}y\,\mathrm{d}z\frac{\partial F_x}{\partial x}.$$

From the other faces we obtain in an analogous way

$$-8\,\mathrm{d}x\,\mathrm{d}y\,\mathrm{d}z\frac{\partial F_y}{\partial y} \quad \text{and} \quad -8\,\mathrm{d}x\,\mathrm{d}y\,\mathrm{d}z\frac{\partial F_z}{\partial z}.$$

At the same time we can write the rate at which the amount of diffusing substance in the element increases as the volume $V$ of the element times the change in concentration per time or

$$V\frac{\partial C}{\partial t} = 8\,\mathrm{d}x\,\mathrm{d}y\,\mathrm{d}z\frac{\partial C}{\partial t},$$

hence we have mass conservation

$$\frac{\partial C}{\partial t} + \frac{\partial F_x}{\partial x} + \frac{\partial F_y}{\partial y} + \frac{\partial F_z}{\partial z} = 0.$$

From Fick's first law of diffusion (1.1) we get the parabolic partial differential equation

$$\frac{\partial C}{\partial t} = D\left(\frac{\partial^2 C}{\partial x^2} + \frac{\partial^2 C}{\partial y^2} + \frac{\partial^2 C}{\partial z^2}\right), \tag{1.2}$$

or

$$\frac{\partial C}{\partial t} = \frac{\partial}{\partial x}\left(D\frac{\partial C}{\partial x}\right) + \frac{\partial}{\partial y}\left(D\frac{\partial C}{\partial y}\right) + \frac{\partial}{\partial z}\left(D\frac{\partial C}{\partial z}\right),$$

in the case where $D$ varies from point to point and may be a function of $x$, $y$, $z$ and $C$. This equation is reduced to

$$\frac{\partial C}{\partial t} = \frac{\partial}{\partial x}\left(D\frac{\partial C}{\partial x}\right),$$

in the one-dimensional case.
Also, $D$ can be time-dependent. In this case we can write $D = f(t)$, introduce the time-scale variable $\mathrm{d}\tau = f(t)\,\mathrm{d}t$ and write eq. (1.2) as

$$\frac{\partial C}{\partial \tau} = \left(\frac{\partial^2 C}{\partial x^2} + \frac{\partial^2 C}{\partial y^2} + \frac{\partial^2 C}{\partial z^2}\right).$$

In this research we will need a cylindrical diffusion model. To derive the corresponding differential equation we will transform our coordinate system to a cylindrical one by putting

$$\begin{cases} x = r\cos(\theta) \\ y = r\sin(\theta) \end{cases}.$$

We obtain the cylindrical diffusion equation

$$\frac{\partial C}{\partial t} = \frac{1}{r}\left[\frac{\partial}{\partial r}\left(rD\frac{\partial C}{\partial r}\right) + \frac{\partial}{\partial \theta}\left(\frac{D}{r}\frac{\partial C}{\partial \theta}\right) + \frac{\partial}{\partial z}\left(rD\frac{\partial C}{\partial z}\right)\right].$$

Also other coordinate systems are possible, but they all can be summarized using the following diffusion equation using vector analysis

$$\frac{\partial C}{\partial t} = \nabla \cdot (D\nabla C).$$

## 1.3 Two scale model of heat and moisture transfer in textiles

### 1.3.1 Setting

This entire research was based upon some existing models for transfer of heat and moisture in textile substrates. These all take into account a particular setting, and several assumptions for this setting. Here, we will summarize the most important ones that also will be taken on for the work in this study. The following section can be seen as background information and is based on [53, 59, 12, 33].

We assume a piece of textile fabric assembled of thin fabrics/films with an inner and outer surface. The inner side is close to the human skin and the outer surface is directed to the external environment. We have a porous textile material with internal structure composed of capillaries that are made up of interconnected pores between the fibers of the fabric, see Fig. 1.2.
The distribution of the liquid phase and the gaseous phase (consisting of water vapor and air) in any tiny element inside the fabric is described by the following relationship between the respective volumetric fractions of liquid water $\epsilon_l$, the gaseous phase consisting of water vapor and air $\epsilon_g$ and the fibers in the particular element $\epsilon_f$:

$$\epsilon_l + \epsilon_g + \epsilon_f = 1.$$

In case of liquid content the porosity of the fabric is defined by

$$\epsilon = 1 - \epsilon_l - \epsilon_f = \epsilon_g.$$

If there is no liquid content, $\epsilon_l = 0$, and $\epsilon_g$ becomes bigger, namely $\epsilon_g'$, so we write

$$\epsilon' = 1 - \epsilon_f = \epsilon_g',$$

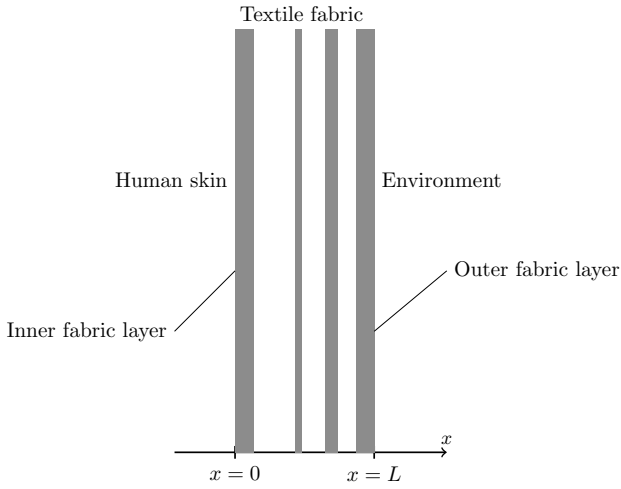


(a) Piece of fabric consisting of thin fabrics/films

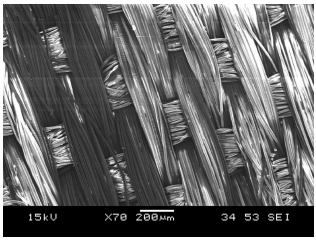


(b) Microscopic view of a piece of fabric with a certain thickness and visible fibers, [52]

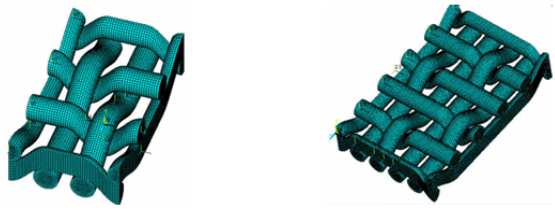

(c) Microscopic reproduction of a piece of woven fabric with visible pores, [52]

Figure 1.2: The piece of textile under consideration for modeling

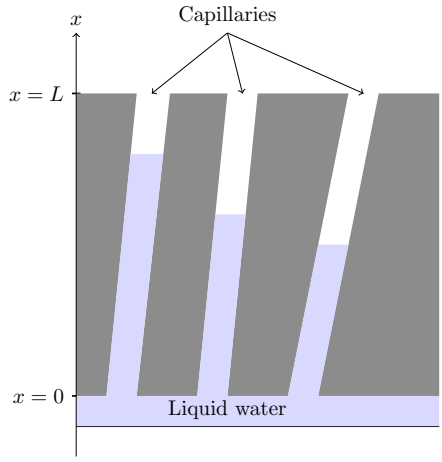


Figure 1.3: Schematic reproduction of the intersection of a textile slab showing the capillaries formed by fibers (gray), filled with liquid water

for the porosity.

Let $x = 0$ and $x = L$ represent the inner and outer surfaces of the porous fabric respectively. Porous textiles are composed of capillaries made up of interconnected pores formed by fibers, see Fig. 1.3. The liquid is propelled by surface tension force from regions of higher liquid content to drier regions. During this action, evaporation and sorption take place.

In what follows also heat transfer will be taken into consideration, nevertheless we will not include this in our research and this part will just be mentioned for informative purposes. The existing models all consist of only two levels of diffusion of moisture, the fabric level represented by the fibers composing it and the air level, the gaseous phase of moisture. Because we work with an open non-dense structure, like a woven net, it will be necessary to include an extra level. This will be an intermediate, so called meso-level, represented by the yarns of the fabric. To construct the governing equation for this level we will extend the existing models with an extra equation of similar form.

### 1.3.2 Assumptions

1. The textile fabric is isotropic in terms of structure and thermal properties.

2. Local thermal equilibrium exists among all phases due to the relatively low velocities considered and the small dimensions of the constituting

fibers.

3. The angular distribution of radiant intensity is approximately constant, and scattering of radiation by fibers can be ignored.
4. Equilibrium is reached instantly between the moisture content at fiber surface and that of the surrounding air.
5. The air-vapor mixture reaches saturation instantly in the presence of liquid.
6. Swelling of the fibers due to absorption of moisture is neglected.
7. The inertial force is ignored due to the relatively low velocities for liquid transfer.
8. Forced convection such as the effect of wind penetration is neglected.

### 1.3.3 The two scale model

#### 1.3.3.1 Governing Equations for Moisture and Heat Diffusion on fabric level

We now write down the four equations governing the mathematical model under assumptions 1.3.2, summarizing the results of the previous mentioned articles into one system of equations. They consist of the conservation of mass for vapor, air and liquid, and the conservation of energy for the mixture of gas, liquid and solid matrix.

- Equation 1: Mass conservation of water vapor:

$$\frac{\partial(C_v\epsilon_g)}{\partial t} = -\frac{\partial(u_g C_v \epsilon_g)}{\partial x} + \frac{\partial}{\partial x}\left(\frac{D_g}{\tau_g} C \frac{\partial}{\partial x}\left(\frac{C_v\epsilon_g}{C}\right)\right) - \epsilon_f \xi_1 \Gamma_f - \Gamma_{lg}$$

- Equation 2: Mass conservation of air:

$$\frac{\partial(C_a\epsilon_g)}{\partial t} = -\frac{\partial(u_g C_a \epsilon_g)}{\partial x} + \frac{\partial}{\partial x}\left(\frac{D_g}{\tau_g} C \frac{\partial}{\partial x}\left(\frac{C_a\epsilon_g}{C}\right)\right)$$

- Equation 3: Mass conservation of liquid water:

$$\frac{\partial(\rho_l\epsilon_l)}{\partial t} = \frac{\partial(\rho_f(1-\epsilon')W_s)}{\partial t} = \frac{\partial}{\partial x}\left(\frac{D_l(\epsilon_l)}{\tau_l}\frac{\partial(\rho_l\epsilon_l)}{\partial x}\right) - \epsilon_f \xi_2 \Gamma_f + \Gamma_{lg}$$

- Equation 4: Energy conservation:

$$\begin{aligned} c_\nu \frac{\partial T}{\partial t} = &- \frac{\partial(\epsilon_g u_g c_{\nu a} T)}{\partial x} + \frac{\partial}{\partial x}\left(K_{\text{mix}}(x)\frac{\partial T}{\partial x}\right) + \frac{\partial F_R}{\partial x} - \frac{\partial F_L}{\partial x} \\ &+ \epsilon_f \Gamma_f (\xi_1 \lambda_\nu + \xi_2 \lambda_l) - \lambda_{lg}\Gamma_{lg} \end{aligned}$$

Table 1.1: Quantities and their units in the model for moisture and heat diffusion in a fabric

| | | |
|---|---|---|
| $D_g$ | Diffusion coefficient of water vapor in the air of the fabric | $\mathrm{m}^2 \cdot \mathrm{s}^{-1}$ |
| $u_g$ | Velocity of water vapor | $\mathrm{m} \cdot \mathrm{s}^{-1}$ |
| $\tau_g$ | Effective tortuosity of the fabric for water vapor and air diffusion | |
| $\xi_n$ | Proportions of moisture sorption at fiber surface covered by air and water vapor (n=1) and liquid water (n=2) | |
| $\Gamma_f$ | Effective sorption rate of moisture of the fibers | $\mathrm{kg} \cdot \mathrm{m}^{-3} \cdot \mathrm{s}^{-1}$ |
| $\Gamma_{lg}$ | Evaporation/condensation rate of liquid/vapor | $\mathrm{kg} \cdot \mathrm{m}^{-3} \cdot \mathrm{s}^{-1}$ |
| $C_a$ | Air concentration in the inter-fiber void space | $\mathrm{kg} \cdot \mathrm{m}^{-3}$ |
| $C_v$ | Water vapor concentration in the air filling the inter-fiber void space | $\mathrm{kg} \cdot \mathrm{m}^{-3}$ |
| $C$ | Total concentration of air and water vapor in the inter-fiber void space | $\mathrm{mol} \cdot \mathrm{m}^3$ |
| $\rho_l$ | Density of the liquid water | $\mathrm{kg} \cdot \mathrm{m}^{-3}$ |
| $\rho_f$ | Density of the textile fiber | $\mathrm{kg} \cdot \mathrm{m}^{-3}$ |
| $W_s$ | Liquid water content on the fiber surface | % |
| $D_l(\epsilon_l)$ | Diffusion coefficient of liquid water in the fabric | $\mathrm{m}^2 \cdot \mathrm{s}^{-1}$ |
| $\tau_l$ | Effective tortuosity of the fabric for liquid water diffusion | |
| $c_\nu$ | Dynamic volumetric specific heat of the fabric | $\mathrm{J} \cdot \mathrm{m}^{-3}$ |
| $T$ | Temperature of the fabric | °C |
| $c_{\nu a}$ | Volumetric heat capacity of the air | $\mathrm{kJ} \,.\, \mathrm{m}^{-3} \cdot \mathrm{K}^{-1}$ |
| $K_{\mathrm{mix}}$ | Effective thermal conductivity of the fabric | $\mathrm{W} \,.\, \mathrm{m}^{-1} \cdot \mathrm{K}^{-1}$ |
| $F_R$ | Total thermal radiation incident inside the clothing traveling to the right | $\mathrm{W} \,.\, \mathrm{m}^{-2}$ |
| $F_L$ | Total thermal radiation incident inside the clothing traveling to the left | $\mathrm{W} \,.\, \mathrm{m}^{-2}$ |
| $\lambda_\nu$ | Heat of sorption or desorption of vapor by fibers | $\mathrm{kJ} \cdot \mathrm{kg}^{-1}$ |
| $\lambda_l$ | Heat of sorption or desorption of liquid water by fibers | $\mathrm{kJ} \cdot \mathrm{kg}^{-1}$ |
| $\lambda_{lg}$ | Heat of evaporation/condensation of liquid/vapor | $\mathrm{kJ} \cdot \mathrm{kg}^{-1}$ |

where $C_v$ and $C_a$ are vapor concentration en air concentration in the inter-fiber void spaces, $\rho_l$ is the liquid density, $T$ stands for temperature in degrees Celsius. An overview of the used quantities and their units can be found in the Table 1.1. The quantities $C_a$, $C_v$, $T$, and all the other quantities, except those for which the dependency is separately stated, are dependent on $x$ and $t$, where $x$ stands

for the distance to the inner surface of the fiber, and $t$ stands for time.
Here the generalized Fick's law has been used for the binary multi-component gas mixture (vapor and air). The concentration $C$ is the total molar concentration of vapor and air, so $C = C_a^M + C_v^M$ with the concentrations of air and vapor converted to molar concentrations, whereby $[C] = \frac{\text{mol}}{\text{m}^3}$. This unit is according to the rule

$$\text{Mass concentration } \left[\frac{\text{kg}}{\text{m}^3}\right] = \text{Molar concentration } \left[\frac{\text{mol}}{\text{m}^3}\right] \times \text{Molar mass } \left[\frac{\text{kg}}{\text{mol}}\right].$$

The molar mass is given by the atomic mass found in the Mendeleev's Table, multiplied with the molar mass constant, $M_u = 10^{-3}\,\frac{\text{kg}}{\text{mol}}$.
The proportions of moisture sorption at fiber surface, $\xi_1$ for water vapor and $\xi_2$ for liquid water, can be defined as follows

$$\xi_1 = \epsilon_g/\epsilon',$$

$$\xi_2 = \epsilon_l/\epsilon'.$$

Here, $\xi_1 + \xi_2 = 1$.
The gas porosity $\epsilon_g$, which is the porosity with liquid water content $\epsilon$, and without liquid water content, $\epsilon'$ are related by introducing the relative free liquid water content on the fiber surface $W_s$ defined by

$$(1-\epsilon')W_s = \frac{\rho_l \epsilon_l}{\rho_f},$$

thus

$$\epsilon = \epsilon_g = \epsilon' - \frac{\rho_f}{\rho_l}(1-\epsilon')W_s.$$

The total volumetric water content $W$ (%) is the sum of this free water content on the fiber surface and the water content absorbed within the fiber $W_f$:

$$W = W_s + W_f,$$

where we can define this total water content in function of the total rate of phase change, i.e. (de)sorption, condensation and/or evaporation of water $\Gamma(x,t)$ as

$$W = \frac{1}{\rho_f(1-\epsilon')}\int_0^t \Gamma(x,t)\,\mathrm{d}t.$$

For this rate of phase change we have that

$$\Gamma(x,t) = \Gamma_{lg}(x,t) - \Gamma_f(x,t),$$

i.e. it is the sum of the rate of evaporation/condensation and the negative sorption rate by the fibers. This last sorption rate can also be written as

$$\Gamma_f = \frac{\partial C_f}{\partial t}.$$

The water content inside the fibers can be described in function of the mean amount of water absorbed by the fibers $C_f$

$$W_f = \frac{C_f M}{\rho_f}.$$

with $M$ the molecular weight of water. This in mind the term $\rho_f(1-\epsilon')W_s$ in equation 3 can also be written as

$$\begin{aligned}\rho_f(1-\epsilon')(W-W_f) &= \rho_f(1-\epsilon')W - \frac{C_f M}{\rho_f}(1-\epsilon')\rho_f \\ &= \int_0^t (\Gamma_{lg} - \epsilon_f \xi_2 \Gamma_f)\,\mathrm{d}t \;-\; C_f M \epsilon_f,\end{aligned}$$

where the sorption rate $\Gamma_f$ is scaled by the volumetric fraction of fibers and the proportion of moisture sorption covered by liquid water. Equation 3 then also can be written as

$$\begin{aligned}\frac{\partial(\rho_l \epsilon_l)}{\partial t} &= \frac{\partial(C_f M \epsilon_f)}{\partial t} - \epsilon_f \xi_2 \Gamma_f(x,t) + \Gamma_{lg}(x,t) \\ &= \frac{\partial}{\partial x}\left(\frac{D_l(\epsilon_l)}{\tau_l}\frac{\partial(C_f M \epsilon_f)}{\partial x}\right) - \epsilon_f \xi_2 \Gamma_f(t) + \Gamma_{lg}.\end{aligned}$$

The volumetric specific heat of the fabric is defined as

$$c_\nu = \epsilon_l c_{\nu l} + \epsilon_f c_{\nu f} + \epsilon_g c_{\nu a},$$

where $c_{\nu l}$ is the volumetric heat capacity of the liquid water and $c_{\nu f}$ that of the fiber.
The diffusion coefficient of liquid water $D_l(\epsilon_l)$ is derived from the physical mechanics of capillary theory and Darcy's law for liquid transfer through porous media as follows

$$D_l(\epsilon_l) = \frac{\gamma \cos(\theta) \sin^2(\alpha) d_c \epsilon_l^{1/3}}{20\eta\epsilon^{1/3}}.$$

Here $\gamma$ is the fiber surface energy, $\theta$ is the contact angle of the liquid water on the fiber surface, $\alpha$ is the effective angle of capillaries in the fabric, $d_c$ the capillary pore distribution, $\eta$ is the dynamic viscosity of the liquid water.

The situation of whether evaporation or condensation occurs is determined by the difference between the water vapor concentration surrounding the fibers $C_v$ and the saturated water vapor concentration at the local temperature $C^\star(T)$:

- when $C_v > C^\star(T)$, condensation occurs at the fiber surface,

- when $C_v < C^\star(T)$ and the local liquid volume $\epsilon_l$ is beyond the critical value for evaporation $\epsilon_{l0}$, i.e. $\epsilon_l > \epsilon_{l0}$, evaporation occurs from the fiber surface.

This saturated water vapor concentration can be calculated from the saturated water vapor pressure at temperature $T$ by use of the standard absolute vapor pressure $P_a$ of $1\,\mathrm{atm}$ or $760\,\mathrm{mmHg}$

$$C_v[\mathrm{ppm}] = \frac{P_v(T)[\mathrm{mmHg}]}{P_a[\mathrm{mmHg}]},$$

and converting this concentration in parts per million to the SI-unit of $\mathrm{mg}\,/\,\mathrm{m}^3$ using

$$C_v[\mathrm{mg}\,/\,\mathrm{m}^3] = C_v[\mathrm{ppm}] \cdot M[\mathrm{g}\,/\,\mathrm{mol}] \cdot 0.04156 \left[\frac{\mathrm{mg}\,/\,\mathrm{m}^3}{\mathrm{ppm}\cdot\mathrm{g}\,/\,\mathrm{mol}}\right].$$

Here the coefficient $0.04156$ is the inverse of the ideal gas volume at $1\,\mathrm{atm}$.
The saturation vapor pressure (in kPa) is obtained from temperature by the following relationship:

$$P^\star(T) = \begin{cases} 1013.25e^{13.3185-1.976s^2-0.6445s^3-0.1299s^4} & T \le 273.16 \\ 10^{10.5380997-2663.91/T} & T > 273.16 \end{cases}, \tag{1.3}$$

where $s = T - 273.16$ and $T$ in Kelvin, [13].
Another way of calculating the saturation vapor pressure (in Pa) is by the empirical expression know as the Tetens' formula

$$P^\star(T) = 0.6108 \exp\left(\frac{17.2694\,T}{T + 237.3}\right),$$

where $T$ is in degrees Celsius and above freezing point.
The saturation water vapor concentration can also be deduced from the ideal gas law as, [13],

$$C^\star(T) = \frac{P^\star(T)}{R_{\mathrm{wv}} \cdot T},$$

where $R_{\mathrm{wv}}$ is the individual gas constant of water vapor equaling $461.5\frac{\mathrm{J}}{\mathrm{kg\,K}}$. Typical values can be found in literature, e.g. [7, 54] and in table 1.2.

The evaporation/condensation rate can be expressed as

$$\Gamma_{lg} = S'_\nu h_{lg}(C^\star(T) - C_v(x,t)),$$

with $h_{lg}$ the mass transfer coefficient for evaporation and condensation which is zero if $C_v < C^\star(T)$ and $\epsilon_l \le \epsilon_{l0}$, $S'_\nu$ the effective area of condensation and evaporation

$$S'_\nu = \frac{\epsilon_g}{\epsilon'}\epsilon_f S_\nu = \xi_1 \epsilon_f S_\nu,$$

| Table 1.2: Saturation vapor concentration of water in air | | | | | |
|---|---|---|---|---|---|
| $T$ [°C] | 0 | 10 | 20 | 30 | 40 |
| $C^\star(T)$ [mol / m$^3$] | 0.269 | 0.521 | 0.959 | 1.684 | 2.834 |

where $S_\nu$ is the surface/volume ratio of the fiber

$$S_\nu = \frac{2\pi R_f l}{\pi R_f^2 l} = \frac{2}{R_f},$$

with $l$ the fiber length and $R_f$ the fiber radius.
The radiation flux inside a textile fabric, i.e. the change of the total thermal radiation incident on a tiny volume element inside the fabric traveling to the right and left direction, $F_R$ and $F_L$ can be described using the absorption constant $\beta$ of the fabric

$$\begin{aligned}\frac{\partial F_R}{\partial x} &= -\beta F_R + \beta\sigma T^4,\\ \frac{\partial F_L}{\partial x} &= \beta F_L - \beta\sigma T^4,\\ \beta &= \frac{1-\epsilon'}{R_f}\epsilon_r,\end{aligned}$$

with $\sigma$ the Stefan-Boltzmann constant of $5.67 \cdot 10^{-8}\,\mathrm{W}\cdot\mathrm{m}^{-2}\cdot\mathrm{K}^{-4}$ and $\epsilon_r$ the thermal emissivity of the fiber, i.e. $\epsilon_r < 1$. The duller and blacker a material is, the closer its emissivity is to 1. The more reflective a material is, the lower its emissivity.

$K_{\text{mix}}$, the effective thermal conductivity for the gas-fiber-liquid mixture is a volumetric average calculated by

$$K_{\text{mix}} = \epsilon_g K_{\text{g}} + (1-\epsilon_g) K_{\text{fab}},$$

where $K_{\text{fab}}$ is the dynamic thermal conductivity of the wetted fabric, and can be obtained from experiments or empirical equations, see [59]. $K_{\text{g}}$ is that of the gas mixture.

To get a numerical solution for this problem, the initial and boundary conditions have to be considered, depending on two possible situations. In the first case direct contact with liquid at the inner side of the fabric (the skin side) is allowed, in the second situation this is prohibited. It is assumed that a porous textile fabric is initially, at $t = 0$, equilibrated to a given surrounding:

- skin surface condition $(T(0,0), C_v(0,0)) = (T_{\text{sk0}}, C_{\text{sk0}})$,

- atmosphere condition $(T(L,0), C(L,0)) = (T_{\text{env0}}, C_{\text{env0}})$,

in terms of temperature and vapor concentration, (we assume $C_a$ constant), with linear distribution across the thickness of the fabric. We assume the liquid water content to be initially zero:

$$W_s(x,0) = 0.$$

1. At the position $(x = 0)$ there are two different boundary conditions depending on the situation:

   (a) direct contact with liquid water

   $$\begin{cases} C_v(0,t) = C^\star(T) \\ \epsilon_l(0,t) = 1 - \epsilon_f \\ K_{\text{mix}} \left.\dfrac{\partial T}{\partial x}\right|_{x=0} = h_{c0}(T - T_{\text{sk}}) \\ F_R(0,t) = (1-\epsilon_0)F_L(0,t) + \epsilon_0 \sigma T^4(0,t) \end{cases},$$

   (b) non-direct contact with liquid water

   $$\begin{cases} D_a \left.\dfrac{\partial (C_v(0,t)\epsilon_g)}{\partial x}\right|_{x=0} = h_{m0}(C_v - C_{\text{sk}}) \\ \epsilon_l(0,t) = 0 \\ K_{\text{mix}} \left.\dfrac{\partial T}{\partial x}\right|_{x=0} = h_{c0}(T - T_{\text{sk}}) \\ F_R(0,t) = (1-\epsilon_0)F_L(0,t) + \epsilon_0 \sigma T^4(0,t) \end{cases}.$$

2. At $(x = L)$ the boundary conditions are described as follows with considering the convective nature of the boundary air layers:

   $$\begin{cases} D_a \left.\dfrac{\partial (C_v(0,t)\epsilon_g)}{\partial x}\right|_{x=L} = -\xi_1 h_{m1}(C_v - C_{\text{env}}) \\ K_{\text{mix}} \left.\dfrac{\partial T}{\partial x}\right|_{x=L} = h_{c1}(T - T_{\text{env}}) - \xi_2 \lambda h_{lg}(C^\star(T) - C_{\text{env}}) \\ D_l \rho_l \left.\dfrac{\partial \epsilon_l}{\partial x}\right|_{x=L} = \xi_2 h_{lg}(C^\star(T) - C_{\text{env}}) F_L(L,t) \\ \qquad\qquad = (1-\epsilon_1)F_R(0,t) + \epsilon_1 \sigma T^4(L,t) \end{cases},$$

with $h_{cn}$ the convective heat transfer coefficient at the clothing surface, $h_{mn}$ the convective vapor transfer coefficient at the clothing surface and $\epsilon_n$ the emissivity of the clothing at the clothing surface ($n = 0$, inner surface; $n = 1$, outer surface).

#### 1.3.3.2 Governing Equations for Moisture Diffusion on fiber level

If we choose to work with a cylindrical coordinate system then we can describe the moisture sorption rate of the fibers as

$$\Gamma_f(x,t) = \frac{\partial C_f}{\partial t},$$

with

$$C_f(x,t) = \frac{2}{R_f^2}\int_0^{R_f} C'_f(x,r,t) r dr, \tag{1.4}$$

the average amount of water absorbed by a fiber at position $x$ in the fabric with radius $R_f$. Here $C'_f$ satisfies he cylindrical diffusion equation

$$\frac{\partial C'_f}{\partial t} = \frac{1}{r}\frac{\partial}{\partial r}\left(rD_f\frac{\partial C'_f}{\partial r}\right), \quad 0 \leq r \leq R_f, \tag{1.5}$$

where the water concentration in the fibers of the fabric $C'_f$ is a function of the position $x$ of the fiber in the fabric, time $t$ and distance $r$ from the middle of the cylindrical fiber [59]. $D_f$ is the diffusion coefficient of moisture in a fiber, which is a function of the water content of the fibers, $W_f(x,t)$, which on its turn depends on the time of sorption and the location of the fiber [32].
The boundary condition for eq. (1.5) for a fiber at position $(x,t)$ can be determined by assuming that the moisture concentration at the fiber surface $C'_f(x,R_f,t)$ is instantaneously in equilibrium with the surrounding air. Consequently $C'_f(x,R_f,t)$ is a known function of the relative humidity of the surrounding air $RH(x,t)$ and its temperature, i.e.

$$C'_{fs} = C'_f(x,R_f,t) = \rho_f f(RH(x,t),T(x,t)),$$

where $RH$ is the relative humidity of the air surrounding a fiber at $x$, and $\rho_f$ is the density of the fibers. This known function $f$ depends on the kind of textile used and is a non-linear function of $RH$ en $T$, that can be obtained from experiments for different fibers with different hygroscopicity, or can be found in data in textile textbooks, [58]. The $RH$-value for a given $x$ and $t$ can be calculated as the ratio of the actual vapor pressure of water vapor in air and the saturation vapor pressure at the same temperature

$$\begin{aligned} RH(x,t) &= \frac{P_v(T)}{P^\star(T)} \times 100\% = \frac{R_{\text{wv}} \cdot T(x,t) \cdot C_v(x,t)\cdot}{P^\star(T(x,t))} \times 100\% \\ &= \frac{T(x,t) \cdot C_v(x,t) \cdot 10^6}{216.5 \cdot P^\star(T(x,t))} \times 100\%, \end{aligned}$$

where $R_{\text{wv}}$ is the individual gas constant of water vapor and the saturation vapor pressure (in kPa) is obtained from temperature by equation (1.3).

In equation (1.4) the volume average has been used. Depending on the distribution of water concentration inside the fibers at the direction of the fiber radius this average water concentration inside the fiber can also be obtained by taking the averaged $\bar{C}_f$ at any space-time position. This average water vapor concentration can be obtained from

$$\bar{C}_f(x,t) = \chi[C'_f(x,r,t)],$$

where $\chi[.]$ is a averaging operator. The water content of the fiber then can be calculated as follows:

$$W_f(x,t) = \frac{\bar{C}_f}{\rho_f},$$

which gives a percentage of the moisture in a fiber on the basis of its dry weight, i.e. the fiber moisture regain. It can be defined as the amount of water a completely dry fiber will absorb from the air at a certain condition of this surrounding air. Table 1.3 gives the regain of different fibers at a standard condition of $21.1°$C and a RH of $100\%$ (expressed as a percentage of the dry fiber weight), [25]. Fig. 1.4 shows the relation between the moisture regain and the RH for wool, cotton, nylon and polyester.

Table 1.3: Saturation moisture regain for different fibers at $T = 21.1°$C and RH $= 100\%$ [percentage of dry fiber weight]

| | |
|---|---|
| wool | 35 |
| cotton | 24 |
| polyamide | 7 |
| polyester | 1 |
| polyolefin | .05 |
| polyarylonitrile | 7 |
| aramide | 6.5 |

### 1.3.4 Numerical solution

In [53, 33, 31] the finite volume method is used to develop a numerical computational scheme to solve the model consisting of the given governing equations. These schemes can be made consistent to the adjustments made to the governing equations and their initial and boundary conditions in Equations 1 to 4. Therefor along the direction of thickness $L$, the fabric is divided into $(N + 1)$

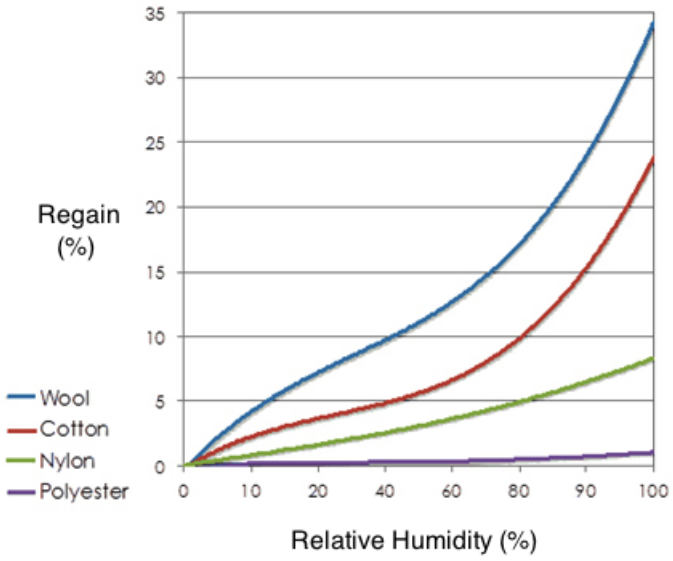


Figure 1.4: Fiber regain against relative humidity for different fibers, from [36]

control cells with equal interval size $\Delta x$. Each control cell is regarded as composed of different volumetric fractions of liquid water $\epsilon_l$ and water vapor $\epsilon_g$.

For the computations we use the central finite difference equations for the space derivatives at a reference point in space $y_j, j = 1 \dots n$,

$$\frac{\partial y}{\partial x} = \frac{y_{j+1} - y_{j-1}}{2\Delta x},$$
$$\frac{\partial^2 y}{\partial x^2} = \frac{y_{j+1} - 2y_j + y_{j-1}}{(\Delta x)^2}.$$

Also the time interval under consideration will be divided into smaller intervals and a backward finite difference scheme at the reference point in time $t_{n+1}$ is used which will lead to a fully implicit scheme for the diffusion equations. This backward difference for the time derivative in the reference point $(x_j,t_{n+1})$ is defined as

$$\frac{\partial y}{\partial t} = \frac{y_j^{n+1} - y_j^n}{\Delta t}.$$

Here we used $y(x_j,t_n) = y_j^n$.

For further solutions of this numerical scheme, the author would like to refer to [53, 33, 31].

## 1.4 Method of lines

The method of lines (MOL) is a technique for solving parabolic partial differential equations in which all but one dimension is discretized. MOL allows standard, general-purpose methods and software, developed for the numerical integration of ordinary differential equations and differential-algebraic equations, to be used. A large number of integration routines have been developed over the years in many different programming languages, and some have been published as open source resources.
The method of lines refers to the construction or analysis of numerical methods for parabolic partial differential equations that proceeds by first discretizing the spatial derivatives only and leaving the time variable continuous. For this purpose finite differences are used which leads to a system of ordinary differential equations to which a numerical method for initial value ordinary equations can be applied, e.g. Runge-Kutta methods.

As an example we could use the two-dimensional diffusion equation, the standard example of a two-dimensional parabolic PDE,

$$\frac{\partial u}{\partial t} = D\left(\frac{\partial^2 u}{\partial x^2} + \frac{\partial^2 u}{\partial y^2}\right).$$

We discretize the space by dividing both the $x$ and $y$ spaces into smaller intervals and thereby creating points $(x_i,y_j)$ where $x_i = i \cdot h$ and $y_j = j \cdot h$ with $h$ the size of an interval in both $x$ and $y$ spaces, $i = 0,\ldots,N,\ j = 0,\ldots,M$.
In each of the points of the created grid we use a central finite difference for the second order derivative in the equation

$$\frac{\partial^2 u}{\partial x^2}(t,x_i,y_j) = \frac{u(t,x_{i-1},y_j) - 2u(t,x_i,y_j) + u(t,x_{i+1},y_j)}{h^2},$$

$$\frac{\partial^2 u}{\partial y^2}(t,x_i,y_j) = \frac{u(t,x_i,y_{j-1}) - 2u(t,x_i,y_j) + u(t,x_i,y_{j+1})}{h^2},$$

leading to the discretized equation

$$\frac{\partial u_{i,j}}{\partial t} = D\frac{u_{i-1,j} + u_{i,j-1} + u_{i+1,j} + u_{i,j+1} - 4u_{i,j}}{h^2},$$

with $u_{i,j} = u(t,x_i,y_j)$.
For every grid point $(x_i,y_j)$ this last equation is an ordinary differential equation which is coupled to four adjacent grid points, where again in each of them an ordinary differential equation is valid. Next to the initial and boundary condition there arises a system of $(N-1)\times(M-1)$ coupled ODE's, which can be solved with the existing methods for ODE's.

## 1.5 Literature Study on DEET

The start of this research was given by the "Novel release system and bio-based utilities for insect repellent textiles and garments" (NO BUG) project, a project financed by the European Union.
In several applications of professional textiles and clothes mosquito repellency is an important issue. Two major problems arise:

- repellents currently in use are harmful, resistance to conventional repellents increases,
- the lifetime of release systems is too short.

Solving these two problems were the main goals of the No Bug project. Novel biorepellents were considered and evaluated as well as two release systems (multilayer coating and textile bioaggregates) in order to repel mosquitoes causing malaria or dengue. Novel release concepts are multilayer coatings and in situ release of the active compounds. Targeted prototypes are textiles for health workers and bed nets (mosquitoes). The project has studied what are the best conditions of use of the biorepellents and how to integrate them in the textile products.

A European consortium has developed novel mosquito bio-repellents to be incorporated into clothing and mosquito nets for health care workers and the public. With NO BUG project, scientists hoped to bypass the aforementioned problems.

They investigated a range of novel bio-repellents and selected the most promising to incorporate into various slow-release systems. Their focus was mainly on multi-layer textiles, but they also investigated microcapsules for improved repellent delivery.

New materials incorporating these release systems were produced and evaluated. These were used to create prototype mosquito nets and protective clothing for health workers.

NO BUG results could play an important role in reducing the number of deadly malaria and dengue fever cases in health workers and the general population. Furthermore, bio-repellents offer an eco-friendly alternative to currently used hazardous chemicals.

The idea was to start with the modeling of the release per time-unit of the widely used chemical compound N,N-Diethyl-m-toluamide (DEET) on a bed net, because these nets already existed and made testing possible for experimental validation. Therefore additional info on DEET, textiles and mosquitoes was needed to answer questions like what are the properties of DEET, what attracts mosquitoes to human beings, what repels them, how come DEET repels

mosquitoes,... In a next step this repellent could be replaced by other volatile products once the mathematical model was finished to achieve an overview of the factors influencing the lifetime and efficiency of the textile end product.

We start with an overview of the physical and chemical properties of DEET in table 1.4.

Table 1.4: Physical-Chemical Properties of DEET

| Property | Information |
|---|---|
| Physical State | colorless to faintly yellow liquid |
| Odor | aromatic |
| Taste | bitter |
| Boiling Point | $160°C$ @ $19\,mmHg$ |
| Melting Point | $-45°C$ |
| Density | $0.996\ g/ml$ $(20°C/4°C)$ |
| Solubility in water | $< 0.1\,g\,/100\,ml$ @ $20°C$ |
| Other solubilities | Soluble in ethanol, benzene, ether<br>Sparingly soluble in petroleum ether<br>Miscible with 2-propanol, cottonseed oil, propylene glycol |
| Vapor Density | $6.7$ (air=1) |
| Vapor Pressure | $1\,mmHg$ @ $111°C$ |
| Flash Point | $155°C$ |
| Evaporation Rate (butyl acetate=1) | $< 1$ |
| Refractive Index | $1.5212$ @ $20°C$ |
| Molecular weight | $191.27\ g/mol$ |

DEET is used primarily by dermal application as an insect repellent against mosquitoes, ticks, fleas, leeches, and black-flies.
DEET is available in $4\%$ to $100\%$ concentrations in insect repellent formulations, including solutions, lotions, creams, gels, aerosols, pump sprays, and impregnated towelettes, usually with an ethyl or isopropyl base.
In the atmosphere, it exists in the vapor phase and is degraded by reaction with photochemically produced hydroxy radicals; its atmospheric half-life is approximately 15 hours. DEET has moderate mobility and is not expected to volatilize in moist or dry soil or to biodegrade under either aerobic or anaerobic conditions. A minimum evaporation flux of 5 $\frac{\mu g}{cm^2\,h}$ (0.03 $\frac{\mu mol}{cm^2\,h}$) for DEET over

5-15 minutes was determined for human skin. DEET acts as a volatile agent to repel mosquitoes at distances of at least 38 cm from their host, [50].

DEET was nominated by the National Institute of Environmental Health Sciences (NIEHS) for toxicity and carcinogenicity testing based on its high U.S. production volume and wide spread consumer use in commercial insect repellents. Exposure to DEET can occur via ingestion, inhalation, or dermal contact. In humans, reported symptoms of overexposure include seizures, coma, hypotension, bradycardia, confusion, acute psychosis, abdominal pain, nausea and vomiting, skin irritation, and urticaria or contact rash. The role of DEET in Gulf War Syndrome continues to be investigated. Veterans who used DEET-containing insect repellents showed signs of arthro-myo-neuropathy, a neurotoxic syndrome with symptoms including joint and muscle pain, fatigue after exertion, and tingling or numbing of the hands, arms, feet, and legs.

A 1980 EPA (Environmental Protection Agency) report estimated that approximately $38\%$ of Americans are exposed to DEET each year and that 200 million people are exposed annually worldwide.

A next question was what attracts mosquitoes to human beings and what the relationship of it is with DEET.
A little litterature study learned that the attraction of moqsuitos to human hosts is largely odor-mediated, with human body emanations such as $CO_2$, lactic acid and 1-octen-3-ol, emitted in human breath and sweat, as strong mosquito attractants. DEET blocks the behavioral attraction of mosquitoes to lactic acid, a component of human sweat, as it mediates a decrease in the amounts of the major compounds released from the skin. This is called the masking effect of DEET.

In relation to this, we can ask ourselves the question what repels mosquitoes in DEET. Two major ideas were publicated in the spring of 2008. The first one [9] stated that DEET inhibits the 1-octen-3-ol-evoked responses by inhibiting the activity of the olfactory receptory neurons (ORN's) on the antennae of the mosquito. In the second study [47] provided convincing evidence suggesting that repellency of the mosquito is a matter of direct detection of DEET in the vapor phase an avoidance of the smell of DEET. The researchers found a DEET-sensitive ORN and pointed out a false positive in the previous research due to trapping of odorants in the Pasteur pipes when a DEET-laden filter paper is added to the cartridge. This means the moqsuitos couldn't smell DEET due to this fact and not due to inhibition of the olfactory system.

## 1.6 Upscaling methods

The mathematical multiscale model described in the previous sections needs an upscaling of the solution from the fiber level to the fabric level. This can be done in numerous ways, but we used two methods well illustrated in literature which we adjusted for the purpose of the problem in mind. These are the volume averaging technique and the overlapping domain decomposition method.

### 1.6.1 Volume Averaging

The volume averaging method was derived by Whitaker and is used for transport of fluids in a multiphase problem. This method provides a foundation for the analysis of these systems and is based on classical continuum physics and can be used for predicting the effective transport coefficients that appear in those equations. It therefor uses a spatially smoothed equation which can be illustrated with the standard diffusion problem as in [55]. Volume averaging shows how two levels of equations, i.e. of each phase, are related and makes it possible to calculate the concentration on a macroscopic level related to that of the microscopic one. Spatial smoothing, or upscaling, of a physical property belonging to the micro scale model leads to the governing equation for the macro scale volume averaged concentration, or vice versa.

To explain the volume averaging method we will use the first example in [55] where a two phase system is assumed. Phase $\kappa$ represents a rigid solid in contact with a fluid phase identified as the $\gamma$-phase. The $\gamma/\kappa$-interface is a catalytic surface at which chemical reactions can take place and both phases are continuous. The governing equation for the concentration of a species $A$ is a diffusion equation in the $\gamma$-phase. Furthermore there is a jump condition for $A$ at the $\gamma/\kappa$-interface. We are interested in the entrances and exits of species $A$ at the $\gamma$-phase boundary. Because the point concentration in the system is unknown we will use the average concentration and the average rate of reaction for upscaling from the $\gamma$-phase to the $\beta$-phase of the system. Therefore it is necessary to define the *averaging volume* $\mathcal{V}$ associated with these averages. We will first define the position vector $\mathbf{r}_\gamma$ to locate any point in the $\gamma$-phase, the position vector $\mathbf{x}$ for the location of the centroid of $\mathcal{V}$ and the relative position vector $\mathbf{y}_\gamma$ for the location of superficial a point in the $\gamma$-phase relative to the centroid. For the upscaling we need to associate an averaging volume to every point in space which is invariant of time and space

$$\mathcal{V} = \mathcal{V}_\gamma(\mathbf{x}) + \mathcal{V}_\kappa(\mathbf{x}),$$

where $\mathcal{V}_\gamma(\mathbf{x})$ represents the volume of phase $\gamma$ with volume fraction, e.g. the porosity, given by

$$\epsilon_\gamma = \frac{\mathcal{V}_\gamma(\mathbf{x})}{\mathcal{V}}.$$

For $\mathcal{V}_\kappa(\mathbf{x})$ an analogous definition exists. Next we define the *superficial average concentration*

$$\langle C_{A\gamma} \rangle|_{\mathbf{x}} = \frac{1}{\mathcal{V}} \int_{\mathcal{V}_\gamma(\mathbf{x})} C_{A\gamma}|_{\mathbf{x}+\mathbf{y}_\gamma} \, \mathrm{d}V.$$

This average is easy to calculate but not the preferred variable because it is not a good representation of the concentration in the $\gamma$-phase. E.g. if $C_{A\gamma}$ were a constant $c_A$, the superficial average concentration would not be equal to $c_A$. The preferred variable is the *intrinsic average concentration* defined as

$$\langle C_{A\gamma} \rangle^\gamma|_{\mathbf{x}} = \frac{1}{\mathcal{V}_\gamma(\mathbf{x})} \int_{\mathcal{V}_\gamma(\mathbf{x})} C_{A\gamma}|_{\mathbf{x}+\mathbf{y}_\gamma} \, \mathrm{d}V.$$

The relation between the superficial and the intrinsic average concentration is given by

$$\langle C_{A\gamma} \rangle = \epsilon_\gamma \langle C_{A\gamma} \rangle^\gamma.$$

Although we want an equation for the intrinsic average concentration, it is convenient to start the spatial smoothing using the superficial average, by integrating the governing equation over $\mathcal{V}_\gamma$ and dividing by $\mathcal{V}$. Afterwards we use the general transport theorem (Whitaker, 1981) to get

$$\begin{aligned} \frac{1}{\mathcal{V}} \int_{\mathcal{V}_\gamma(\mathbf{x})} \left. \frac{\partial C_{A\gamma}}{\partial t} \right|_{\mathbf{x}+\mathbf{y}_\gamma} \mathrm{d}V &= \frac{d}{dt} \left[ \frac{1}{\mathcal{V}} \int_{\mathcal{V}_\gamma(\mathbf{x})} C_{A\gamma}|_{\mathbf{x}+\mathbf{y}_\gamma} \, \mathrm{d}V \right] = \frac{d}{dt} \langle C_{A\gamma} \rangle|_{\mathbf{x}} \\ &= \frac{1}{\mathcal{V}} \int_{\mathcal{V}_\gamma(\mathbf{x})} \nabla \cdot (D_\gamma \nabla C_{A\gamma}) \, \mathrm{d}V. \end{aligned} \tag{1.6}$$

The superficial average concentration is associated to the fixed centroid $\mathbf{x}$ so we can write the derivative as a partial derivative and express equation (1.6) as

$$\left. \frac{\partial}{\partial t} \langle C_{A\gamma} \rangle \right|_{\mathbf{x}} = \langle \nabla \cdot (D_\gamma \nabla C_{A\gamma}) \rangle|_{\mathbf{x}} \, .$$

Because the porosity is independent of time this leads to the equation for the accumulation of species $A$ in terms of the preferred dependent variable, the intrinsic average concentration

$$\epsilon_\gamma \left. \frac{\partial}{\partial t} \langle C_{A\gamma} \rangle^\gamma \right|_{\mathbf{x}} = \langle \nabla \cdot (D_\gamma \nabla C_{A\gamma}) \rangle|_{\mathbf{x}} \, .$$

The term on the right hand side of this expression can be rewritten using the spatial averaging theorem in order to express the diffusive flux in terms of

the intrinsic average concentration. This theorem gives a three-dimensional Leibniz rule for interchanging differentiation and integration for some quantity $\Psi$ corresponding with the $\gamma$-phase in a $\gamma/\kappa$-system:

$$\langle \nabla \Psi \rangle = \nabla \langle \Psi \rangle + \frac{1}{\mathscr{V}} \int_{A_{\gamma\kappa}} \mathbf{n}_{\gamma\kappa} \Psi \, \mathrm{d}A,$$

where $A_{\gamma\kappa}$ is the area of the $\gamma/\kappa$-interface. This theorem yields

$$\begin{aligned} \epsilon_\gamma \left. \frac{\partial}{\partial t} \langle C_{A\gamma} \rangle^\gamma \right|_{\mathbf{x}} =& \nabla \cdot \left[ (D_\gamma \left( \epsilon_\gamma \nabla \langle C_{A\gamma} \rangle)^\gamma + \langle C_{A\gamma} \rangle^\gamma \nabla \epsilon_\gamma + \frac{1}{\mathscr{V}} \int_{A_{\gamma\kappa}} \mathbf{n}_{\gamma\kappa} C_{A\gamma} \, \mathrm{d}A \right) \right] \\ & - a_v k \langle C_{A\gamma} \rangle_{\gamma\kappa}, \end{aligned} \tag{1.7}$$

where $a_v$ is the surface area per unit volume, $\frac{A_{\gamma\kappa}}{\mathscr{V}}$ $k$ is the conductivity and the area averaged concentration is defined by

$$\langle C_{A\gamma} \rangle_{\gamma\kappa} = \frac{1}{A_{\gamma\kappa}} \int_{A_{\gamma\kappa}} C_{A\gamma} \, \mathrm{d}A.$$

However equation (1.7) still contains the point concentration this can be overcome by using *spatial decomposition*, see [55] for further information.

### 1.6.2 Overlapping Domain Decomposition

A special class of numerical methods for solving partial differential equations (PDEs) is that of the domain decomposition (DD) methods. The methods of concern are based on a physical decomposition of a global solution domain. The global solution to a PDE is then sought by solving the smaller subdomain problems collaboratively and "patching together" the subdomain solutions. There are two kinds of DD methods, overlapping methods, where the subdomains are physically overlapping and non-overlapping methods, where they only share an adjacent boundary. These methods have multiple advantages compared with many other numerical methods, such as superior efficiency, applicability for parallel computing, easy handling of solution domains of irregular shape and the possibility to use different numerical methods in different subdomains for e.g. special treatment of singularities, [2].

Since in the stated physical problem the fiber is entirely lying in the room domain, the overlapping domain decomposition method can be used for upscaling the solution in the subdomain of the fiber scale to solution in the subdomain of the fabric scale. The concentration of an active ingredient can be tracked in the global domain consisting of both the fabric and the air surrounding it, which can be decomposed into two domains, one on each level. This

overlapping DD method has a simple algorithmic structure and is an iterative procedure, where the PDE is alternately solved within each subdomain. For each iteration the solution of the other subdomain(s) is used as an artificial internal boundary condition and is provided by the solution of the previous step in the algorithm, where the PDE is solved on the other subdomain(s). Each iteration step has to be done in a certain order to achieve convergence, because convergence of the solution on the internal subdomains ensures the convergence of the solution in the global solution domain, and this subdomain convergence depends on the artificial internal boundary condition used.

The method that will be used here is based upon the classical alternating Schwarz method. This method was developed to solve a Poisson equation in a domain $\Omega = \Omega_1 \cup \Omega_2$, where subdomain $\Omega_1$ is a circle overlapping with the rectangular subdomain $\Omega_2$, see Fig. 1.5. The boundary-value problem under

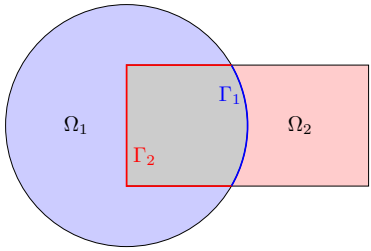


Figure 1.5: Domain decomposition for the classical alternating Schwarz method

consideration is

$$\begin{aligned} Lu &= f \quad \text{in } \Omega, \\ u &= g \quad \text{on } \partial\Omega, \end{aligned}$$

where operator $L$ can be $-\boldsymbol{\nabla}^2$ for example. The part of the boundary of subdomain $\Omega_i$ which is not part of the global physical boundary $\partial\Omega$ is the artificial internal boundary $\Gamma_i$. Schwarz proposed an iterative algorithm to find an estimation of the solution to this problem by starting from an initial guess $u^0$ in each subdomain. Denote the approximate solution in subdomain $\Omega_i$ in the $n$th iteration by $u_i^n$, and the restriction of $f$ to $\Omega_i$ by $f_i$, then we will first solve the Poisson problem restricted to the circle $\Omega_1$ using the solution of the previous iteration for the restriction to the rectangle $\Omega_2$, i.e. $u_2^{n-1}$, as the

artificial internal boundary condition:

$$\begin{aligned} Lu_1^n &= f_1 && \text{in } \Omega_1, \\ u_1^n &= g && \text{on } \partial\Omega_1 \setminus \Gamma_1, \\ u_1^n &= u_2^{n-1}|_{\Gamma_1} && \text{on } \Gamma_1. \end{aligned}$$

Afterwards, we will solve the problem within the second subdomain $\Omega_2$, using the latest solution of this iteration of subdomain $\Omega_1$, i.e. $u_1^n$ on the artificial boundary $\Gamma_2$:

$$\begin{aligned} Lu_2^n &= f_2 && \text{in } \Omega_2, \\ u_2^n &= g && \text{on } \partial\Omega_1 \setminus \Gamma_2, \\ u_2^n &= u_1^n|_{\Gamma_2} && \text{on } \Gamma_2. \end{aligned}$$

This means that the solution of the problem changes on both subdomains from iteration to iteration, while converging to the true solution by updating the Dirichlet boundary conditions on $\Gamma_1$ en $\Gamma_2$ by exchanging data from one domain to another. This Schwarz alternating method is an additive and sequential method, which means that the iterations must be carried out in a predetermined sequence, first in $\Omega_1$, then in $\Omega_2$, for convergence.

Next to this basic additive overlapping domain decomposition technique, there exist several other techniques such as the multiplicative Schwarz method and non-overlapping techniques. For further information on these topics we refer to [49, 43]. An overview of the method especially for parabolic equations like the diffusion equation under consideration can be found in [35].

CHAPTER 2

# The Three Scale Model

## 2.1 Three Scale modeling and Introduction to the Application

The diffusion of substances in and through polymers is studied in a large variety of engineering applications. It is found in settings where controlled release plays an important role such as drug delivery and their encapsulation in the medical context, polymer melts and the inflation of elastic membranes for the construction of plastic materials, architecture and building, transfer of particles through polymer coated materials such as textiles and many others. In the latter textile context polymer coating and encapsulation of substances for application on fibers creates functional materials such as dyes, fragrances, phase change materials, smart polymers and nanomaterials found in sports, defense, health care, environmental pollution control, space, and even everyday use products like rain coats or floor mats. Our interest is the development of protective clothing.

Health-workers, soldiers, and other people who are frequently exposed to vector-borne diseases during missions in hot and tropical conditions, are recommended to use a combination of repellent-based creme on exposed body parts and treated garments to protect themselves against mosquitoes infected with malaria and other life threatening diseases. Current solutions have some deficits because they are not used in a proper way, application is too complex or

people don't want to use them because of a certain degree of toxicity mentioned in the press. Next to product failure, the limited lifetime of effectiveness is a matter of concern. Therefore the NO BUG project, in the framework of the European Commission program FP7, focuses on the improvement of treated garments, and the future construction of garments with natural and bio-repellents.

We focus on the mathematical modeling of these garments, in particular the emphasis is on the diffusion of a substance to the outer boundary of textiles that are coated with a polymer solution of an active ingredient (AI), e.g. a perfume or a healing substance. This substance can easily be replaced by other volatiles which have a repellent effect or other substances under consideration. Based on the results of this study an inverse problem is encountered and once solved it can answer the question of how much of the AI has to be present on the textile fiber, so the concentration at the outer boundary of the textile stays high enough for as long as possible to be effective (e.g. repel or even kill mosquitoes, have a noticeable odor for humans, a healing effect ...).

Existing models for mass transfer in textiles only consist of two levels, a fiber and fabric level, with no level in between, [60, 59, 29, 13, 38, 22, 24]. Most of them are concentrating on the transfer of water through textiles, whereas the use of an AI hasn't been studied yet. It has been proved that neglecting the yarn-scale usually works very well in the simulation for a dense fabric. But neglecting the yarn scale has several drawbacks. It introduces an error in the simulations, because upscaling techniques based on volume averaging are difficult to construct due to the specific geometry of a fabric. It is difficult to perform optimization of textile properties related to the yarn structure (e.g. a blend of different kinds of fibers). Also, modeling the yarn allows to investigate the influence of the placement of the different fibers in the yarn. These existing models and algorithms for standard multilayer systems were extended to the needs that have arisen during the research on the polymer finishes. The application in mind has the purpose to track the diffusion of an active component released by the fibers of a scrim, e.g. a gauze bandage. For textile substrates with an open structure like these scrims the previous approach is no longer suitable. This is because a scrim consists of loosely woven yarns so the release of the active component from the scrim actually equals the release of the component from the yarns. Furthermore the number of fibers and the configuration of these fibers in the yarn plays a role. Finally, the vapor pressure of the active component in the gaps of the yarn will influence the release rate from the fibers and varies over the yarn cross-section. As a conclusion we could say that a meso-level model that describes the release of the active component in the yarn cross-section is needed. Because of this extra level in the model, we need a method to upscale the results from one level to

another.

It was decided to concentrate only on multilayer finishes of open structures, e.g. lattices like nets and simple fabrics. Hence, with 'multilayer structures' we indicate the full coupling between three levels of modeling, the micro-level which in practice could be the fibers, a meso-level corresponding to the yarns, and the macro-level, or thus the level of the total fabric. This approach gives the possibility to optimize for fiber-yarn layouts, to obtain a better understanding of the life cycle of the textile and eventually the ability to consider some additional mechanisms to provide toxicity/repellency: micro-capsules or bio-repellents. It was decided not to consider the effects of water and heat, as these don't play a major role in the use-scenario's of the finished fabrics at the moment.

The models have been developed and solved using the programming language Python in a toolbox called STICK (Sophisticated Textile Information Computation Kit), see section 2.8. It uses the finite volume method which has been implemented with the FiPy package [21]. A full coupling between the three scales is present and the effect of different micro and meso-level layouts can be determined. The mathematical model under consideration is a complete multilayer model for volatiles with three levels, the fiber, yarn and net level, where upscaling is done by volume averaging and the overlapping domain decomposition method, respectively.

In this section we use the general moisture and heat transfer model and use the upscaling methods given in Chapter 1 for a novel application. As stated, this application consists of modeling a bednet or textile fabric which is impregnated with one or more substances. In this case we consider two chemical substances, namely DEET and permethrin. Another possibility is the use of natural products such as bio repellents (products from plants or $\mu$-organisms).

Permethrin is a common synthetic chemical, widely used as an insecticide, acaricide, and insect repellent. It belongs to the family of synthetic chemicals called pyrethroids and functions as a neurotoxin, affecting neuron membranes by prolonging sodium channel activation. Mosquito nets used to cover beds may be treated with a solution of permethrin. This increases the effectiveness of the bed net by killing parasitic insects before they are able to find gaps or holes in the net.

N,N-Diethyl-meta-toluamide, abbreviated DEET, is a slightly yellow oil. It is the most common active ingredient in insect repellents. It is intended to be applied to the skin or to clothing, and is primarily used to repel mosquitoes. In particular, DEET protects against tick bites, preventing several rickettsioses, tick-borne meningoencephalitis and other tick-borne diseases such as Lyme disease. It also protects against mosquito bites which can transmit dengue fever, West Nile virus, eastern equine encephalitis, and malaria. Recent evidence

shows that DEET serves as a true repellent in that mosquitoes intensely dislike the smell of the chemical repellent.

To model a bednet we make a distinction on three levels of the textile material, namely the fiber, yarn and fabric level respectively. First we model the fiber with a coating consisting of different layers of active ingredients DEET and permithrin. To this end the fiber will be seen as a cylindric object. The boundary conditions depend on the chosen textile and the void space characteristics. Secondly we model the yarn, a porous structure built out of fibers, upscaling the outcome of the fiber model using an volume averaging technique. The yarn level can be developed in two ways, a two-dimensional model and a one-dimensional cylindric model. The third model represents the net or fabric itself, i.e. the total fabric, with its environment, again using an upscaling method to calculate the overall properties of the fabric using the resulting yarn properties.

## 2.2 Scale of the Fibers

To construct a model on the scale of fibers we started with a Representative Elementary Volume (REV) in a cylindric coated fiber of infinite length. The fiber is a cylinder with radius $R$. On this cylindric fiber there are $\kappa$ coatings of different chemical substances with thickness $d_i$, $i = 1..\kappa$. These coatings consist of a binder that contains a chemical substance, the active ingredient (AI). The binder makes a firm bond between the fiber and the chemical substance or between the underlaying coating and the substance. The concentration of chemical substance in the binder is expressed as a percentage, e.g. there can be a coating with $4\%$ of DEET on top of a coating with $2\%$ of permethrine.

Based on the model prescribed above in section 1.3.3.2, we choose to work with cylindrical coordinates $(\rho,\theta,z)$, in which diffusion is everywhere radial. The governing model for diffusion of the AI in the fiber is then generally described by

$$\frac{\partial C_f}{\partial t} = \frac{1}{\rho}\left\{\frac{\partial}{\partial \rho}\left(\rho D_f \frac{\partial C_f}{\partial \rho}\right) + \frac{\partial}{\partial \theta}\left(\frac{D_f}{\rho}\frac{\partial C_f}{\partial \theta}\right) + \frac{\partial}{\partial z}\left(\rho D_f \frac{\partial C_f}{\partial z}\right)\right\},$$

where $C_f$ is the concentration of the AI in the fiber and $D_f$ is the diffusion coefficient of the AI in the fiber, which can be concentration dependent. According to a radial symmetric diffusion in a long cylinder [5] concentration is a function of the radial position $\rho$ and time $t$ only, so azimuth $\theta$ and height $z$ can be ignored and the diffusion equation becomes

$$\frac{\partial C_f(\rho,t)}{\partial t} = \frac{1}{\rho}\frac{\partial}{\partial \rho}\left(\rho D_f \frac{\partial C_f(\rho,t)}{\partial \rho}\right), 0 \leq \rho \leq R_f,$$

with boundary conditions

$$\nabla C_f(R,t) = 0,$$

at the fiber radius $R$, where it is assumed that the AI is not absorbed by the fiber itself, and

$$\nabla C_f(R_f,t) = \alpha \left(C_f(R_f,t) - C_{f_s}(t)\right) \cdot \mathcal{H}\left(C_f(R_f,t) - C_b, C^*(T) - C_{f_s}(t)\right).$$

at the coated fiber radius $R_f$. Here, $\alpha$ is a proportionality constant, $C^*(T)$ is the equilibrium or saturation concentration at temperature $T$, $C_{f_s}$ is the concentration of the volatile at the outside-surface of the fiber which will be determined from the meso-level or yarn model, $C_b$ is the concentration bound to the fiber that cannot be released and $\mathcal{H}(x,y)$ is defined as the Heaviside function $H(x)$ if $y > 0$, otherwise it is the identity, extending the BC in [33, 61]. This models evaporation of AI ($C^* > C_{f_s}$) and condensation ($C^* \leq C_{f_s}$).

Because we study diffusion through a polymer the diffusion coefficient $D_f$ is taken to be concentration dependent, i.e. of the form $D_f(C_f) = D_{f_0} \exp\left(-c\, C_f\right)$, with $D_{f_0}$ and $c$ known constants.

This model has been solved using both a finite differences approach and the method of lines (MOL) based on a finite volume approach (FVM), [18].

We will first model the flux in a cylindrical fiber which is coated with one layer of polymer with the AI of thickness $d$. Then an extension is made using several coating layers. Based on this model it is possible to describe the concentration release for other chemical coatings by adjusting the diffusion coefficients and mass transfer coefficients to these of the AI in question.

### 2.2.1 Initial and boundary conditions for a one layer coating

1. The prescribed concentration on the surface at starting time,

$$C_{f_s}^0 = C_f(R+\rho,0), \text{ with } 0 \leq \rho \leq d. \tag{2.1}$$

2. The outer flux is determined by the evaporation rate $\Gamma_{lg}$, that is defined as

$$\Gamma_{lg} = h_{lg}\left(C^\star(T) - C_{f_s}\right) S_f,$$

wherein $C^\star$ is the equilibrium concentration in the void space, $h_{lg}$ is the mass transfer coefficient, $[h_{lg}] = m \cdot s^{-1}$, that can be derived from the Churchill-Bernstein equation for mass transfer, [57], [3]. It is a relation of the form $\mathrm{Sh} = f(\mathrm{Re}\,, \mathrm{Sc}) = \frac{h_{lg} L}{D}$ where $\mathrm{Sh}$ is the Sherwood number, $\mathrm{Re}$ is the Reynolds number and $\mathrm{Sc}$ is the Schmidt number, $L$ is the length and $D$ is the diffusivity. $S_f$ is the surface/volume ratio of the fiber and equals $2/R_f$.

For the evaporation process it is important to make the assumption that the equilibrium is reached instantly between the moisture content at fiber surface and that of the surrounding air. This means that the surface of the fiber is assumed to reach equilibrium with the outside atmosphere instantaneously when evaporation begins, i.e. if the atmosphere is free of vapor the concentration at the surface falls immediately to zero; if the vapor pressure in the atmosphere is $p$, the surface of the fiber immediately reaches the concentration which is in equilibrium with $p$.

This gives the BC on the surface

$$- D_{fs} \left. \frac{\partial C_f}{\partial \rho} \right|_{\rho=R+d} = \Gamma_{lg} = h_{lg} \left( C_{f_s} - C^\star(T) \right) S_f, \tag{2.2}$$

where the diffusion coefficient $D_{fs}$ is the value corresponding to the actual concentration on the surface $C_{f_s}$.

3. If we use a polyester fiber the inner flux is zero due to the impermeable surface, so

$$\left. \frac{\partial C_f}{\partial \rho} \right|_{\rho=R} = 0. \tag{2.3}$$

For a cotton fiber or a blend of several fibers water and thus also other liquid chemicals could enter the inner fiber. To adjust for this the right-hand side of this above flux equation becomes a constant depending on the kind of fiber, or it is necessary to use a polymer that meets the assumption of no absorption by the fiber itself by creating an impermeable coating under-need the AI coating.

4. We assume radial diffusion only,

$$\frac{\partial C_f}{\partial z} = \frac{\partial C_f}{\partial \theta} = 0. \tag{2.4}$$

5. For the REV, the left and right flux should be the same

$$D_{\mathrm{L}} \partial_\rho C_f^+ = D_{\mathrm{R}} \partial_\rho C_f^- , \tag{2.5}$$

where $C_f^+$ is the concentration that diffuses into the REV from the left and $C_f^-$ the concentration that diffuses out of the REV tot the right. These two concentrations are assumed to be known since they are at the boundary of the REV.

### 2.2.2 Initial and boundary conditions for a coating consisting of multiple layers

If we have multiple coating layers, say $\kappa$, the model and its IC and BC are similar,

$$\frac{\partial C_{f_i}}{\partial t}(\rho,t) = \frac{1}{\rho}\frac{\partial}{\partial \rho}\left(\rho D_i \frac{\partial C_{f_i}}{\partial \rho}(\rho,t)\right), \quad i = 1,\ldots,\kappa,$$

with $C_{f_i}$ the concentration of the component from coating layer $i$ and $D_i$ the corresponding diffusion coefficient that again can be concentration dependent.

Lets focus on the example where we have three coatings of thickness $d_i$ respectively. All layers satisfy BC (2.4) and (2.5). Furthermore, for the inner coating we only have IC (2.1) and BC (2.3), because the evaporation doesn't occur since this coating is covered with another coating. The outer coating satisfies IC (2.1) and BC (2.2). For the middle layer we only have the initial condition. Formally we can describe the IC's and BC's as

1. The prescribed concentration on the surface

$$\left(C^0_{f_s}\right)_i = C_{f_i}(R + d_{i-1} + \rho,0), \text{ with } 0 \le \rho \le d_i, \quad d_0 = 0, i = 1,\ldots,3.$$

2. The outer flux for the outer coating

$$\left(D_{fs}\right)_3 \left.\frac{\partial C_{f_3}}{\partial r}\right|_{\rho=R+d} = -\Gamma_{lg} = -h_{lg}\left(\left(C_{f_s} - C^\star(T)\right)_3\right) S_f,\ d = d_1+d_2+d_3,$$

   where $\left(D_{fs}\right)_3$ is the diffusion coefficient for the active ingredient in layer 3 corresponding to the actual concentration on the surface $\left(C_{f_s}\right)_3$ .

3. The impermeable surface flux on the left

$$\left.\frac{\partial C_{f_i}}{\partial r}\right|_{\rho=R} = 0.$$

4. If the coatings cannot diffuse into each other we have a similar no-flux condition for each layer:

$$\left.\frac{\partial C_{f_i}}{\partial r}\right|_{\rho=R+d_i} = 0, \quad i = 1,2,$$

5. We assume radial diffusion only,

$$\frac{\partial C_{f_i}}{\partial z} = \frac{\partial C_{f_i}}{\partial \theta} = 0.$$

6. For the REV, the left and right flux should be the same

$$D_{\mathrm{L}}\partial_\rho C_{f_i}^{+} = D_{\mathrm{R}}\partial_\rho C_{f_i}^{-},$$

where $C_{f_i}^{+}$ is the concentration of substance $i$ that diffuses into the REV from the left and $C_{f_i}^{-}$ the concentration that diffuses out of the REV tot the right. These two concentrations are assumed to be known since they are at the boundary of the REV.

### 2.2.3 Active ingredient in a polymer binder coating

In the above sections we considered a fiber coated with one or more layer(s) of an AI. In practice these AI's are bound to the fiber using a polymer coating in which the AI is dissolved. The thickness of the fiber is approximately 12 $\mu$m. In our case the polymer binder contains or DEET, or permethrin.
Mostly 2 to 5 layers with a thickness of 1 to 3 $\mu$m are deposited. The aim is to find the optimal coating in order to achieve a sufficiently high concentration of DEET around the fiber and permethrin on the fiber surface to repel mosquitoes and kill when landing.

We consider a domain $(0,R_f)$ with $R_f = R + \sum_{j=1,\ldots,n_c} R_j$, where $R_j$ is the thickness of coating $j$, and $n_c$ is the number of coatings. We use $u_1$ for the concentration of DEET, and $u_2$ for permethrin.

In the simplest model, the diffusion coefficient of $u_p$, $(p = 1, 2)$ in the polymer layer is constant: $D_p$ is small, and the two components do not influence each other, thus they can be considered independent. At the binder-air boundary at $R_f$, DEET evaporates with a speed $\alpha(u_1(R_f,t) - u_1^\star(T))$, with $\alpha$ a constant of proportionality and $u_1^\star(T)$ the equilibrium concentration of DEET remote from the surface at temperature $T$. Considering the fact that DEET will not accumulate in the surrounding air, we can ignore the part $u_1^\star$ in the evaporation equation and only consider the flux in the direction of $\rho$ as $\alpha u(R_f,t)$. Due to the form of the polymer binding, the diffusion coefficient will however decrease as the concentration of the components decreases. Hence, a concentration dependent diffusion coefficient is needed, instead of a constant diffusion. We consider:

$$D_{p,q}(u_p) = D_{0,q} \exp(c_p u_p),$$

for AI $p$ in polymer layer $q$, where $D_{0,q}$ is the diffusion coefficient at the limiting concentration $u_p \to 0$ and $c_p$ is a constant to determine further-on.

Hence, the full direct model for two coating layers, one for each AI, is given

by:

$$
\begin{cases}
\partial_t u_p &= \frac{1}{\rho}\partial_\rho\left(\rho D_{p,q}(u_p)\partial_\rho u_p\right), \quad \rho \in (R, R_f) \\
u_1(\rho,0) &= \begin{cases} u_{1,0} & \rho \in (R, R+R_1) \\ 0 & \rho \in (R+R_1, R_f) \end{cases} \\
u_2(\rho,0) &= \begin{cases} 0 & \rho \in (R,R+R_1) \\ u_{2,0} & \rho \in (R+R_1, R_f) \end{cases} \\
\partial_\rho u_1(R,t) &= 0 \\
\partial_\rho u_2(R,t) &= 0 \\
\partial_\rho u_1(R_f,t) &= \alpha u_1(R_f,t) \\
\partial_\rho u_2(R_f,t) &= 0 \\
\partial_z u_1(\rho,t) &= \partial_\theta u_1(\rho,t) = 0 \qquad \rho \in (0, R_f) \\
\partial_z u_2(\rho,t) &= \partial_\theta u_2(\rho,t) = 0 \qquad \rho \in (0, R_f)
\end{cases}
$$

Here $u_{1,0}$ and $u_{2,0}$ are the original piecewise constant concentration profiles after creating the coatings. So in a coating layer with DEET, $u_{2,0}$ is zero, and vice-versa. Further we have,

$$\alpha = \frac{h_m}{D_{1,1}(u_1)} S_f,$$

with $h_m$ the mass transfer coefficient and $S_f$ the surface/volume ratio, so $\alpha$ is a dimensionless constant.

More precisely we consider 2 layers: the first consisting of the polymer polyacrylate and the active ingredient DEET, the second consisting of silicone elastomer and the active ingredient permethrin. We assume the above stated concentration dependent diffusion coefficient $D_{p,q}(u_p)$ for AI $p$ trough the layer of polymer $q$, where $p = 1$ for DEET and $p = 2$ for permethrin, $q = 1$ for polyacrylate and $q = 2$ for silicone elastomer. The initial conditions of DEET $u_{1,0}$ and of permithrin $u_{2,0}$ are taken to be $1500\,\mathrm{mg}\,/\,\mathrm{m}^3$.

The above direct problem is a BVP with Dirichlet initial conditions for $t$ and Neumann boundary condition for $\rho$ and is solved using a forward finite difference scheme and with a standard method in Maple.
Therefor we construct a mesh of $(N+1)\times(M+1)$ dividing the interval $[R,R_f]$ in $N$ equal intervals $[\rho_i,\rho_{i+1}], i = 0,\ldots,n-1$ and choosing an interval $[0,T]$ for

$t$ that is divided into $M$ equal intervals

$$\begin{aligned}
h &= \frac{R_f - R}{N},\\
k &= \frac{T-0}{M},\\
\rho_i &= R + ih, \quad i = 0,1,\ldots,N,\\
t_j &= 0 + jk, \quad j = 0,1,\ldots,M,\\
u_{1i,j} &= u_1(\rho_i,t_j), \quad i = 0,1,\ldots,N \text{ and } j = 0,1,\ldots,M,\\
u_{2i,j} &= u_2(\rho_i,t_j), \quad i = 0,1,\ldots,N \text{ and } j = 0,1,\ldots,M.
\end{aligned}$$

We denote $u_{i,j}$ for $u_{p_{i,j}}, p = 1,2$.

The finite difference that are used are

$$\begin{aligned}
\partial_t u(\rho_i,t_j) &= \frac{u_{i,j+1} - u_{i,j}}{k},\\
\partial_r u(\rho_i,t_j) &= \frac{u_{i+1,j} - u_{i-1,j}}{2h},\\
\partial^2_\rho u(\rho_i,t_j) &= \frac{u_{i+1,j} - 2u_{i,j} + u_{i-1,j}}{h^2}.
\end{aligned}$$

To be able to differentiate the function $D_{p,q}(u_p)$ we first define the smoothed step function

$$S(\rho,a,b,c,d) = a + \frac{b-a}{1+\exp\left(-c(\rho-d)\right)},$$

visible in Fig. 2.1.

Using this function we define

$$\begin{aligned}
c(\rho) &= S(\rho,c_1,c_2,100,R+R_1),\\
d(\rho) &= S(\rho,D_{0,1},D_{0,2},100,R+R_1),\\
f(\rho,t) &= d(\rho)\exp(c(\rho)\cdot u(\rho,t)),\\
f_{i,j} &= f(\rho_i,t_j),\\
f'_{i,j} &= \frac{\partial f}{\partial \rho}(\rho_i,t_j)\\
&= d'(\rho_i)\cdot\exp(c(\rho_i)\cdot u_{i,j}) + f_{i,j}\cdot\left(c'(\rho_i)\cdot u_{i,j} + c(\rho_i)\frac{\partial u}{\partial \rho}(\rho_i,t_j)\right)\\
&= d'(\rho_i)\cdot\exp(c(\rho_i)\cdot u_{i,j}) + f_{i,j}\cdot\left(c'(\rho_i)\cdot u_{i,j} + c(\rho_i)\frac{u_{i+1,j} - u_{i-1,j}}{2h}\right).
\end{aligned}$$

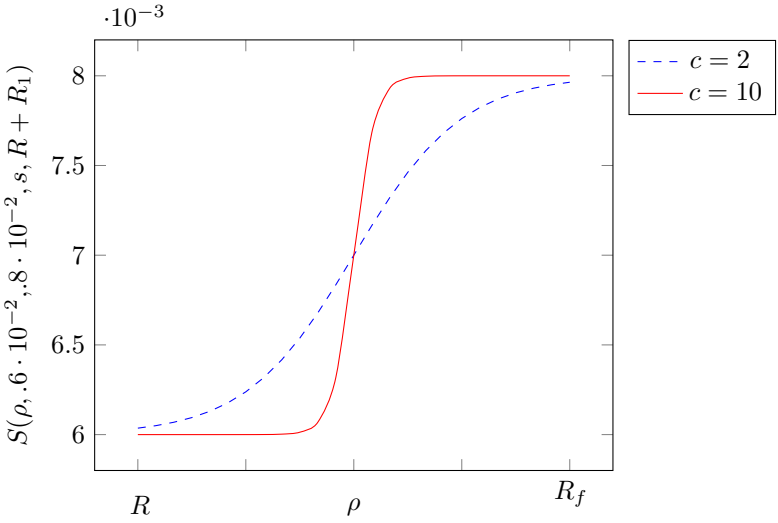


Figure 2.1: The smoothed step function $S$ for different values of $c$

In point $(\rho_i, t_j)$ the model becomes , $i = 1, \ldots, N$ and $j = 1, \ldots, M$:

$$
\begin{cases}
u_{i,j+1} = u_{i,j} + kf_{i,j}\dfrac{u_{i+1,j} - u_{i-1,j}}{2\rho_i h} + kf'_{i,j}\dfrac{u_{i+1,j} - u_{i-1,j}}{2h} \\
\qquad\qquad + kf_{i,j}\dfrac{u_{i+1,j} - 2u_{i,j} + u_{i-1,j}}{h^2} \\
u_1(\rho,0) = \begin{cases} 1500 \text{ mg / m}^3 & \rho \in (R, R + R_1) \\ 0 & \rho \in (R + R_1, R_f) \end{cases} \\
u_2(\rho,0) = \begin{cases} 0 & \rho \in (R, R + R_1) \\ 1500 \text{ mg / m}^3 & \rho \in (R + R_1, R_f) \end{cases} \\
\frac{u_{1_{1,j}} - u_{1_{-1,j}}}{2h} = 0 \\
\frac{u_{2_{1,j}} - u_{2_{-1,j}}}{2h} = 0 \\
\frac{u_{1_{N+1,j}} - u_{1_{N-1,j}}}{2h} = \alpha u_{1_{N,j}} \\
\frac{u_{2_{N+1,j}} - u_{2_{N-1,j}}}{2h} = 0
\end{cases}
$$

Solving this model in Maple gives the solution in Fig. 2.2 for DEET using the above constructed finite difference method and the solution for both AI's in Fig. 2.3 using the standard built-in Maple method.

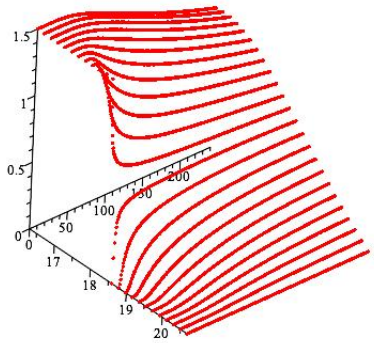


(a) Pointplot of solution for DEET

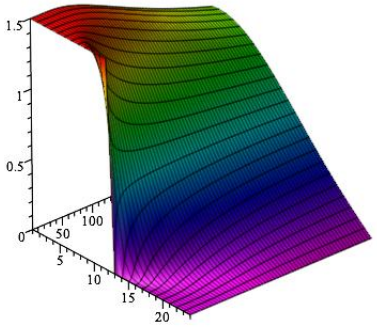


(b) Fitted surface through pointsolution for DEET

Figure 2.2: Solution for DEET using the above constructed finite difference method

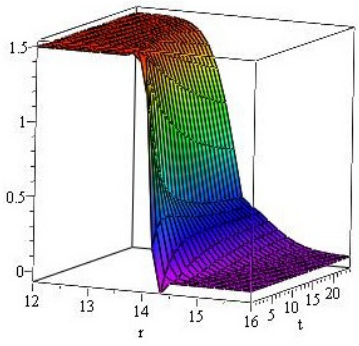


(a) Solution for DEET

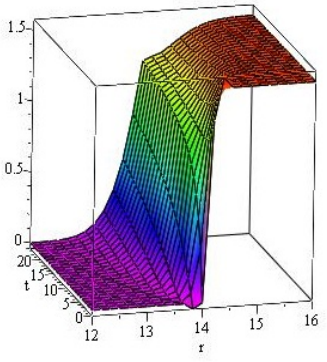


(b) Solution for permethrine

Figure 2.3: Solution for DEET, permethrin and both using the standard built in finite difference method in Maple

Instead of using finite differences and Maple we can also solve the model

$$\frac{\partial C_f(\rho,t)}{\partial t} = \frac{1}{\rho}\frac{\partial}{\partial \rho}\left(\rho D_f \frac{\partial C_f(\rho,t)}{\partial \rho}\right), \quad 0 \leq \rho \leq R_f,$$

with boundary conditions

$$\nabla C_f(R,t) = 0,$$

at the fiber radius $R$ and

$$\nabla C_f = \alpha \left( C_f(R_f,t) - C_{f_s}(t) \right) \cdot \mathcal{H} \left( C_f(R_f,t) - C_b, C^*(T) - C_{f_s}(t) \right). \qquad (2.6)$$

at the coated fiber radius $R_f$, using the method of lines (MOL). This has been implemented in Python code. Two possible derivations can be made. An error analysis is made to pick the best method. The set-up is given in Fig. 2.4.

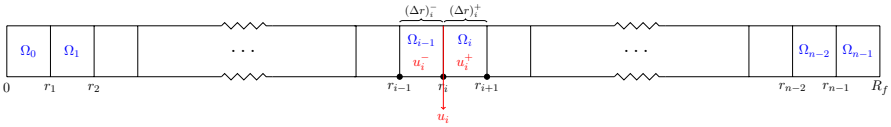


Figure 2.4: Domain for MOL

We will use

$$\begin{aligned}
(\Delta\rho)_i^+ &= \rho_i - \rho_{i-1}, \\
(\Delta\rho)_i^- &= \rho_{i+1} - \rho_i, \\
\rho_i^+ &= \rho_{i+\frac{1}{2}} = \rho_i + \frac{(\Delta\rho)_i^+}{2}, \\
\rho_i^- &= \rho_{i-\frac{1}{2}} = \rho_i - \frac{(\Delta\rho)_i^-}{2}.
\end{aligned}$$

Derivation 1

Denote $w = u\rho$. Then

$$\partial_t w = \partial_\rho \left( \rho D \partial_\rho \frac{w}{\rho} \right),$$

where

$$D = D_0 e^{-c\frac{w}{\rho}}.$$

If we integrate over the domain $\Omega = [L,R]$ we get

$$\int_\Omega \partial_t w \, \mathrm{d}\rho = \left[ \rho D \partial_\rho \frac{w}{\rho} \right]_L^R.$$

If we divide the domain into $n$ cells we can write this for every cell $\Omega_i = [\rho_i,\rho_{i+1}]$, denoting the scaled concentration on time $t$ on space location $\rho_i$ as

$w_i(t)$. The scaled concentration in de centers of the adjacent cells are denoted by $w_i^-$ and $w_i^+$ in $\Omega_{i-1}$ and $\Omega_i$ respectively. Doing so we calculate the flux on the edge $\rho_i$ as

$$\begin{aligned}\int_{\Omega_i} \partial_t w_i(t)\,\mathrm{d}\rho = \partial_t w_i^+ \int_{\Omega_i} \mathrm{d}\rho &= \left[\rho D \partial_\rho \frac{w}{\rho}\right]_{\rho_i}^{\rho_{i+1}} \\ &= \rho_{i+1} D_{i+1} \partial_\rho \frac{w}{\rho}\bigg|_{\rho_{i+1}} - \rho_i D_i \partial_\rho \frac{w}{\rho}\bigg|_{\rho_i}.\end{aligned}$$

The first term on the right hand side is the flux along edge $\rho_{i+1}$, the second term is the flux along edge $\rho_i$.
For the flux along edge $\rho_i$ we have

$$\begin{aligned}\text{flux}_{\text{edge}_i} &= \rho_i D_i \left(\partial_\rho \frac{w}{\rho}\right)\bigg|_{\rho_i} \\ &= \rho_i \left(\frac{D_{0,i}^+ \exp\left(-c\frac{w_i^+}{\rho_i^+}\right) + D_{0,i}^- \exp\left(-c\frac{w_i^-}{\rho_i^-}\right)}{2}\right)\left(\frac{\frac{w_i^+}{\rho_i^+} - \frac{w_i^-}{\rho_i^-}}{\frac{(\Delta\rho)_i^+ + (\Delta\rho)_i^-}{2}}\right),\end{aligned}$$

where we have taken the average diffusion coefficient of the adjacent cell centers.
According to the above derivation we get

$$\partial_t w_i^+ = \left(\text{flux}_{\text{edge}_{i+1}} - \text{flux}_{\text{edge}_i}\right)\frac{1}{(\Delta\rho)_i^+}.$$

Derivation 2

We do not make the substitution to the scaled concentration $w = u\rho$ and work with the original concentration $u$. We then get for every cell $\Omega_i$

$$\int_{\Omega_i} \partial_t u_i(t)\rho\,\mathrm{d}\rho = \partial_t u_i^+ \int_{\Omega_i} \rho\,\mathrm{d}\rho = \left[D\rho\partial_\rho u\right]_{\rho_i}^{\rho_{i+1}}.$$

Like in derivation 1 we write

$$\begin{aligned}\text{flux}_{\text{edge}_i} &= \rho_i D_i \left(\partial_\rho u\right)\big|_{\rho_i} \\ &= \rho_i \left(\frac{D_{0,i}^+ \exp\left(-cu_i^+\right) + D_{0,i}^- \exp\left(-cu_i^-\right)}{2}\right)\left(\frac{u_i^+ - u_i^-}{\frac{(\Delta\rho)_i^+ + (\Delta\rho)_i^-}{2}}\right).\end{aligned}$$

For the flux we get

$$\partial_t u_i^+ = \left(\text{flux}_{\text{edge}_{i+1}} - \text{flux}_{\text{edge}_i}\right)\frac{2}{2\rho_i(\Delta\rho)_i^+ + \left((\Delta\rho)_i^+\right)^2}. \tag{2.7}$$

This last result is the same as in derivation 1 where we do the inverse transformation from the scaled to the original concentration using $w_i^+ = u_i^+ \left(\rho_i + \frac{(\Delta\rho)_i^+}{2}\right)$. The difference is the number of calculations. Considering the fact that more calculations induce more rounding errors and slower computation time, the preference is given to derivation 2.

Results for the diffusion model of the AI in time using MOL where the AI is directly at the fiber surface and taken to be $961\,\mathrm{mg}\,/\,\mathrm{m}^3$ at $t = 0$ are shown in Fig. 2.5. Here the `cvode`-package is used to solve the ODE's. This is a subpackage of python's Sundials-packages that uses backward differential formulas (BDF) or the Adams-Moulton method to solve the system of ODE's. In the example BDF was used.

## 2.3 Scale of the Yarn

On the yarn level we only model the concentration of an evaporating AI, such as DEET.

Based on the model prescribed in [59], we choose to work with cylindrical coordinates $(r,\theta,z)$. By assuming we can neglect diffusion in the $\theta$ and $z$ direction and diffusion is everywhere radial and symmetrical we can work in only one dimension. The governing model for the concentration of the AI on the yarn level then is, according to the radial diffusion equation in a cylinder,

$$\epsilon \frac{\partial C_y(r,t)}{\partial t} = \frac{1}{r}\frac{\partial}{\partial r}\left(\epsilon r \frac{D_y}{\tau_y}\frac{\partial C_y(r,t)}{\partial r}\right) + \Gamma_{\text{in}}(r,t), \tag{2.8}$$

with as BC's a diffusive flux to the outside

$$-D_y \frac{\partial C_y}{\partial r}(R_y,t) = -\frac{1}{d_{\text{out}}}\left(C_y(R_y,t) - C_{\text{out}}(t)\right),$$

a no-flux condition on the left boundary

$$\frac{\partial C_y}{\partial r}(0,t) = 0,$$

and initially a zero concentration

$$C_y(r,0) = 0,$$

where $D_y$ is the diffusion coefficient of the AI in the yarn air gaps, $\epsilon$ is the porosity depending on position and $\tau_y$ is the tortuosity of the yarn. In the BC $C_{\text{out}}(t)$ is the concentration of AI in the air surrounding the yarn at a prescribed distance $d_{\text{out}}$ to the yarn.
The term $\Gamma_{\text{in}}(r,t)$ in the equation above is a source term that describes the

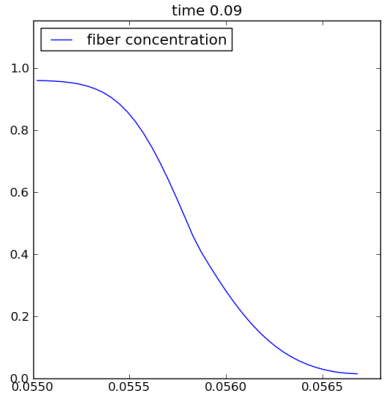


(a) AI concentration in the fiber after 0.09s

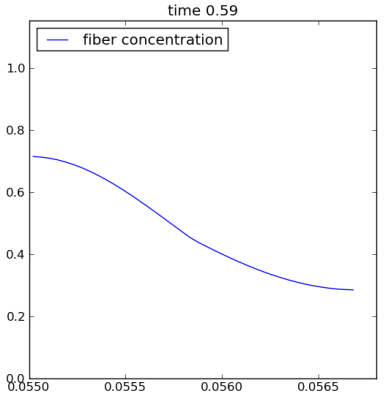


(b) AI concentration in the fiber after 0.59s

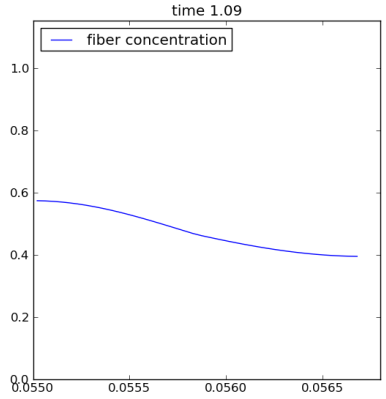


(c) AI concentration in the fiber after 1.09s

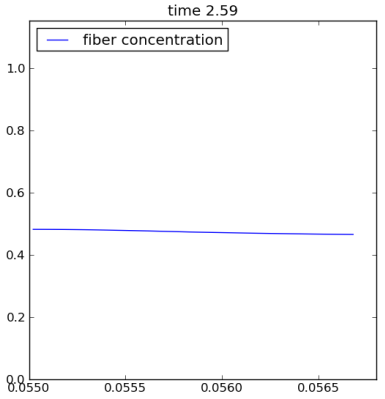


(d) AI concentration in the fiber after 2.59s

Figure 2.5: The diffusion of the AI in time using MOL where the AI is directly at the fiber surface and taken to be $961\,\mathrm{mg}\,/\,\mathrm{m}^3$ at $t = 0$

amount of AI coming out of a cross-section of the fibers into the yarn air space. It is calculated by upscaling the boundary condition at the fiber level (2.6), representing the flux of AI over the boundary, using the volume averaging technique [55].

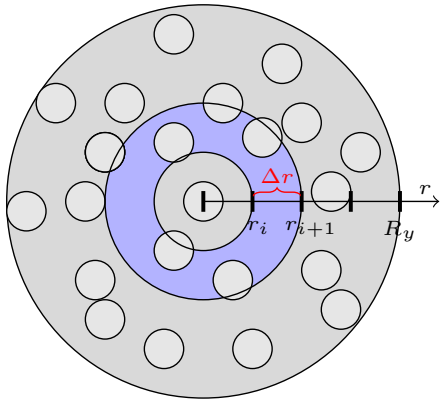


Figure 2.6: Yarn discretization in cylindrical coordinates

In order to solve this model we divide the radial space $[0,R_y]$ in $N$ intervals $\Omega_i = [r_i,r_i + \Delta r] = [r_i,r_{i+1}]$ with length $\Delta r = \frac{R_y}{N}$, where $R_y$ is the yarn radius. If afterwards we also consider the $\theta$-coordinate we get concentric circles for each space interval, Fig. 2.6. In each of these shells we consider $n$ fibers. $N$ is chosen in such way that in each interval we can describe one fiber model, with the same initial conditions and boundary conditions. Considering the fact that the area of such a shell between $[r_i,r_{i+1}]$ is

$$V_{\text{shell}} = \int_0^{2\pi} \mathrm{d}\theta \int_{r_i}^{r_{i+1}} r \,\mathrm{d}r = \pi(r_{i+1}^2 - r_i^2) = \pi\Delta(r^2)_i$$

and the area of a coated fiber intersection with radius $R_f$ is $\pi R_f^2$, we have

$$\epsilon_f = \frac{nR_f^2}{\Delta(r^2)_i}.$$

On the other hand, the area of a yarn intersection with radius $R_y$ is $\pi R_y^2$. So if we have $m$ fibers per yarn cross section, the fiber volumetric fraction also can be expressed as

$$\epsilon_f = \frac{mR_f^2}{R_y^2}.$$

This means we can calculate the number of fibers in a shell $[r_i,r_{i+1}]$ as

$$n = \frac{m(r_{i+1}^2 - r_i^2)}{R_y^2}.$$

In every time step $t_j$ and space interval $[r_i,r_{i+1}]$ we solve one fiber model, assuming all $n$ fibers in the same shell satisfy the same evaporation boundary condition

$$-D_f \frac{\partial C_f^{i,j}}{\partial \rho}(R_f) = S_f h_{b\to f}\left(C_f^{i,j-1}(R_f) - C_y^{i+,j-1}\right) \cdot \mathcal{H}\left(C_f^{i,j-1}(R_f) - C_b, C^*(\mathrm{T}) - C_y^{i+,j-1}\right),$$

where $C_y^{i+,j-1} = C_y(r_i^+,t_{j-1})$ is the concentration in the middle of the space interval $\Omega_i$, i.e. $r_i^+ = r_i + \frac{\Delta r}{2}$, of the previous time step, and $C_f^{i,j-1}(R_f) = C_f(R_f,r_i,t_{j-1})$ is the concentration on the fiber surface of a fiber in $\Omega_i$ of the previous time step. Furthermore, $S_f$ is the effective area of evaporation $\epsilon\frac{2}{R_f}$, $h_{b\to f}$ is the mass transfer coefficient for the AI from bounded to free material and $\mathcal{H}$ is the adjusted Heaviside function as defined earlier, [33, 53]. Therefore we can calculate the resulting averaged fiber mass from the intrinsic averaged fiber concentration times the *averaging volume* of the fiber void space $V_f\epsilon$, using the volume average technique to calculate the, [55],

$$\begin{aligned}
M_f^{i,j} &= \left(\frac{1}{V_f}\int_0^{2\pi} \mathrm{d}\theta \int_R^{R_f} C_f^{i,j}(\rho)\,\rho\,\mathrm{d}\rho\right) V_f\epsilon \\
&= 2\pi\epsilon \int_R^{R_f} C_f^{i,j}(\rho)\,\rho\,\mathrm{d}\rho \\
&= 2\pi\epsilon \sum_{k=0}^{N-1} \int_{\rho_k}^{\rho_{k+1}} C_f(\rho)\rho\,\mathrm{d}\rho \\
&= 2\pi\epsilon \sum_{k=0}^{N-1} C_f(\rho_k^+) \int_{\rho_k}^{\rho_{k+1}} \rho\,\mathrm{d}\rho \\
&= 2\pi\epsilon \sum_{k=0}^{N-1} C_f(\rho_k^+) \frac{\rho_{k+1}^2 - \rho_k^2}{2} \\
&= \pi\epsilon \sum_{k=0}^{N-1} C_f(\rho_k^+)(\rho_{k+1}^2 - \rho_k^2),
\end{aligned}$$

for fibers at $[r_i,r_{i+1}]$ at time $t_j$ and then take the difference between this fiber mass and the mass at the previous time step $M_f^{i,j-1}$. Here $V_f$ is the *averaging volume* of the fiber coating. The difference $\Delta M_f^{i,j} = (M_f^{i,j} - M_f^{i,j-1})$ gives the amount removed from the fibers at yarn interval $[r_i,r_{i+1}]$ during that time step. Next we find the source term $\Gamma_{\text{in}}$ for a shell at $[r_i,r_{i+1}]$ representing the amount

coming from all $n$ fibers in the shell per timestep,

$$\Gamma_{\text{in}}(r_i^+,t_j) = n\frac{\Delta M_f^{i,j}}{\epsilon V_{\text{shell}}\Delta t}.$$

If in (2.8) we denote $rC_y$ by $u$ the equation becomes

$$\epsilon\frac{\partial u}{\partial t} = \frac{\partial}{\partial r}\left(\epsilon r\frac{D_y}{\tau}\frac{\partial}{\partial r}\left(\frac{u}{r}\right)\right) + r\Gamma_{\text{in}}(r,t).$$

Using MOL in $\Omega_i = [r_i,r_{i+1}]$ we get

$$\epsilon\int_{r_i}^{r_{i+1}}\frac{\partial u}{\partial t}\,\mathrm{d}r = \epsilon\frac{D_y}{\tau}\int_{r_i}^{r_{i+1}}\frac{\partial}{\partial r}\left(r\frac{\partial}{\partial r}\left(\frac{u}{r}\right)\right)\mathrm{d}r + \int_{r_i}^{r_{i+1}}\Gamma_{\text{in}}(r,t)r\,\mathrm{d}r,$$

which becomes

$$\epsilon\frac{\partial u(r_i^+,t)}{\partial t}\Delta r_i^+ = \epsilon\frac{D_y}{\tau}\left[r\frac{\partial}{\partial r}\left(\frac{u}{r}\right)\right]_{r_i}^{r_{i+1}} + \Gamma_{\text{in}}(r_i^+,t)\frac{(\Delta r^2)_i}{2}.$$

This means we need to implement the partial derivative of $u_i^+ = u(r_i^+,t) = r_i^+C_y(t)$ as

$$\frac{\partial u_i^+}{\partial t} = \frac{1}{\Delta r_i^+}\left(\frac{D_y}{\tau_y}\left[\text{flux}_{\text{edge}_{i+1}} - \text{flux}_{\text{edge}_i}\right] + n\frac{\Delta M_f(r_i,t)}{2\epsilon^2 V_{\text{shell}}\Delta t}(\Delta r^2)_i\right), \qquad (2.9)$$

with

$$\text{flux}_{\text{edge}_i} = \left(r\frac{\partial}{\partial r}\left(\frac{u}{r}\right)\right)\Big|_{r_i} = r_i\frac{\frac{u_i^+}{r_i^+} - \frac{u_i^-}{r_i^-}}{\Delta r},$$

where $r_i^- = r_i - \frac{\Delta r}{2} = r_{i-1} + \frac{\Delta r}{2} = r_{i-1}^+$ and $u_i^- = u(r_i^-,t)$.
The equation (2.9) has been implemented in Python-code next to the previously derived equation for the fiber (2.7) in order to be able to solve the system of equations of the complete three scale model. The last step in finding the solution of the complete system of equations is implementing the equation of the room model and upscaling the solution for one yarn model to the amount of AI coming into the room from all yarns together.

Another way of solving this problem is using a 2D diffusion model of the 2D yarn cross section containing fibers. Then only the $z$ direction is neglected, and we can write in $(x,y)$ coordinates

$$\frac{\partial C_y(x,y,t)}{\partial t} = \boldsymbol{\nabla}\cdot\left(D_y\nabla C_y(x,y,t)\right),$$

where the tortuosity $\tau_y$ needed in the 1D model is no longer necessary. This model takes as a domain the circle circumscribing the yarn intersection with

the fiber intersection circles cut out. On each boundary that arises like this a a certain concentration of the AI is introduced through a flux boundary condition for the fiber model which in this case also is also a 2D model

$$\frac{\partial C_f(x,y,t)}{\partial t} = \boldsymbol{\nabla} \cdot \left( D_f \nabla C_f(x,y,t) \right),$$

with BC

$$\nabla C_{f_s} = \alpha (C_{f_s} - C_y(x,y,t))\, \mathcal{H}(C_{f_s} - C_b, C^*(T) - C_y(x,y,t)),$$

where the subscript s stands for surface and $\mathcal{H}, C_b$ and $C^*(T)$ are defined as before.

This 2D model can be solved using a finite element method or a finite volume method. For this purpose it is necessary that we can create a suitable representation of the yarn cross-section. We have to focus on the creation of a realistic grid for the yarn cross-section, which is suitable for mass and heat transfer models. Therefor we extended and adapted the virtual location method (VLM) which allows the quick creation of a range of 2D yarn-fiber layouts. We overcame two of its main disadvantages: the presence of too much regularity, and the inability to produce yarn-fiber layouts when blends of fibers with different sizes are present. Our method is based on the standard ring configuration VLM, creating two sets of virtual locations per fiber type, which causes some overlap of the fibers. The overlap is removed with an iteration scheme based on induced movement. The final result is a realistic 2D cross-section of a yarn. A reference implementation is available, and it is shown how the layout can be used to create a grid.

## 2.4 The Extended Virtual Location Method

We present an improved yarn-fiber layout construction algorithm, which forms the first step in a multiscale simulation: domain construction of the different scales. For porous materials there are several packing algorithms available, see e.g. Software Package for the Assessment of Compositional Evolution (SPACE) and other methods [46], but these are oriented towards ground structures and large-scale repetition, and are therefore ill-suited to construct the specific fiber layout found in textiles. A thorough analysis of this fiber layout for single fiber materials was done in [19]. In the same article a VLM was introduced to generate computer-generated yarn cross-sections mimicking the experimental fiber layout.

There are some drawbacks to the VLM proposed in [19]. These are also present in the extension to elliptical virtual locations to account for yarn-twist

given in [45]. Firstly, the results show more regularity than what is commonly found in the experimental results. Secondly, the method is only valid for yarns consisting of a single type of fiber. Although fibers of different size can be generated in the virtual location, the virtual location itself is based upon a single size. We adapted the method to obtain a final result with less regularity, also we are capable of handling blends of fibers with very different sizes. To validate the approach, we compared the results with yarn cross-sections of a polyester-cotton blend obtained by optical microscopy.

In multiscale modeling one specific yarn realization can give qualitative insights into the physical processes. However, over an entire fabric, some averaging should be performed when upscaling is done to the fabric level. This can be done using some volume averaging or via a Monte-Carlo approach or via overlapping domain decomposition. For all methods it is important to verify that a given yarn cross-section realization satisfies the structure of the yarn one wanted to generate in the first place. We also provided the statistical tests needed to verify this.

The method presented is only valid for a cross-section of a yarn. From this, one can construct 3D yarns as done in [45] for the standard virtual location method. For the application we have in mind (heat and tracer transfer), a 3D yarn is not required. Hence, we only present how a 2D grid can be constructed from the generated cross-sections. All algorithms presented are available in the STICK-toolkit[1].

### 2.4.1 Conventional approach

The standard algorithm used to create a 2D yarn structure is the "virtual location method" (VLM). It has been developed by [19], and has been applied to generate the structure of the yarn cross-section [20, 44, 42]. "Virtual Location" (VL) stands for a cell in a yarn cross-section which might be occupied by a fiber. In this method, VLs are generated first, then fibers are assigned a VL. In this way the optimal packing is determined first via VLs, next the actual yarn-fiber layout is determined. Usually, for simplification, it is assumed that the diameter $D_{\mathrm{VL}}$ of each VL remains constant and equal to $D_{\mathrm{VL}} = D_f^{\mathrm{av}} + \sigma_f$, where $D_f^{\mathrm{av}}$ is the average diameter of the fibers and $\sigma_f$ the mean deviation of the fiber diameter. The total number of VLs equals at least the number of fibers. The location of a fiber within a VL is random. Often, it is assumed that the shape of the fibers in the cross-section, and hence in the VL, is elliptical. How many VLs contain fibers, depends on the fiber-distribution probability $p(r)$ or $p(r, \theta)$, with $r$ the radius of each ring zone from the center of the yarn and $\theta$ the angle of each location in polar coordinates. Three types of models that use

[1] See `http://gitorious.org/stickproject`

VLs are considered: "one fiber-one location", "one fiber-several locations" and "ring configuration model". In general, only the last one is used, as it gives the best results.

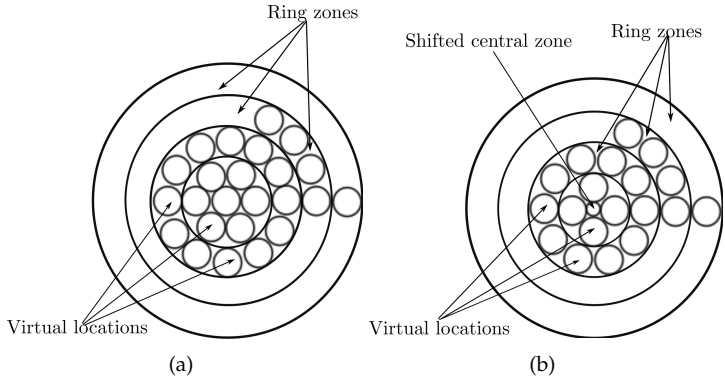


Figure 2.7: (a) normal ("non-shifted") ring configuration as used in VLM; (b)"shifted" ring configuration where the central zone has 'shifting' value $\Delta d_{\text{shift}} = R_f/2$

In this ring configuration model, the yarn cross-section is divided into several ring zones, see Fig. 2.7(a), [19, 20]. All of them have the same width $h = D_{\text{VL}}$ and the outer radii $R_j$ of these zones are

$$R_j = h/2 + jh; \quad j = 0,1,\ldots,n_z,$$

where $n_z$ is chosen so that $R_{n_z}$ is near the imposed yarn radius $R_y$.

Each ring zone is filled up with VLs. The number of virtual locations within any $j$th zone does not depend on the diameter of the VLs and is calculated as

$$M_0 = 1, \quad M_j = \lfloor 2\pi j \rfloor, \quad 1 \le j \le n_z,$$

where $\lfloor x \rfloor$ is the greatest integer less than or equal to $x$.

To generate a yarn-fiber layout according to this conventional approach, the following input data is required:

1. fiber-dimension parameters, namely, $R_f^{\max}$, $R_f^{\min}$, $R_f^{\text{av}}$ and $\sigma_f$: the maximum, minimum and average radius of the fibers, and mean deviation of the fiber diameter, respectively;

2. $R_y$, the yarn radius;

3. $N_f$ ,the total number of fibers in the cross-section;

4. $p_{\mathrm{VL}}(r,\theta)$, the VL fiber-distribution probability over the yarn cross-section in polar coordinates.

Here, $p_{\mathrm{VL}}(r,\theta)$ is the probability that a VL at position $(r,\theta)$ contains a fiber. This probability can indirectly be obtained from measurements. The general algorithm then consists of the following steps:

1. divide the yarn domain (a disc) in ring zones;

2. construct VLs in every ring zone;

3. determine those VL that are occupied by fibers in accordance with the VL fiber-distribution probability $p_{\mathrm{VL}}(r,\theta)$ or $p_{\mathrm{VL}}(r)$. For example, in [44], the following distribution is used

$$p_{\mathrm{VL}}(r) = (1-\varepsilon)\left\{\frac{\exp(1)-\exp(r/R_y)}{\exp(1)-1}\right\}^{\beta} + \varepsilon, \qquad r \in (0,R_y), \quad (2.10)$$

   where $\beta$ and $\varepsilon$ are parameters that are fitted to experimental data; and

4. for every occupied VL in the yarn cross-section, define the dimensions of the occupying fiber and locate them randomly within the VL.

See Fig. 2.8 for the typical result of such a computation. The advantage of this algorithm is that by using VLs, one can quickly create fiber-yarn layouts with the typical ring structure that satisfy the obtained virtual-location fiber-distribution, $p_{\mathrm{VL}}(r,\theta)$ or $p_{\mathrm{VL}}(r)$. Other methods have difficulty with this, and several trials are needed to achieve a correct realization.

### 2.4.2 New approach: Extended VLM

The conventional approach has some shortcomings. To start with, there is the regularity seen in Fig. 2.8, which does not match experimentally retrieved data of yarn cross-sections. Secondly, many applications deal with blended yarns, containing for example both cotton and polyester fibers. Therefore a method that is able to generate yarn-fiber layouts with different fiber types, is needed. To resolve both issues, we present an extension to the VLM.

**Area fraction.** The first important change is that we drop the requirement of a VL fiber-distribution probability. Instead, we use the more natural area fraction, $f_A(r,\theta)$. This function expresses how much area at position $(r,\theta)$ will be fiber area. For every type of fiber present in a yarn cross-section the fraction can be determined as follows. One obtains several images of cross-sections of

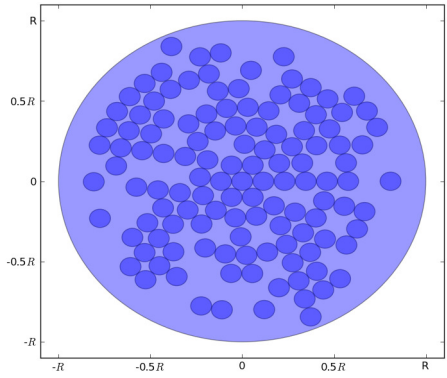


Figure 2.8: Fiber distribution in virtual locations constructed with the standard algorithm

the yarn under consideration. The images are divided in zones, and per zone the fraction of fiber area is determined by

$$f^i_{A_j} = \frac{A^i_{j,f}}{A_j}. \tag{2.11}$$

Here, $A^i_{j,f}$ indicates the average over the images of the area of fibers of type $i$ in the $j$th zone; $A_j$ is the total area of the $j$th zone. We call $f^i_{A_j}$ the area fraction of fibers of type $i$ in the $j$th zone. Then, the discrete values of $f^i_{A_j}$ are interpolated to obtain a continuous function $f^i_A(r,\theta)$. Note that

$$\int_0^{2\pi}\int_0^{R_y} f^i_A(r,\theta)\, r\mathrm{d}r\mathrm{d}\theta = A^i_f \approx N^i_f \pi {R^i_f}^2,$$

with $A^i_f$ the total fiber area for fiber type $i$, and $N^i_f$ the total number of fibers of type $i$, which have average radius $R^i_f$.

The above construction of the area fraction from images can be automatized using image recognition software. The area fraction is useful as it contains all information of the production method used to create the yarn. The processes of yarn twist, fiber movement, yarn deformation, etc. would need to be considered if one would like to determine the area fraction from first principles. Using images of the final resulting yarn, this information is not needed. We now show an example of typical area fractions.

**Example.** Consider two types of yarns as also given in [44]: filament yarn and ring spun yarn. Note that there is a single fiber type, and that the fibers are circular. Here, we have $R_y = 0.83$mm, $R_f = 0.0295$mm and as number of fibers $N_f^{\mathrm{f}} = 262$ for the filament and $N_f^{\mathrm{rs}} = 193$ for the ring spun yarn. Analyzing the images of these yarns, we can determine the area fraction function. We obtain

$$\begin{aligned} f_A^{\mathrm{f}}(u) &= 5.88u^4 - 12.97u^3 + 8.23u^2 - 1.74u + 0.60, \\ f_A^{\mathrm{rs}}(u) &= 1.05u^4 - 2.24u^3 + 0.87u^2 - 0.11u + 0.42, \end{aligned}$$

with $u = \frac{r}{R_y}$, $u \in (0,1)$, and $f_A^{\mathrm{f}}(u)$, $f_A^{\mathrm{rs}}(u)$ being the area fraction functions for a filament and a ring spun yarn. We have indeed that $2\pi R_y^2 \int_0^1 f_A^f(u) u \, \mathrm{d}u =$

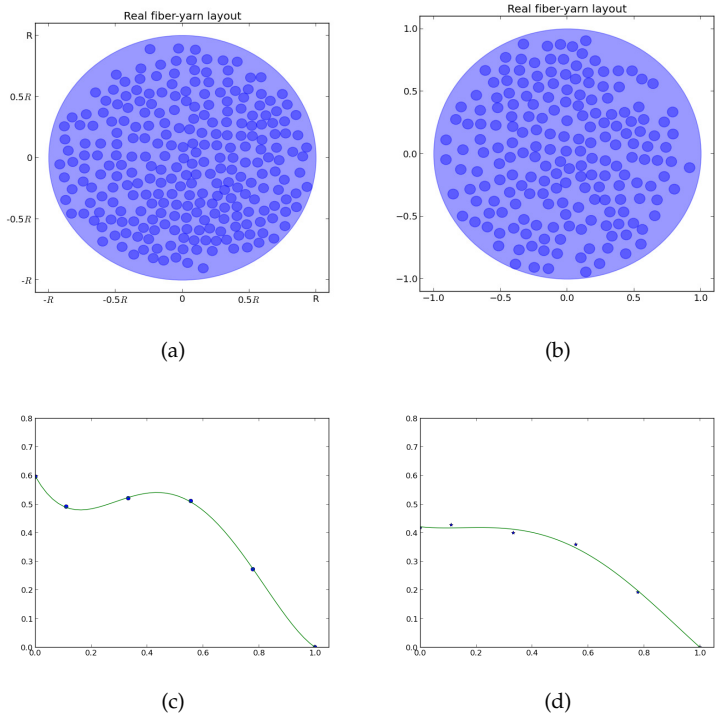


Figure 2.9: (a) Typical cross-section for a filament yarn with 262 fibers; (b) Typical cross-section for a ring spun yarn with 193 fibers; (c) The area fraction function for fibers in the filament yarn; (d) The area fraction function for fibers in the ring spun yarn

$1.027R_y \approx \bar{N}_f^{\mathrm{f}} \pi R_f^2$. We have $|N_f^{\mathrm{f}} - \bar{N}_f^{\mathrm{f}}| < 0.02$ and $|N_f^{\mathrm{rs}} - \bar{N}_f^{\mathrm{rs}}| < 0.02$. Typical

fiber-yarn layouts for these yarns are given in Fig. 2.9(a) & 2.9(b), with the area fraction function given in Fig. 2.9(c) & 2.9(d). It is clear that the different mechanical processes to create the yarns give rise to qualitatively different fiber area fractions.

Here, and in the following, we use circular fibers. This is for simplicity reason, only. The extension to elliptical fibers (as they arise also due to twisting) can be done similarly as [44] did for the standard VLM.

**Combining layouts.** The second important change is to combine several standard VL setups. This will allow blends instead of only single fiber setups. With this technique, we will also be able to generate more realistic yarn cross-sections for yarns with a single fiber type (less regularity as compared to the VLM).

In our approach, we use a VL size which is based on the fiber size of the fiber under consideration in the blend. We consider blends with $N_t$ fiber types. Thus, for instance, a cotton-polyester blend has $N_t = 2$. When necessary a super index is used to indicate the fiber type, e.g. $f_A^1(r,\theta)$ for the area fraction of fiber type 1. VLs are used to generate a good start structure satisfying the area fraction $f_A$. For each fiber type, the cross-section of the yarn is divided into several ring zones containing VLs, see Fig. 2.7(a). This process is repeated as many times as the number of fiber types in the blend. The VLs of a specific fiber type have constant radius

$$R_{\mathrm{VL}}^i = (1+\beta)R_f^i, \quad i = 1,\ldots,N_t,$$

where $R_f^i$ is the mean radius of each fiber type and $\beta$ is a small non-touch factor which prevents most fibers touching each other (it allows some extra freedom to place the actual fiber in the VL).

The amount of VLs that are filled with fibers in each ring zone $k$, viz $N_{f,k}^i$, is determined by the area fraction $f_A^i(r,\theta)$. Fibers are added from the center to the yarn radius. For example, for a radially dependent fraction, the number of fibers in the previous ring zones is $\sum_{k=0}^{j-1} N_{f,k}^i = N_{f,0\to j-1}^i$. Therefore, in ring zone $j$

$$A_{f,j}^i = \int_0^{2\pi}\int_0^{R_j} f_A^i(r,\theta) r \,\mathrm{d}r\mathrm{d}\theta - N_{f,0\to j-1}^i \pi (R_f^i)^2, \quad N_{f,j}^i = \left\lfloor \frac{A_{f,j}^i}{\pi (R_f^i)^2} \right\rfloor, \tag{2.12}$$

where $R_f^i$ is the mean value of the radius of the fiber of type $i$, and $R_j$, as before, is the outer radius of the virtual zone. The integral in (2.12) is computed with the trapezium rule (as $f_A$ itself is determined numerically from experiments).

Once we determined how many fibers are in each ring zone, the fibers for each ring zone are distributed to the VLs in the ring zone by using a uniform

distribution function. Apart from the fact that this procedure uses an area fraction, the result per fiber type will be the same as the standard VLM, so a high regularity is obtained.

To avoid this typical regularity resulting from the conventional VLM, we also construct a shifted VL configuration for every fiber type, and repeat the procedure to determine the occupied VLs. The shifted configuration only differs from the normal one in that the central ring zone for each kind of fiber is shifted $\Delta d_{\text{shift}} = \gamma R_f^i$, $0 < \gamma < 1$, where $\Delta d_{\text{shift}}$ is the shifting value, and $\gamma$ the shifting coefficient. For our computations we use $\gamma = 1/2$. As a result, both the ring zones and the VLs in the domain have new positions, see Fig. 2.7(b). Consequently, for each fiber type, there is the normal VL configuration and the shifted one, Fig. 2.7.

The construction of a shifted version of the VLM is a crucial step to allow for fast generation of yarn-fiber layouts that satisfy the given area fraction $f_A^i$. The two configurations have $2N_f^i$ fibers per fiber type $i$. The two VLM realizations are merged so that the final result still satisfies $f_A^i$ and has $N_f^i$ fibers in the domain: we randomly take $N_{f,j}^i/2$ from each $j$th ring zone of the "non-shifted" and "shifted" configurations.

Having the correct amount of fibers per fiber type, we merge the different fiber type configurations to a single layout. In the case of several fiber types (blends), but also as a consequence of the shifted ring zone, several fibers will overlap. To remove this overlap, an iteration scheme based on an induced movement is used. This induced movement is explained in details in Section 2.4.3. It's main characteristic is that it leaves the area fraction function largely unchanged. The result of this step is the final yarn-fiber layout. In Section 2.4.5 it is shown that after removing the overlap, the layout indeed satisfies the original fiber area fraction function. As we can verify that a generated layout satisfies the area fraction within preset margins, it is straightforward to reject a layout that does not satisfy this requirement, and start again. In our experience, this is seldom needed.

This extended VLM requires as input data:

1. The number of fiber types $N_t$, the fiber-dimension parameters, and the number of fibers $N_f^i$ in the yarn cross-section per fiber type $i$, with total number of fibers $N_f = \sum_i^{N_t} N_f^i$ and blend percentage $P_f^i = N_f^i/N_f$;
2. $R_y$, the yarn radius;
3. The fiber area fraction $f_A^i(r,\theta)$ per fiber type $i$ in polar coordinates;
4. The shifting coefficient $\gamma$.

The Extended VLM consists of the following steps:

1. Divide the yarn domain (a disk) per fiber type in ring zones for normal VLs and shifted VLs.

2. Construct VLs in every constructed ring zone (a configuration).

3. Determine per configuration those VLs that are occupied by fibers in accordance with the fiber area fraction function $f_A^i(r,\theta)$.

4. Merge the normal and shifted VL in accordance with the fiber fraction $f_A^i(r,\theta)$ by making the sum of fibers' area from the normal and shifted VL up to the $j$th ring zone equal to $A_{f,j}^i$ from (2.12).

5. For every selected occupied VL, define the dimensions of the occupying fiber and locate them randomly within the VL.

6. Merge all the different configurations to one single yarn-fiber layout. Thus, we end up with $N_f$ fibers in a blended yarn cross-section.

7. Remove all the overlappings between the fibers in the domain using the induced movement.

8. Calculate the resulting area fraction. If this is in agreement with the given $f_A^i(r,\theta)$, retain the final result, otherwise reject it.

We now present the scheme to remove the overlap and show that this scheme is a valid approach leading to acceptable fiber-yarn layouts.

### 2.4.3 Removing Overlap

Merging configurations generates overlap. There is no overlap in the real structure of a yarn, so all the overlap in the cross-section domain must be removed. During this step VLs are of no importance since we are working with representations of real fibers. For the sake of clarity, we consider here circular fibers, that resemble the VLs in which they are placed. In case of non circular fibers, it is best to use a circular representation (or another geometrical shape that is easy to calculate overlap with) of the fiber for this step, and only at the end move back to the actual form of the fibers: ellipsoid fibers, or triangular ones, ...

Let there be $N_f$ circular fibers with radii $R_f^n$, $n = 1,\ldots,N_f$. We set the origin of the $XY$-axes at the center of the yarn. The center of the $n$-th fiber is denoted by the vector $\mathbf{u}_n = (x_n,y_n)$. Given two fibers $n$ and $m$, the Eudiclean distance between them is denoted by

$$D_{mn} = \|\mathbf{u}_n - \mathbf{u}_m\|. \tag{2.13}$$

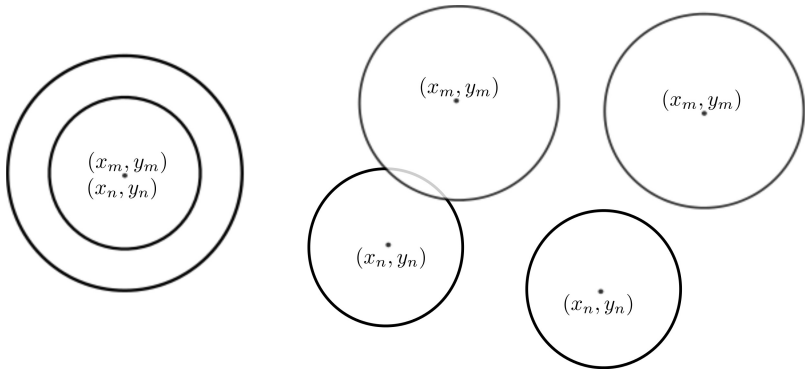


Figure 2.10: Three possible positions between fibers in the yarn domain

Three situations may occur: $D_{mn} = 0$, i.e. total overlap; $0 < D_{mn} < R_f^m + R_f^n$, i.e. partial overlap; and $D_{mn} \geq R_f^m + R_f^n$, i.e. no overlap, see Fig. 2.10.

To determine whether the fibers overlap, a minimum distance between two fibers, denoted as $D_{mn}^{\text{req}}$, is defined by

$$D_{mn}^{\text{req}} = R_f^n + R_f^m.$$

At the same time the condition

$$R_y \geq R_f^m + D_c^m,$$

guarantees that all fibers are inside the yarn domain, here $D_c^m$ being the distance between the center of fiber $m$ and the center of the yarn. As the center of the yarn is the origin, $D_c^m = \|\mathbf{u}_m\|$.

The algorithm to remove the overlap consists of a loop with the following steps:

1. All the distances $D_{mn}$, $m$,$n = 1, \ldots, N_f$, are computed using (2.13). One determines which fibers overlap. This can be done efficiently by a vectorized computation (or even parallelized as they are independent computations).

2. The required movement, needed to have the situation of no overlap, is computed as
$$\Delta D_{mn} = D_{mn}^{\text{req}} - D_{mn} > 0,$$
and the vector, along which the movement should occur, is $\mathbf{u}_{mn} = \mathbf{u}_n - \mathbf{u}_m$. Hence, the needed movement required is
$$\Delta \mathbf{u}_{mn} = \Delta D_{mn} \frac{\mathbf{u}_{mn}}{\|\mathbf{u}_{mn}\|}. \tag{2.14}$$

3. It is necessary to divide (2.14) over the two fibers. We write the induced movement of fiber $m$ under fiber $n$ as $\Delta\mathbf{u}_m^n$. Hence,

$$\Delta\mathbf{u}_{mn} = \Delta\mathbf{u}_n^m - \Delta\mathbf{u}_m^n.$$

The minus sign is needed because the two fibers should move in opposite directions. As we consider different fiber types with different radii, it makes sense to move the smaller fiber more then the larger one. This is a consequence of the fact that if we move the larger fiber, there is more chance of creating new overlap with other fibers, Fig. 2.11. Therefore, we impose the relationship

$$R_f^m \Delta\mathbf{u}_m^n = -R_f^n \Delta\mathbf{u}_n^m. \tag{2.15}$$

This shows the correct limiting behavior that, for an infinitely small fiber, all movement would be assigned to this fiber. From (2.15) we can eliminate one of the movements as,

$$\Delta\mathbf{u}_n^m = \alpha\Delta\mathbf{u}_m^n, \quad \alpha = -\frac{R_f^m}{R_f^n}. \tag{2.16}$$

From (2.14)-(2.16) we can calculate the movement value for the $m$th fiber,

$$\Delta\mathbf{u}_m^n = \frac{D_{mn} - D_{mn}^{\text{req}}}{R_f^m + R_f^n} R_f^n \frac{\mathbf{u}_{mn}}{\|\mathbf{u}_{mn}\|}.$$

4. The previous step is done for all overlapping fiber pairs. At the end, a new location $\mathbf{u}_m^{'}$ for every fiber is calculated from the original location by

$$\mathbf{u}_m^{'} = \mathbf{u}_m + (1+\epsilon)\sum_{k=1}^{N_{\text{ov}}} \Delta\mathbf{u}_m^k,$$

where $N_{\text{ov}}$ indicates the indexes of the overlapping fibers. The parameter $\epsilon$ is a random value, which is added to avoid repetitive oscillations in the movement. We take $\epsilon \in (0.0, 0.01)$.

5. If the location of the fiber moves outside of the yarn domain, it needs to be moved back inside. This is achieved as follows, see Fig. 2.12. Define the distance between the yarn boundary and the outermost boundary of the $m$th fiber by

$$\Delta D_{y/f}^m = (R_f^m + D_c^m) - R_y,$$

If $\Delta D_{y/f}^m > 0$, the fiber is outside of the domain. If this is the case, the fiber should be moved by

$$\Delta\mathbf{u}_m^y = (-\Delta D_{y/f}^m)\frac{\mathbf{u}_m}{D_c^m}.$$

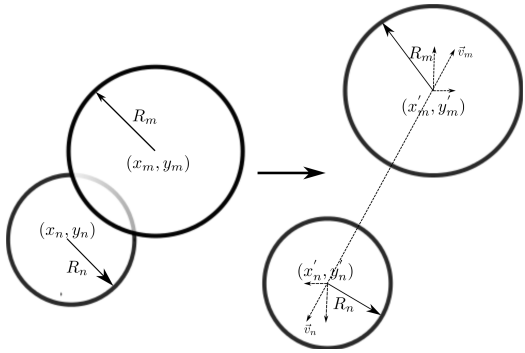


Figure 2.11: From overlap to non-overlap

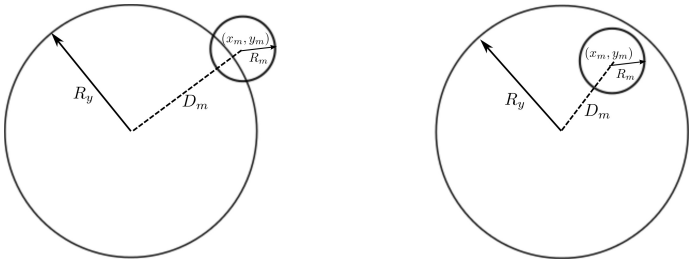


Figure 2.12: Move a fiber back into the domain of the yarn

Hence the new position is

$$\mathbf{u}'_m = \mathbf{u}_m + (1+\epsilon)\Delta\mathbf{u}^y_m.$$

6. The induced movement is stopped when no fibers overlap anymore and no fibers are outside of the yarn domain, or when the number of iterations in this step exceeds a preset maximum value.

In Section 2.4.5, the advantage of the above procedure is discussed. We show that the movement is localized around the original fiber position, and does not perturb the area fraction. Hence, the realization of a yarn layout still satisfies the preset area fraction after the induced movement, and the computational time is reasonable. The preset maximum number of iterations is normally only reached when wrong initial data is given, for example more fibers than what can fit in the radius domain. As an alternative to stopping the iterations, one can continue the iteration but without the step that limits the positions to the inside of the yarn radius.

### 2.4.4 Results

The main result we want to verify is that the generated fiber-yarn layouts satisfy the originally computed area fraction we started with. We do this mathematically by determining the area fraction for a generated layout and by computing the difference with the original one. We can also define an error in terms of the difference with the original area fraction. A low error then indicates a correct fiber-yarn construction.

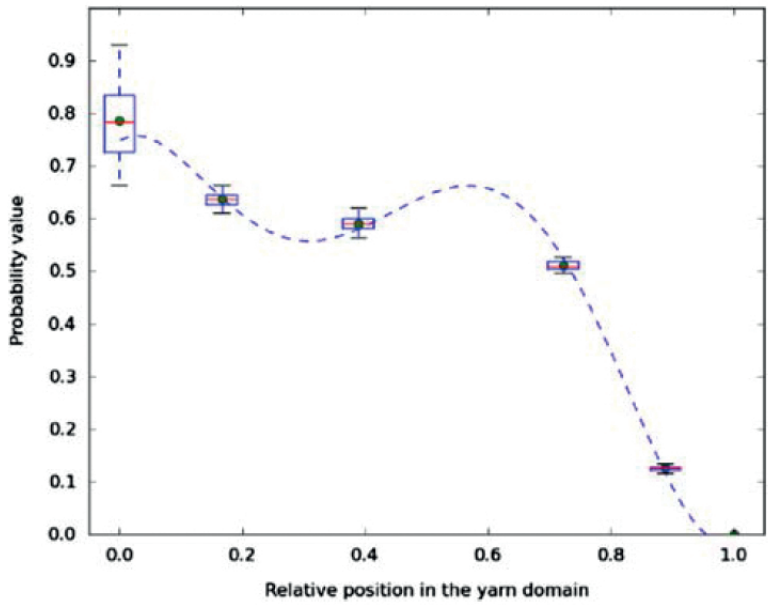


Figure 2.13: Original area fraction for a yarn with one fiber type (dashed line) and the area fraction as box plots from layouts generated with the Extended VLM (dots indicate the mean values)

### 2.4.5 Satisfying a given area fraction

**Satisfying the area fraction function of yarn with a single fiber type**

We consider a yarn with one fiber type. The result of the yarn-fiber layout should satisfy a given fiber area fraction. We consider the fiber-distribution probability, Eq. (2.10), used in the standard VLM. Though this is not directly related to the area fraction, an area fraction function can be fitted to the obtained

layout. We consider a yarn with $R_y = 0.196$mm, $N_t = 1$, $R_f^1 = 0.014$mm, and

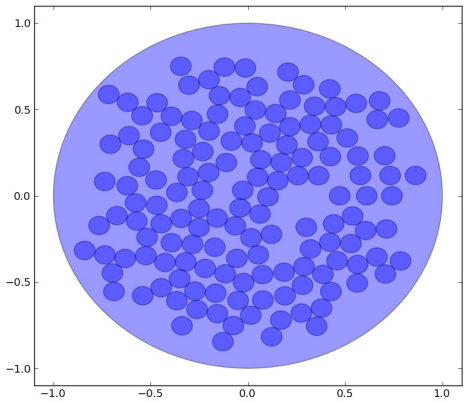


Figure 2.14: The irregular fiber-yarn layout obtained with the Extended VLM

with the number of fibers being $N_f = N_f^1 = 144$. We obtain

$$f_A^1(r) = 32.91r^5 - 77.29r^4 + 59.14r^3 - 16.24r^2 + 0.73r + 0.75.$$

The Extended VLM is applied and the results are depicted in Fig. 2.13 and Fig. 2.14. To compare the generated layout with the given area fraction, we divided the yarn in 5 ring zones $A_m$, and computed the discrete fiber area fraction, $\bar{f}_{A_m}$, in that zone with 10 realizations, according to equation (2.11). This gives 5 computed points and box plots, which are shown in Fig. 2.13 together with the area fraction.

The result of the Extended VLM matches the area fraction function of the yarn layout. The Extended VLM can generate the fiber-yarn layout satisfying the fiber distribution and nevertheless has the irregularity of the layout, as seen from experiments, Fig. 2.14.

**Satisfying the area fraction function of a blend**

To test a blended fiber-yarn layout, a polyester-cotton blend is used. We retrieved the cross-section of a yarn by means of a microtome. To this end a fabric was embedded in a resin. A typical result can be seen in Figs. 2.15(a), 2.15(b). Based on these images, the parameters of the yarn have been determined, see Table 2.1.

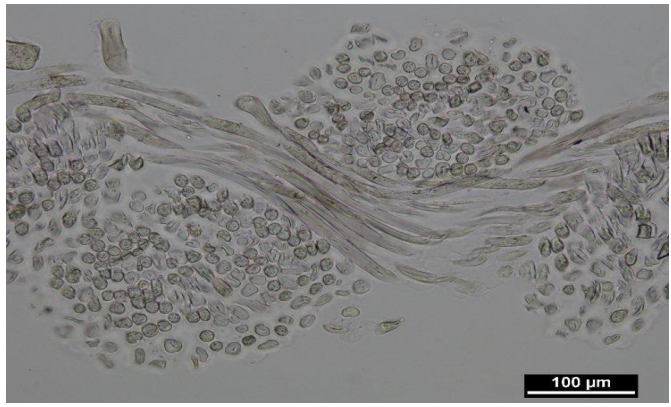


(a)

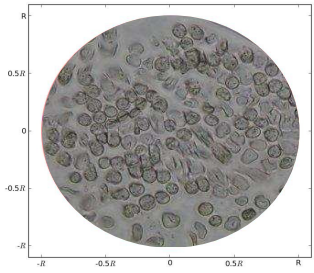

(b)

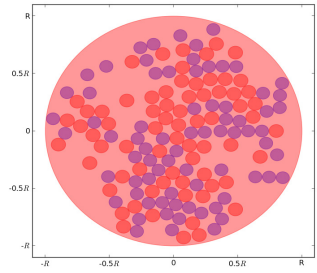

(c)

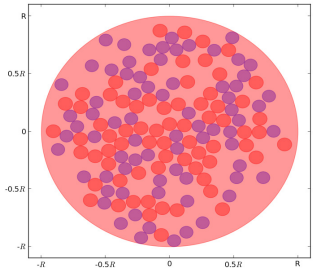

(d)

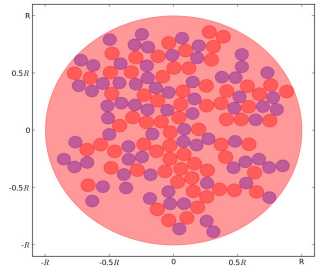

(e)

Figure 2.15: Comparison between the real yarn cross-section and three different realizations generated from our simulations

| Table 2.1: Data of a cotton-polyester blend yarn | |
|---|---|
| Parameters | Value |
| Yarn diameter | $0.0273\,\mathrm{cm}$ |
| Number of polyester fibers $N_f^1$ | $74$ |
| Number of cotton fibers $N_f^2$ | $70$ |
| Mean radius polyester $R_f^1$ | $0.00517\,\mathrm{mm}$ |
| Mean radius cotton $R_f^2$ | $0.00551\,\mathrm{mm}$ |
| Standard deviation polyester radius | $0.00074\,\mathrm{mm}$ |
| Standard deviation cotton radius | $0.00120\,\mathrm{mm}$ |

The cotton is approximated as circles. As this is a blend with two fiber types, two area fraction functions have been computed based upon the images of the cross sections:

$$f_A^1(r) = -7.03r^4 + 13.22r^3 - 8.34r^2 + 2.16r + 0.004,$$
$$f_A^2(r) = 1.13r^4 - 4.14r^3 + 4.39r^2 - 1.91r + 0.53.$$

Based on this, we generate yarn-fiber layouts using the Extended VLM . The results are given in Fig. 2.16, where the area fraction function is given as a dashed line, and the points represent again numerically computed values for the area fraction, obtained by dividing the generated layouts in 5 ring zones. They are the mean values computed from 10 realizations. Each box plot shows the median and standard deviation of the area fraction from 10 realizations. It can be seen that for this blend the area fractions from the simulated layout match well the given area fraction function for each kind of fiber. The examples which keep the area fraction characteristics and the natural irregularity of the yarn layout, corresponding to the microtome experiment Fig. 2.15(b), are shown in Figs. 2.15(c), 2.15(d) and 2.15(e).

Although the results above demonstrate that the Extended VLM works very well for this specific blend, the mean radii of the two kinds of fibers are close. Other cases are considered for further testing. First, we increase the difference between the fibers' radii, so that $R_f^1 = 3R_f^2$, see Fig. 2.17. The comparison of the original and obtained area fraction function is given in Fig. 2.18. We can conclude that again the generated yarn layouts satisfy the given area fraction.

As a third test, we generate a very dense yarn layout. The resulting layout satisfies the original area function, and is given in Fig. 2.19. There is no difficulty for the Extended VLM to obtain this layout, while at the same time the highly regular result of the standard VLM is not visible.

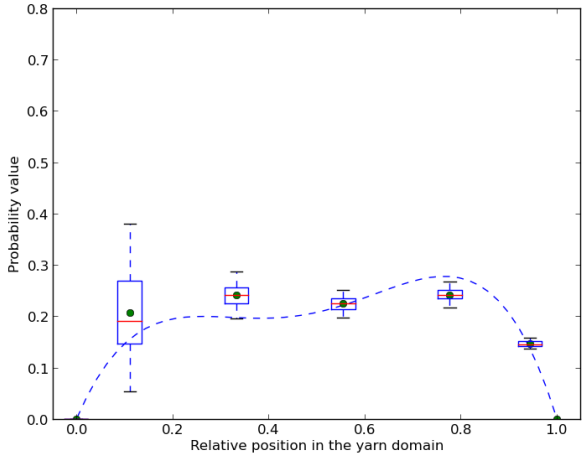


(a)

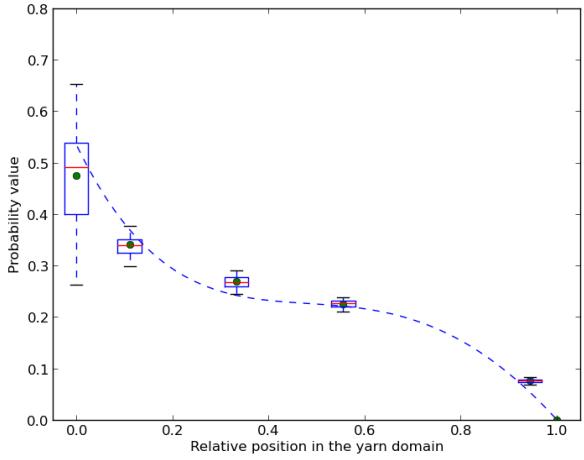


(b)

Figure 2.16: Comparison between the original (dashed line) and via the Extended VLM obtained area fraction functions for fiber type 1 and 2 (box plots, dots)

### 2.4.6 Validation of induced movement

From Section 2.4.5 it is clear that the presented induced movement algorithm removes the overlap, and does not disturb the area fraction function of the final

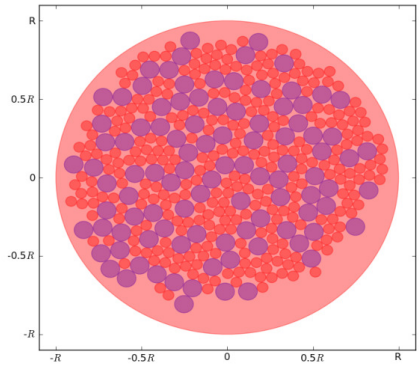


Figure 2.17: A yarn layout for fiber type radii that satisfy $R_f^m/R_f^n = 3$.

Table 2.2: The number of iterations for different $\alpha$ values (Two fiber types)

| $\alpha$ value | Minimum | Maximum | Average |
|---|---|---|---|
| $\alpha = -\frac{1}{2}$ | 112 | 171 | 144 |
| $\alpha = -1$ | 55 | 71 | 62 |
| $\alpha = -R_f^m/R_f^n$ | 130 | 247 | 194 |

result. We now show that other movement schemes do disturb this function. In Fig. 2.20 we present a typical result of the algorithm. The start layout is given in Fig. 2.20(a), with apparent overlap. The final configuration is given in Fig. 2.20(b), which retains the qualitative features of the original, but without the overlap, resulting in a realistic layout.

The distribution of the induced movement over the two fibers, (2.15-2.16), is very important to obtain the correct layout. In Table 2.2 the different number of iterations, needed for different values of $\alpha$, are given. We test the Extended VLM with

1. $\alpha = -\frac{R_f^m}{R_f^n}$. Each of the two fibers do a proportional movement, which depends on the radii ratio;

2. $\alpha = -\frac{1}{2}$. Each of the two fibers do half of the required movement;

3. $\alpha = -1$ . Both fibers do the full movement.

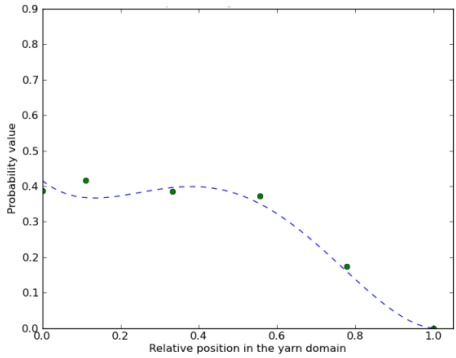


(a)

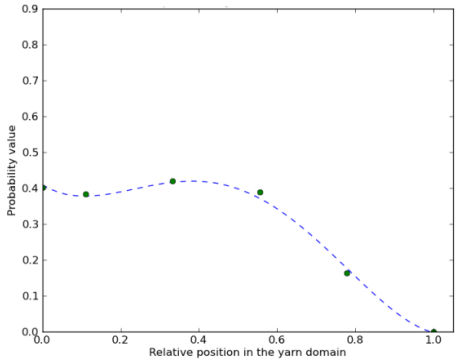


(b)

Figure 2.18: Comparison between the original area fraction functions (dashed line) and the (from the Extended VLM) obtained numerical area fraction for a blend with fiber type radii that satisfy $R_f^1/R_f^2 = 3$ (points)

Note that in the second case the overlap is over-corrected. We consider a yarn with two types of fibers, $N_t = 2$. The other parameters are as in Table 2.1. We repeat the layout generation 10 times, and notice the number of iterations needed to remove the overlap, see Table 2.2. From Table 2.2, it is obvious that $\alpha = -1$ requires the least number of iterations, followed by $\alpha = -\frac{1}{2}$. This would suggest that the proposed choice of $\alpha = -\frac{R_f^m}{R_f^n}$ is the worst. However, one also has to determine whether the obtained layouts satisfy the given area

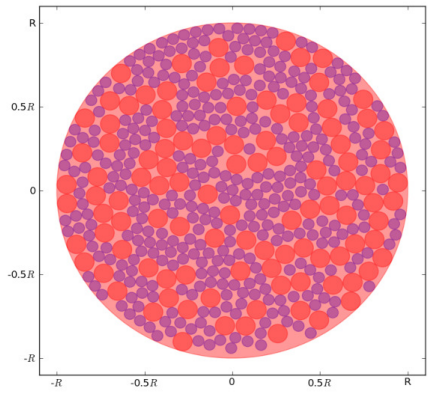


Figure 2.19: Example of a very dense fiber-yarn layout

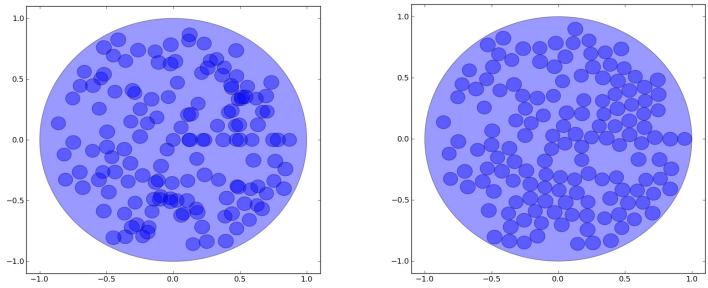

(a) (b)

Figure 2.20: (a) Fiber distribution with overlap created with Extended VLM; (b) Result after removing the overlap

fraction function. As expected, $\alpha = -\frac{R_f^m}{R_f^n}$ has the smallest relative error value, see Fig. 2.21 for both fiber types. The double movement obtained with $\alpha = -1$ gives the worst result. Here, the relative error is defined as:

$$\varepsilon_{A_m}^n = \left| \frac{\bar{f}_{A_m}^n - f_A^n(R_m)}{f_A^n(R_m)} \right|^2,$$

where $n$ is the fiber type and $m$ indicates a ring zone in the yarn domain. So

we compare the discrete values according to equation (2.11) with the values of the area fraction function at the radii of the $m$th ring, $R_m$. We conclude that, to maintain the original area fraction, our method should be chosen to remove the overlap between fibers, although it requires a higher number of iterations.

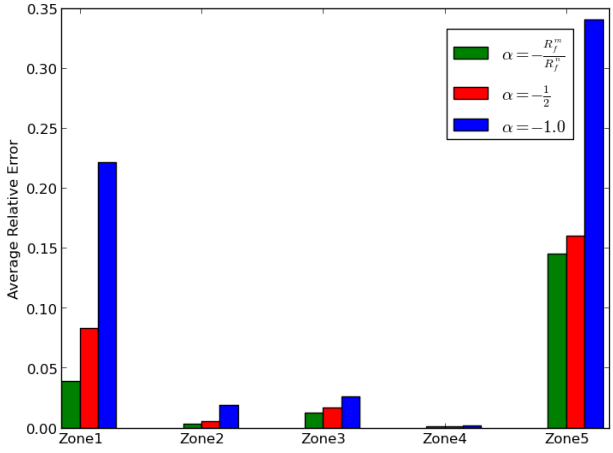


(a)

Figure 2.21: Analysis of the average relative error for $\alpha = -\frac{R_f^m}{R_f^n}$, $\alpha = -\frac{1}{2}$ and $\alpha = -1.0$ in Eq. 2.16 (a) for cotton and (b) polyester

### 2.4.7 Conclusion

We presented an extension of the VLM that can produce realistic fiber-yarn layouts, showing the irregularity observed in experiments. The method is fast, since it does not use a packing algorithm. Instead it uses merged results of the standard VLM (using it twice per fiber type), and a step to remove the overlap, without disturbing the fiber area fraction. The numerical experiments presented confirm the validity of the approach. The resulting 2D fiber-yarn layouts, can be used to construct 3D yarns, or to perform a deformation procedure, or to construct a realistic grid for the yarn scale of a multiscale mass transfer model. This last result is what is used in our python code to solve the yarn level model using a finite element method. A irregular mesh is constructed using the extended VLM for a blend of cotton and polyester. A colleague introduced

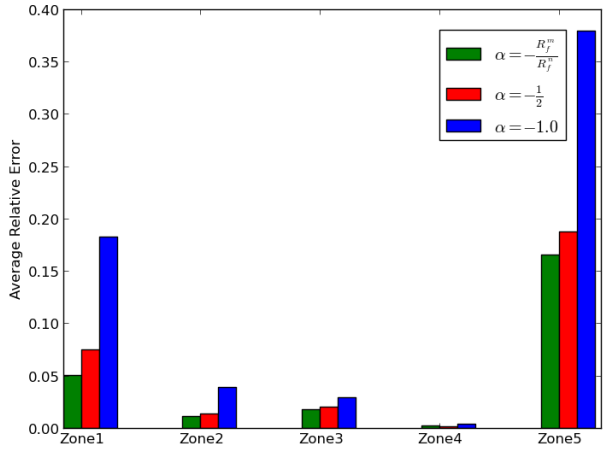


(b)

Figure 2.21: Analysis of the average relative error for $\alpha = -\frac{R_f^m}{R_f^n}$, $\alpha = -\frac{1}{2}$ and $\alpha = -1.0$ in Eq. 2.16 (a) for cotton and (b) polyester (continued)

the aforementioned elliptic fibers in the python code giving Fig. 2.22(a) as an example and an example of a finite element mesh in Fig. 2.22(b). As an

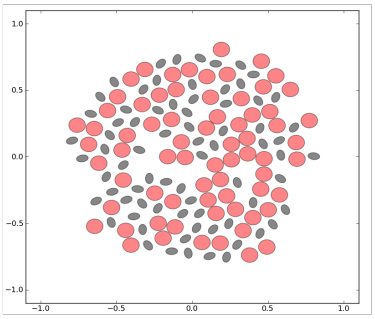

(a) Extended VLM generation of fiber-yarn layout

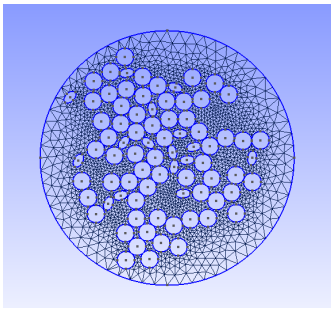

(b) Constructed mesh for a fiber-yarn layout

Figure 2.22: Construction of a suitable mesh for the finite element method

example we close this section with Fig. 2.23, where an example is shown of the calculations for the diffusion problem in a 2D yarn domain consisting of only circular fibers using the STICK toolbox, see section 2.8

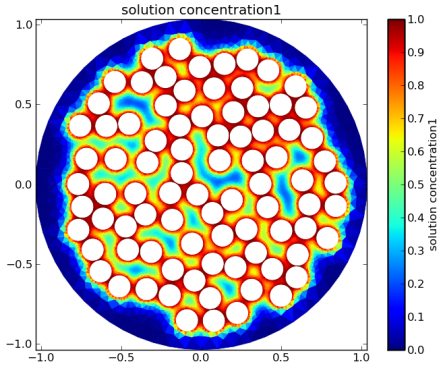


Figure 2.23: Solution of the diffusion problem for a 2D yarn domain with circular fibers using the constructed mesh corresponding to the extended VLM

## 2.5 Upscaling to the macro level

To upscale to the macro-level model of the total fabric the volume averaging technique can be used. Another way of upscaling is the overlapping domain decomposition technique. Therefor the original domain $[0,R_y]$ is extended with an overlapping zone $\Omega_o$ to the new domain $[R_y, R_y+\Omega_o]$ where the PDE (2.8) is slightly adapted with an extra sink term to

$$\epsilon \frac{\partial C_y(r,t)}{\partial t} = \frac{1}{r}\frac{\partial}{\partial r}\left(\epsilon r \frac{D_y}{\tau_y}\frac{\partial C_y(r,t)}{\partial r}\right) + \Gamma_{\text{in}}(r,t) - \Gamma_{\text{out}}(t,\Omega_o), \tag{2.17}$$

where the diffusive flux to the outside is replaced with a homogeneous Neumann BC

$$\frac{\partial C_y}{\partial r}(R_y+\Omega_o) = 0.$$

The sink term $\Gamma_{\text{out}}(t,\Omega_o)$ is the amount of AI that is removed from the meso-scale due to diffusion to the macro-level, see section 2.6.

## 2.6 Scale of the Net

### 2.6.1 Practical application within the NOBUG project

For the purpose of the NOBUG project we let us inspire by section 1.3.3 where only two levels were considered, a fiber level and a fabric level. For a densely woven or knitted fabric, e.g. a impregnated T-shirt, these two levels are appropriate. If we assume two coating layers on the fibers, one with DEET as AI, and one with permethrin as AI the governing equations for a textile fabric are

$$\frac{\partial(C_D(\epsilon_g+\epsilon_l))}{\partial t} = -\frac{\partial(u_g C_D \epsilon_g)}{\partial x} + \frac{\partial}{\partial x}\left(\frac{D_D^\star}{\tau_D}\frac{\partial(C_D(\epsilon_g+\epsilon_l))}{\partial x}\right) - \Gamma_{lg,D} + \epsilon_f \xi_2 \Gamma_{f,D},$$

$$\frac{\partial(C_p\epsilon_l)}{\partial t} = \frac{\partial}{\partial x}\left(\frac{D_p\epsilon_l}{\tau_p}\frac{\partial(C_p\epsilon_l)}{\partial x}\right) + \xi_2\Gamma_{f,p},$$

where

$$D_D^\star = \epsilon_g D_D^g + \epsilon_l D_D^l,$$

with $D_D^g$ and $D_D^l$ are the diffusion coefficients in gas and liquid, respectively. $\Gamma_{lg,D}$ is the evaporation rate of DEET from the fabric. $\Gamma_{f,D}$ and $\Gamma_{f,p}$ are the sorption rates of respectively DEET and permethrin of the fibers covered by liquid water. These last two terms only exist if liquid is present, for example during washing. Considering what is valid for water and the sorption rate $\Gamma_f$ in the governing equations of section 1.3.3 (where the volume averaging method of Whitaker) is used, we came to the following reasoning to find the sorption rates of DEET and permethrin.

We first solve an equation on fiber level for both AI's

$$\frac{\partial C_f'}{\partial t} = \frac{1}{\rho}\frac{\partial}{\partial\rho}\left(\rho D_f \frac{\partial C_f'}{\partial\rho}\right), \quad R_f \le \rho \le R.$$

After that we get a solution $C_f'(\rho,t)$ and use the volume averaging method to get the overall concentration, only depending on time, by integrating out the independent variable $\rho$.

$$C_f(t) = \frac{1}{V}\int_{R_f}^{R} C_f'(\rho,t)\rho\,\mathrm{d}\rho,$$

where

$$V = \int_{R_f}^{R}\rho\,\mathrm{d}\rho = \frac{1}{2}(R^2 - R_f^2).$$

Once we know this $C_f(t)$ we can differentiate to get

$$\Gamma_f(t) = \frac{\partial C_f(t)}{\partial t}.$$

If we take under consideration the number of fibers in the fabric we now can calculate the total sorption rate of the fabric as $\epsilon_f \xi_2 \Gamma_f(t)$.

In the above reasoning the $x$-dependence was left out, because of the simplification assumption that DEET and permethrin are evenly distributed on the fabric. Another assumption could be that there is an $x$-dependence because of the method used to construct the treated fabric. The active ingredient (AI) is applied on the fabric by soaking the total fabric in a bath. For multilayer coating this is done in several steps. The first bath is filled with water, the first AI to apply on the fabric and the polymer binder of this first AI. This can for example be DEET and polyacrylate. Then the fabric is squeezed, so most of the water is extruded. Next a heat treatment follows to remove the remaining water. Subsequently the fabric gets a next bath filled with water, the second AI and the polymer binder for this AI. For example the AI of the second layer can be permethrin and its polymer binder silicone elastomer. Then the fabric is again squeezed. A extra layer of just polymer without an AI can be applied for strength. Afterwards the fabric is dried. The water evaporates completely and only the separate layers with polymer binders and the AI's remain. In the drying process a crosslinking between the polymers develops, which gives extra strength to the fabric.
It is also possible to treat the yarns on a bobbin instead of the whole fabric, but the waste water cannot be disposed as easily as in the other process.
By treating the fabric it is possible that not all fibers are treated evenly. In the average coating however the measured concentration of permethrin is $1500 \text{ mg} / \text{m}^2$ of AI. This way there would be an $x$-dependence, the starting concentration could be higher on the outer sides of the fabric and lower on the inside of the fabric.

For DEET we can also consider the evaporation rate $\Gamma_{lg}$ from the fabric. We can compute this rate using the Hertz-Knudsen equation [59, 55] for condensation and evaporation (molar rate),

$$\Gamma_{lg,D} = -\frac{E}{R_f}\sqrt{\frac{(1-\epsilon)\epsilon_f}{2\pi \bar{R} M}}\left(\frac{P^\star - P_v}{\sqrt{T_s}}\right),$$

where $E$ is the evaporation coefficient, $\bar{R}$ is the universal gas constant and $T_s$ is the surface temperature. $P^\star$ is the saturation pressure, depending on time and can be determined from experimental measurements. The vapor pressure $P_v$ is given by

$$P_v = \bar{R} C_v T.$$

If we know what the evaporative flux of DEET is for one fiber, we might be able to calculate the total evaporation rate $\Gamma_f$ of the fabric as

$$\Gamma_{lg,D} = \epsilon_f \partial_r u_1(R,t) = \epsilon_f \alpha u_1(R,t),$$

where $u_1$ is defined as in section 2.2.3.

The inverse problem to solve here is what should be the initial concentration in a fabric coating on the level of the fiber so that on the level of the fabric we have the threshold concentration of $4\,\mathrm{mg}\,/\,\mathrm{m}^2$ needed to repel moquitoes. Each of the AI's used here can be substituted by any other chemical once we know the physical and chemical properties of the substance used.

If we concentrate on an open net structured fabric rather than a densely woven fabric an intermediate level is needed in the model. The yarn level is inserted the way mentioned in the previous section. The final model then consists of three levels with on each level a diffusion model to be solved that is coupled to the other two levels and where an upscaling technique is used to update the concentration of the AI from one level to another.

### 2.6.2 Analytical solution: Cauchy problem

For a scrim like structure, e.g. a treated bednet we can consider a model using the assumption that the yarns are infinitely long and the scrim is infinitely big for an observer close enough. The scrim can be visualized as a rectangular grid in 2D, with holes of width $d_W$ and height $d_H$. In 3D space we thus consider an infinite scrim in the $YZ$ plane, with an observer in $(x_0,0,0)$, see Fig. 2.24 and the Cauchy problem for $-\infty < x,y,z < +\infty$,

In 3D space we consider the Cauchy problem for $-\infty < x,y,z < +\infty$,

$$\begin{aligned}\frac{\partial C}{\partial t}(x,y,z,t) &= D_g \Delta C + \Phi(x,y,z,t) \\ &= D_g \left( \frac{\partial^2 C}{\partial x^2} + \frac{\partial^2 C}{\partial y^2} + \frac{\partial^2 C}{\partial z^2} \right) + \Phi(x,y,z,t), \end{aligned} \tag{2.18}$$

with initial condition

$$C = f(x,y,z) \quad \text{at} \quad t = 0.$$

Here the source term $\Phi(x,y,z,t)$ is the amount of AI coming out of the yarn at position $(x,y,z)$ at time $t$.

Due to symmetry, we can consider the $XY$ plane for the vertical yarns, and the $XZ$ plane for the horizontal yarn. Doing so one derivative becomes zero each time and the problem can be solved in 2D instead of 3D, i.e. separately for vertical and horizontal yarns.

For a vertical yarn at position $y = y_v$ the amount of AI at $t = 0$ is taken to be the delta function scaled with the flux coming out of a yarn cross section, denoted by $F_{y_v}(0)$. Using the symmetry we know that $C_{zz} = 0$. We then arrive at a 2D Cauchy problem of the form

$$\frac{\partial C}{\partial t}(x,y,t) = D_g \left( \frac{\partial^2 C}{\partial x^2} + \frac{\partial^2 C}{\partial y^2} \right) + \Phi(x,y,t), \quad -\infty < x,y < +\infty,$$

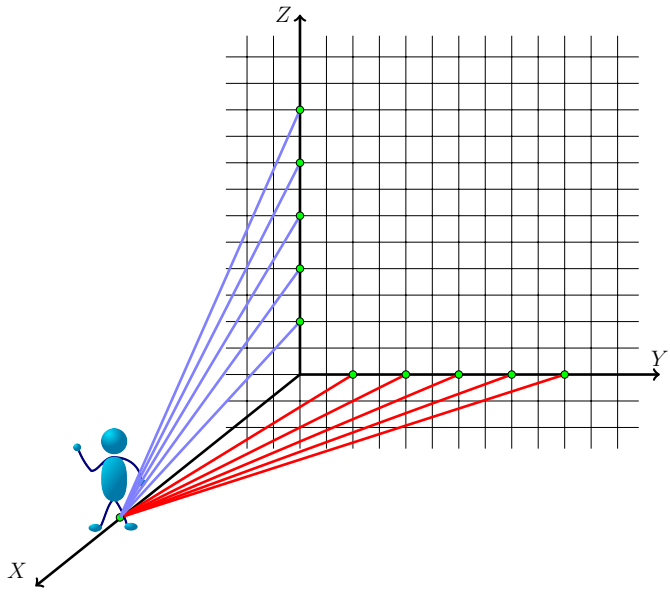


Figure 2.24: The observer at distance $x_0$ from the scrim

subject to

$$C(x,y,0) = F_{y_v}(0)\delta(x)\delta(y - y_v),$$

where $D_g$ is the diffusion coefficient of the compound in air and we assume a source at $(0,y_v)$. The source term is

$$\Phi(x,y,t) = F_{y_v}(t)\delta(x)\delta(y - y_v),$$

where $F_{y_v}(t)$ is the amount of AI coming from a cross section of the yarn at $y = y_v$ at time $t$.

For a horizontal yarn at position $z = z_h$ a similar problem and initial condition holds

$$\frac{\partial C}{\partial t}(x,z,t) = D_g \left( \frac{\partial^2 C}{\partial x^2} + \frac{\partial^2 C}{\partial z^2} \right) + \Phi(x,z,t), \quad -\infty < x,z < +\infty,$$

subject to

$$C(x,z,0) = F_{z_h}(0)\delta(x)\delta(z - z_h),$$

assuming a point source at $(0,z_h)$ and source term

$$\Phi(x,z,t) = F_{z_h}(t)\delta(x)\delta(z - z_h).$$

The solution of the general Cauchy problem for a vertical yarn is [40]

$$C_v(x,y,t) = \int_{-\infty}^{+\infty}\int_{-\infty}^{+\infty} F_{y_v}(0)\delta(\xi)\delta(\eta - y_v)G(x,y,\xi,\eta,t)\,\mathrm{d}\xi\,\mathrm{d}\eta + \int_0^t \int_{-\infty}^{+\infty}\int_{-\infty}^{+\infty} \Phi(\xi,\eta,\tau)G(x,y,\xi,\eta,t-\tau)\,\mathrm{d}\xi\,\mathrm{d}\eta\,\mathrm{d}\tau,$$

where the Green's function is

$$G(x,y,\xi,\eta,t) = \frac{1}{4\pi D_g t}\exp\left[-\frac{(x-\xi)^2+(y-\eta)^2}{4D_g t}\right].$$

Further calculations lead to

$$C_v(x,y,t) = \frac{F_{y_v}(0)}{4\pi D_g t}\exp\left[-\frac{x^2+(y-y_v)^2}{4D_g t}\right] + \int_0^t \frac{F_{y_v}(\tau)}{4\pi D_g(t-\tau)}\exp\left[-\frac{x^2+(y-y_v)^2}{4D_g(t-\tau)}\right]\mathrm{d}\tau.$$

By discretizing the past time period $[0,t]$ into N timesteps of length $\Delta t$: $[0,1\Delta t, 2\Delta t, \ldots,$
$(k-1)\Delta t, k\Delta t, \ldots, (N-1)\Delta t, t]$, we can calculate the last integral of the solution (with integrandum $I(\tau)$) as a sum

$$\int_0^{\Delta t} I(\tau)\,\mathrm{d}\tau + \int_{\Delta t}^{2\Delta t} I(\tau)\,\mathrm{d}\tau + \cdots + \int_{(k-1)\Delta t}^{k\Delta t} I(\tau)\,\mathrm{d}\tau + \cdots + \int_{(N-1)\Delta t}^{t} I(\tau)\,\mathrm{d}\tau.$$

We use the following estimation in each time interval for a given function $g(t)$

$$\int_{(k-1)\Delta t}^{k\Delta t} g(\tau)F_{y_v}(\tau)\,\mathrm{d}\tau \approx F_{y_v}(k\Delta t)\int_{(k-1)\Delta t}^{k\Delta t} g(\tau)d\tau \overset{\text{not.}}{=} F_{y_v,k\Delta t}\int_{(k-1)\Delta t}^{k\Delta t} g(\tau)d\tau,$$

so we obtain

$$\int_{(k-1)\Delta t}^{k\Delta t} I(\tau)\,\mathrm{d}\tau \approx F_{y_v,k\Delta t}\int_{(k-1)\Delta t}^{k\Delta t}\frac{1}{4\pi D_g(t-\tau)}\exp\left[-\frac{x^2+(y-y_v)^2}{4D_g(t-\tau)}\right]\mathrm{d}\tau = -\frac{F_{y_v,k\Delta t}}{4\pi D_g}\left[E_1\left(-\frac{x^2+(y-y_v)^2}{4D_g(\tau-t)}\right)\right]_{(k-1)\Delta t}^{k\Delta t},$$

where $E_1(\cdot)$ is the exponential integral function defined by

$$E_1(z) = \int_z^{+\infty}\frac{e^{-t}}{t}\,\mathrm{d}t.$$

The total solution for one vertical yarn at $y = y_v$ then is

$$C_v(x,y,t) = \frac{F_{y_v}(0)}{4\pi D_g t} \exp\left[-\frac{x^2+(y-y_v)^2}{4D_g t}\right] + \sum_{k=1}^{N} \frac{F_{y_v,k\Delta t}}{4\pi D_g}\left[E_1\left(-\frac{x^2+(y-y_v)^2}{4D_g((k-1)\Delta t - t)}\right) - E_1\left(-\frac{x^2+(y-y_v)^2}{4D_g(k\Delta t - t)}\right)\right].$$

The solution of the general Cauchy problem for a horizontal yarn is [40]

$$C(x,z,t) = \int_{-\infty}^{+\infty}\int_{-\infty}^{+\infty} F_{y_v}(0)\delta(\xi)\delta(\eta - z_h)G(x,y,\xi,\eta,t)\,\mathrm{d}\xi\,\mathrm{d}\eta + \int_0^t \int_{-\infty}^{+\infty}\int_{-\infty}^{+\infty} \Phi(\xi,\eta,\tau)G(x,z,\xi,\eta,t-\tau)\,\mathrm{d}\xi\,\mathrm{d}\eta\,\mathrm{d}\tau,$$

where

$$G(x,z,\xi,\eta,t) = \frac{1}{4\pi D_g t}\exp\left[-\frac{(x-\xi)^2+(z-\eta)^2}{4D_g t}\right],$$

and $\Phi(x,z,t)$ as given above.

Following similar calculations as for the vertical yarn we find for a horizontal yarn at $z = z_h$

$$C_h(x,z,t) = \frac{F_{z_h}(0)}{4\pi D_g t} \exp\left[-\frac{x^2+(z-z_h)^2}{4D_g t}\right] + \sum_{k=1}^{N} \frac{F_{z_h,k\Delta t}}{4\pi D_g}\left[E_1\left(-\frac{x^2+(z-z_h)^2}{4D_g((k-1)\Delta t - t)}\right) - E_1\left(-\frac{x^2+(z-z_h)^2}{4D_g(k\Delta t - t)}\right)\right].$$

We suppose that the yarns are on such distance from one another that they do not influence each other. By doing so we can take the total solution of problem (2.18) to be a superposition of the seperate solutuions for all vertical and horizontal yarns. If we take the number of vertical and horizontal yarns to be $n$ and $m$ respectively we get, with $y_v^n$ the $n$'th vertical yarn, i.e. the yarn with Cartesian equation $y = nd_W$ and $z_h^m$ the $m$'th horizontal yarn, i.e. with

Cartesian equation $z = md_H$,

$$
\begin{aligned}
&C(x,y,z,t) \\
&\quad = \sum_n C_v(x,y,t) + \sum_m C_h(x,z,t) \\
&\quad = \sum_n \left\{ \frac{F_{y_v^n}(0)}{4\pi D_g t} \exp\left( -\frac{x^2 + (y - y_v^n)^2}{4D_g t} \right) \right. \\
&\quad \left. + \sum_{k=1}^{N} \frac{F_{y_v^n,k\Delta t}}{4\pi D_g} \left[ E_1\left( -\frac{x^2 + (y - y_v^n)^2}{4D_g((k-1)\Delta t - t)} \right) - E_1\left( -\frac{x^2 + (y - y_v^n)^2}{4D_g(k\Delta t - t)} \right) \right] \right\} \\
&\quad + \sum_m \left\{ \frac{F_{z_h^m}(0)}{4\pi D_g t} \exp\left( -\frac{x^2 + (z - z_h^m)^2}{4D_g t} \right) \right. \\
&\quad \left. + \sum_{k=1}^{N} \frac{F_{z_h^m,k\Delta t}}{4\pi D_g} \left[ E_1\left( -\frac{x^2 + (z - z_h^m)^2}{4D_g((k-1)\Delta t - t)} \right) - E_1\left( -\frac{x^2 + (z - z_h^m)^2}{4D_g(k\Delta t - t)} \right) \right] \right\}.
\end{aligned}
$$

For an observer at position $(x_0,0,0)$ the amount of observed AI coming out of the scrim will be, with $V$ and $H$ the set of all vertical and horizontal yarns, resp.,

$$
\begin{aligned}
&C(x_0,0,0,t) \\
&\quad = \frac{1}{4\pi D_g} \sum_{n=-\infty}^{+\infty} \left\{ \frac{F_{nd_W}(0)}{t} \exp\left( -\frac{r_{v,n}^2}{4D_g t} \right) \right. \\
&\quad \left. + \sum_{k=1}^{N} F_{nd_W,k\Delta t} \left[ E_1\left( -\frac{r_{v,n}^2}{4D_g((k-1)\Delta t - t)} \right) - E_1\left( -\frac{r_{v,n}^2}{4D_g(k\Delta t - t)} \right) \right] \right\} \\
&\quad + \frac{1}{4\pi D_g} \sum_{m=-\infty}^{+\infty} \left\{ \frac{F_{md_H}(0)}{t} \exp\left( -\frac{r_{h,m}^2}{4D_g t} \right) \right. \\
&\quad \left. + \sum_{k=1}^{N} F_{md_H,k\Delta t} \left[ E_1\left( -\frac{r_{h,m}^2}{4D_g((k-1)\Delta t - t)} \right) - E_1\left( -\frac{r_{h,m}^2}{4D_g(k\Delta t - t)} \right) \right] \right\},
\end{aligned}
$$

which leads to

$$C(x_0,0,0,t) = \frac{1}{4\pi D_g} \sum_{n=-\infty}^{+\infty} \left\{ \frac{F_{nd_W}(0)}{t} \exp\left(-\frac{r_{v,n}^2}{4D_g t}\right) + \sum_{k=1}^{N} F_{nd_W,k\Delta t} \int_{\frac{r_{v,n}^2}{4D_g((k-1)\Delta t - t)}}^{\frac{r_{v,n}^2}{4D_g(k\Delta t - t)}} \frac{e^{-u}}{u} du \right\}$$
$$+ \frac{1}{4\pi D_g} \sum_{m=-\infty}^{+\infty} \left\{ \frac{F_{md_H}(0)}{t} \exp\left(-\frac{r_{h,m}^2}{4D_g t}\right) + \sum_{k=1}^{N} F_{md_H,k\Delta t} \int_{\frac{r_{h,m}^2}{4D_g((k-1)\Delta t - t)}}^{\frac{r_{h,m}^2}{4D_g(k\Delta t - t)}} \frac{e^{-u}}{u} du \right\},$$

where $r_{v,n}^2 = x_0^2 + n^2 d_W^2$ and $r_{h,m}^2 = x_0^2 + m^2 d_H^2$ are the shortest distances to the yarn in question, and where we used $y_v^n = nd_W$ and $z_h^m = md_H$.

If the horizontal en vertical yarns are of the same type this further simplifies to

$$C(x_0,0,0,t) = \frac{1}{4\pi D_g} \sum_{n=-\infty}^{+\infty} \left\{ \frac{F_y(0)}{t} \exp\left(-\frac{r_{v,n}^2}{4D_g t}\right) + \sum_{k=1}^{N} F_{y,k\Delta t} \int_{\frac{r_{v,n}^2}{4D_g((k-1)\Delta t - t)}}^{\frac{r_{v,n}^2}{4D_g(k\Delta t - t)}} \frac{e^{-u}}{u} du \right\}$$
$$+ \frac{1}{4\pi D_g} \sum_{m=-\infty}^{+\infty} \left\{ \frac{F_y(0)}{t} \exp\left(-\frac{r_{h,m}^2}{4D_g t}\right) + \sum_{k=1}^{N} F_{y,k\Delta t} \int_{\frac{r_{h,m}^2}{4D_g((k-1)\Delta t - t)}}^{\frac{r_{h,m}^2}{4D_g(k\Delta t - t)}} \frac{e^{-u}}{u} du \right\},$$

since the amount coming from a yarn is the same in each direction and at each position.

### 2.6.3 Numerical solution: Domain decomposition method

In the previous approach an analytical solution was given for the macro-level model based on solving a Cauchy problem. Implementing these analytical solutions though was unstable due to the need to cut-off the infinite series arising in them. So a numerical analysis was asserted. This numerical method is the overlapping domain decomposition method. As indicated in section 2.5, we use an overlap zone to upscale from the meso-level to the fabric level.

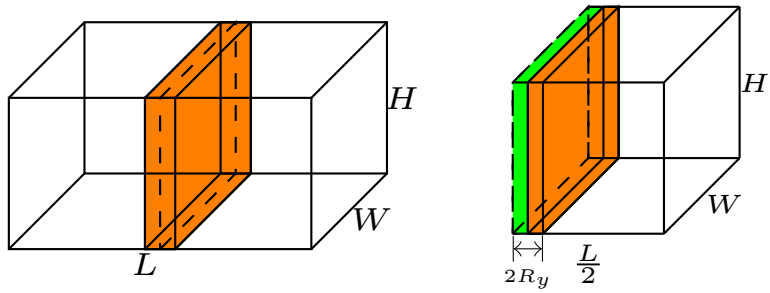


(a) 3D room with scrim hanging in the middle

(b) Scrim and overlap zone, half of the 3D room

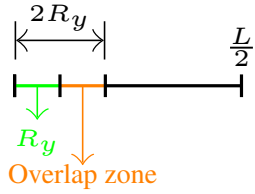


(c) 1D domain for fabric modeling

Figure 2.25: Simplification from a 3D room to a 1D domain for fabric modeling via ODD

Here a room with dimensions $L \times W \times H$ is modelled with a net hanging in the middle of the room, so at $\frac{L}{2}$, see Fig. 2.25. This can be reduced to a 1D model. The domain under consideration is the interval $[0, \frac{L}{2}]$. The yarn in the net is modelled as a 1D cylindrical object over an extended domain $[0,2R_y]$ with two *no flux*-BC's $\partial_r C_y(0,t) = 0$ and $\partial_r C_y(2R_y,t) = 0$, the way mentioned in section 2.5. The mass coming from the yarn is going to the surrounding

air of the yarn into the overlap zone $[R_y, 2R_y]$. The room model on its turn runs over $[R_y, \frac{L}{2}]$, again with *no flux*-BC's $\partial_x C\,(R_y,t) = 0$ and $\partial_x C\,\left(\frac{L}{2},t\right) = 0$, because no AI is leaving the room. The calculations made only serve for one side of the net, but due to symmetry the other site behaves in the same way, so we can predict the outcome for the whole room domain $[0,L]$.

The room 1D diffusion equation is

$$\partial_t C = \partial_x(D\partial_x C) + \Gamma_s(x,t),$$

with $D$ the diffusion of the AI in air and $\Gamma_s(x,t)$ the concentration per time unit added/removed at $x$. To solve this differential equation the domain $[0, \frac{L}{2}]$ is divided into smaller intervals of length $\Delta x$ and integrating over one cell gives

$$\partial_t C_i = \frac{\text{flux}_{\text{edge}_{i+1}} - \text{flux}_{\text{edge}_i}}{\Delta x_i} + \Gamma_s(\Delta x_i),$$

where $\Gamma_s(\Delta x_i)$ is the concentration per time unit added to or removed from the interval $[x_i,x_{i+1}]$ and the fluxes are obtained via MOL.

We situate the overlap zone in the first cell for integration so there the source term is corresponding to the amount of AI coming out of the yarns.

Now the yarn and fabric models will be solved alternately per time step, using the outcome of one model as the source term for the other model.

Per time step $t_j$ the overlapping domain decomposition method exists of three steps:

1. We solve the 1D yarn model, calculate the mass coming out of one yarn using the above meso-level model with the sink term $\Gamma_{\text{out}}(t_{j-1},\Omega_o)$ of the previous time step and calculate the corresponding concentration by dividing by the volume of a yarn cross-section $\pi R_y^2$.

2. We solve the room model to obtain a new concentration value near a yarn. For this model we use the mass released by one yarn to the overlap zone in the first step which needs to be upscaled to a concentration source per second per $\text{mm}^3$ for all yarns in the scrim. To upscale we need to calculate how many yarns are present in the scrim. Because we model only half the room eventually everything should be multiplied by 2.

3. For the next time step, due to domain overlap, the BC is now homogeneous Neumann always. Then, we need to set a correct $\Gamma_{\text{out}}(t_j,\Omega_o)$ on the yarn level, so we need to downscale the mass calculated from the room model in this time step to keep mass balance. The sink term $\Gamma_{\text{out}}(t_j,\Omega_o)$ for the yarn model is what was present in the overlap zone, so being the mass removed from the yarns, approximated from the concentration given by the solved room model, downscaled to one yarn and again using a factor 2 as we model only half the room.

## 2.7 The total three step model and discussion

On each time step one complete three step model is solved. Beginning with the fiber level with all initial conditions and boundary concentrations set to zero. Afterwards a yarn model is solved over a domain $[0,2R_y]$, including an overlap zone, with an upscaled source term $\Gamma_{\text{in}}$ calculated via volume averaging of the fiber results, a sink term $\Gamma_{\text{out}}(t,\Omega_o) = 0$ and with a homogeneous Neumann BC. Next a fabric model is solved over a domain $[R_y, \frac{L}{2}]$ using a source term $\Gamma_s$ calculated from the upscaled yarn results in the overlap zone. In the next time step we again begin by solving a fiber model, but now with adjusted initial conditions en boundary concentrations, afterwards a yarn level model and a fabric level model, and so on.

For the numerical scheme of the algorithm we make the distinction between the radial coordinate of the fiber level, $\rho_i$, $1 \leq i \leq I$ and that of the yarn level, $r_k$, $1 \leq k \leq K$.

In time step $t_1$ we use the initial conditions and first solve the fiber system:

$$\begin{cases} \partial_t C_f(\rho,r,t)|_{\rho=\rho_i,r=r_k,t=t_1} &= \frac{1}{\rho_i}\partial_\rho \left(\rho D_f \partial_\rho C_f(\rho,r,t)\right)|_{\rho=\rho_i,r=r_k,t=t_1} \\ C_f(\rho_i,r_k,t_0) &= C_{\text{init}}(r_k) \\ D_f\partial_\rho C_f(R,r_k,t_1) &= 0 \\ D_f\partial_\rho C_f(R_f,r_k,t_1) &= -S_f h_{b\to f} C_f(R_f,r_k,t_0) \end{cases},$$

where per $r_k$ index $i$ runs from 1 to $l$, to get $C_f(\rho_i,r_k,t_1)$, $1 \leq i \leq I$, and $1 \leq k \leq K$. $C_{\text{init}}$ is the initial concentration of AI applied in the fiber coating during fabrication.

Then we solve the yarn system:

$$\begin{cases} \epsilon\, \partial_t C_y(r,t)|_{r=r_k,t=t_1} &= \frac{1}{r_k}\partial_{r'}\left(\epsilon r \frac{D_y}{\tau_y}\partial_r C_y(r,t)\right)\Big|_{r=r_k,t=t_1} + \Gamma_{\text{in}}(r_k,t_1) \\ C_y(r_k,t_0) &= 0 \\ \partial_r C_y(0,t_1) &= 0 \\ \partial_r C_y(R_y,t_1) &= 0 \end{cases},$$

to get $C_y(r_k,t_1)$, for $1 \leq k \leq K$.

Then we solve the fabric system:

$$\begin{cases} \partial_t C(x,t)|_{x=x_l,t=t_1} &= \partial_x \left(D\partial_x C(x,t)\right)|_{x=x_l,t=t_1} + \Gamma_s(\Delta x_l,t_1) \\ C(x_l,t_0) &= 0 \\ \partial_x C(R_y,t_1) &= 0 \\ \partial_x C\left(\frac{L}{2},t_1\right) &= 0 \\ \Gamma_s(\Delta x_1,t_1) &= \text{upscaled change in } C_y(t_1,\Omega_o) \end{cases},$$

to get $C(x_l,t_1)$ for $1 \leq l \leq L$.

For the next time steps $t_j$, $2 \leq j \leq J$ the three systems are per time step:

$$\begin{cases} \partial_t C_f(\rho,r,t)|_{\rho=\rho_i,r=r_k,t=t_j} &= \frac{1}{\rho_i}\partial_\rho \left(\rho D_f \partial_\rho C_f(\rho,r,t)\right)|_{\rho=\rho_i,r=r_k,t=t_j} \\ D_f \partial_\rho C_f(R,r_k,t_j) &= 0 \\ D_f \partial_\rho C_f(R_f,r_k,t_j) &= -S_f h_{b\to f}\left(C_f(R_f,r_k,t_{j-1}) - C_y(r_k,t_{j-1})\right) \\ & \quad \cdot \mathcal{H}\left(C_f(R_f,r_k,t_{j-1}) - C_b, C^*(T) - C_y(r_k,t_{j-1})\right) \end{cases},$$

where per $r_k$ index $i$ runs from 1 to $l$, to get $C_f(\rho_i,r_k,t_j)$, $1 \leq i \leq I$, and $1 \leq k \leq K$.

$$\begin{cases} \epsilon\, \partial_t C_y(r,t)|_{r=r_k,t=t_j} &= \frac{1}{r_k}\partial_r \left(\epsilon r \frac{D_y}{\tau_y}\partial_r C_y(r,t)\right)\Big|_{r=r_k,t=t_j} \\ & \quad + \Gamma_{\text{in}}(r_k,t_j) - \Gamma_{\text{out}}(t_{j-1}), \\ \partial_r C_y(0,t_j) &= 0 \\ \partial_r C_y(2R_y,t_j) &= 0 \\ \Gamma_{\text{out}}(t_{j-1}) &= \text{downscaled change in } C(t_{j-1},\Omega_o) \end{cases},$$

to get $C_y(r_k,t_j)$, for $1 \leq k \leq K$.

$$\begin{cases} \partial_t C(x,t)|_{x=x_l,t=t_j} &= \partial_x \left(D\partial_x C(x,t)\right)|_{x=x_l,t=t_j} + \Gamma_s(\Delta x_l,t_j) \\ \partial_x C(R_y,t_j) &= 0 \\ \partial_x C(\frac{L}{2},t_j) &= 0 \\ \Gamma_s(\Delta x_1,t_j) &= \text{upscaled change in } C_y(t_j,\Omega_o) \end{cases},$$

to get $C(x_l,t_j)$ for $1 \leq l \leq L$.

If we know $C(x_l,t_j)$ for all $0 \leq l \leq L$ and $0 \leq j \leq J$ we can study the concentration of AI in the air at a certain distance from the scrim.

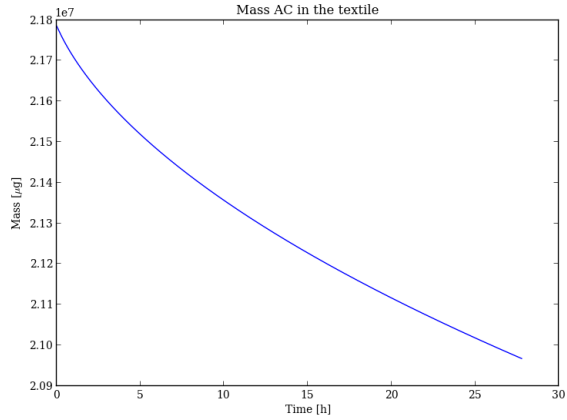


(a) Mass of the AI in the bed net

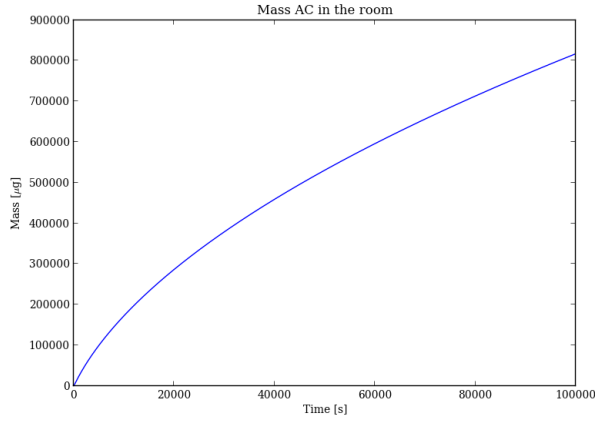


(b) Mass of the AI in the room

Figure 2.26: Mass of DEET diffusing to the outside from a polymer coating on a fiber in a room with standard dimensions

When simulating a closed room of length $5\,\mathrm{m}$, width $3\,\mathrm{m}$ and height $2.1\,\mathrm{m}$ for $100000\,\mathrm{s}$ and starting from an initial concentration of $0.9 \cdot 10^3 \frac{\mu\mathrm{g}}{\mathrm{mm}^3}$ for the AI DEET captured in one polymer coating on a cotton scrim placed in the middle of the room we get the following results, presented in Figs. 2.26 and 2.27.

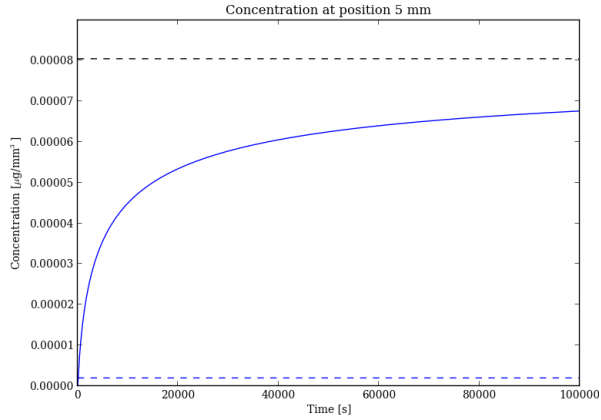


(a) Concentration of AI at 5mm from the scrim

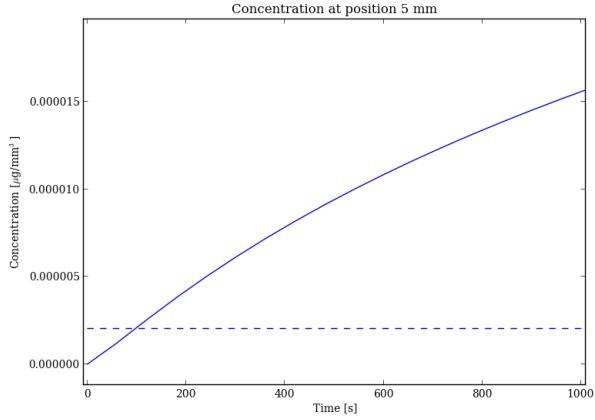


(b) Concentration of AI at 5mm from the scrim in the first 1000 seconds

Figure 2.27: Concentration of DEET diffusing to the outside from a polymer coating on a fiber in a room with standard dimensions at 5 mm and 500 mm from the scrim

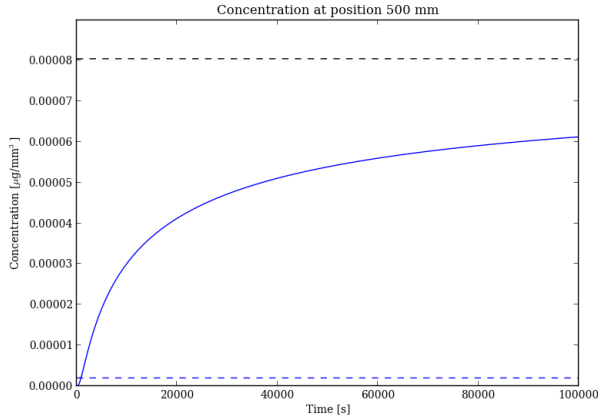


(c) Concentration of AI at 500mm from the scrim

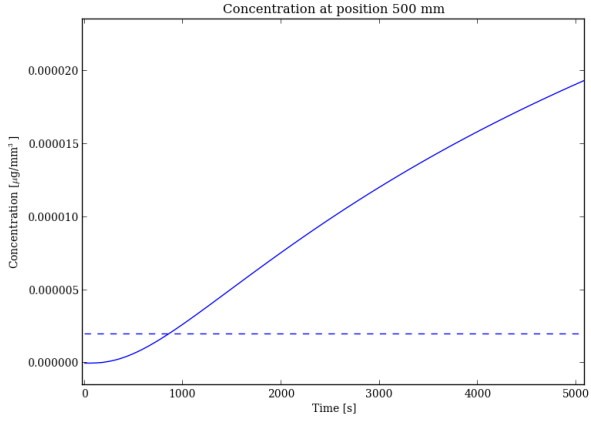


(d) Concentration of AI at 500mm from the scrim in the first 5000 seconds

Figure 2.27: Concentration of DEET diffusing to the outside from a polymer coating on a fiber in a room with standard dimensions at 5 mm and 500 mm from the scrim (continued)

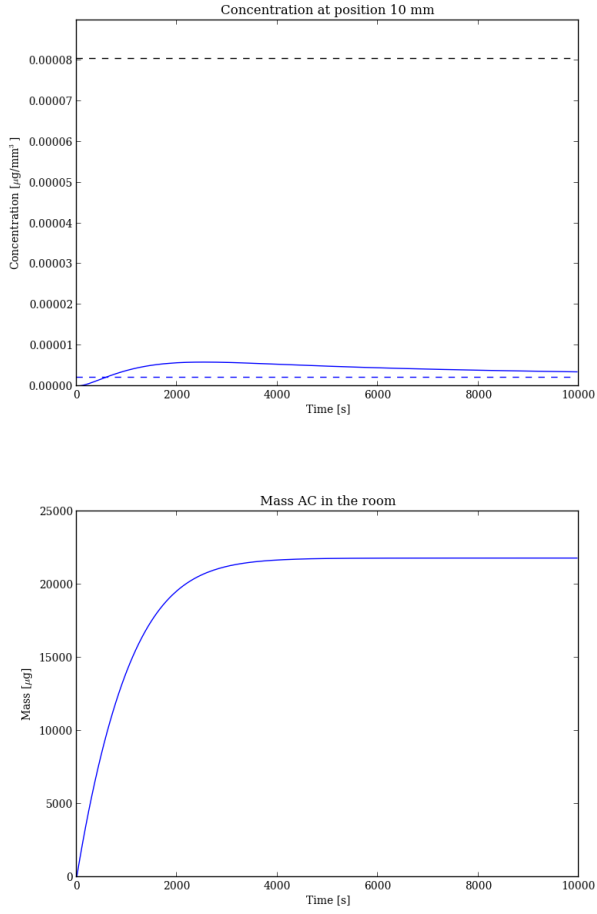


Figure 2.28: The concentration and mass in the room stays constant after the AI in the fiber coating is depleted

The mass of the AI in the scrim is dropping down, in the room it is increasing. First the AI is diffusing to the surface of the polymer coating around the fibers. Once the concentration in this coating is depleted the AI is diffusing to the surrounding air until no mass is coming from the fibers any longer. Since no ventilation is allowed concentration should go to a constant value or the saturation concentration should be reached after a certain time. For the application in mind the concentration is not yet depleted after $100000$ s. For illustrative purposes we have used a much smaller initial concentration and a higher evaporation coefficient (which is not in accordance with the application)

to visualise this effect in Fig. 2.28.

By construction of our algorithm, the total mass remains constant during simulation. The concentration at the given different positions (5mm, 500mm) in the room increases and exceeds the threshold concentration for repellency represented by the lower dashed line quickly enough to satisfy required standards. The higher dashed line represents the saturation concentration for the AI used in the simulation.

## 2.8 STICK-toolbox

The three scale model of the previous section was implemented in python code. The toolbox was named STICK, *Sophisticated Textile Information Computing Kit* and is available at `https://github.com/tinegoessens/stickproject`. To be able to run the stick.py code the following must be installed:

1. a terminal from which the code is run;
2. the latest Python distribution available at `https://www.python.org/`;
3. the mathematical packages:
   (a) Numpy: a fundamental package for scientific computing with Python. It contains, among other things, a powerful $n$-dimensional array object, sophisticated (broadcasting) functions, tools for integrating C/C++ and Fortran code, useful linear algebra, Fourier transform, and random number capabilities;
   (b) Scipy: a library that contains modules for optimization, linear algebra, integration, interpolation, special functions, FFT, signal and image processing, ODE solvers and other tasks common in science and engineering;
   (c) Fipy: an object oriented, PDE solver, written in python, based on a standard finite volume approach;
   (d) Pysparse: a fast sparse matrix library for Python. It provides several sparse matrix storage formats and conversion methods. It also implements a number of iterative solvers, preconditioners, and interfaces to efficient factorization packages;
   (e) scikits.odes: a module with ordinary differential equation and differential algebraic equation solvers that can be found on `https://github.com/bmcage/odes`;
4. a plotting environment, e.g. matplotlib.

To run the STICK code one needs to make initial files (inifile) containing all information on the textile under consideration. An inifile should be made for each level of the model, one for the fiber, one for the yarn and one with the external room conditions where the textile product is present. For the fiber the inifile contains the characteristics of the fiber used, e.g. Fig. 2.29. The yarn inifiles contains the characteristics of the yarn in question and points to the fiber inifile(s) of the fibers building up the yarn. The fabric inifile contains the fabric's and the room's characteristics and points to the yarn inifile of the yarns building up the total fabric.

**/defaultfiber.ini**

```
[general]
;; following solution methods and submethods are possible:
;; FVM : finite volume method based discretization method of
;;   --> odew, odew_step : solve via method of lines ode solver using substition
;;        w=ur (stepwise plotting)
;;   --> odeu : solve via method of lines ode solver WITHOUT substition w=ur
;;   --> fipy : solve via fipy
;;   --> cvode, cvode_step: solve via method of lines cvode solver (stepwise plotting)
;; SIMPLE: A constant mass approximation: dM/dt = - flux_surface
;;   --> standard
;;method='FVM'
;;submethod='odew_step'
method = 'FVM'
submethod = 'cvode_step'
read = False
verbose = False

[fiber]
radius_pure_fiber = 0.01 ;; in mm
form = 'circle'
nrlayers = 2
;;total number of coating layers in the domain
internal_diffusion = False
;; diffusion in the fiber section itself or not
therm_cond_K = 0.1
;;conductivity of the fiber in W / (m K)
spec_heat_c = 1.17e-3
;;Volumetric Specific heat of the fiber J/(mm^3 K)
density = 1.55
water_absorbed_rel_dens = 0.1
;; Water content absorbed by fiber relative to fiber density in
;; [-] =[kg/m^3] / [kg/m^3], eg 0.1 for viscose at 60% relative humidity
n_edge = 21
;;discretization points in the fiber cross section domain
porosity_in = 0.2
mean_deviation = 0.00074

[fiberlayer_0]
n_edge = 21
;; nr discretization points
thickness = 0.00085
;; thickness of the layer
diffusion_coef = 5.2e-7
porosity_layer = 1.
diffusion_polymer_exp_factor = 0.3
init_conc = 'lambda x: 0.90'
porosity_layer = 1.0
```

In each of the inifiles a choice can be made for the used numerical method. For the fiber model it is possible to choose from the FVM, including the Finite Volume Method both with or without substitution of $ur = w$ as mentioned in section 2.2 making it possible to compare both in cpu-time and efficiency, with the built-in FVM solver of Fipy or with the method of lines solver cvode. Next it is possible to choose for the option SIMPLE, made possible for testing the

```
48
49 [fiberlayer_1]
50 n_edge = 6
51 ;; nr discretization points
52 thickness = 0.00085
53 ;; thickness of the layer
54 diffusion_coef = 7.2e-7
55 porosity_layer = 1.
56 diffusion_polymer_exp_factor = 0.3
57 init_conc = 'lambda x: 0.0'
58
59
60 [boundary]
61 type_left = 'flux'
62 type_right = 'evaporation'
63 ;;type_right = 'flux, transfer, evaporation'
64 boundary_fib_left = 0.0
65 ;;the boundary flux left of the fiber - 1D domain,
66 ;;-D &C/&x = boundary_fib_left, meaning, flux in is this
67 boundary_fib_right = 0.0
68 ;;then boundary flux right of the fiber - 1D domain
69 ;; D &C/&x = boundary_fib_right, meaning, flux out is this
70 transfer_right =  5.0e-10
71 ;;DEET mass transfer coefficient on the surface of fiber(MT-1)
72 ;;then boundary flux right of the fiber - 1D domain
73 ;;D &C/&x = transfer_right C
74 evap_satconc = 'lambda T: 0.04'
75 evap_transfer = 5.0e-5
76 evap_minbound = 0.
77 out_conc = 'lambda t, data: 0.'
78
79 [time]
80 time_period = 600.
81 ;;the time domain for the simulation (s)
82 dt = 1.
83 ;;time step
84
85 [plot]
86 plotevery = 1
87
```

Figure 2.29: Initial fiber file containing all fiber characteristic as input for the STICK toolbox

code using a simple constant mass approximation.
If different time periods are given in each of the inifiles the time-period is set to that of the fabric. For the yarn model it is possible to make a blend consisting of more than one type of fiber by pointing to each of the inifiles of the fibers in the blend. In fact every part registers the defaults for it's settings by inheriting a custom written ConfigManager, see Fig. 2.32. A configuration file hence acts as a datastore of the user settings which is accessible everywhere via a singleton type implementation: e.g. `config.get('fiber.radius_pure_fiber')`.
The code is run through a terminal (no user interface was made, due to time restraints and little programming skills) using the inifiles as input: e.g.

`python stick.py fiber1d -i ~/defaultfiber.ini,`
`python stick.py yarn2d -i ~/defaultyarn.ini,`
`python stick.py room -i ~/defaultfabric.ini.`

The model one wants to run can be passed on the command line after calling the stick.py program. One of the possibilities is `fiber1d` modeling the fiber as in section 2.2. Using `yarn1d` or `yarn2d` depending on the requirement, a

**/defaultyarn.ini**

```
[general]
;; following solution methods and submethods are possible:
;; FVM : finite volume method based discretization method of
;;    --> fipy : fipy finite volume method
method = 'FVM'
submethod = 'fipy'
read = False
verbose = True

[domain]
fiberlayout_method = 'virtlocoverlap'
;; method to use to determine fiber position in yarn
;; choose from random, virtloc, virtlocoverlap
distribute_fiber = 'integral'
cellsize_centre = 1.0e-1
;;preferred edge length of each mesh for yarn
cellsize_fiber = 2.50e-2
;;preferred edge length of each mesh for fiber
yarnradius = 1.0
;;radius of yarn domain
n_edge = 10
theta_value = 0.05
beta_value = 0.1

[fiber]
number_type = 2
number_fiber = 144
;;number of fibers in the yarn
blend = [51.4, 48.6]
eps_value = 0.001
;;radius_fiber = [0.052]
radius_fiber = [0.055, 0.0052]
fiber_config = ['../fiber/defaultfiber.ini', '../fiber/defaultfiber2.ini']
prob_area = '[lambda r: 0.0178 * (0.360 * r**4  -3.397 * r ** 3 + 4.531 * r ** 2 ..'
            '..- 1.979 * r + 0.496), lambda r: 0.0241 * (-1.061 * r ** 4 ..'
            '.. + 0.397 * r ** 3 + 0.606 * r ** 2 - 0.093* r + 0.152)]'

[initial]
init_conc2d = 'lambda x, y: 0.'
init_conc1d = 'lambda x: 0.'
;;initial concentration DEET

[yarn]
tortuosity = 1.
;; tortuosity of a yarn

[diffusion]
diffusion_coeff = 25
;;diffusion coefficient of DEET in the void space

[boundary]
type_right = 'transfer'
;;'diff_flux'
conc_out = 0.
D_out = 25
;; typical: 2.5e-5 m**2/s, here in mm
dist_conc_out = 0.1
transfer_coef = 5.3e-9
;;DEET mass transfer coefficient on the surface of yarn(MT-1)
;;then boundary flux right of the yarn ~ 1D domain D &C/&x = -transfer_coef C

[time]
time_period = 5000.
;;the time domain for the simulation (s)
dt = 5.
;;time step

[plot]
maxval = 0.0005
plotevery = 10
writeevery = 5
```

Figure 2.30: Initial yarn file containing all fiber and yarn characteristic as input for the STICK toolbox

yarn can be modelled as a one-dimensional radial model as in section 2.3, or a two-dimensional model with a specific yarn-fiber layout as in 2.4. Furthermore there are the options `fiberfabric` where the mesolevel is neglected, and

**/defaultfabric.ini**

```
[general]
;; following solution methods and submethods are possible:
;; FVM : finite volume method based discretization method of
;;   --> cvode : solve via method of lines cvode solver
method = 'FVM'
submethod = 'cvode'
read = False
verbose = False

[observer]
#a few possible x_positions of the observer
x0 = [5, 10, 500, 1000]

[domain]
nr_vert_yarns = 50
nr_hor_yarns= 100
domain_size = [5e-2, 1.5e-1]
;;the whole domain size - width, length
dx = 1.21
;;distance between yarns in x direction in mm
dy = 2.21
;;distance between yarns in y direction in mm

[sample]
yarn_config = ['../yarn/defaultyarn.ini']

[diffusion]
diff_coef = 25
;;diffusion coefficient in air in mm²/s
tortuosity_fab = 2.
;;tortusity value in fabric void space

[active_component]
saturation_conc = 5.589e-5
treshold_effect = 2e-6

[initial]
init_conc = 0.0
init_void = 0.0

[plot]
maxval = 0.0005
plotevery = 100
writeevery = 100
extra_time_room = 'r.|[0,100, 200]|[0,1e-6, 2e-6]'

[time]
time_period = 500
;;s
dt = 0.1
```

Figure 2.31: Initial fabric file containing all fabric, yarn and fiber characteristic as input for the STICK toolbox

`bednet` modeling a room containing a complete fabric with a open structure and exhibiting some environmental conditions as in 2.6.

```
class FiberIdConfigManager(ConfigManager):

    __instance = {}

    def get_instance(inifile):
        """ Use this function to get the instance of the ConfigManager
        that will work on inifile
        """
        if not (inifile in FiberIdConfigManager.__instance):
            FiberIdConfigManager.__instance[inifile] = None # Set for __init__()
            FiberIdConfigManager.__instance[inifile] = FiberIdConfigManager(inifile)
        return FiberIdConfigManager.__instance[inifile]
    get_instance = staticmethod(get_instance)

    def __init__(self, filename = INIFILE_DEFAULT):
        """
        A singleton implementation of config.ConfigManager
        """
        if filename not in FiberIdConfigManager.__instance:
            raise Exception("This class is a singleton per filename. "
                            "Use the get_instance() method")
        ConfigManager.__init__(self, filename)

    def register_defaults(self):
        """default ini settings for a fiberid problem"""
        self.register("general.read", False)
        self.register("general.verbose", False)
        self.register("general.method", 'FVM')
        self.register("general.submethod", 'odew')
        self.register("general.fiber_kind", 'polyester')
```

Figure 2.32: Part of the ConfigManager for the fiber

CHAPTER 3

# Validation of the model with experimental data and field testing

## 3.1 Validation of the model with experimental data

In collaboration with the Department of Organic Chemistry of Ghent University some experimental test were done on the coated fabrics delivered by one of the textile companies. A headspace analysis and a liquid extraction was carried out to determine the release rate of DEET from the fabric, the saturated DEET concentration in the air and the amount of AI on the fabric. These tests can be used to estimate the real life values needed in the models discussed above and a simulation of the release can be done and compared with the test results to check for the correct behavior of the models. Firstly we will itemize some facts about the textile substrate under consideration in the NOBUG project.

### 3.1.1 Textile properties, fact sheets

To make clear which product we are mathematical modeling we will first summarize some properties of the used treated textile as provided by Utexbel N.V., one of the research partners in the NO BUG Consortium and the Organic Chemistry and Textile Department of Ghent University.

- **Cotton**
  Cotton is a vegetable fiber obtained from the cotton plant. In one seed of

the plant there have developed an average of 4000 fibers. For manufacturing yarns and fabrics, $7/8'' - 11/4''$ or $2.22 - 3.18\,\mathrm{cm}$ is the standard fiber length. Cotton fibers are spun then woven or knitted into fabrics such as velvet, corduroy, chambray, velour, jersey and flannel.
The cotton fiber has a weight of $1.67$ decitex, that is $0.167$ tex, where $1$ tex is $1\ \mathrm{mg}\,/\,\mathrm{m}$. This means that 1 meter of cotton fiber weighs $0.167\ \mathrm{mg}$.
The radius of a cotton fiber is estimated at $11$ à $15\ \mu\mathrm{m}$. Optical measurements of samples were carried out by the lab of the Textile Department of Ghent University leading to the result of $11.7\,\mu\mathrm{m}$.
For a spun yarn we assume it to be perfectly even, i.e. we need two conditions, see Fig. 3.1:

1. The constituent fibers are uniform in thickness;
2. The yarn has the same number of fibers in all cross sections along its length.

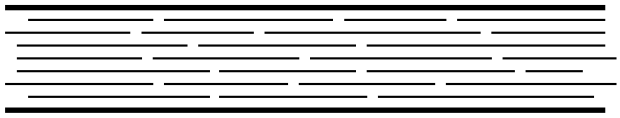

Figure 3.1: perfectly even yarn build out of fibers

Since we know the weight of $1\,\mathrm{m}$ of both the fiber and yarn, we are able to calculate the number of fibers in a yarn cross section

$$\begin{aligned}\text{Number of fibers/yarn cross section} = N &= \frac{\text{weight } 1\,\mathrm{m} \text{ yarn}}{\text{weight } 1\,\mathrm{m} \text{ fiber}} \\ &= \frac{30\,\mathrm{mg}}{0.167\,\mathrm{mg}} = 179.6.\end{aligned}$$

The porosity is defined as the fraction of void space in a porous medium. Once we know the diameter of a yarn, see table 3.1, we can calculate the porosity of a cotton yarn from the diameter of a fiber and the number of fibers per yarn as

$$\text{Porosity} = 1 - \frac{d_{\text{yarn}}}{N \cdot d_{\text{fiber}}} = 0{,}9584,$$

where we've used the mean diameter.

The cotton fiber and the cotton yarn are not cylindrical but look like a twisted noodle.

Cotton absorbs water. The regain of cotton at $65\%$ relative humidity (RH) at $20°$C is 6 to $7\%$, and It can absorb approximately $20$ percent of its own weight of water at $100\%$ RH [1].

Table 3.1: Cotton fact sheet

| Structure | Parameter | Estimation | Unit |
|---|---|---|---|
| Fiber | weight | $1.67$ | $\mathrm{dtex}$ |
| | radius | $18.3$ (long axis) | $\mu\mathrm{m}$ |
| | | $9.8$ (short axis) | |
| | length | $2.2 - 3.2$ | $\mathrm{cm}$ |
| | density | $1.55$ | $\mathrm{mg\,/\,mm^3}$ |
| Yarn | weight | $30$ | $\mathrm{tex}$ |
| | diameter | $210$ | $\mu\mathrm{m}$ |

- **Polyester**
  Polyester is a synthetic fiber derived from coal, air, water, and petroleum. Developed in a 20th-century laboratory, polyester fibers are formed from a chemical reaction between an acid and alcohol. In this reaction, two or more molecules combine to make a large molecule whose structure repeats throughout its length. Polyester fibers can form very long molecules that are very stable and strong.
  The polyester fiber has a weight of $1.5$ decitex. The weight of a polyester yarn is approximately $20$ tex. Once we know the number of fibers per yarn and the diameter of a yarn and a fiber, we can calculate the porosity of a polyester yarn in a similar way as for the cotton yarn

$$\text{Porosity} = 1 - \frac{d_{\text{yarn}}}{N \cdot d_{\text{fiber}}} = 1 - \frac{d_{\text{yarn}}}{133.3 \cdot d_{\text{fiber}}} = 0{,}9213 \text{ á } 0{,}9314.$$

  Polyester does not absorb water and it is perfectly cylindrical.

- **Blend fabric**
  The combination cotton/polyester yarn is made by Utexbel in different percentages of both types, with every time the same weight of $30$ tex. If you have for example a $50\%/50\%$ sample you have $15$ tex of polyester and $15$ tex of cotton. This means you need more polyester fibers in the yarn because of the lower weight of polyester to get the same weight of

[1] FYI: Viscose can absorb to 30 % of its own weight.

| Table 3.2: Polyester fact sheet | | | |
|---|---|---|---|
| Structure | Parameter | Estimation | Unit |
| Fiber | weight | $1.5$ | $\mathrm{dtex}$ |
| | radius | $12.2 - 14$ | $\mu\mathrm{m}$ |
| | density | $1.38$ | $\mathrm{mg}\,/\,\mathrm{mm}^3$ |
| Yarn | weight | $20$ | $\mathrm{tex}$ |
| | diameter | $256$ | $\mu\mathrm{m}$ |

$15$ tex as compared to the cotton fibers. A consequence of this is that the diameter of the yarn wil be bigger compared to a sample of cotton yarn of $30$ tex. The two most common blends are $65\%$ of cotton combined with $35\%$ of polyester fiber for a normal wearable fabric and $47{,}3\%$ of cotton and $52{,}7\%$ of polyester for a net structure.
The combination yarn also absorbs water.

The blended fabric for the net is constructed out of yarns in a twisted/single configuration (see Fig. 3.2):

- 2 “superyarns" (see Fig. 3.2(b)), each consisting of the 2 twisted yarns in one direction (the weft);
- 1 superyarn, in the weft direction;
- again 2 superyarns in the weft direction;
- etc.
- 2 superyarns in the other direction (the warp);
- 1 superyarnin the warp direction;
- again 2 superyarns in the warp direction;
- etc.

A twisted yarn contains 2 yarns (one of each kind) of each 15 tex for a total weight of 30 tex.

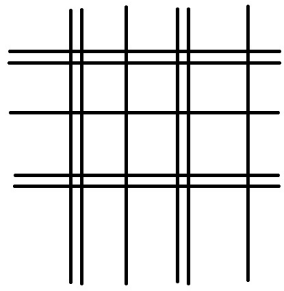

(a) The net configuration

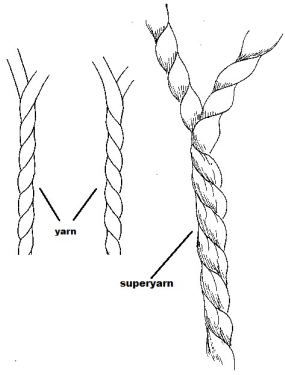


(b) A superyarn consisting of 2 twisted yarns

Figure 3.2: Twisted/single configuration of the net

This twisted-single configuration is used because otherwise the holes in a net would be that big that the yarns would move. The detail of an intersection looks like Fig. 3.3.

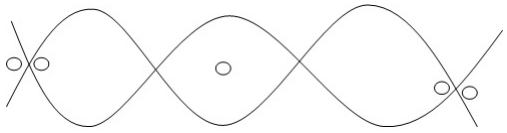

Figure 3.3: Intersection detail

- **Impregnated fabric**
  The active ingredient (AI) is applied on the fabric by soaking the total fabric in a bath. The used polymer is different for both AI's. For DEET polyacrylate is used, whereas silicone elastomer is used for permethrin. To secure the DEET layer it is also possible to add an extra layer of polymer binder without an AI, e.g. polyacrylate. DEET attacks plastic, so we can assume it also invades polyester. Permethrin does not. Both AI's probably infiltrate cotton together with the absorbed water.
  We will assume that by soaking the fabric every fiber will be impregnated, as it would be the case if the fiber is impregnated and the fabric is woven or knitted afterwards. The thickness of the resulting AI-layers is a fraction of the diameter of the fiber. Impregnating the fiber is impossible for the

moment due to environmental restrictions for the produced waste water. By drying the fabric all water has disappeared out of the fibers, but it is assumed the polymers are still in rubbery state. If they were in the glassy state the fabric should break and be uncomfortable to wear. This makes sure we can use a normal Fickian diffusion model, whereas diffusion through polymers in glassy state needs a non-Fickian diffusion model.

Tests with living mosquitoes performed by the University of Wageningen (The Netherlands), have pointed out that $4\,\mathrm{mg}\,/\,\mathrm{m}^2$ of DEET on the fabric is enough to have a repellent effect on mosquitoes. This repellent effect is caused by the evaporation of the AI and makes sure that the insects do not approach the wearer of the fabric or the net and are repelled by the AI. The evaporation rate of DEET will be determined further, together with the delay time corresponding to the model where DEET is applied under other coating layers of AI or pure polymer layers.

A concentration of at least $200\,\mathrm{mg}\,/\,\mathrm{m}^2$ of permethrin is necessary to get the hot-feet effect. This effect is established by a non-evaporating AI. When the insects do land on the textile, the AI is transported to the ends of the insects nerves, the insects clearly feel the influence of the agent, which causes them to move away - they are literally getting hot feet. It is imported to know how fast this hot-feet effect is diminishing after washing the fabric. Test have pointed out that after approximately 5 washes the fabric looses $40\%$ of its starting permethrin concentration of $1500\,\mathrm{mg}\,/\,\mathrm{m}^2$, after that the rate of concentration loss is slower. After 100 washes the permethrin concentration is still $200\,\mathrm{mg}\,/\,\mathrm{m}^2$, which is still above the threshold concentration.

If mosquitoes are on the fabric for a certain amount of time, ignoring the repelent and hot-feet effect, the insecticide has a knock-down effect/kill-effect: due to absorption of AI in the system of the insects, they are immobilized and sometime later they will be killed.

The concentration of AI on the fabric was measured with a HPLC (High Performance Liquid Chromotography) which is calibrated for permethrin and DEET separately.

### 3.1.2 Headspace Analysis and Liquid Extraction

In practice the set up looks like in Fig. 3.4. A piece of textile with dimensions $4 \times 0.5\,\mathrm{cm}$ is put into a $20\,\mathrm{ml}$ vial. After weight determination, the vial is closed and kept at at $30\,^{\circ}\mathrm{C}$. After a predetermined time, the vial is shaken and 1 mL of the gas is taken from the vial using a Hamilton Gastight syringe. To keep de volume in the vial constant, 1 mL of nitrogen is added to the vial with the

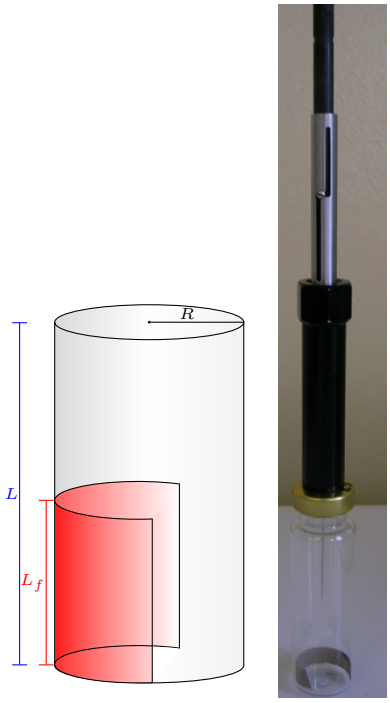


Figure 3.4: Test set up headspace analysis

Gastight syringe. Next a gas chromatography/mass spectrometry (GC/MS) is carried out to determine the peak area of the AI. The instrumental conditions of the GC/MS were reported by the Department of Organic Chemistry of Ghent University as produced by a HP6890 series GC system coupled to a HP5973 MS system, with a HP-5MS column of $30\,\mathrm{m} \times 0.25\,\mathrm{mm}$ (length $\times$ inner diameter), $0.25\,\mu\mathrm{m}\,d_f$ ($d_f$ stands for film thickness). The gas flow in the GC-oven was taken to be $1\,\mathrm{ml}\,/\,\mathrm{min}$ He, splitless mode, with an inlet temperature of $250°\mathrm{C}$. The temperature program was set to $40°\mathrm{C}$ increasing with $10°\mathrm{C}$ every minute to a temperature of $300°\mathrm{C}$. The MS-temperature was $300°\mathrm{C}$ and the solvent delay was $6\,\mathrm{min}$.

In GC/MS, the sample is injected into a gas chromatograph which volatilizes the sample, then separates the various components of the sample based on size and/or polarity. The separated components then go into a mass selective detector. The resulting mass spectrum allows for the identification of the components using standard reference libraries. If identification is not the goal, like in our case, measuring the area of the peak resulting from the GC/MS is

useful to calculate the concentration of the volatile in the air above the sample (headspace). Before we can quantitate our analyte, we must know the relationship between peak area and concentration. The simplest method is to determine a response factor and a calibration curve. The response factor ($\mathrm{RF}$) is the proportionality constant for the analyte. Each analyte will have a unique $\mathrm{RF}$ under given instrumental conditions. We know that the $\mathrm{RF}$ is simply the concentration ($C$) divided by the area ($A$),

$$\mathrm{RF} = \frac{C}{A}.$$

If we prepare a sample of a known concentration (called a standard) and evaluate it, we can measure the peak area and determine the $\mathrm{RF}$. This process is referred to as the calibration. The user will repeat this several times at different concentrations, the data points are then plotted and a line is fitted through these points to get a calibration curve, where concentration is plotted along the $x$-axis and area is plotted along the $y$-axis. If we now get a peak area out of the GC/MS analysis we can calculate the concentration out of the calibration curve. The calibration curve of DEET is given in Fig. 3.5.

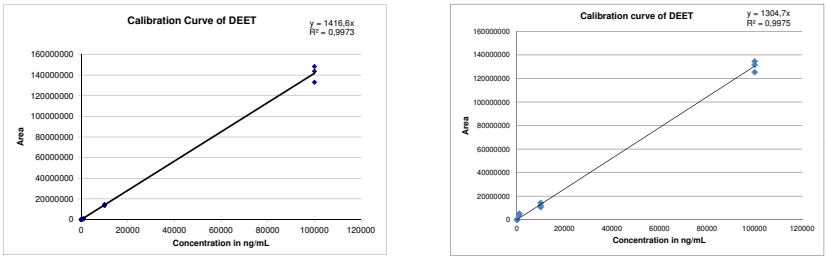


(a) First calibration

(b) Second calibration one week later

Figure 3.5: Calibration curves of DEET

Using the experimental values in table 3.3 we can calculate the concentration from the calibration curve $y = 1416.6x$.

Asuming that after $1615$ minutes saturation has been reached a saturated concentration of $673.20\,\mathrm{ng}\,/\,\mathrm{ml}$ DEET can be considered.

Next to the headspace analysis the Department of Organic Chemistry of Ghent University carried out two liquid extractions of the samples. For the first extraction a piece of textile of $4 \times 0.5\,\mathrm{cm}$ was inserted in a $4\,\mathrm{ml}$ vial. The weight of this piece was determined earlier. $3\,\mathrm{ml}$ of methyl-tert-butyl-ether

Table 3.3: Experimental data for DEET and the calculated concentration according to the calibration curve $y = 1416.6x$

| Time in oven [min] | Peak Area | Concentration [ng/ml] |
|---|---|---|
| 10 | 31648 | 22.34081604 |
| 20 | 141540 | 99.91529013 |
| 30 | 287440 | 202.9083722 |
| 40 | 197025 | 139.0830157 |
| 50 | 239792 | 169.272907 |
| 1440 | 714855 | 504.6272766 |
| 1615 | 953652 | 673.1977975 |

(MTBE) was added to the vial. This vial is put into an ultrasonic bath during $30$ minutes. In a $2\,\mathrm{ml}$ vial, $10\,\mathrm{ml}$ of this solution and $990\,\mathrm{ml}$ ofn MTBE are added giving a dilution factor of $100$. For the second extraction the MTBE is removed from the vial which is put into an oven at $60°$C for $15$ minutes. Then, $2\,\mathrm{ml}$ of MTBE is added to the vial which is again put into the ultrasonic bath during $30$ minutes. In a $2\,\mathrm{ml}$ vial, we have put $1\,\mathrm{ml}$ of this solution (no dilution). On the resulting liquid extraction vials a GC/MS analysis is carried out with the same instrumental conditions as mentioned for the headspace analysis. The results are given in Tables 3.4, 3.5 and 3.6. In these tables each sample received a code (A5, C5, C6, A3, C3). These codes stand for the production process used to achieve each specific textile piece. There are two different ways of drying the fabric, coded with A or C, and different orders of coating layers, indicated by the used numbers (only 3, 5 and 6 are in the experiments because these coatings were assumed to give the best results for repellency based upon experience from the textile company, together with the abilities of the production process). These codes are of particular interest for the textile company producing the samples, but will be used for notation purpose only in this work.

### 3.1.3 Saturation concentration

We can compute the equilibrium concentration of DEET using vapor pressure, $P_v$, values from literature. We know vapor pressure increases with temperature, so we can calculate the corresponding saturation concentrations for different temperatures.

To convert a vapor pressure to a concentration in the air at standard absolute

pressure, $P_a$ of $101.325\,\mathrm{kPa}$, $1\,\mathrm{atm}$ or $760\,\mathrm{mmHg}$ we use, [51, 4]

$$C_v[\mathrm{ppm}] = \frac{P_v(T)[\mathrm{mmHg}]}{P_a[\mathrm{mmHg}]},$$

and converting this concentration in parts per million to the SI-unit of $\mathrm{mg}\,/\,\mathrm{m}^3$ using

$$C_v\left[\frac{\mathrm{mg}}{\mathrm{m}^3}\right] = C_v[\mathrm{ppm}] \cdot M\left[\frac{\mathrm{g}}{\mathrm{mol}}\right] \cdot 0.04156\left[\frac{\mathrm{mg}\,/\,\mathrm{m}^3}{\mathrm{ppm}\cdot\mathrm{g}\,/\,\mathrm{mol}}\right].$$

Here the quantity $M$ stands for the molecular weight of the chemical substance. The molecular weight of DEET is $191.27\,\mathrm{g}\,/\,\mathrm{mol}$. The factor $0.04156$ is the inverse of the ideal gas volume at $1\,\mathrm{atm}$ which is $24.06\,\mathrm{l}$ at $20°C$ for $1$ mole of ideal gas.

We use the vapor pressures given in literature for $20°C$, $30°C$, $111°C$ and $160°C$:

- $20°C$ :

$$\frac{P_v}{P_a} = \frac{5.6\cdot 10^{-3}\,\mathrm{mmHg}}{760\,\mathrm{mmHg}} = 7.37\cdot 10^{-6} = 7.37\,\mathrm{ppm}\,,$$
$$C_v\left[\frac{\mathrm{mg}}{\mathrm{m}^3}\right] = 7.37\cdot 191.27\cdot 0.04156 = 58.59\frac{\mathrm{mg}}{\mathrm{m}^3} = 58.59\frac{\mathrm{ng}}{\mathrm{ml}}.$$

- $30°C$ :

$$\frac{P_v}{P_a} = \frac{7.69\cdot 10^{-3}\,\mathrm{mmHg}}{760\,\mathrm{mmHg}} = 10.12\cdot 10^{-6} = 10.12\,\mathrm{ppm}\,,$$
$$C_v = 10.12\cdot 191.27\cdot 0.04156 = 80.47667303\frac{\mathrm{mg}}{\mathrm{m}^3} = 80.47667303\frac{\mathrm{ng}}{\mathrm{ml}}.$$

- $111°C : P_v = 1\,\mathrm{mmHg}$ which leads to $C_v = 10459.44895\frac{\mathrm{ng}}{\mathrm{ml}}$.
- $160°C : P_v = 19\,\mathrm{mmHg}$ which leads to $C_v = 1.987295300\cdot 10^5\frac{\mathrm{ng}}{\mathrm{ml}}$.

The oven in the experiments was set at $30°C$ so we must have found a saturation concentration of $80.47667303\,\mathrm{ng}\,/\,\mathrm{ml}$ instead of the above given $673.20\,\mathrm{ng}\,/\,\mathrm{ml}$. Therefore we assume the oven was set to high in the experiments or something else went wrong. We ask for feedback at the Department of Organic Chemistry of Ghent University but could not find any other cause.

### 3.1.4 Diffusion coefficient in air

According to [10] the diffusion of a chemical in air can be calculated as

$$D_{\mathrm{g}} = 0.0067\,T^{1.5}(0.034 + M^{-1})^{0.5}\,M^{-0.17}\left[\left(\frac{M}{2.5d}\right)^{0.33} + 1.81\right]^{-2},$$

where

$$\begin{aligned} T &= \text{temperature, in } K, \\ M &= \text{molecular weight of chemical, in } \mathrm{g\,/\,mol}\,, \\ d &= \text{density of liquid chemical, in } \mathrm{g\,/\,cm^3}, \end{aligned}$$

and $D_{\mathrm{g}}$ is in $\mathrm{cm^2\,/\,s}$.

For DEET we know the density is $0.998\,\mathrm{g\,/\,cm^3}$ and the molecular weight is $191.27\,\mathrm{g\,/\,mol}$ so we derive that the needed diffusion coefficient is

$$D_{\mathrm{g,DEET}} = 0.07778168884\,\mathrm{cm^2\,/\,s}\,.$$

### 3.1.5 Evaporation rate

Another unknown coefficient in the model is the evaporation rate $\Gamma_{\mathrm{evap}}$.The evaporation flux is defined by

$$\Gamma_{\mathrm{evap}} = -D_{f_s}\left.\frac{\partial C_f}{\partial r}\right|_{r=R} = k_{\mathrm{evap}}(C^\star(\mathrm{T}) - C_{f_s}),$$

with $C^\star(\mathrm{T})$ the saturated concentration. We thus can estimate $\Gamma_{\mathrm{evap}}$ by $k_{\mathrm{evap}}C^\star(\mathrm{T})$ based upon the experiments using the amount of DEET measured in the first liquid extraction compared to those from the second test or use the known effective evaporation rate out of literature.

To repel mosquitoes a minimum effective evaporation rate of $1.2 \pm 0.3\,\mu\mathrm{g}\,/(\mathrm{cm^2}\cdot\mathrm{h}) = 3.3\cdot 10^{-6}\,\mu\mathrm{g}\,/(\mathrm{mm^2}\cdot\mathrm{s})$ should be achieved, [26]. Using this value and the previously estimated saturation concentration of $8.047\cdot 10^{-5}\,\mu\mathrm{g\,/\,mm^3}$ we get

$$k_{\mathrm{evap}} = 0.0414193\frac{\mathrm{mm}}{\mathrm{s}}.$$

A concentration of $2\,\mu\mathrm{g}\,/\,\mathrm{l}$ air of DEET is needed for repellancy, [23] . In research of Bonn University, it was found that a polymer layer technique needs $\geq 4\mathrm{g/m^2}$ of DEET for a bed net to be repellent. If we assume this is released over 6 months (15552000s), a sample of $10\,\mathrm{cm^2}$ was used, and 100s buildup is needed for repellency, then we have

$$\frac{4\,\mathrm{g}\,/10^4\,\mathrm{cm^2}}{15552000s}\cdot 100\,\mathrm{s}\cdot 10\,\mathrm{cm^2} = 2.5720\cdot 10^{-2}\,\mu\mathrm{g}\,,$$

around the sample. Estimating the volume around it as $1\,\mathrm{cm}$ high, we arrive for this experiment at

$$\frac{2.5720\cdot 10^{-2}\,\mu\mathrm{g}}{1\cdot 10^{-2}\,\mathrm{l}} = 2.57\,\mu\mathrm{g}\,/\,\mathrm{l}\,,$$

of DEET in the air around the sample which indicates the technique would work. The release can be slower (eg effective over 3 years ($0.0714\,\mu\mathrm{g}\,/\,\mathrm{l}$)), or buildup in a larger volume above the textile.

For a polymer layer on the textile consisting of DEET, the calculation above for $4\,\mathrm{g}\,/\,\mathrm{m}^2$ active over 6 months gives a release rate estimate of

$$\Gamma_{\mathrm{evap}} = 2.57 \cdot 10^{-7} \frac{\mu\mathrm{g}}{\mathrm{mm}^2\,\mathrm{s}}.$$

This leads to

$$k_{\mathrm{evap}} = 3.194 \cdot 10^{-3} \frac{\mathrm{mm}}{\mathrm{s}}.$$

In [41] an evaporation coefficient for a DEET layer on skin is given as

$$\begin{aligned} k_{\mathrm{evap}} &= \frac{\tilde{k}_{\mathrm{evap}}\rho}{C^\star} = \frac{2.6 \cdot 10^{-5}\frac{\mathrm{cm}}{\mathrm{h}} \cdot 0.998\frac{\mathrm{g}}{\mathrm{cm}^3}}{8.0477 \cdot 10^{-5}\frac{\mu\mathrm{g}}{\mathrm{mm}^3}} \\ &= \frac{7.22 \cdot 10^{-8}\frac{\mathrm{mm}}{\mathrm{s}} \cdot 0.998\frac{\mathrm{g}}{\mathrm{cm}^3}}{8.0477 \cdot 10^{-5}\frac{\mu\mathrm{g}}{\mathrm{mm}^3}} \\ &= 0.89535\frac{\mathrm{mm}}{\mathrm{s}}, \end{aligned}$$

with evaporation rate of pure DEET from skin given by $\Gamma_{\mathrm{evap}} = \tilde{k}_{\mathrm{evap}}\rho = 7.206 \cdot 10^{-5}\frac{\mu\mathrm{g}}{\mathrm{mm}^2\,\mathrm{s}}$, where pure DEET has density $\rho = 0.998\,\mathrm{g}\,/\,\mathrm{cm}^3$.

We can also estimate the evaporation rate from the experimental values given by the Department of Organic Chemistry of Ghent University. They measured twice the amount of DEET present at the textile using liquid extraction on a piece of textile of $2\,\mathrm{cm}^2$. Measurements were $91$ days or $7.862 \cdot 10^6\,\mathrm{s}$ apart from each other and can be found in Tables 3.4 and 3.5.

Table 3.4: First liquid extraction sample A5

| Sample weight [g] | Estimation DEET [$\mu$g / g] | Estimation of DEET on sample [$\mu$g] |
|---|---|---|
| 0.045 | 643 | 28.935 |
| 0.048 | 559 | 26.664 |
| 0.048 | 500 | 24.000 |
| Mean | | 26.533 |

Over $3$ months $23.461\,\mu\mathrm{g}$ per sample was released. The size of a sample is $2\,\mathrm{cm}^2$ so this gives a release rate of

$$\Gamma_{\mathrm{evap}} = \frac{23.461\,\mu\mathrm{g}}{7.862 \cdot 10^6\,\mathrm{s} \cdot 2\,\mathrm{cm}^2} = 1.492 \cdot 10^{-8}\frac{\mu\mathrm{g}}{\mathrm{mm}^2\,\mathrm{s}},$$

| Table 3.5: Second liquid extraction sample A5 | | |
|---|---|---|
| Sample weight [g] | Estimation DEET [$\mu$g / g] | Estimation of DEET on sample [$\mu$g] |
| 0.0476 | 68 | 3.237 |
| 0.0529 | 53 | 2.804 |
| 0.0515 | 60 | 3.090 |
| 0.0554 | 57 | 3.158 |
| Mean | | 3.072 |

with

$$\mathrm{k_{evap}} = 1.854 \cdot 10^{-4} \frac{\mathrm{mm}}{\mathrm{s}}.$$

A complete overview of experimental values for the different samples can be found in Table 3.6.

| Table 3.6: Experimental average values for liquid extraction (LE) | | | | | |
|---|---|---|---|---|---|
| Sample | Average estimation of DEET first LE [$\mu$g] | Average estimation of DEET second LE [$\mu$g] | Difference [$\mu$g] | $\Gamma_{\mathrm{evap}}$ [$10^{-8} \frac{\mu\mathrm{g}}{\mathrm{mm}^2\,\mathrm{s}}$] | $k_{\mathrm{evap}}$ [$10^{-4} \frac{\mathrm{mm}}{\mathrm{s}}$] |
| A5 | 26.533 | 3.072 | 23.461 | 1.492 | 1.854 |
| C5 | 2.179 | 3.879 | $-1.700$ | - | - |
| C6 | 120.607 | 10.521 | 110.086 | 7.001 | 8.700 |
| A3 | 30.661 | 1.893 | 28.768 | 1.830 | 2.274 |
| C3 | 24.188 | 3.435 | 20.754 | 1.320 | 1.640 |

Because in the experiments a closed fabric was considered instead of an open net the fiber surface is larger than the fabric surface and the evaporation rate can be smaller than this value. To know how much smaller we need to calculate the ratio of the total fiber surface per fabric surface:

$$\frac{S_{\mathrm{fib}}}{S_{\mathrm{fab}}} = \frac{(n_{\mathrm{vertyarns}} \cdot S_{\mathrm{vertfib}} + n_{\mathrm{horyarns}} \cdot S_{\mathrm{horfib}}) \cdot n}{W \cdot H},$$

with

$$
\begin{aligned}
S_{\text{fib}} &= \text{total fiber surface},\\
S_{\text{fab}} &= \text{fabric surface},\\
n_{\text{vertyarns}} &= \text{number of vertical yarns in the fabric},\\
n_{\text{horyarns}} &= \text{number of horizontal yarns in the fabric},\\
S_{\text{vertfib}} &= \text{surface of a vertical fiber},\\
S_{\text{horfib}} &= \text{surface of a horizontal fiber},\\
n &= \text{number of fibers in a yarn cross section},\\
W &= \text{width of the fabric},\\
H &= \text{height of the fabric}.
\end{aligned}
$$

We know that

$$
\begin{aligned}
n_{\text{vertyarns}} &= \frac{W}{\Delta x},\\
n_{\text{horyarns}} &= \frac{H}{\Delta y},\\
S_{\text{vertfib}} &= 2\pi HR,\\
S_{\text{horfib}} &= 2\pi WR,
\end{aligned}
$$

where

$$
\begin{aligned}
\Delta x &= \text{space in between yarns in horizontal direction},\\
\Delta y &= \text{space in between yarns in vertical direction}.
\end{aligned}
$$

For the sample of the bed net fabric we have an open net structure with room dimensions of $3\,\mathrm{m}$ by $2.1\,\mathrm{m}$, made of very fine fibers with radius $0.0052\,\mathrm{mm}$, coated with two polymer layers of thickness $0.0085\,\mathrm{mm}$, we have:

$$
\begin{aligned}
n_{\text{vertyarns}} &= \frac{3000\,\mathrm{mm}}{1.21\,\mathrm{mm}},\\
n_{\text{horyarns}} &= \frac{2100\,\mathrm{mm}}{2.21\,\mathrm{mm}},\\
S_{\text{vertfib}} &= 2\pi \cdot 2100\,\mathrm{mm}(0.0052\,\mathrm{mm} + 2 \cdot 0.0085\,\mathrm{mm}) = 292.922\,\mathrm{mm}^2\,,\\
S_{\text{horfib}} &= 2\pi \cdot 3000\,\mathrm{mm}(0.0052\,\mathrm{mm} + 2 \cdot 0.0085\,\mathrm{mm}) = 418.460\,\mathrm{mm}^2\,,\\
n &= 100,\\
W &= 3000\,\mathrm{mm}\,,\\
H &= 2100\,\mathrm{mm},
\end{aligned}
$$

with $\Delta x = 1.21\,\mathrm{mm}$ and $\Delta y = 2.21\,\mathrm{mm}$ and $100$ fibers per yarn cross-section. This leads to

$$\begin{aligned} S_{\text{fib}} &= \left(\frac{3000}{1.21} \cdot 292.922\,\mathrm{mm}^2 + \frac{2100}{2.21} \cdot 418.460\,\mathrm{mm}^2\right) \cdot 100 \\ &= 72625313.807\,\mathrm{mm}^2 + 39763180.863\,\mathrm{mm}^2 \\ &= 112388494.669\,\mathrm{mm}^2, \end{aligned}$$

for the total fiber surface and

$$S_{\text{fab}} = 3000\,\mathrm{mm} \cdot 2100\,\mathrm{mm} = 6300000\,\mathrm{mm}^2\,,$$

for the fabric surface. The ratio then is

$$\begin{aligned} \frac{S_{\text{fib}}}{S_{\text{fab}}} &= \frac{112388494.669\,\mathrm{mm}^2}{6300000\,\mathrm{mm}^2} \\ &= 17.839. \end{aligned}$$

Considering this factor the estimated $k_{\text{evap}}$ is

$$k_{\text{evap}} = \frac{1.854 \cdot 10^{-4}\,\mathrm{mm\,/\,s}}{17.839} = 1.0393 \cdot 10^{-5} \frac{\mathrm{mm}}{\mathrm{s}}.$$

In case of the closed fabric as in sample A5 this value become much larger. We then have a blended fabric with $65\%$ of cotton and $35\%$ of polyester. The radius of a polyester fiber in this sample is estimated at 0.0122. The cotton fiber has an elliptical cross section with long axis $0.0183$ and short axis $0.0098$. The area of this cross section is the same if we take a circular fiber with radius $0.01339$. Per $\mathrm{cm}$ in the warp direction of the fabric there are $43$ yarns, in the weft direction it has $27$ yarns per $\mathrm{cm}$. In a yarn cross-section the number of fibers is estimated at $190$ fibers. For a piece of fabric of dimensions $4 \times 0.5\,\mathrm{cm}$ this gives

$$\begin{aligned} n_{\text{vertyarns}} &= 27 \cdot 4 = 108, \\ n_{\text{horyarns}} &= 43 \cdot 0.5 = 21.5, \\ S_{\text{vertfib}} &= 2\pi \cdot 5\,\mathrm{mm}[65\%(0.01339\,\mathrm{mm} + 2 \cdot 0.0085\,\mathrm{mm}) + 35\%(0.0122 + 2 \cdot 0.0085)] \\ &= 0.94165\,\mathrm{mm}^2\,, \\ S_{\text{horfib}} &= 2\pi \cdot 40\,\mathrm{mm}[65\%(0.01339\,\mathrm{mm} + 2 \cdot 0.0085\,\mathrm{mm}) + 35\%(0.0122 + 2 \cdot 0.0085)] \\ &= 7.53316\,\mathrm{mm}^2\,, \\ n &= 190, \\ W &= 40\,\mathrm{mm}\,, \\ H &= 5\,\mathrm{mm}, \end{aligned}$$

which leads to

$$\begin{aligned} S_{\text{fib}} &= \left(108 \cdot 0.9417\,\text{mm}^2 + 21.5 \cdot 7.5332\,\text{mm}^2\right) \cdot 190 \\ &= 50095.6166\,\text{mm}^2, \end{aligned}$$

for the total fiber surface and

$$S_{\text{fab}} = 40\,\text{mm} \cdot 5\,\text{mm} = 200\,\text{mm}^2\,,$$

for the fabric surface. The ratio then is

$$\begin{aligned} \frac{S_{\text{fib}}}{S_{\text{fab}}} &= \frac{50095.6166\,\text{mm}^2}{200\,\text{mm}^2} \\ &= 250.4781. \end{aligned}$$

Considering this factor the estimated $k_{\text{evap}}$ is

$$k_{\text{evap}} = \frac{1.854 \cdot 10^{-4}\,\text{mm}\,/\,\text{s}}{250.4781} = 7.402 \cdot 10^{-7}\frac{\text{mm}}{\text{s}}.$$

For pure DEET which is not captured in a polymer layer we can use a known formula for the evaporation flux/rate:

$$\Phi_{\text{evap}} = \frac{k_{\text{evap}} N_A (P_v - P_h)}{\sqrt{2\pi MRT}}, \qquad \left[\frac{\text{mol}}{\text{cm}^2\,s}\right],$$

where

$$\begin{aligned} k_{\text{evap}} &= \text{coefficient of evaporation} (0 < k_{\text{evap}} < 1), \\ N_A &= \text{Avagadro's constant} = (6.02214129 \pm 0.00000027) \cdot 10^{23}\,\text{mol}^{-1}\,, \\ P_v &= \text{vapor pressure (in Torr or mmHg)}, \\ P_h &= \text{ambient pressure (in Torr or mmHg)}, \\ M &= \text{molecular weight } (\text{g}\,/\,\text{mol}), \\ R &= \text{universal gas constant}, \\ \text{T} &= \text{temperature at which the corresponding } P_v \text{ is met.} \end{aligned}$$

To have a more convenient unit we can multiply the evaporation flux with the molecular weight of the chemical to get the evaporation rate

$$\Gamma_{\text{evap}} = 5.84 \cdot 10^{-2}\sqrt{\frac{M}{T}}P_v, \qquad \left[\frac{\text{g}}{\text{cm}^2\,\text{s}}\right].$$

For DEET we then get

$$\begin{aligned} \Gamma_{\text{evap}} &= 5.84 \cdot 10^{-2}\sqrt{\frac{191.27\,\text{g}\,/\,\text{mol}}{20°C}}\,7.69 \cdot 10^{-}3\frac{\text{g}}{\text{cm}^2\,\text{s}} \\ &= 13.888\frac{\mu\text{g}}{\text{mm}^2\,\text{s}}, \end{aligned}$$

with an corresponding $k_{\text{evap}} = 172574.188\frac{\text{mm}}{\text{s}}$.

### 3.1.6 Initial concentration of DEET per fiber in the coating

The cross sectional area of a fiber is given by

$$A = \pi R_f^2 = \frac{\pi \varnothing_f^2}{4}.$$

The volume of a fiber with length $\ell$ then is

$$V = \frac{\pi \varnothing_f^2}{4} \ell.$$

The linear density of a fiber is

$$\rho_f = \frac{m}{\ell}, \text{with } m \text{ the mass given by } m = \rho V,$$

where $\rho$ is the density of the material. From this we end up with the relation

$$\rho_f = \frac{\rho \pi \varnothing_f^2}{4}.$$

For polyester fibers the linear density is $1.5\,\mathrm{dtex}$ or $1.5\,\mathrm{g}\,/10000\,\mathrm{m}$, for cotton fibers it is $1.67\,\mathrm{dtex}$. The material density of polyester is $1.38\,\mathrm{g}\,/\,\mathrm{cm}^3$ and of cotton $1.55\,\mathrm{g}\,/\,\mathrm{cm}^3$ .

From the derivation above we can calculate the diameter of the fibers $\varnothing_f$ in the fabric from the known linear density and fabric density as

$$\varnothing_f = \sqrt{\frac{4 \cdot 10^{-6} \cdot \rho_f}{\rho \pi}},$$

where the diameter is in $\mathrm{cm}$, the linear density in $\mathrm{dtex}$ and the density of the material is in $\mathrm{g}\,/\,\mathrm{cm}^3$. The estimated diameter of a cotton fiber is $0.01171\,\mathrm{mm}$, that of a polyester fiber is $0.01176\,\mathrm{mm}$. Using the above values we can estimate the amount of DEET per fiber coating as follows.

- Weight of a piece of fabric of $2\,\mathrm{cm}^2$:

$$G = \frac{0.045\,\mathrm{g}}{2\,\mathrm{cm}^2} = 0.0225 \frac{\mathrm{g}}{\mathrm{cm}^2};$$

- Volume of the fibers per $\mathrm{cm}^2$ of fabric:

$$V = \frac{G}{\rho} \qquad \left[\frac{\mathrm{mm}^3}{\mathrm{cm}^2}\right];$$

- Volume of one fiber:

$$V_f = \pi R_f^2 \ell \qquad \left[\mathrm{mm}^3\right];$$

- Number of fibers per $\mathrm{cm}^2$ of fabric:

$$\mathrm{N} = \frac{V}{V_f} = \frac{G}{\rho V_f};$$

- Mass of DEET on a piece of fabric of $1\,\mathrm{g}$:

$$A = \pm 600 \frac{\mu\mathrm{g}}{\mathrm{g}};$$

- Mass of DEET per fiber:

$$\begin{aligned} M = \frac{A \cdot G}{\mathrm{N}} &= \frac{A[\mu\mathrm{g}\,/\,\mathrm{g}] \cdot G[\mathrm{g}\,/\,\mathrm{cm}^2] \cdot \rho[\mathrm{g}\,/\,\mathrm{mm}^3] \cdot V_f[\mathrm{mm}^3]}{G[\mathrm{g}\,/\,\mathrm{cm}^2]} \\ &= 600 \cdot 1.38 \cdot 10^{-3} \left(\frac{0.01176}{2}\right)^2 \pi\ell \qquad [\mu\mathrm{g}] \qquad \text{for polyester,} \end{aligned}$$

and

$$= 600 \cdot 1.67 \cdot 10^{-3} \left(\frac{0.01171}{2}\right)^2 \pi\ell \qquad [\mu\mathrm{g}] \qquad \text{for cotton;}$$

- Volume of coating $V_c$ with thickness $\Delta c$:

$$V_c = ((\mathrm{R}_f + \Delta c)^2 - \mathrm{R}_f^2)\pi\ell;$$

- Concentration of DEET in coating per fiber:

$$\begin{aligned} \frac{M}{V_c} &= \frac{A \cdot G}{G} \cdot \frac{\rho \cdot V_f}{\pi((R_f + \Delta c)^2 - R_f^2)\ell} \\ &= \frac{A \cdot \rho \cdot V_f}{[2R_f \Delta c + (\Delta c)^2]\pi\ell} \\ &= \frac{600 \cdot 1.38 \cdot 10^{-3} \left(\frac{0.01176}{2}\right)^2 \pi\ell}{[2\left(\frac{0.01176}{2}\right) 0.00085 + (0.00085)^2]\pi\ell} \qquad \left[\frac{\mu\mathrm{g}}{\mathrm{mm}^3}\right] \\ &= 1.809754604 \qquad \left[\frac{\mu\mathrm{g}}{\mathrm{mm}^3}\right] \qquad \text{for polyester,} \end{aligned}$$

and

$$\begin{aligned} &= \frac{600 \cdot 1.67 \cdot 10^{-3} \left(\frac{0.01171}{2}\right)^2 \pi\ell}{[2\left(\frac{0.01171}{2}\right) 0.00085 + (0.00085)^2]\pi\ell} \qquad \left[\frac{\mu\mathrm{g}}{\mathrm{mm}^3}\right] \\ &= 2.177331836 \qquad \left[\frac{\mu\mathrm{g}}{\mathrm{mm}^3}\right] \qquad \text{for cotton.} \end{aligned}$$

### 3.1.7 Tests

For adjusting the end product a few suggestions can be made to the textile companies:

- more layers;
- thicker layers (this results in lesser fibers per yarn, or a thicker yarn);
- a higher initial concentration of the active ingredient;
- other fabric choice, polyester/cotton in other blend percentage;
- bigger/smaller holes in the net;

In the next section we will give the exact reproduction of the article 'Model based determination of the influence of textile fabric on bioassay analysis and the effectiveness of a textile slow release system of DEET in mosquito control' as published in Pest Management Science, by John Wiley & Sons, Ltd in 2015, as it summarizes the previous sections and consequently is the end-product of the more physical part of these thesis.

## 3.2 Model based determination of the influence of textile fabric on bioassay analysis and the effectiveness of a textile slow release system of DEET in mosquito control.

**Benny Malengier, Tineke Goessens, Flora F. Mafo, Mike De Vrieze, Lieva Van Langenhove, Samuel Wanji, Frederic Lynen** [1]

**published by John Wiley & Sons, Ltd in Pest Management Science, 2015.**
[doi:10.1002/ps.3902]

**Abstract**

*BACKGROUND: : Determining the effectiveness of a product in repelling mosquitoes or other flying insects is a difficult task. One approach is to use a bioassay with textile fabric. We investigated the role of the textile substrate in a bioassay with a numerical model, and compared the outcome with known results for DEET. The model was then used to determine the effectiveness of textile slow-release formulations based on coatings, and results were compared with those of a field study in the Cameroon. Slow-release formulations are difficult to evaluate with standard tests, as the compound needs a build-up time not present in these tests.*

*RESULTS: We found excellent correspondence between the model and the known DEET results without matching parameters. Slow-release approaches are deemed possible but have several drawbacks. Modeling can help in identifying optimal use conditions. The field test with a slow-release system performed better than the model anticipated with initially more than 90% repellency. DEET-coated textile was considered not marketable however.*

*CONCLUSION: We advise that bioassays also characterize in more detail the type of textile fabric used so as to allow conclusions to be drawn by textile modeling. As regards coated textile slow-release systems, more research is needed. We nevertheless advise usage mainly at entry points, e.g. as scrims.*

**Keywords:** *Anopheles, DEET, slow-release, spatial repellent, textile modeling*

### 3.2.1 Introduction

Mosquitoes transmit several pathogens that cause serious illnesses: malaria, yellow fever, dengue, and many more diseases. As a consequence, much

[1] We wish to acknowledge the support from European Union project: NMP2-2009-228639, FP7, NOBUG project.

research is done to determine new insecticides and mosquito repellents. Our work focuses on repellents, which have the ability to disrupt the host-seeking abilities of the mosquitoes and induce movement away from the repellent. Once a product is determined to be a repellent, the next step is to determine the effective dosage needed for optimal repellence of mosquitoes, and how this dosage can be best provided.

Different testing setups exist to determine the spatial repellency of products. A common test is the arm-in-cage, in which a product is applied to an open section of a human arm and introduced into a cage with up to $500$ mosquitoes, see eg. [34]. The difficulty with this test is the variability in attractiveness of the humans used, and the personnel cost. However, given that the final aim of any spatial repellent is to repel mosquitoes from humans, an *in vivo* test like the arm-in-cage is a necessity.

Alternative *in vitro* tests have been developed. For example, cup designs like the Klun & Debboun (K&D) test module, [27, 28]. In these a bait is used that mimics the human. Over this bait there is a cup, and mosquitoes are released into this cup. A distinction must be made here between a *feeding deterrent*, that is, a chemical that inhibits feeding when present in a place where the insects feed in its absence, [8], a *spatial repellent*, which is a chemical that causes mosquitoes to make a movement away from its source, and *attraction inhibitors*, which mask the presence of an attractant and hence prevent mosquitoes taking flight in the presence of an attractant and causing them to have difficulty locating the attractant. In cup tests the mosquito typically has no possibility of leaving the cup, so the compound is tested like a feeding deterrent or attraction inhibitor. However, results are often used in the sense of a spatial repellent.

Depending on the tests, different textiles are used, or no textile at all. For example, in [28, 1] nylon organdy cloths are used in some biting bioassays, while others use muslin cloth for the repellency bioassay, [1]. The nylon cloth typically only serves as a delivery mechanism on top of the human skin or bait. The compound normally will remain as a layer on the nylon fibers, applied in such a way as not to touch the human skin, and allowing mosquitoes still to bite the arm or bait underneath. Muslin cloth on the other hand consists of cotton fibers, which will absorb the compound. This offers the possibility of testing different concentrations of a compound.

In this study we use a model to investigate the influence of the textile used. In essence, for a repellent, the important aspect is the concentration in the air, which is almost never determined. Instead, different compounds and concentrations are applied to textile, which is the delivery system of the compound into the air. With a model, this delivery system can be investigated. Several problems can occur with the textile that are of importance: the compound could bind with the textile aggregate, causing an incorrect negative

result; different research groups may use different textiles, making the results not comparable; different ventilation set-ups might be used, resulting in very different air concentrations. With a model, the gradient of the compound in a domain (a cup or a room) can also be determined. This can help in determining whether a feeding deterrent test might be valid as a repellent result: if a strong gradient is present in the environment of the mosquito, it stands to reason that the mosquito can move towards the lowest concentration, even if it cannot actually move away.

We will concentrate on DEET (N,N-diethyl-3-methylbenzamide) in this study, given the large amount of information available on this successful insect repellent. DEET is an attraction inhibitor, [6, 11], that requires a bait to function as a repellent. Commercial products based on DEET give a mean time of protection of around $4\,\mathrm{h}$ in academic studies, [34]. Using known data, we can simulate the release of DEET and its hypothetical effect on mosquitoes.

Taking the results into account, we carried out tests to create a slow-release system for DEET based on the technology of the Belgian company Utexbel, enabling an extension of the protection offered by DEET. We evaluated the binding capacity of this system, its theoretical performance over time and the results of a field test.

### 3.2.2 Simulation

#### 3.2.2.1 Simulation Code

Details about the simulation code can be found in an earlier article, [16]. The code is freely available at https://gitorious.org/stickproject. The components of the code are:

1. A fiber model that implements the fiber as a layered cylindrical structure, with an evaporation law at the boundary.

2. A fiber-yarn multiscale coupling via an overlap zone in the fiber and yarn model. This makes it possible to convert the system of a yarn consisting of hundreds of fibers into a single yarn model and $4Đ10$ representative fiber models, interacting via a designated overlap zone. The fiber result in the overlap zone (corresponding to void space in the yarn model) is upscaled to the yarn overlap zone via a source/sink term, while the yarn result in the yarn overlap zone is likewise downscaled to the fiber model in the next time step.

3. A yarn model that implements the yarn as a cylindrical structure consisting of radial zones with a specific fiber composition. Every zone interacts with its own representative fiber model.

4. A yarn-fabric/environment multiscale coupling via an overlap zone in the yarn and fabric/environment models. This makes it possible to reduce the problem of a fabric consisting of thousands of yarn threads to a fabric model interacting with some representative yarn models via a designated overlap zone. Now, the yarn overlap zone (corresponding to the volume outside the yarn) is upscaled to the fabric, and the fabric overlap zone (corresponding to the volume closest to the fabric) is downscaled to the yarn in the next time step.

5. A fabric/environment model with basic ventilation. All test set-ups considered have a simple geometry allowing reduction to a 1D model.

The simulation code allows many different textile optimizations: changes in fibers, different blend proportions, weaving changes, etc.

Important in the model is how evaporation is handled. In [41] the evaporative flux $F_{\text{evap}}$ from skin is given as

$$F_{\text{evap}}(t) = \tilde{k}_{\text{evap}} \frac{\rho}{C^*_{\text{m}}} C_B(t), \tag{3.1}$$

where $\tilde{k}_{\text{evap}}$ is the evaporation coefficient, $C^*_{\text{m}}$ is the saturation concentration in the medium (e.g. skin), $\rho$ is the density of the component, and $C_B(t)$ is the concentration at the boundary. For a pure DEET layer, $C^* = C_B(t)$, and the equation reduces to

$$F_{\text{evap}}(t) = \tilde{k}_{\text{evap}} \rho.$$

One can interpret the $\frac{\rho}{C^*_{\text{m}}}$ factor as a membrane partition coefficient. It effectively works like a porosity of the medium considered.

Equation (3.1) can be improved. We do this by considering a water liquid-vapor term, [59, 24]:

$$F_{\text{evap}}(t) = Sh_{lg}(C^*_{\text{a}} - C_{a,B})\mathcal{H}(C_B, C^*_{\text{a}} - C_{a,B}), \tag{3.2}$$

where $S$ is the effective area fraction, $h_{lg}$ is the mass transfer coefficient from liquid to gas (unit $\text{mm/s}$), $C^*_{\text{a}}$ is the saturated concentration in air, $C_{a,B}$ is the concentration of the component in the air at the boundary, $C_B(t)$ is the concentration at the boundary, and $\mathcal{H}$ is a Heaviside type function defined as:

$$\mathcal{H}(v, c) = \begin{cases} 1, & c \leq 0 \\ 0, & c > 0 \;\&\; v < 0 \\ 1, & c > 0 \;\&\; v > 0 \end{cases},$$

which indicates that condensation occurs if the control $c$ is less than $0$, otherwise evaporation is governed by the presence of the component at the boundary. If

we assume $C_{a,B} \approx 0$, and that the entire surface is available for evaporation ($S = 1$), the equation reduces to

$$F_{\text{evap}}(t) = h_{lg} C^*_{\text{a}},$$

which makes it possible to obtain the approximate relationship

$$\tilde{k}_{\text{evap}} = h_{lg} C^*_{\text{a}} / \rho.$$

Further, $S$ is proportional to $C_B(t)/C^*_{\text{m}}$, which shows that the improved equation (3.2) is indeed analogous to (3.1).

#### 3.2.2.2 DEET

We concentrate on DEET, as a great deal of information is known about this compound. Important for mosquito repellency is the air concentration needed for DEET to behave like a repellent. DEET is used primarily by dermal application as an insect repellent against mosquitoes, ticks, fleas, leeches and black-flies. DEET is available in $4\%$ to almost $100\%$ concentrations in insect repellent formulations, including solutions, lotions, creams, gels, aerosols, pump sprays, and impregnated towelettes, usually with an ethyl or isopropyl base.

In the atmosphere it exists in the vapor phase and is degraded by reaction with photochemically produced hydroxy radicals; its atmospheric half-life is approximately $15$ hours. DEET has moderate mobility and is not expected to volatilize in moist or dry soil or to biodegrade under either aerobic or anaerobic conditions.

A minimum evaporation rate of $5\,\mu\text{g}/(\text{cm}^2\,\text{h})$ ($0.03\,\mu\text{mol}/(\text{cm}^2\,\text{h})$) for DEET over 5-15 minutes was determined for human skin. DEET then acts as a volatile agent to repel mosquitoes at distances of at least $38\,\text{cm}$ from their host, [48].

The question on how DEET repels mosquitoes has been investigated in different studies. One such study, [9] stated that DEET inhibits the 1-octen-3-ol-evoked responses by inhibiting the activity of the olfactory receptory neurons (ORN's) on the antennae of the mosquito. Another study, [47] provided convincing evidence suggesting that repellency of the mosquito is a matter of direct detection of DEET in the vapor phase and avoidance of the smell of DEET. The researchers found a DEET-sensitive ORN and pointed out a false positive in the previous research on account of trapping of odorants in the Pasteur pipes when a DEET-laden filter paper is added to the cartridge. It was because of this that the mosquitoes could not smell DEET, and not because of inhibition of the olfactory system.

We estimate the diffusion coefficient of DEET in air according to the methods used by the Emission Standards Division [10], which gives $D_{g,\text{DEET}} = 0.07778\,\text{cm}^2/\text{s}$.

From [41] we can estimate an evaporative flux of DEET around $7.2{\cdot}10^{-3}$ $\mu\mathrm{g}/(\mathrm{cm}^2\,\mathrm{s})$. This translates into a build-up of several micrograms of DEET after some minutes. The different evaporative laws (3.1)-(3.2) have corresponding coefficients $\tilde{k}_{\mathrm{evap}} = 7.2 \cdot 10^{-8}\,\mathrm{mm/s}$ and $h_{lg} = 0.897\,\mathrm{mm/s}$.

Pure DEET evaporates more rapidly than needed to repel mosquitoes, so a slow-release system would be beneficial. It has been determined in [23] that a DEET concentration of $2$ $\mu\mathrm{g}/\mathrm{l}$ air is needed for repellency. In [26] an encapsulation technique was used to slow down the release. They determined that, to repel mosquitoes, a minimum effective evaporation rate of $3.3 \pm 0.8 \cdot 10^{-4}\,\mu\mathrm{g}/(\mathrm{cm}^2\,\mathrm{s})$ should be achieved. The different evaporative laws (3.1)-(3.2) then have corresponding coefficients $\tilde{k}_{\mathrm{evap}} = 3.3 \cdot 10^{-9}\,\mathrm{mm/s}$ and $h_{lg} = 0.041\,\mathrm{mm/s}$, indicating the evaporation can be reduced 22-fold and still give rise to repellency.

#### 3.2.2.3 Muslin cloth

The muslin cloth used in bioassays is normally not characterized. Therefor, we consider some typical values. We will examine a fabric of $5$ by $10\,\mathrm{cm}$, consisting of yarns that are $0.6\,\mathrm{mm}$ apart center to center in the vertical and horizontal directions. A yarn has a radius of $0.105\,\mathrm{mm}$ and typically contains $160$ cotton fibers. A cotton fiber has a typical radius of $0.0052\,\mathrm{mm}$ and density of $1.55\,\mathrm{g/cm}^2$. The moisture regain (absorbed water expressed in percentages of dry weight) of cotton at $65\%$ relative humidity (RH) at $20°\mathrm{C}$ is $6$ to $7\%$, and $20\%$ at $100\%$ RH, indicating that cotton can absorb water up to $20\%$ of it's own weight in water. If we assume the muslin cloth used to be originally fully dry, we can conclude that $20\%$ regain is also possible for DEET, allowing a maximum of $0.31\,\mathrm{g/cm}^3$ in the cotton, which translates to a porosity of DEET in cotton of $n = 0.31$.

The total volume of cotton in the muslin cloth is $V_c = 228.6\,\mathrm{mm}^3$, which leads to a maximum absorbed DEET content of $0.071\,\mathrm{g}$ or $1.4\,\mathrm{mg/cm}^2$.

In a typical bioassay, a stock solution is diluted to produce test concentrations of $1.5$, $0.75$, $0.375$, $0.187$, $0.094$, $0.047$, $0.023$, $0.011$ and $0.006\,\mathrm{mg/cm}^2$, which corresponds to a dose range of $7841$ down to $31\,\mathrm{nmol/cm}^2$. We see that these concentrations can be absorbed by the muslin cloth, except for the first, which should result in a thin surface layer of unabsorbed DEET. Converting this to the fraction $n_D$ of the porosity available used, we obtain $1.07$, $0.54$, $0.27$, $0.13$, $0.067$, $0.033$, $0.017$, $0.008$, $0.004$. The comparison article also uses $25\,\mathrm{nmol/cm}^2$ or $0.0048\,\mathrm{mg/cm}^2$, which translates into a used fraction $n_D$ of $0.0034$. These fractions allow us to set the initial conditions correctly for the

numerical model. In equation (3.2) we set

$$S(t) = n\frac{C_B(t)}{\rho}, \tag{3.3}$$

and consider the initial DEET concentration in the fiber to be

$$C(0) = C_B(0) = n_D\rho,$$

where $n_D$ is the fraction of the porosity used for the start concentration.

#### 3.2.2.4 Numerical Experiments

As a first experiment, we compare with Fig. 4 of [1], which is a dose response study for DEET at $25, 20, 15, 10, 5\,\mathrm{nmol/cm^2}$. In that study, $25\,\mathrm{nmol/cm^2}$ provided a repellency of $90\%$, $20$ and $15\,\mathrm{nmol/cm^2}$ gave equal reduced repellency of $70\%$, while $10$ and $5\,\mathrm{nmol/cm^2}$ showed results similar to solvent control. In the dose response, the fabrics are dried for $3$ to $5$ minutes, which we estimate can remove a maximum of $1\,\mu\mathrm{g}$ of DEET, which is sufficiently low. The patch is attached to a human arm, which is then introduced into a screened cage with mosquitoes exhibiting host-seeking behavior. The movement of the arm will create an unknown amount of forced convection over the muslin cloth. The arm is held in the cage for $1\,\mathrm{min}$, after which the number of mosquitoes that could feed is counted.

As we cannot know the influence of the forced convection, we simulate this with a run of the simulation code over $2\,\mathrm{min}$, starting with the initial known concentration and no DEET present in the surrounding air. We then consider the last minute of the simulation as meaningful for comparison with the results of Fig. 4 of [1]. This because the forced convection will remove the surface layers above the muslin cloth containing DEET, but not the DEET concentration accumulated inside the cloth void spaces. The simulation results are shown in Fig. 3.6.

The results nicely match the bioassay: $25\,\mathrm{nmol/cm^2}$ achieves the required minimum amount of $2\,\mu\mathrm{g}$ DEET per $\mathrm{l}$ air almost for the entire duration of the last minute of simulation. However, the $10$ and $5\,\mathrm{nmol/cm^2}$ remain under $2\,\mu\mathrm{g}$ DEET per $\mathrm{l}$ air, and cannot offer protection against the mosquitoes.

We stress that no parameter matching was done - all parameters used in the simulation were estimated on the basis of previous DEET studies. Hence, this test could be used to estimate the required amount of DEET in the air for repellency.

As a second experiment, we will consider the case of the application of $25\,\mathrm{nmol/cm^2}$ on the muslin cloth and a duration test. These results should be

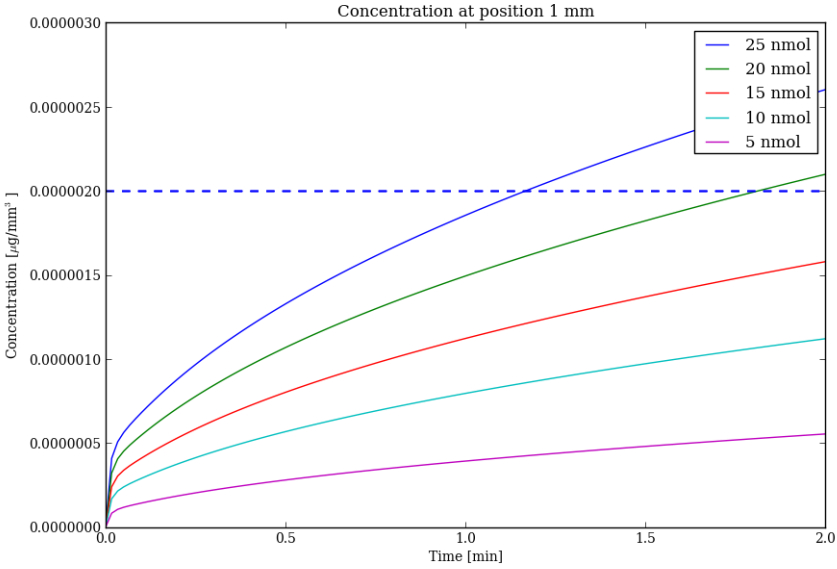


Figure 3.6: Concentration $1\,\mathrm{mm}$ from the cloth over $2$ minutes as obtained with a dose-response simulation. The dashed line is the required amount for good repellency

compared with the results in Fig. 3 of [1]. The results there can be summarized as the muslin cloth giving almost full protection for $2\,\mathrm{h}$, after which there is a linear decrease, with a repellency still of $70\%$ (proportion not biting) at $6\,\mathrm{h}$ and little difference from the positive control after $12\,\mathrm{h}$. We simulate this by considering a sample that evaporates in an open environment with an initial concentration $25\,\mathrm{nmol/cm^2}$. At $0, 1, 3, 6, 12$ and $24\,\mathrm{h}$, the sample is moved for testing to a cage. Hence, we consider the concentrations obtained at those time points, and conduct tests as in our first numerical experiment with those values.

We obtain Fig. 3.7, the relevant data of which for comparison with the reference [1] is given in Table 3.7. Comparing with the results in Fig. 3.6, we see that a good correspondence with the experiment is obtained. In Fig. 3.8, we show the protection over $1$ day given by the muslin cloth if the cloth remains fixed in position. The bottom dashed line in Fig. 3.8 corresponds to the determined lower boundary of DEET concentration needed to have good repellency.

| Table 3.7: Duration test concentration values in the textile | | |
|---|---|---|
| Duration [h] | Mass DEET [$\mu$g] | Conc [$\mathrm{nmol/cm^2}$] |
| 0 | 152.5 | 25 |
| 1 | 140.5 | 23 |
| 3 | 120.5 | 19.8 |
| 6 | 97.0 | 15.9 |
| 12 | 62.5 | 10.2 |
| 24 | 23.2 | 5.3 |

By moving the muslin cloth to the testing cage, the surface layer above the fabric will be replaced by mostly fresh air (forced convection), and hence the protection right after movement (Fig. 3.6) is considerably decreased from this ideal consideration of an arm that remains fixed in position. By the movement of the user, the result after $6\,\mathrm{h}$ is already much reduced owing to the slower build-up of DEET at the lower concentrations, while not moving the muslin cloth gives good protection even at $5\,\mathrm{mm}$ for the full $24\,\mathrm{h}$. It is important to note that forced convection over the muslin cloth would change this considerably.

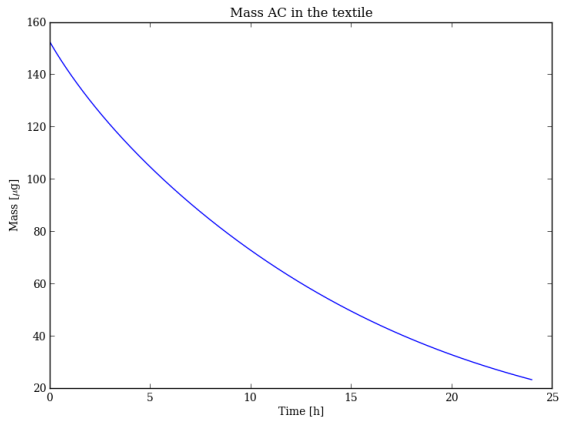


Figure 3.7: Mass of DEET in the textile, starting with a $25\,\mathrm{nmol/cm^2}$ concentration, over $1$ day

In the simulation, air diffusion and convection reduce the DEET concen-

tration around the muslin cloth at a slow rate as the model mimics open cup evaporation.

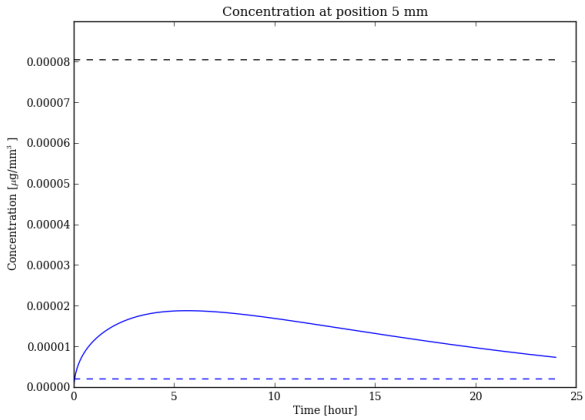


Figure 3.8: Concentration $5\,\mathrm{mm}$ from the cloth over $1$ day as obtained with the simulation code. Top dashed line is the saturation concentration, bottom dash required amount for repellency

Although the computational results match the experiment satisfactorily, not everything was taken into account. The following processes will lead to differences:

- The muslin cloth sample was soaked in a DEET solution in a closed cup and allowed to dry for $3$ to $5$ minutes after extraction from the cup. The closed cup will see a high DEET concentration, lowering the actual DEET concentration present in the muslin cloth. We estimate this can reduce the total DEET mass by a maximum of $1\,\mu\mathrm{g}$. As $5\,\mathrm{nmol/cm^2}$ corresponds to $30\,\mu\mathrm{g}$, this is a small error lowering the actual effectiveness.

- We assume in the model that all DEET is absorbed in the cotton fibers. In reality, some will remain attached to the surface, where it can evaporate rapidly at the beginning. This also reduces the amount of DEET present when the experiment starts. As the saturation concentration for DEET can be easily obtained close to the fiber in both cases for the absorbed concentrations considered, we estimate this effect to be negligible.

- The muslin cloth used in the original paper is not given, but can have some influence on the results. For the simulation we consider yarns that

are $0.6\,\mathrm{mm}$ apart (midline to midline), with a yarn radius of $0.105\,\mathrm{mm}$, consisting of $160$ cotton fibers of $5.2\,\mu\mathrm{m}$ radius, all values typical for cotton cloth. Tests with the simulation code show the effect of changes to be small within realistic variations.

- We consider a slow convection, driven by a boundary condition of $0$ sufficiently far from the muslin cloth. Any actual forced convection, as can be expected from time to time in an experimental environment, will reduce the DEET concentration more rapidly than the model considers. This can be assumed to have a large influence. We take it into account by setting the outside concentration to $0$ when movement occurs (moving the hand in a test cage), and add a minute of simulation time to determine a new initial outside concentration to work with.

- We give the DEET concentration at $1$ or $5\,\mathrm{mm}$ away from the target in Figs 3.6 and 3.8 as values to determine whether repellency is working or not. It could be that concentrations farther away from the muslin cloth must be considered for effective repellency (as the host attraction might overrule the DEET present at these distances). As DEET is considered to repel mosquitoes effectively, taking the value at $1\,\mathrm{mm}$ should be a good assumption for the cage test, while for static conditions $5\,\mathrm{mm}$ seems a good sampling position.

We conclude that these assumptions yield the same results as an actual bioassay using the known characteristics of DEET as the only input, and that, if not previously known, the minimum required concentration for repellency of a new product could, it appears, be determined by this method.

### 3.2.3 Slow-release

#### 3.2.3.1 Lab tests

The results obtained show that there is room to develop a slow-release adaptation. Such an application might require some time to achieve repellency, but would not be depleted as rapidly. Utexbel, a Belgian textile company, provided us with textile samples where DEET was embedded in a polymer coating. In this paper we do not concern ourselves with the actual polymer coating, which is an internal Utexbel product, but instead characterize it's effect. The coating process used was analogous to the one Utexbel has available for permethrin in their BuzzX (http://www.buzzx.info/) range of products. We wanted to investigate whether a slow-release system for DEET could be obtained like this, as permethrin has very low vapor pressure and is not considered to be volatile.

Different slow-release systems based on encapsulation have been tested before, [26, 37] with varying results. Depending on the encapsulation used, the release of DEET can be spread over 1week to several months. Encapsulation is an interesting technique, but obtaining the optimal release rate of repellent is not straightforward. It requires a step to create the capsules, and another step to bind the capsules to the fabric. A polymer coating technique has the advantage that it is a coating technique, comparable with other textile finishes. Which technique is preferred will depend on production considerations. The modeling presented can be adapted to simulate release by microcapsules, provided a model is available for how rapidly the capsules release DEET.

The samples received from Utexbel had to be characterized in terms of DEET content. Conducting mass balance experiments to determine the evaporation rate proved troublesome, as the polymer layer and textile will only slowly come to equilibrium when exposed to a different relative humidity. A test showed that, in a climate chamber, several hours were needed to reach equilibrium, during which the sample increased in weight. As a weight test would need to run longer than the time for which we could reserve the climate chamber, a chemical approach using GC-MS was chosen instead. The actual initial amount of DEET can be obtained in this way also. Hence, the samples were tested on arrival, and after $91$ days. In between, the samples were kept under a fume hood. GC-MS was used to determine the DEET and permethrin contents. A HP6890 series GC system coupled to a HP5973 MS system was used, with an injection volume of $1\mu\mathrm{l}$ for liquids. SPME stayed in the inlet for the whole run. The column used was HP-5MS, $30\,\mathrm{m} \times 0.25\,\mathrm{mm}$ I.D., $0.25\,\mu\mathrm{m}$ df, with as temperature program of $40°\mathrm{C}$ to $300°\mathrm{C}$ at $10°\mathrm{C/min}$. The liquid extractor analysis was done on strips of $4$ by $0.5\,\mathrm{cm}$ obtained from the samples. They were extracted with $3\,\mathrm{ml}$ methyl-tert-butyl-ether (MTBE) in a $4\,\mathrm{ml}$ vial. Sonication for $30\,\mathrm{min}$ provided $> 85\%$ recovery for the DEET and permethrin. Calibration was done with pure DEET and a stock solution of permethrin.

For permethrin, no reduction in concentration was found after $91$ days, as expected, because permethrin is not volatile. The results for DEET can be found in Table 3.8, where from the given measurements the long term evaporative flux $F_{\mathrm{evap}}$ is estimated, and also long-term values for $\tilde{k}_{\mathrm{evap}}$ and $h_{lg}$. Note that, for this, the fiber surface is used, and not the muslin cloth surface of $2\,\mathrm{cm}^2$. To obtain this fiber surface, we took into account that the samples were a blended fabric with $65\%$ cotton and $35\%$ polyester. The cotton fiber has an elliptical shape with average long axis of $0.0183\,\mathrm{mm}$ and short axis of $0.01339\,\mathrm{mm}$. The polyester fiber has average radius of $0.00551\,\mathrm{mm}$. There are $190$ fibers in a yarn, and $27$ yarns per $\mathrm{cm}$ in the vertical direction, and $43$ yarns per $\mathrm{cm}$ in the horizontal direction. As a consequence, we estimate the fiber surface where evaporation occurs to be $29$ times the fabric surface.

| Table 3.8: Experimental average values for liquid extraction and deduced parameters | | | | | | |
|---|---|---|---|---|---|---|
| Sample | Avg. DEET start $[\mathrm{nmol}\,/\,\mathrm{cm}^2]$ | Avg. DEET 91 days $[\mathrm{nmol}\,/\,\mathrm{cm}^2]$ | Diff. $[\mu g]$ | $F_{\mathrm{evap}}$ $[10^{-8}\frac{\mu g}{\mathrm{mm}^2\,\mathrm{s}}]$ | $\tilde{k}_{\mathrm{evap}}$ $[10^{-13}\frac{\mathrm{mm}}{\mathrm{s}}]$ | $h_{lg}$ $[10^{-4}\frac{\mathrm{mm}}{\mathrm{s}}]$ |
| A5 | 61.5 | 8 | 23.46 | 1.492 | 5.1 | 0.064 |
| C6 | 315 | 27.5 | 110.09 | 7.001 | 24 | 0.299 |
| A3 | 80 | 5 | 28.77 | 1.830 | 6.2 | 0.077 |
| C3 | 63 | 9 | 20.75 | 1.320 | 4.5 | 0.056 |

The polymer treatment reduced the release of DEET enormously, with $h_{lg}$ dropping from $0.897\,\mathrm{mm/s}$ in pure form to a value of $0.06 \cdot 10^{-4}$ and $-0.3 \cdot 10^{-4}\,\mathrm{mm/s}$, or a reduction of 29900 to 149500. However, in the deduction, we have assumed that the entire area of the fiber surface coating was available for evaporation, so $S = 1$. Previously, for the $25\,\mathrm{nmol/cm^2}$ dilution on cotton, we had, see (3.3), $S = 0.001$, so this cotton sample, which had good repellent properties, also had a reduction in evaporation compared to pure DEET of 1000. We conclude that a further reduction of 29.9 to 149.5 in evaporation speed was obtained after polymer coating. In other words, where Fig. 3.7 shows that the $25\,\mathrm{nmol/cm^2}$ sample was almost depleted after $24\,\mathrm{h}$, for the polymer coated version with the same concentration this would be around $24 \times 29.9\,\mathrm{h}$, or after 30 days. Compared with the required evaporation rate given in [26] of $F_{\mathrm{evap}} = 3.3 \pm 0.8 \cdot 10^{-6}\,\mu\mathrm{g}/(\mathrm{mm}^2\,\mathrm{s})$, the determined $F_{\mathrm{evap}}$ of our textile slow-release system seems to be 35 to 58-fold too low. Note, however, that the fiber surface of the textile is typically 25-30 times larger than the textile surface, so this discrepancy can be overcome by selection of the fabric used to construct the repellent textiles.

The estimates done are rough, but nevertheless give an idea of the order of magnitudes to work with. We are specifically lacking in knowledge about the polymer: how does DEET diffuse in the polymer, and how is the evaporation process working? We can deduce from Table 3.8 that evaporation of DEET will be higher at higher concentrations in the polymer. We have, however, too few data points to characterize the evaporation behavior fully. If we consider a least-squares fit through the points formed by the midpoint concentration $(C_{\text{start}} + C_{\text{91 days}})/2$, and the long-term computed $h_{lg}$ in Table 3.8 , we obtain

$$h_{lg} = 10^{-7}(4.9 + 2C), \tag{3.4}$$

where $C$ is the concentration on this textile ($\mathrm{nmol/cm^2}$).
For the modeling, we will make the following assumptions:

- We assume that the evaporation is not diffusion limited; that is, diffusion in the polymer is more rapid than evaporation, and no specific knowledge about the diffusion process is needed apart from the fact it is sufficiently rapid.
- Through lack of knowledge about the specific binding of DEET in the polymer, we will set $S = 1$ in equation (3.2), and use $h_{lg}$ from equation (3.4).
- The derivation of equation (3.4) is for the textiles tested. Other textiles can use the same formula provided their fiber surface area is comparable; that is, the evaporation rate depends on the DEET concentration in the polymer layer, not on the measured fabric surface concentration expressed in $\mathrm{nmol/cm^2}$.

As evaporation is now a slow-release process, this modeling will be adequate to obtain qualitative results. Having $S = 1$ and $h_{lg}$ fixed on the basis of equation (3.4) will make it possible to see the effectiveness of a textile over a typically night. We will consider a bed net that has a total fiber surface area comparable with that of the tested textiles, and consider an initial concentrations of $400, 200, 100$ and $50\,\mathrm{nmol/cm^2}$. With $S = 1$, this corresponds to mass transfer coefficients $h_{lg}$ of $8 \cdot 10^{-5}, 6 \cdot 10^{-5}, 4 \cdot 10^{-5}, 2 \cdot 10^{-5}$, and $10^{-5}$. A reduction from $400$ to $50\,\mathrm{nmol/cm^2}$ will occur over 3 to $4$ months, or, if carefully stored in a plastic bag and only used for $8\,\mathrm{h}$ a day, over a year. We do not simulate values above $400\,\mathrm{nmol/cm^2}$ although that is theoretically possible. This is because, based on Table 3.8, we cannot assume that equation (3.4) is still valid at higher concentrations.

The results of the simulation are shown in Fig. 3.9. Here, we see the effect of a sheet or curtain of the bed net textile put in the middle of a rectangular room. To interpret this figure, we need to consider that an actual bed net will consist of a sheet to the right and left of the bed, so the concentrations observed will be at least double that of a single sheet. As we are far from the saturation concentration of DEET, we can indeed approximate the effect of the bed net by doubling the simulation result, which is indicated with dashed lines in Fig. 3.9. The simulation uses a 1D representation of the room, so it is currently not possible to take the actual geometry of a testing hut (e.g. window traps) into account. As we indicated, the build-up of DEET around the bed net is slow. Considering the double action of a net, we reach protection against mosquitoes at $1\,\mathrm{mm}$ after $70\,\mathrm{min}$ for the $400\,\mathrm{nmol/cm^2}$ bed net. Further away from the bed net, more time is needed. Forced convection would spread the results faster

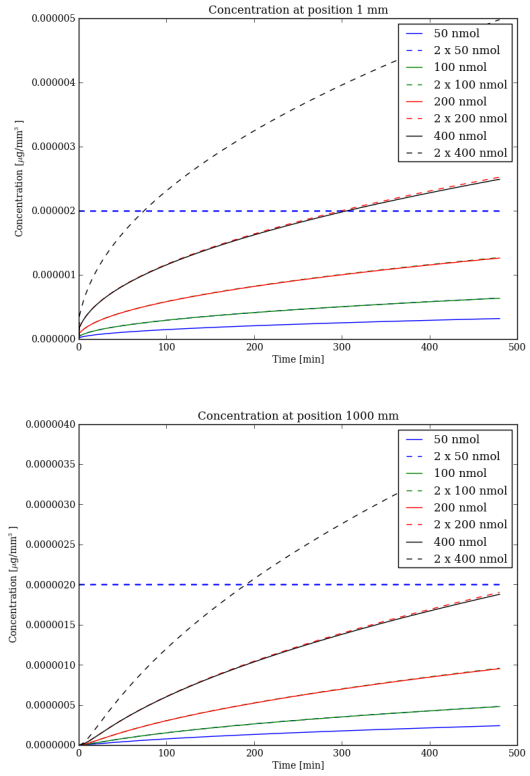


Figure 3.9: Concentration of DEET due to a single sheet of bed net material, at 1 mm and 1000mm from the curtain. The straight dashed line is the required amount for repellency. The dashed curves are the double of full lines to indicate the effect of a real bed net

over the room, which would have a positive effect. The actual ventilation of the room would have to be taken into account to match the experimental setup fully. This could lead to higher or lower values depending on whether the ventilation is lower or higher than considered in the model. The model uses a fixed boundary condition of $0$ DEET at $2.5\,\mathrm{m}$ to simulate the ventilation.

Qualitatively, we can deduce from the simulation that

1. A slow-release system does not give adequate protection for the first hour. In reality however, the product would be stored in a bag, which would create a build-up of DEET in the bag and in the void zones of the

textile. As a consequence, in reality, full protection might be present from the start, depending on when and where the bag is opened, if the forced convection is sufficiently low.

2. Over time, provided sufficient initial concentration is present, the bed net will provide full protection from mosquitoes present in the room. It therefore offers effective protection from entry via cuts or holes in the bed net.

3. To avoid entry of mosquitoes into the sleeping chamber, the slow-release system still needs more time. At $200\,\mathrm{nmol/cm^2}$, even after $8\,\mathrm{h}$, there is insufficient DEET at the entry points to prevent entry. As real rooms will have varying size, using a DEET-treated bed net commercially to avoid mosquitoes in the room does not seem feasible.

As a consequence, the following recommendation can be made:

1. To maximize the effective duration of the treated textiles, they would better be used only at the points of entry of the mosquitoes, e.g. as a curtain or scrim (light gauzy material).

2. It is useful to add DEET to bed nets so as to avoid biting through holes in the bed net or by body parts touching the bed net. However, the initial hours need to be overcome to achieve full protection. This could be done in other ways, e.g. by using a spray before going to bed.

3. In practical use, a consumer would need to be made well aware that a repellent textile has a limited durability, governed by the dose initially applied. Our modeled bed net with $400\,\mathrm{nmol/cm^2}$, corresponds to a use of only $76\,\mu\mathrm{g}$ DEET per $\mathrm{cm^2}$, which is a very modest use of repellent. If higher amounts can be added to a slow-release coating, a long adequate extra protection could be offered by comparison with current pyrethroid-only bed nets.

#### 3.2.3.2 Field tests

Based on knowledge gained, two types of bed nets (Utexbel types Y412 and Y335) were coated for field testing in the Cameroon. Field testing should realistically evaluate the efficacy of the slow-release system, as the technique will require an accumulation of active component, making a short arm-in-cage test in a small cage not indicative. At the same time, a field test can be considered as the gold standard for testing.

A total of five different coatings were prepared: DEET with and without washing binder, DEET combined with permethrin with and without washing

binder, and permethrin without washing binder. The washing binder should have no influence on the performance, it is needed for textile treated with permethrin to keep the permethrin stable and to avoid the polymer layer being removed by washing.

The DEET content was maximized as much as possible. As a consequence, the bed nets had an oily feel. A typical DEET odor could also be distinguished. For these reasons, the nets would probably not be marketable. As the fabrics used in GC-MS did not have this, we can conclude that the concentration is considerably higher than $400\,\mathrm{nmol/cm^2}$ obtained as maximum in those tests. Furthermore, the production process was manual. The upscaling of DEET application to an industrial finishing process involves some challenging issues, such as:

- environmental specifications concerning the volatile concentration in the ambient air and preventing operators from coming into contact with vapors;
- minimizing contamination of the process equipment;
- managing cleaning procedures;
- managing recycling issues;
- dealing with the aggressivity of DEET towards plastic parts, including end-user packaging.

Testing was done at the research institute REFOTDE Research Institute in Cameroon. The textiles where cut and knitted into usable bed nets. Three experimental huts in Meanja were used. At this location, the testing huts are between a breeding place and a small community. The testing schedule was based on a Latin square design, with a positive control present during all tests in a fixed hut, and one net in the other huts used for $4$ days. The nets were mounted each evening, remaining exposed for $12\,\mathrm{h}$ (from $6$ p.m. to $6$ a.m.), dismounted the next morning, kept in plastic bags and mounted again the next evening ($12\,\mathrm{h}$ a day for $4$ days).

A hut functionality test showed that $18.4\%$ of mosquitoes were captured inside the huts. An average number of $4.5$ mosquitoes per hut per night was found in this test. The dominant species was *Anopheles* ($50\%$), followed by *Mansonia* ($48\%$) and *Aedes* ($1\%$). A schematic of the sleeping hut is given in Fig. 3.10.

The results with the different nets are given in Table 3.9. Here, repellency is defined as the reduction in entry rate into a hut, while feeding inhibition is the reduction in feeding (control number - test number)/control number (%). In

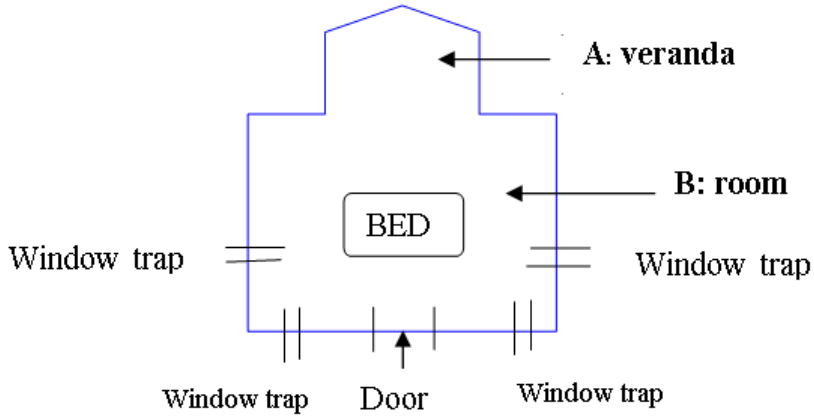


Figure 3.10: Top view schematic of the sleeping huts

the control, in which an untreated net was used, it is possible also to have no mosquitoes feeding over the $4$ days of testing.

From Table 3.9, we can see that the bed nets with DEET performed better than anticipated by the model: the DEET-treated bed nets could prevent mosquitoes from entering the hut (percentage repellency column), and in two cases even provided $100\%$ prevention. For the products with DEET, not a single fed mosquito was recorded. In the case of a traditional permethrin-treated net, we can see that the repellency dropped to $66$ à $77\%$, but the mosquitoes that entered were also prevented from feeding by the permethrin coating. The DEET-treated nets also caused all mosquitoes to be found on the veranda.

To substantiate that the products can survive storage, the nets were stored for $12$ months in plastic bags, and the best-performing nets were retested. The results of this retesting are in Table 3.10. Note that one product had a seriously reduced functionality, with the repellency dropping to $66\%$. The other three products, however, performed only slightly less well than in the original test.

### 3.2.4 Discussion and conclusion

We can conclude from the results that a slow-release system for DEET can be developed, and that the effect of DEET is discernible in field testing, giving the best possible protection. The slow-release is optimized in such a way that no excessive amount of DEET is used, maximizing the time to depletion.

We attribute the better performance than obtained by the model to a higher initial concentration than the $400\,\mathrm{nmol/cm^2}$, and to the preparation time before

Table 3.9: Bed net hut testing, showing the repellency and the feeding inhibition of the products. The amount of mosquitoes found in the control hut, and the amount of mosquitoes that fed in the control hut is also given

| Product | % Repel | % feeding inhibition | # mosq. control | # mosq. fed control |
|---|---|---|---|---|
| DEET+ BINDER Y421 | 100 | 100 | 16 | 0 |
| DEET+ BINDER Y335 | 97.5 | 100 | 16 | 0 |
| PERM.+DEET Y421 | 100 | 100 | 22 | 5 |
| PERM.+DEET Y335 | 97.5 | 100 | 22 | 5 |
| PERM.+DEET+BINDER Y421 | 95.2 | 100 | 13 | 2 |
| PERM.+DEET+BINDER Y335 | 95.2 | 100 | 13 | 2 |
| DEET Y421 | 97.6 | 100 | 43 | 8 |
| DEET Y335 | 97.6 | 100 | 43 | 8 |
| PERM. Y421 | 77.7 | 100 | 18 | 7 |
| PERM. Y335 | 66.6 | 100 | 18 | 7 |

the start of testing (6 p.m.), which reduced the time needed for building up an initial concentration of DEET in the sleeping huts.

However, the sleepers complained that the DEET nets were sticky and had an oily feel. The odor was also considered to be unpleasant overnight. As indicated previously, the production process also cannot be upscaled. All this indicates that further research should be carried out to bind a more pleasant repellent in a slow-release product, or to adapt the production process with DEET in a way that is feasible for industrial production. In this way, the high repellency (mosquitoes not entering the sleeping huts) values found when using DEET bed nets could become a reality for people around the world.

We have modeled repellent compounds being released from textile fabrics. Comparison with known results for DEET bioassays shows that the observed data, be it the active working duration of DEET or the dose response study, can be explained via the study. This opens up the possibility of determining the required effective air concentration of repellents by a coupling of the numerical

model and a bioassay. Next, a slow-release model has been developed for repellents applied to textile. In this model, the textile properties, specifically the effective fiber surface, can be adapted in such a way as to interact optimally with the reduced evaporation due to the polymer coating. A test was conducted with bed nets in the Cameroon, showing that this approach is viable. Further research should be done, however, to repeat this approach with a more pleasant repellent, or to convert the DEET coating technique to allow higher dosage in the textile fabric so as to achieve a longer durability. The modeling should also be extended so as to allow a correct representation of the room used and a correct inclusion of the effect of air movement on the repellent concentration in and around the textile. Based on the model of a slow-release product, we would nevertheless advise that slow-release products be considered mainly at the entry points, for example in the form of a scrim.

Table 3.10: Bed net hut retesting, showing the repellency and the feeding inhibition of the products. The amount of mosquitoes found in the control hut, and the amount of mosquitoes that fed in the control hut is also given

| Product | % Repel | % feeding inhibition | # mosq. control | # mosq. fed control |
|---|---|---|---|---|
| PERM.+DEET Y421 | 93.75 | 100 | 32 | 2 |
| PERM.+DEET Y335 | 93.75 | 100 | 32 | 2 |
| DEET Y421 | 98 | 100 | 66 | 2 |
| DEET Y335 | 66.66 | 100 | 66 | 2 |

CHAPTER 4

# Characteristic Times

As the previous article was the end-product of the more physical part of this thesis we now start the more mathematical part where the three scale diffusion model is further analyzed and where it is investigated how the model interacts on the different levels. Therefor it may be convenient to firstly explain the notion of characteristic times. Afterwards the exact reproduction of three A1-classified articles will be added where the analysis of these characteristic times is carried out:

1. 'Characteristic times for multiscale diffusion of active ingredients in coated textiles' as published in Journal of Computational and Applied Mathematics, by Elsevier in 2015;

2. 'Characteristic times and inverse problems for diffusion in coated textiles' as published in Applied Mathematics and Information Sciences, by NSP in 2015;

3. 'Characteristic times in a three scale model with overlapping domain decomposition' as accepted for publication in Journal of Computational and Applied Mathematics, by Elsevier in 2016.

The study of characteristic times for a partial differential equation representing a physical and/or chemical reaction of a system is key to understanding the system and its scaled components, in our case the three levels of the textile model and their interactions. At some particular moments in time the system

reaches an equilibrium, where the different levels in the model tend to continue the process cooperating as one level. Furthermore one of the characteristic times provides the physical concept of the average time a particle passes a certain point in space, another shows the time needed for a particle to travel from one position to some other position. To this end a C-language program was written as a simplification of the more complex STICK-toolbox that provides a visualization in a much shorter computation time, but still reaches satisfying accuracy for the mathematical analysis of the problem.

The characteristic times can be deduced from the moment-generating function and the cumulant-generating function. Therefor the diffusion problem should be seen from the earlier mentioned atomistic view of diffusion where it is considered as a result of the random walk of the diffusing particles, i.e. molecules or atoms of a substance. For a more elaborate explanation on random walks, the author would like to cite [30].

The cumulative distribution function $F(x)$ of a random variable $X$ describes the probability that the real-valued random variable $X$ with a given probability density function $f_X(x)$ will be found to have a value less than or equal to $x$ and

$$F(x) = \int_{-\infty}^{x} f_X(u)\,\mathrm{d}u.$$

This probability distribution alternatively also can be expressed as a moment-generating function $M_X(t)$ instead of the cumulative distribution $F(X)$, defined as the expected value of the exponential values of the random variable $X$ multiplied with a real-valued variable $t$

$$M_X(t) = E[e^{tX}] = \int_{-\infty}^{+\infty} e^{tx} f_X(x)\,\mathrm{d}x,$$

wherever this expectation exists. The $n$th moment of a distribution about a value $c$ is defined as

$$m_n = E[(x-c)^n] = \int_{-\infty}^{+\infty} (x-c)^n f_X(x)\,\mathrm{d}x.$$

The zeroth moment about $0$ is the total probability, the first moment about $0$ is the mean $\mu$ of the distribution. For the second and higher moments, the central moments i.e. moments about the mean, are usually used rather than the moments about zero, because they provide clearer information about the distribution's shape. The second central moment is the variance, $\sigma$ and the third central (normalized) moment is the skewness. Moments are normalized (or *standardized*) as

$$m_n^s = \frac{m_n}{\sigma^n}.$$

The moment-generating function $M_X(x)$ can be used to define each moment in a straightforward way because the Taylor expansion of the exponential function reads

$$e^{tX} = 1 + tX + \frac{(tX)^2}{2} + \frac{(tX)^3}{3!} + \cdots + \frac{(tX)^n}{n!} + \cdots,$$

hence

$$\begin{aligned} M_X(t) &= 1 + tE[X] + t^2\frac{E[X]^2}{2} + t^3\frac{E[X]^3}{3!} + \cdots + t^n\frac{E[X]^n}{n!} + \cdots \\ &= 1 + tm_1 + \frac{t^2}{2}m_2 + \frac{t^3}{3!}m_3 + \cdots + \frac{t^n}{n!}m_n + \cdots, \end{aligned}$$

where $m_n$ is the $n$th moment about $0$. As a consequence each moment can be derived from $M_X$ as

$$m_n = \left.\frac{\partial^i M_X(t)}{\partial t^i}\right|_{t=0}.$$

The cumulant-generating function is defined by

$$C_X(t) = \log(M_X(t)) = \log(E[e^{tX}]),$$

and generates the cumulants of the distribution

$$c_n = \left.\frac{\partial^i C_X(t)}{\partial t^i}\right|_{t=0},$$

which like the moments describe the shape of and information about the distribution.

If we now interpret the diffusive flux $\mathcal{F}_T(x)$ as the probability distribution function of all possible moments in time $T$ when a particle passes a certain point in space $x$ we can derive the moments of the distrubution of the random walk of particles in the diffusion problem. This can give information on how the system works, how the different levels interact and which characteristics of the textile are of high influence. The moment-generating function then is evaluated in $-s$

$$M_T(-s) = E_T[e^{-sT}] = \int_{-\infty}^{+\infty} e^{-st}\mathcal{F}_T(t)\,\mathrm{d}t = \mathcal{L}[\mathcal{F}_T(t)](s),$$

where $\mathcal{L}$ is the two-sided Laplace transform and $s$ is in the Laplace domain.

If we now take the logarithm of this moment-generating function in $-s$ we have the cumulant-generating function over the Laplace domain

$$C_T(-s) = \log(\mathcal{L}[\mathcal{F}_T(t)](s)) = c_0 - sc_1 + \frac{s^2}{2}c_2 - \cdots,$$

generating the first cumulant, i.e. the *residence time*,

$$\begin{aligned}
c_1 &= -\left.\frac{\partial}{\partial s} C_T(-s)\right|_{s=0} = -\left.\frac{\partial}{\partial s}\log M_T(-s)\right|_{s=0} \\
&= -\left.\frac{\partial}{\partial s}\log(\mathcal{L}[\mathcal{F}_T(t)](s))\right|_{s=0} \\
&= -\left.\frac{1}{\mathcal{L}[\mathcal{F}_T(t)](s)}\cdot\frac{\partial}{\partial s}(\mathcal{L}[\mathcal{F}_T(t)](s))\right|_{s=0} \\
&= -\left.\frac{1}{\left(m_0 - sm_1 + \frac{s^2}{2}m_2 - \cdots\right)}\cdot(-m_1 + m_2 s - \cdots)\right|_{s=0} \\
&= \frac{m_1}{m_0},
\end{aligned}$$

which equals the first moment if the zero'th moment equals one, and can be interpreted as the mean moment in time where a particle passes a certain point. The second cumulant, i.e. the *variance* of the distribution of possible moments in time is also an important characteristic time and is also related to the moments about zero:

$$\begin{aligned}
c_2 &= -\left.\frac{\partial^2}{\partial s^2} C_T(-s)\right|_{s=0} = -\left.\frac{\partial^2}{\partial s^2}\log M_T(-s)\right|_{s=0} \\
&= \frac{\partial}{\partial s}\left[-\frac{1}{\mathcal{L}[\mathcal{F}_T(t)](s)}\cdot\frac{\partial}{\partial s}(\mathcal{L}[\mathcal{F}_T(t)](s))\right]\Bigg|_{s=0} \\
&= -\left.\frac{(-m_1 + m_2 s - \cdots)^2}{\left(m_0 - sm_1 + \frac{s^2}{2}m_2 - \cdots\right)^2}\right|_{s=0} + \left.\frac{(m_2 - sm_3 + \cdots)}{\left(m_0 - sm_1 + \frac{s^2}{2}m_2 - \cdots\right)}\right|_{s=0} \\
&= \frac{m_2}{m_0} - \frac{m_1^2}{m_0^2}.
\end{aligned}$$

If $m_0$ equals 1, this second cumulant equals the second moment about the mean. For the third cumulant a analogous derivation can be made and it can be shown that it equals the third moment about the mean, $E[(T - m_1)^3]$. Also higher-order cumulants have a similar relation to the moments, although they are not longer equaling the moments about the mean. Each of these moments and cumulants are of importance as they are the characteristic times of the diffusion model as described in the following 3 sections.

## 4.1 Characteristic times for multiscale diffusion of active ingredients in coated textiles

**T. Goessens, R.H. De Staelen and D. Constales**

**published by Elsevier in Journal of Computational and Applied Mathematics, 2015.**
[doi:10.1016/j.cam.2014.10.015]

**Abstract** *A three-scale approach for textile models was given in [16]: a one-dimensional fiber model and a room model, with a meso-level in between, which is the yarn scale. To analyze and simplify the model, its characteristic times are investigated here. At these times the fiber and yarn model, and the yarn and room model, respectively, tend to reach a partial equilibrium concentration. The identification of these characteristic times is key in reducing the model to its variously scaled components when simplifying it.*

### 4.1.1 Introduction

We focus on the diffusion of a substance to the outer boundary of textiles. The fibers used to construct this fabric are coated with a polymer solution of an active ingredient (AI), e.g. an insect repellent, a perfume or a healing substance. This substance can easily be replaced by other volatiles. The goal is to investigate how much of the AI has to be present on the textile fiber and which polymer substance to use to coat the fiber so that the concentration at the outer boundary of the textile stays high enough for as long as required to be effective (e.g. repel or even kill mosquitoes, spread a noticeable odor for humans, have a healing effect ...).

The application in mind has the purpose to track the diffusion of an active component released by the fibers of an open textile structure, like a woven scrim, e.g. a gauze bandage. Models and algorithms for this application were based on [53, 59, 12, 33] and discussed in [16, 18, 17] where a meso-level model that describes the release of the active component in the yarn cross-section is included in between the standard fiber model and the room model. Upscaling from one level to another is done by volume averaging or overlapping domain decomposition (future work). Implementation was done in C language using lsoda, [39].

### 4.1.2 Characteristic times for the three-level diffusion

The governing system of equations of the complete three-level model is

$$\begin{cases} \dfrac{\partial C_f(\rho,t)}{\partial t} = \dfrac{1}{\rho}\dfrac{\partial}{\partial \rho}\left(\rho D_f \dfrac{\partial C_f(\rho,t)}{\partial \rho}\right), & \rho \in [\rho_{\min},\rho_{\max}] \quad (4.1a) \\ \dfrac{\partial C_y(r,t)}{\partial t} = \dfrac{1}{r}\dfrac{\partial}{\partial r}\left(r\dfrac{D_y}{\tau_y}\dfrac{\partial C_y(r,t)}{\partial r}\right) + \dfrac{1}{\epsilon}\Gamma_{\text{in}}(r,t), & r \in [0,R_y] \quad (4.1b) \\ \dfrac{\partial C_r(x,t)}{\partial x} = \dfrac{\partial}{\partial x}\left(D\dfrac{\partial C_r(x,t)}{\partial x}\right), & x \in [0,L] \quad (4.1c) \end{cases}$$

with a homogeneous Neumann BC at the left boundaries and an evaporation flux at the right boundaries for the fiber and yarn model (4.1a) and (4.1b):

$$\begin{aligned} &\frac{\partial C_f}{\partial \rho}(0,t) = 0, && -D_f\frac{\partial C_f}{\partial \rho}(\rho_{\max},t) = v_f(C_f(\rho_{\max},t) - C_y(r,t)), \\ &\frac{\partial C_y}{\partial r}(0,t) = 0, && -D_y\frac{\partial C_y}{\partial r}(R_y,t) = v_y(C_y(R_y,t) - C_r(0,t)). \end{aligned}$$

For the room model (4.1c) a homogeneous Neumann BC is present at the right boundary and at the left boundary there exists an evaporation flux coming from the concentration in the yarn evaporating to the room:

$$D\frac{\partial C_r}{\partial x}(0,t) = \alpha_{yr}v_x(C_r(0,t) - C_y(R_y,t)), \qquad \frac{\partial C_r}{\partial x}(L,t) = 0.$$

In the above system of equations (4.1) the subscript $f, y$ and $r$ stand for a quantity in the fiber, yarn and room respectively, $C$ represents the concentration of the AI, $D$ is the diffusion coefficient, $v$ is the evaporation speed and $\alpha_{yr}$ is a constant of proportion for the evaporation from yarn to room. The constants $\tau$ and $\epsilon$ are the tortuosity and porosity of the textile used. The term $\Gamma_{\text{in}}$ in (4.1b) is the volume averaged condensation/evaporation rate and is calculated as $\alpha_{fy}v_f(C_f(\rho_{\max}) - C_y(r))$ with $\alpha_{fy}$ the surface/volume ratio of the fiber.

At certain points in time equilibrium is essentially reached between the three models. Plotting the logarithmic concentration against the logarithmic time scale (Fig. 4.1) shows that, for standard parameters, after a rather short time (approximately $5\,\text{s}$) the yarn and room concentrations coincide, the fiber and yarn concentrations coincide at $100\,\text{s}$ and after approximately $1 \times 10^6\,\text{s}$ all concentrations reach the same value.

As an upscaling method volume averaging is used, the averaged outcome of one model serves as boundary conditions for the other.

These moments in time where equilibria are reached correspond with the systems characteristic times. These are the time scales $\tau$ for a particle to travel over a distance $x$ and on average these are given by $\tau^d \approx x^2/D$ for diffusion and $\tau^e = x/v$ for evaporation.

As a first estimation of these times one may calculate them by this rule of thumb for each of the levels as

$$\begin{cases} \tau_f^d = \frac{(\Delta\rho)^2}{D_f}, & \tau_f^e = \frac{\Delta\rho}{v_{\text{fiya}}}, \\ \\ \tau_y^d = \frac{(\Delta r)^2}{D_y}, & \tau_y^e = \frac{\Delta r}{v_{\text{yaro}}}, \end{cases}$$

where $v_{\text{fiya}}$ is the evaporation speed for the AI from the fiber surface to the yarn gaps, $v_{\text{yaro}}$ is the evaporation speed for the AI from the yarn surface to the room, $\Delta\rho$ and $\Delta r$ are the thickness of the fiber and yarn cross-section, and $D_f$ and $D_y$ are the respective diffusion coefficients of the first two levels.

A more precise way to calculate these characteristic times uses the Laplace transform of the flux. At interesting points of the system we interpret the diffusive flux $\mathcal{F}(x,t)$ as the probability distribution function of the times $T$ when a particle passes by position $x$. The moment-generating function is then related to the Laplace transform of the flux:

$$M_x(-s) = E_x(e^{-sT}) = \int_0^{+\infty} e^{-st}\mathcal{F}(x,t)dt = \mathcal{L}[\mathcal{F}(x,t)](s),$$

and the cumulant-generating function $g(-s)$ is the logarithm of the Laplace transform of the flux, where $s$ is in the Laplace domain.

Doing so, we are particularly interested in the first and second cumulants. The first cumulant is

$$c_1 = -\frac{\partial}{\partial s}g(s)\bigg|_{s=0} = -\frac{\partial}{\partial s}\left[\log(\mathcal{L}[\mathcal{F}(x,t)](s))\right]\bigg|_{s=0},$$

which is the mean of the probability distribution, i.e. the residence time of the diffusion equation or the average time it takes a particle to pass a certain point.

Also the second cumulant or the second derivative of the logarithm of the Laplace transform of the flux in $s = 0$, i.e. the variance of the flux, is useful for interpreting the system.

### 4.1.3 Calculation of the characteristic times

All of the characteristic values can be exactly calculated in function of the parameters in the above equations and will help to understand the diffusion in open textile structures. To calculate the exact characteristic times the Laplace transform of each of the three governing equations is taken.

The PDE for the fiber equation then is

$$s\mathcal{L}_f(\rho,s) - C_f(\rho,0) = D_f\frac{\partial^2}{\partial\rho^2}\mathcal{L}_f(\rho,s) + \frac{1}{\rho}D_f\frac{\partial}{\partial\rho}\mathcal{L}_f(\rho,s),$$

with

$$\rho_{\min} \leq \rho \leq \rho_{\max}, \quad s \in \mathbb{C}, \quad \Re(s) > \gamma_0$$

and Laplace transformed BC's

$$\left(\frac{\partial}{\partial\rho}\mathcal{L}_f\right)(\rho_{\min},s) = 0, \quad -D_f\left(\frac{\partial}{\partial\rho}\mathcal{L}_f\right)(\rho_{\max},s) = v_f(\mathcal{L}_f(\rho_{\max},s) - \mathcal{L}_y(r,s)),$$

where $\mathcal{L}_f = \mathcal{L}[C_f(\rho,t)](s)$ and $\mathcal{L}_y = \mathcal{L}[C_y(r,t)](s)$.

Solving for $\mathcal{L}_f(s)$ gives

$$\mathcal{L}_f(\rho,s) = \frac{C_f(\rho,0)}{s} + C_1\mathcal{I}_0\left(\frac{\sqrt{s}}{\sqrt{D}}\rho\right) + C_2\mathcal{K}_0\left(\frac{\sqrt{s}}{\sqrt{D}}\rho\right),$$

where $\mathcal{I}_i$ and $\mathcal{K}_i$ are the modified Bessel functions of the first and second kind, respectively, of order $i$. We define the characteristic time and the Peclet number of the equation as

$$t_f = \rho_{\max}^2/D_f, \qquad p_f = v_f\rho_{\max}/D_f.$$

The Laplace transformed BC on the right boundary of the fiber is rewritten in function of the initial concentration $C_f(\rho,0)$ because $C_f(\rho_{\max},t)$ is not yet known. One can notice that when the initial concentration equals the concentration in the immediate neighborhood of the fiber, i.e. $C_y(r)$, their is no longer any flux. This can be expressed in a way following naturally from the Laplace transformed PDE itself:

$$s\left(\mathcal{L}_f(\rho,s) - \frac{C_f(\rho,0)}{s}\right) = D_f\frac{\partial^2}{\partial\rho^2}\mathcal{L}_f(\rho,s) + \frac{1}{\rho}D_f\frac{\partial}{\partial\rho}\mathcal{L}_f(\rho,s),$$

so we can instead of taking the flux of $\mathcal{L}[C_f(\rho,t)]$ take the flux of $\mathcal{L}[C_f(\rho,t) - C_f(\rho,0)] \overset{\text{not.}}{=} \mathcal{L}_f - \frac{C_0}{s}$ at the right boundary and express it in terms that are known or are possible to be calculated, namely the difference between the initial concentration and the concentration in the immediate neighborhood of the fiber's right end. The BC on the right of the fiber domain then becomes

$$\frac{D_f}{v_f}\frac{\partial}{\partial\rho}\left(\mathcal{L}_f - \frac{C_0}{s}\right) = X\left(\mathcal{L}_y - \frac{C_0}{s}\right),$$

where $\mathcal{L}_y$ and $X$ (a dimensionless constant) will be determined further on.

Using the BC on the left of the fiber domain and the new BC on the right

we can determine $C_1$ and $C_2$ as

$$C_1 = \frac{p_f}{\sqrt{st_f}} \frac{X\left(\mathcal{L}_y(r,s) - \dfrac{C_0}{s}\right)}{\mathcal{I}_1\left(\sqrt{st_f}\dfrac{\rho_{\min}}{\rho_{\max}}\right)} \left[\frac{\mathcal{I}_1(\sqrt{st_f})}{\mathcal{I}_1\left(\sqrt{st_f}\dfrac{\rho_{\min}}{\rho_{\max}}\right)} - \frac{\mathcal{K}_1(\sqrt{st_f})}{\mathcal{K}_1\left(\sqrt{st_f}\dfrac{\rho_{\min}}{\rho_{\max}}\right)}\right]^{-1},$$

$$C_2 = \frac{p_f}{\sqrt{st_f}} \frac{X\left(\mathcal{L}_y(r,s) - \dfrac{C_0}{s}\right)}{\mathcal{K}_1\left(\sqrt{st_f}\dfrac{\rho_{\min}}{\rho_{\max}}\right)} \left[\frac{\mathcal{I}_1(\sqrt{st_f})}{\mathcal{I}_1\left(\sqrt{st_f}\dfrac{\rho_{\min}}{\rho_{\max}}\right)} - \frac{\mathcal{K}_1(\sqrt{st_f})}{\mathcal{K}_1\left(\sqrt{st_f}\dfrac{\rho_{\min}}{\rho_{\max}}\right)}\right]^{-1}.$$

These choices for the constant make sure the BC's are satisfied because

$$\frac{\partial}{\partial x}\mathcal{I}_0(x) = \mathcal{I}_1(x) \qquad \text{and} \qquad \frac{\partial}{\partial x}\mathcal{K}_0(x) = -\mathcal{K}_1(x),$$

and

$$(\mathcal{L}_f(\rho_{\max},s) - \mathcal{L}_y(r,s)) = X\left(\frac{C_f(\rho,0)}{s} - \mathcal{L}_y(r,s)\right),$$

with the dimensionless $X$ defined as

$$\begin{aligned} X &= \left[1 + \frac{p_f}{\sqrt{st_f}} \frac{\dfrac{\mathcal{I}_0(\sqrt{st_f})}{\mathcal{I}_1\left(\sqrt{st_f}\dfrac{\rho_{\min}}{\rho_{\max}}\right)} + \dfrac{\mathcal{K}_0(\sqrt{st_f})}{\mathcal{K}_1\left(\sqrt{st_f}\dfrac{\rho_{\min}}{\rho_{\max}}\right)}}{\dfrac{\mathcal{I}_1(\sqrt{st_f})}{\mathcal{I}_1\left(\sqrt{st_f}\dfrac{\rho_{\min}}{\rho_{\max}}\right)} - \dfrac{\mathcal{K}_1(\sqrt{st_f})}{\mathcal{K}_1\left(\sqrt{st_f}\dfrac{\rho_{\min}}{\rho_{\max}}\right)}}\right]^{-1} \\ &= \frac{t_f}{2p_f}\left(1 - \frac{\rho_{\min}^2}{\rho_{\max}^2}\right)s + \cdots. \end{aligned}$$

It is straightforward to prove that the function $\mathcal{L}_f$ with these constants is a solution of the given fiber equation and complies to the constraints.

For the yarn model the Laplace transformed equation is given by

$$s\mathcal{L}_y(r,s) = D_y\frac{\partial^2}{\partial r^2}\mathcal{L}_y(r,s) + \frac{1}{r}D_y\frac{\partial}{\partial r}\mathcal{L}_y(r,s) + \frac{S_2}{s} - S_1\mathcal{L}_y(r,s), \quad 0 \le r \le R_y,$$

where the volume averaged condensation/evaporation rate $\Gamma_{\text{in}}$ is calculated as $\alpha_{fy}v_f(C_f(\rho_{\max}) - C_y(r))$ with $\alpha_{fy}$ the surface/volume ratio $\dfrac{2}{\rho_{\max}}$ and using

the above equality to get $\Gamma_{\text{in}} = \dfrac{2v_f X}{\rho_{\max}}(C_{0,f} - C_y(r))$. This leads to

$$S_1 = 2\frac{p_f}{t_f}X = \frac{2v_f X}{\rho_{\max}},$$
$$S_2 = 2\frac{p_f}{t_f}XC_0 = \frac{2v_f XC_0}{\rho_{\max}}.$$

The BC's are

$$\left(\frac{\partial}{\partial r}\mathcal{L}_y\right)(0,s) = 0, \qquad -D_y\left(\frac{\partial}{\partial r}\mathcal{L}_y\right)(R_y,s) = v_y(\mathcal{L}_y(R_y,s) - \mathcal{L}_r(0,s)),$$

with $\mathcal{L}_r(x,s) = \mathcal{L}[C_r(x,t)](s)$.

Solving for $\mathcal{L}_y$ gives

$$\mathcal{L}_y(r,s) = \frac{S_2}{s(s+s_1)} + C_1\mathcal{I}_0\left(\sqrt{\frac{s+S_1}{D_y}}r\right) + C_2\mathcal{K}_0\left(\sqrt{\frac{s+S_1}{D_y}}r\right).$$

Since $\mathcal{K}_1(0)$ is not defined the left BC immediately gives $C_2 = 0$. We again rewrite the BC on the right of the yarn in function of the initial concentration value inspired by the Laplace transformed PDE

$$s\mathcal{L}_y(r,s) - \frac{S_2}{s} + S_1\mathcal{L}_y(r,s) = D_y\frac{\partial^2}{\partial r^2}\mathcal{L}_y(r,s) + \frac{1}{r}D_y\frac{\partial}{\partial r}\mathcal{L}_y(r,s),$$

or

$$(s+S_1)\left(\mathcal{L}_y(r,s) - \frac{S_2}{s(s+S_1)}\right) = D_y\frac{\partial^2}{\partial r^2}\mathcal{L}_y(r,s) + \frac{1}{r}D_y\frac{\partial}{\partial r}\mathcal{L}_y(r,s).$$

This means we can look at the difference in concentration in the yarn and the surrounding air and introduce a new dimensionless parameter Y such that

$$\mathcal{L}_y(R_y,s) - \mathcal{L}_r(0,s) = Y\left(\frac{S_2}{s(s+S_1)} - \mathcal{L}_r(0,s)\right),$$

leading to the BC at $r = R_y$,

$$\frac{D_y}{v_y}\frac{\partial}{\partial r}\left(\mathcal{L}_y(r,s) - \frac{S_2}{s(s+S_1)}\right) = Y\left(\mathcal{L}_r(0,s) - \frac{S_2}{s(s+S_1)}\right).$$

Here $S_1$ and $S_2$ are defined as above, we use the characteristic time and Peclet number for the yarn equation defined as

$$t_y = R_y^2/D_y, \qquad p_y = v_y R_y/D_y,$$

and

$$Y = \left[1 + \frac{\mathcal{I}_0\left(\sqrt{(s+S_1)t_y}\right)}{\mathcal{I}_1\left(\sqrt{(s+S_1)t_y}\right)} \frac{p_y}{\sqrt{(s+S_1)t_y}}\right]^{-1} = \frac{1}{2}\frac{t_y}{p_y}\left(2 - \frac{\rho_{\min}^2}{\rho_{\max}^2}\right)s + \cdots .$$

This $Y$ makes sure the BC can be expressed in terms of the initial concentration and the concentration on a higher level $\mathcal{L}_r$ which can be calculated from the Laplace transformed room PDE. This new BC leads to

$$\begin{aligned} C_1 &= \frac{Y\left(\mathcal{L}_r(0,s) - \dfrac{S_2}{s(s+S_1)}\right)}{\mathcal{I}_1\left(\sqrt{(s+S_1)t_y}\right)} \frac{p_y}{\sqrt{(s+S_1)t_y}} \\ &= \frac{\left(\mathcal{L}_r(0,s) - \dfrac{S_2}{s(s+S_1)}\right)}{\mathcal{I}_0\left(\sqrt{(s+S_1)t_y}\right) + \mathcal{I}_1\left(\sqrt{(s+S_1)t_y}\right)\dfrac{\sqrt{(s+S_1)t_y}}{p_y}}. \end{aligned}$$

Doing so we find

$$\mathcal{L}_y(s) = \frac{S_2}{s(s+s_1)} + \frac{\left(\mathcal{L}_r(0,s) - \dfrac{S_2}{s(s+S_1)}\right)\mathcal{I}_0\left(\dfrac{\sqrt{(s+S_1)t_y}}{R_y}r\right)}{\mathcal{I}_0\left(\sqrt{(s+S_1)t_y}\right) + \mathcal{I}_1\left(\sqrt{(s+S_1)t_y}\right)\dfrac{\sqrt{(s+S_1)t_y}}{p_y}}.$$

Again, it is not hard to prove that this $\mathcal{L}_y$ is a solution of the above yarn equation that satisfies the given BC's.

To be able to find the constants in $\mathcal{L}_f$ and $\mathcal{L}_y$ on the fiber and yarn level we search for a solution on the room level. For the room PDE the Laplace transform gives

$$s\mathcal{L}[C_r(x,t)](s) = D\frac{\partial^2}{\partial x^2}\mathcal{L}[C_r(x,t)](s), \quad 0 \le x \le L,$$

with BC's

$$\begin{aligned} D\left(\frac{\partial \mathcal{L}_r}{\partial x}\right)(0,s) &= \alpha_{yr}v_x\left(\mathcal{L}[C_r(0,t)](s) - \mathcal{L}[C_y(R_y,t)](s)\right), \\ \left(\frac{\partial \mathcal{L}_r}{\partial x}\right)(L,s) &= 0, \end{aligned}$$

with $\alpha_{yr}$ the ratio of active yarn surface to the surface of the left wall of the room. Solving for $\mathcal{L}_r(x,s)$ gives

$$\mathcal{L}_r(x,s) = C_1 \exp\left(\sqrt{\frac{s}{D}}x\right) + C_2 \exp\left(-\sqrt{\frac{s}{D}}x\right).$$

Using the BC in $x = L$ gives

$$C_1 = \frac{C_2\sqrt{\frac{s}{D}}\exp\left(-\sqrt{\frac{s}{D}}L\right)}{\sqrt{\frac{s}{D}\exp\left(\sqrt{\frac{s}{D}}L\right)}},$$

which leads to

$$\mathcal{L}_r(x,s) = \frac{2\,C_2\cosh\left(\sqrt{\frac{s}{D}}L\right)\cosh\left(\sqrt{\frac{s}{D}}x\right) - 2\,C_2\sinh\left(\sqrt{\frac{s}{D}}L\right)\sinh\left(\sqrt{\frac{s}{D}}x\right)}{\cosh\left(\sqrt{\frac{s}{D}}L\right) + \sinh\left(\sqrt{\frac{s}{D}}L\right)}.$$

Using the flux of the first BC in $x = 0$ and defining

$$t_x = \frac{L^2}{D}, \qquad p_x = \frac{v_x L}{D},$$

we find the correct $C_2$ and

$$\mathcal{L}_r(x,s) = \frac{p_x\cosh\left(\sqrt{st_x}\left(1-\frac{x}{L}\right)\right)Y\left(\frac{S_2}{s(s+S_1)} - \mathcal{L}_r(0,s)\right)}{\sinh\left(\sqrt{st_x}\right)\sqrt{st_x}}, \tag{4.2}$$

where $\mathcal{L}_r(0,s)$ can be calculated by putting $x = 0$ in (4.2). Using this and the previously found expression for $Y$ we arrive at a solution for the Laplace transformed room PDE

$$\mathcal{L}_r(x,s) = \frac{S_2}{s(s+S_1)}\frac{\cosh((1-x/L)\sqrt{st_x})}{\cosh\sqrt{st_x}} \cdot\left[1 + \left(1 + \frac{p_y}{\sqrt{(s+S_1)t_y}}\frac{\mathcal{I}_0(\sqrt{(s+S_1)t_y})}{\mathcal{I}_1(\sqrt{(s+S_1)t_y})}\right)\frac{\sqrt{st_x}\sinh\sqrt{st_x}}{p_x\cosh\sqrt{st_x}}\right]^{-1}.$$

This $\mathcal{L}_r$ is a solution of the room PDE satisfying the BC's. Because on the right of the room domain a zero flux is imposed it is possible to calculate $X$ and $Y$ and as a consequence the constants in the PDE solutions on the yarn and fiber level respectively.

To calculate the characteristic times, i.e. the first and second moment, and the residence time of diffusion and the variance of the flux, i.e. the first and second cumulant of the system, we look at the flux of the above found solutions $-D_f\frac{\partial\mathcal{L}_f}{\partial\rho}$, $-D_y\frac{\partial\mathcal{L}_y}{\partial r}$ and $-D\frac{\partial\mathcal{L}_r}{\partial x}$.

For the first and second moments we write the fluxes to their series expansion and look for the constant term and the coefficient of $-s$.

$$M_{0,f} = \frac{D_f}{2}\frac{t_f\,\left(\rho^2 - {\rho_{\min}}^2\right)\left(p_x\,t_y + 2\,p_y\,t_x\right)C_0}{\left(2\,p_x\,\rho_{\max}{}^2 t_y - p_x\,\rho_{\min}{}^2 t_y + 2\,p_y\,\rho_{\max}{}^2 t_x\right)\rho},$$

$$M_{0,y} = D_y \frac{t_y\, r\, \left({\rho_{\max}}^2 - {\rho_{\min}}^2\right)\, C_0\, p_y\, t_x}{{R_y}^2\, (2\, p_x\, {\rho_{\max}}^2 t_y - p_x\, {\rho_{\min}}^2 t_y + 2\, t_x\, p_y\, {\rho_{\max}}^2)},$$

$$M_{0,r} = D \frac{t_x\ (L-x)\, \left({\rho_{\max}}^2 - {\rho_{\min}}^2\right)\, C_0\, p_x\, t_y}{(2\, p_x\, {\rho_{\max}}^2 t_y - p_x\, {\rho_{\min}}^2 t_y + 2\, t_x\, p_y\, {\rho_{\max}}^2)\, L^2},$$

$$\begin{aligned}
M_{1,f} &= D_f \frac{\partial}{\partial s} \left( \frac{\partial \mathcal{L}_f}{\partial \rho}(s) \right) \Bigg|_{s=0}, & M_{2,f} &= D_f \frac{\partial^2}{\partial s^2} \left( \frac{\partial \mathcal{L}_f}{\partial \rho}(s) \right) \Bigg|_{s=0}, \\
M_{1,y} &= D_y \frac{\partial}{\partial s} \left( \frac{\partial \mathcal{L}_y}{\partial r}(s) \right) \Bigg|_{s=0}, & M_{2,y} &= D_y \frac{\partial^2}{\partial s^2} \left( \frac{\partial \mathcal{L}_y}{\partial r}(s) \right) \Bigg|_{s=0}, \\
M_{1,r} &= D \frac{\partial}{\partial s} \left( \frac{\partial \mathcal{L}_r}{\partial x}(s) \right) \Bigg|_{s=0}, & M_{2,r} &= D \frac{\partial^2}{\partial s^2} \left( \frac{\partial \mathcal{L}_r}{\partial x}(s) \right) \Bigg|_{s=0}.
\end{aligned}$$

The cumulants $c_1$ and $c_2$ can be found from the chain rule for

$$\begin{aligned}
c_{1,f} &= -\frac{\partial}{\partial s} \left[ \log \left( \frac{\partial \mathcal{L}_f}{\partial \rho}(s) \right) \right] \Bigg|_{s=0} = \frac{M_{1,f}}{M_{0,f}}, \\
c_{2,f} &= \frac{\partial^2}{\partial s^2} \left[ \log \left( \frac{\partial \mathcal{L}_f}{\partial \rho}(s) \right) \right] \Bigg|_{s=0} = \frac{M_{2,f}}{M_{0,f}} - \left( \frac{M_{1,f}}{M_{0,f}} \right)^2,
\end{aligned}$$

and analogously for the other cumulants.

### 4.1.4 Application

As a illustration of the theory above we now take some fixed values for the quantities in the found equations. The data we will work with is

$$\begin{aligned}
\alpha_{fy} &= 1\,\mathrm{m}^{-1}, & v_f &= 1\,\mathrm{m}/\mathrm{s}, \\
\alpha_{yr} &= 1, & v_y &= 1\,\mathrm{m}/\mathrm{s}, \\
\rho_{\min} &= 0.0000\,\mathrm{m}, & v_x &= 1\,\mathrm{m}/\mathrm{s}, \\
\rho_{\max} &= 0.0001\,\mathrm{m}, & D_f &= 1 \times 10^{-10}\,\mathrm{m}^2/\mathrm{s}, \\
R_y &= 0.001\,\mathrm{m}, & D_y &= 1 \times 10^{-6}\,\mathrm{m}^2/\mathrm{s}, \\
L &= 5\,\mathrm{m}, & D &= 1 \times 10^{-5}\,\mathrm{m}^2/\mathrm{s}, \\
C_0 &= 1\,\mathrm{mg}/\mathrm{m}^3, &&
\end{aligned} \tag{4.3}$$

and we will run the code using $\Delta t = 1 \times 10^{-8}$ as the initial time step for the yarn and room model, $\Delta t_f = 1.01$ for the scale factor used to get the geometric sequence of time values for calculations and plotting, $n_f = 20$ , $n_y = 20$ and $n_r = 40$ for the number of cells in the respective models.

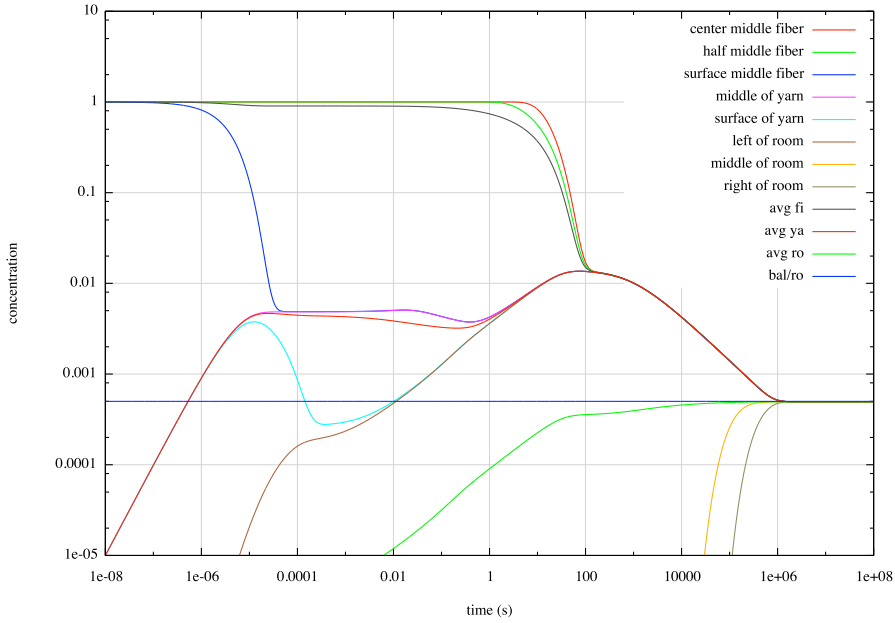


Figure 4.1: Log-log plot of the concentrations in function of time for the data (4.3)

For this example we find for the middle of the room, fiber and yarn, i.e. $x = 2.5$, $\rho = 0.00005$, $r = 0.0005$, the residence times (mean of the flux) and variances of the flux in Table 4.1.

Table 4.1: Cumulants for the middle of the fiber, yarn and room

| Cumulant | Fiber | Yarn | Room |
|---|---|---|---|
| $c_1$ | $105.37010\,\mathrm{s}$ | $179.57059\,\mathrm{s}$ | $3.12679 \times 10^5\,\mathrm{s}$ |
| $\sqrt{c_2}$ | $5271.88198\,\mathrm{s}$ | $7454.84040\,\mathrm{s}$ | $2.55264 \times 10^5\,\mathrm{s}$ |

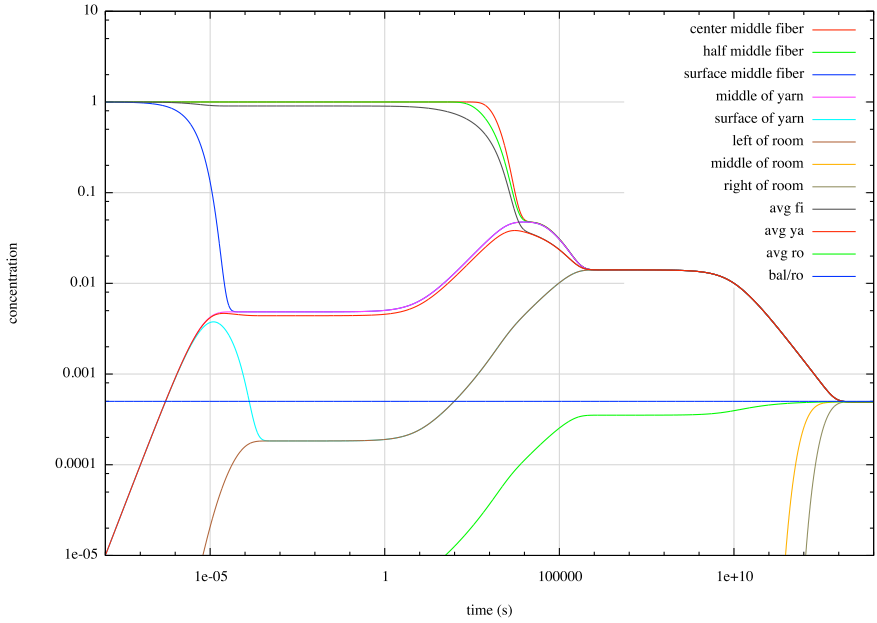


Figure 4.2: Log-log plot of the concentrations in function of time for the data (4.3), but with diminished diffusion coefficients to $1 \times 10^{-12}\,\mathrm{m}^2\,/\,\mathrm{s}$

These values are also visible in the plot of the logarithmic concentration vs. the logarithmic time scale. They correspond to the times where the concentration of the fiber in the middle of the yarn cross-section and that in the middle of the room coincide, and the moment where the latter concentration reaches equilibrium with the room concentration. This means the plot supports the calculated values of the residence times. By enlarging or diminishing some parameters, for example the diffusion coefficients, the plots also suggests the residence times have to shift to the left or right, see Fig. 4.2. This is in accordance with calculated values.

### 4.1.5 Conclusion and future work

A three-scale model consisting of a micro-, meso- and macrolevel was implemented in C language. Upscaling was done by volume averaging for the concentration calculated from the smaller level to serve as a source term and BC for the larger level. This can be adapted to the previously used overlapping domain decomposition method. Characteristic times were confirmed using the Laplace transform of the flux.

## 4.2 Characteristic times and inverse problems for diffusion in coated textiles

**T. Goessens, R.H. De Staelen and D. Constales**

**published by NSP in Applied Mathematics and Information Sciences, 2015.**
[doi:10.12785/amis/092L09]

**Abstract** *We study diffusion of active ingredients in coated textiles by a three-scale model. These scales consist of a fiber level representing the fiber with its polymer coating containing an active ingredient, a yarn level, and the level of the room holding the textile. An analysis of the model is carried out using the characteristic times of the different levels. We investigate the influence of the parameters in the model by solving several inverse problems.*

### 4.2.1 Introduction

We study the diffusion of a volatile trapped in a polymer coating on textiles fibers. These fibers are used to construct an intelligent textile. The coating consists of a polymer solution of an active ingredient (AI), e.g. an insect repellent, a perfume or a healing substance. This substance can easily be replaced by other volatiles. The goal is to slow down the release of the AI in order to increase the active lifetime of the textile. We want to investigate how much of the AI has to be present on the textile fiber and which polymer substance to use, to coat the fiber so that the concentration at the outer boundary of the textile stays high enough for as long as required to be effective (e.g. repel or even kill mosquitoes, spread a noticeable odor for humans, have a healing effect ...). Therefore a forward problem is implemented in C-language and an inverse problem is solved using the Levenberg-Marquardt method. The forward model consists of a three-scale approach based upon [53, 59, 12, 33] . The model is given in [16]: a one-dimensional cylindrical diffusion equation on the fiber and yarn levels and a one-dimensional diffusion model for the room. To analyse and simplify the model, its characteristic times are further investigated in this paper. At these times the fiber and yarn model, and the yarn and room model, respectively, tend to reach an equilibrium concentration. The identification of these characteristic times is key in reducing the model to its variously scaled components when simplifying it.

The characteristic times are calculated using Laplace transformation based on [15] and compared to generated outcomes of the model. Implementation of both the forward as the inverse problem was done in C-language using `lsoda` [39] and the `fit` command in `Gnuplot`.

### 4.2.2 Characteristic times for the three-level diffusion

The governing system of equations of the complete three-level model [16] is

$$\begin{cases} \dfrac{\partial C_f(\rho,t)}{\partial t} &= \dfrac{1}{\rho}\dfrac{\partial}{\partial \rho}\left(\rho D_f \dfrac{\partial C_f(\rho,t)}{\partial \rho}\right), \\ \epsilon\dfrac{\partial C_y(r,t)}{\partial t} &= \dfrac{1}{r}\dfrac{\partial}{\partial r}\left(\epsilon r D_y \dfrac{\partial C_y(r,t)}{\partial r}\right) + \Gamma_{\text{in}}(\Omega,t), \\ \dfrac{\partial C_{\text{r}}(x,t)}{\partial x} &= \dfrac{\partial}{\partial x}\left(D\dfrac{\partial C_{\text{r}}(x,t)}{\partial x}\right), \end{cases}$$

with $\rho \in [R_f,2R_f]$, $r \in [0,2R_y]$ and $x \in [R_y, L]$. There is an evaporation flux at the right boundaries for the fiber and yarn model, and a homogeneous Neumann BC at their left boundaries. For the room model a homogeneous Neumann BC is present at the right boundary and an evaporation flux at the left boundary coming from the concentration in the yarn evaporating to the room.

The concentration of the AI is tracked starting in the fiber coating. Once the outer boundary of the coating is reached the AI is evaporating to the yarn air gaps, and further on to the outside of the textile into the room. Plotting the logarithmic concentration against the logarithmic time scale shows that, for standard parameters, after a rather short time (approximately $100\,\text{s}$) the fiber and yarn concentrations coincide and after approximately $10 \times 10^6\,\text{s}$ those concentrations coincide with the concentration in the middle of the room, see Fig. 4.3. We will further investigate these moments in time where equilibrium is reached between the different levels to have a better understanding of the interactions in the model and to be able to predict when the concentration of the AI reaches a certain position in the textile and in the room. As a consequence it becomes possible to adjust the textile product to the standards needed.

A way to calculate these characteristic times uses the Laplace transform of the flux. At interesting points of the system we interpret the diffusive flux $\mathcal{F}_T(x)$ as the probability distribution function of the times $T$ when a particle passes a certain position $x$. The moment-generating function is then related to the Laplace transform of the flux:

$$M_T(-s) = E_T(e^{-sT}) = \int_0^{+\infty} e^{-st}\mathcal{F}_T(t)dt = \mathcal{L}[\mathcal{F}_T(t)](s).$$

A series expansion of this function

$$\mathcal{L}[\mathcal{F}_T(t)](s) = M_0 - M_1 s + M_2\frac{s^2}{2!} - M_3\frac{s^3}{3!} + ...,$$

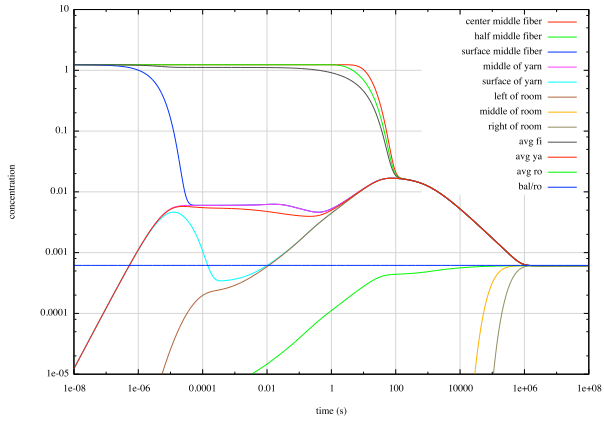


Figure 4.3: Logarithmic concentration vs logarithmic time with $D_f = 1 \times 10^{-10} \frac{\text{mm}^2}{\text{s}}$, $D_y = 1 \times 10^{-6} \frac{\text{mm}^2}{\text{s}}$ and $D = 1 \times 10^{-5} \frac{\text{mm}^2}{\text{s}}$

gives the respective moments of the probability distribution function, e.g. the mean $M_0$ and variance $M_1$. We also look at the series expansion of the cumulant-generating function $g(-s)$, i.e. the logarithm of the Laplace transform of the flux, where $s$ is in the Laplace domain. The cumulants are given by

$$c_n = \frac{\partial^n}{\partial s^n} g(-s)\bigg|_{s=0}.$$

We are particularly interested in the first and second cumulant. The first cumulant is

$$c_1 = \frac{\partial}{\partial s} \left[\log(\mathcal{L}[\mathcal{F}_T(t)](s))\right]\bigg|_{s=0},$$

which is the mean of the probability distribution, i.e. the residence time of the diffusion equation or the average time it takes a particle to pass a certain point. Also the second cumulant or the second derivative of the logarithm of the Laplace transform of the flux in $s = 0$, i.e. the variance of the logarithmic flux, is useful for interpreting the system. All of the characteristic values can be exactly calculated in function of the parameters in the above equations and will help to understand the diffusion in open textile structures.

### 4.2.3 Calculation of the characteristic times

To calculate the exact characteristic times the Laplace transformation of each of the three governing equations is taken. More details can be found in [15].

We use the notation $\mathcal{L}_f = \mathcal{L}[C_f(\rho,t)](s)$, $\mathcal{L}_y = \mathcal{L}[C_y(r,t)](s)$ and $\mathcal{L}_r = \mathcal{L}[C_r(x,t)](s)$ and introduce the function

$$\mathcal{B}_n(x,y) = \frac{\mathcal{I}_n(\sqrt{s\,t_f}\,x)}{\mathcal{I}_1(\sqrt{s\,t_f}\,y)} + (-1)^n \frac{\mathcal{K}_n(\sqrt{s\,t_f}\,x)}{\mathcal{K}_1(\sqrt{s\,t_f}\,y)},$$

which is a combination of modified Bessel functions of first and second kind, where $t_f = \frac{\rho_{\max}^2}{D_f}$ is the diffusion time.

For the fiber equation we define

$$X = \left[1 + \frac{p_f}{\sqrt{s\,t_f}} \frac{\mathcal{B}_0(1,\frac{\rho_{\min}}{\rho_{\max}})}{\mathcal{B}_1(1,\frac{\rho_{\min}}{\rho_{\max}})}\right]^{-1} = \frac{t_f}{2p_f}\left(1 - \frac{\rho_{\min}^2}{\rho_{\max}^2}\right) s + \cdots,$$

where $p_f = \frac{t_f}{t_{ff}}$ is the Peclet number for the fiber level and $t_{ff} = \frac{\rho_{\max}}{v_f}$ is the transport time.

This dimensionless $X$ makes sure the BC on the right can be written in the form

$$\frac{D_f}{v_f}\frac{\partial}{\partial\rho}\left(\mathcal{L}_f - \frac{C_0}{s}\right) = X\left(\mathcal{L}_y - \frac{C_0}{s}\right),$$

which we can use to calculate $\mathcal{L}_f$ once we have $\mathcal{L}_y$ as

$$\mathcal{L}_f(\rho,r,s) = \frac{C_0}{s} + \left(\mathcal{L}_y(r,s) - \frac{C_0}{s}\right) \cdot \frac{\mathcal{B}_0(\frac{\rho}{\rho_{\max}},\frac{\rho_{\min}}{\rho_{\max}})}{\mathcal{B}_0(1,\frac{\rho_{\min}}{\rho_{\max}}) + \frac{\sqrt{s\,t_f}}{p_f}\mathcal{B}_1(1,\frac{\rho_{\min}}{\rho_{\max}})}.$$

For the yarn level the same strategy is followed taking the Laplace transformed equation and solving it for $\mathcal{L}_y(r,s)$, with

$$S_1 = 2\frac{p_f}{t_f}X = \frac{2v_f X}{\rho_{\max}}, \quad S_2 = 2\frac{p_f}{t_f}XC_0 = \frac{2v_f XC_0}{\rho_{\max}},$$

and

$$Y = \left[1 + \frac{\mathcal{I}_0\left(\sqrt{(s+S_1)t_y}\right)}{\mathcal{I}_1\left(\sqrt{(s+S_1)t_y}\right)} \frac{p_y}{\sqrt{(s+S_1)t_y}}\right]^{-1} = \frac{1}{2}\frac{t_y}{p_y}\left(2 - \frac{\rho_{\min}^2}{\rho_{\max}^2}\right) s + \cdots,$$

where we use the diffusion time, the Peclet number for the yarn level and the transport time for the yarn equation defined as

$$t_y = r_{\max}^2/D_y, \quad p_y = v_y r_{\max}/D_y = t_y/t_{fy}, \quad t_{fy} = r_{\max}^2/v_y.$$

The BC on the right can again be written as

$$\mathcal{L}_y(R_y,s) - \mathcal{L}_r(0,s) = Y\left(\frac{S_2}{s(s+S_1)} - \mathcal{L}_r(0,s)\right),$$

which allows to solve for $\mathcal{L}_y$ in function of $\mathcal{L}_r(0,s)$. This last term will be calculated by taking the Laplace transformation of the room PDE, which leads to

$$\mathcal{L}_r(x,s) = \frac{p_x \cosh\left(\sqrt{st_x}\left(1-\frac{x}{L}\right)\right) Y\left(\frac{S_2}{s(s+S_1)} - \mathcal{L}_r(0,s)\right)}{\sinh\left(\sqrt{st_x}\right)\sqrt{st_x}}, \tag{4.4}$$

with $S_1$, $S_2$ and $Y$ as above and the diffusion time $t_x = \frac{L^2}{D}$, transport time $t_{fx} = \frac{L}{v_x}$ and the Peclet number for the room level $p_x = \frac{t_x}{t_{fx}} = \frac{v_x L}{D}$. By setting $x = 0$ in (4.4), we arrive at a linear, thus solvable, equation in $\mathcal{L}_r(0,s)$. Mind that we first need the solution for $\mathcal{L}_r$ to be able to calculate $\mathcal{L}_y$, which, on its turn, is needed for $\mathcal{L}_f$.

To calculate the characteristic times, i.e. the first and second moment, and the residence time of diffusion and the variance of the flux (the first and second cumulant of the system), we look at the fluxes of the solutions found above $\frac{\partial \mathcal{L}_f}{\partial \rho}$, $\frac{\partial \mathcal{L}_y}{\partial r}$ and $\frac{\partial \mathcal{L}_r}{\partial x}$.

For the zeroth, first and second moments we write the fluxes in their series expansion and look for the constant term, the coefficient of $-s$ and the coefficient of $s^2$ by differentiating and setting $s$ equal to zero. We will do this for the most interesting interfaces in the model, that is the transition from one level to another.

When we look at concentration passing from the fiber level to the yarn level, $\rho = \rho_{\max}$, we can calculate the zero'th moment,

$$M_{0,f} = \frac{1}{4}\left(\frac{(2t_{fx}+t_{fy})C_0}{t_{fx}+t_{fy}}\right)\rho_{\max}.$$

For the yarn and room similar results are achieved. The transition from yarn to room, thus taking $r = R_y$ and $x = 0$ leads to

$$M_{0,y} = \frac{1}{2}\left(\frac{t_{fx}C_0}{t_{fx}+t_{fy}}\right)R_y,$$

where now in the numerator only the transport time in the room appears. For the room flux, which gives an idea of how the particles in the room are distributed, the zero'th moment is

$$M_{0,r} = \frac{1}{2}\left(\frac{t_{fy}C_0}{t_{fx}+t_{fy}}\right)L,$$

where in the nominator the dependence of the flux on the evaporation rate in the air gaps of the yarn becomes clear. Also for the first and second moments

the same dependencies appear, but now in a quadratic relation, since a variance has been calculated. For example, for the flux in the room the first moment is

$$\begin{aligned} M_{1,r} &= -\frac{\partial}{\partial s}\left(\frac{\partial \mathcal{L}_r}{\partial x}(-s)\right)\Big|_{s=0} \\ &= \frac{1}{2}\left(\frac{t_{fy}C_0}{(t_{fx}+t_{fy})^2}\right) L\left[\frac{(2t_{fx}+t_{fy})}{16}t_f + \frac{t_{fx}}{4}t_y \right. \\ &\qquad \left. + \frac{t_{fy}}{3}t_x + \frac{(2t_{fx}+t_{fy})}{4}t_{ff} + 2t_{fx}t_{fy}\right]. \end{aligned}$$

Analogous results are found for the second moments on fiber and yarn level,

$$M_{1,f} = -\frac{\partial}{\partial s}\left(\frac{\partial \mathcal{L}_f}{\partial \rho}(-s)\right)\Big|_{s=0},$$

$$M_{1,y} = -\frac{\partial}{\partial s}\left(\frac{\partial \mathcal{L}_y}{\partial r}(-s)\right)\Big|_{s=0},$$

where we need to stress that for the interesting transition from yarn to room (at $r = R_y$ and $x = 0$) these last two moments can be found in two ways resulting twice in the same expression. We can look at the series expansion of the derivatives of the fluxes $\mathcal{L}_y$ and $\mathcal{L}_r$ and calculate them for the position $r = R_y$ and $x = 0$, or we can look at the derivatives of the difference $(\mathcal{L}_y - \mathcal{L}_r)$, once representing the flux at the right boundary of the yarn ($r = R_y$) and once representing the flux at the left boundary of the room ($x = 0$).
In each of these first moments there is an expected dependence on the initial concentration and the denominator each time has the same structure, depending on the distance that should be travelled by the particle.

Even more interesting to look at are the cumulants, which represent the several times were the actual transition from one level to another happens. The cumulants $c_1$ (the mean of the flux, or thus the mean position in time where a particle passes at a certain position) and $c_2$ (the variance of the flux) can be found from the above calculated moments, using the chain rule for the cumulant-generating function:

$$\begin{aligned} c_{1,*} &= -\frac{\partial}{\partial s}\left(\log\frac{\partial \mathcal{L}_*}{\partial \bullet}\right)\Big|_{s=0} = \frac{M_{1,*}}{M_{0,*}}, \\ c_{2,*} &= \frac{1}{2}\frac{\partial^2}{\partial s^2}\left(\log\frac{\partial \mathcal{L}_*}{\partial \bullet}\right)\Big|_{s=0} = \left(\frac{M_{2,*}}{M_{0,*}}\right) - \left(\frac{M_{1,*}}{M_{0,*}}\right)^2, \end{aligned}$$

where $*$ stands for $f$, $y$ or $r$ and $\bullet$ for $\rho$, $r$ or $x$, respectively.

For the fiber the first cumulant at $\rho = \rho_{\max}$, i.e. the residence time at the position where the AI leaves the fiber coating and evaporates to the yarn air

gaps, is

$$
\begin{aligned}
c_{1,f} = & \frac{t_f}{16}\left(\frac{2t_{fx}+t_{fy}}{t_{fx}+t_{fy}}\right) \\
& - \frac{t_y}{4}\left(\frac{t_{fx}\left(2r^2(t_{fx}+t_{fy}) - R_y^2(2t_{fx}+t_{fy})\right)}{R_y^2(t_{fx}+t_{fy})(2t_{fx}+t_{fy})}\right) \\
& + \frac{t_x}{3}\left(\frac{t_{fx}t_{fy}}{(t_{fx}+t_{fy})(2t_{fx}+t_{fy})}\right) + \frac{t_{ff}}{4}\left(\frac{2t_{fx}+t_{fy}}{t_{fx}+t_{fy}}\right) \\
& + \frac{t_{fx}^2 t_{fy}}{(t_{fx}+t_{fy})(2t_{fx}+t_{fy})}.
\end{aligned}
$$

We get an expected dependence between the residence time and the fiber's diffusion time, or the time for a particle to travel over distance $\rho_{\max}$ via diffusion with diffusion coefficient $D_f$. In the coefficient of $t_f$ the transport times $t_{fx}$ and $t_{fy}$ (the times it takes a particle to travel via evaporation in the room and yarn air gaps) are also likely to appear, since movement out of the fiber is controlled by the evaporation rate. It is also worth mentioning that the transport time of the room seems to be twice as sensitive as the transport time in the yarn air gaps. This is because of the dimension of the system ($d = 2$), which plays an important role in all coefficients, e.g. the $\frac{1}{16}$ in the first term. The coefficient of $t_{fx}$ is always equal to $d$.
Also a dependence on $t_y$ and $t_x$ is present. The respective coefficients again show the same linear combination $(2t_{fx} + t_{fy})$ multiplied with the quadratic distance to travel which is present in all the terms. The coefficient of $t_y$ has a factor $t_{fy}$ which is logical when we bear in mind that this is the transport time for a particle to get from the coating to the air gaps by evaporation. The sign is negative because the concentration of AI present in the yarn air gaps inhibits this evaporation and the $\frac{1}{4}$ again comes from the system's dimensions. For the coefficient of $t_x$ we only get both the transport times to travel inside of the yarn and in the room.
There is also a term in $t_{ff}$, the transport time in the fiber, with the same coefficient as $t_f$, the diffusion time, but four times as large.

The residence time at the transition point from yarn to room level, at $r = R_y$

and $x = 0$ is

$$c_{1,y} = c_{1,r} = \frac{t_f}{16}\left(\frac{2t_{fx}+t_{fy}}{t_{fx}+t_{fy}}\right) + \frac{t_y}{4}\left(\frac{t_{fx}}{t_{fx}+t_{fy}}\right) + \frac{t_x}{3}\left(\frac{t_{fy}}{t_{fx}+t_{fy}}\right) + \frac{t_{ff}}{4}\left(\frac{2t_{fx}+t_{fy}}{t_{fx}+t_{fy}}\right) + \frac{t_{fx}t_{fy}}{t_{fx}+t_{fy}}.$$

Again the same coefficients are present, i.e. $\frac{1}{16}$ for the term in $t_f$, $\frac{1}{4}$ for the terms in $t_y$ and $t_{ff}$ and $\frac{1}{3}$ for the term in $t_y$. The coefficient of $t_{ff}$ again is four times as large as the one of $t_f$. Every term has a positive sign since there can only be a positive effect from each of the underlying levels. The recurring denominator is the combined effect of the transport times in the yarn and the room.

The second cumulants both are of the same form and represent quadratic times since they stand for variances of the flux distribution,

$$c_{2,*} = \frac{1}{(t_{fx}+t_{fy})^2}\left[\frac{t_f}{16}\left(\frac{1}{48}a_1 + \frac{1}{2}a_2 t_y + \frac{1}{2}a_3 t_{ff} + 2a_4\right) + \frac{t_y}{4}\left(\frac{1}{12}a_5 t_y + \frac{1}{2}a_6 t_{ff} + 2a_7\right) + \frac{t_x}{3}\left(\frac{1}{15}a_8 t_x + \frac{1}{8}a_9 t_f + \frac{1}{2}a_{10} t_y + \frac{1}{2}a_{11} t_{ff} + 2a_{12}\right) + \frac{t_{ff}}{4}\left(\frac{1}{4}a_{13} + 2a_{14}\right)t_{ff} + t_{fx}^2 t_{fy}^2\right].$$

The coefficients of the respective terms are completely similar as for the residence times and again can be attributed to the system's dimensions.

For a general pair dimension $d$ the residence time for the room is

$$c_{1,r} = \frac{t_f}{a}\frac{dt_{fx}+t_{fy}}{bt_{fx}+ct_{fy}} + \frac{t_y}{e}\frac{t_{fx}}{bt_{fx}+ct_{fy}} + \frac{ct_x}{3}\frac{t_{fy}}{bt_{fx}+ct_{fy}} + \frac{t_{ff}}{e}\frac{dt_{fx}+t_{fy}}{bt_{fx}+ct_{fy}} + c\frac{t_{fx}t_{fy}}{bt_{fx}+ct_{fy}},$$

with coefficients $a$, $b$, $c$, and $e$

$$a = 4(d+2), \quad b = \frac{d^2}{4}, \quad c = \frac{d+2}{4}, \quad e = 4.$$

if $d$ is not divisible by $4$, and if $d$ is divisible by $4$ the coefficients are twice as large. These coefficients are also present in the other cumulants.

At these residence times the system reaches an equilibrium. In [15] the theoretical values were compared with these numerical solutions of the model. These numerical values are visible in the plot of the logarithmic concentration vs. the logarithmic time scale, Fig. 4.3. The symbolic form calculated above now makes it possible to explain even further the accordance between both.

### 4.2.4 Inverse problem

With the programming code utilized it is possible to use Gnuplot's fit command to calculate some inverse problems. Starting from an estimated initial value for the unknown parameter, the model will be fitted to experimental values of the forward problem using nonlinear least squares regression.
In practice measurements of the concentration of the AI in a room can be done, and the model could be fitted to these values. That way the right polymer may be chosen depending on the required diffusion coefficient in the coating and the initial concentration could be determined. It becomes possible to decide on the right composition of the textile, answering the questions of how many fibers are needed to get to the right surface/volume ratio, on its turn determining the needed evaporation rate. The inverse problem is using the same C-code of the 3 level diffusion system as the forward model. Although this does not work for all parameters due to high complexity of some of them and the dependencies between them, it is possible to estimate those of high impact.

For example it is possible to fit the initial concentration $C_0$ and the diffusion coefficient in the room $D$ starting for $C_0$ at an initial guess of $1.1$ and for $D$ at $1.1 \times 10^{-5}$. As data points we use the values optioned by the forward model with $C_0 = 1.234$ and $D = 2.345 \times 10^{-5}$ and a uniform error in $[-\frac{3}{2}; \frac{3}{2}] \times 10^{-5}$ is superimposed. We want to trace back the values for $C_0$ and $D$ after fitting the inverse problem.
This is the case after 5 iterations with a root-mean-square of residuals (RMS) of $8.635 \times 10^{-6}$. The calculated set of parameters is $C_0 = 1.23401$ with an asymptotic SE of $\pm 0.002$ or $0.179\%$ and $D = 2.33142 \times 10^{-5}$ with an SE of $\pm 0.016$ or $0.682\%$. The data fitting of this problem is shown in Fig. 4.4(a).

However if we start from a very bad initial guess for $D$ at $0.001 \times 10^{-5}$ the inverse problem does not converge because a singular matrix is encountered, resulting in an estimation of $8388.17$ for $D$. Using the least squares method of Gnuplot thus requires some a priori knowledge about the parameters, but our earlier analysis of characteristic times helps in selecting these. The model plot corresponding to this problem is found in Fig. 4.4(b). If for example we try to estimate $D_f$ and $D$ from data fitting, the inverse problem does not converge to the correct values. This is because the time frame wherein the AI's particles are moving through the fiber is much smaller than the time these particles

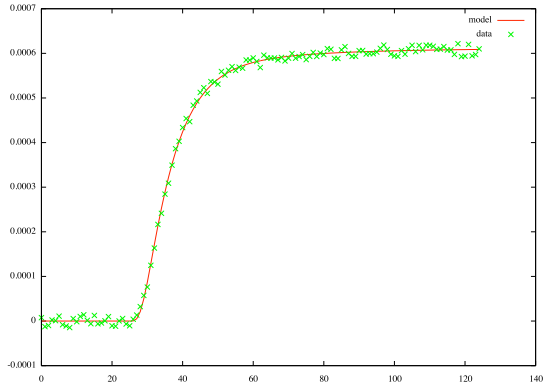


(a) Initial guess of 1.1 for both parameters

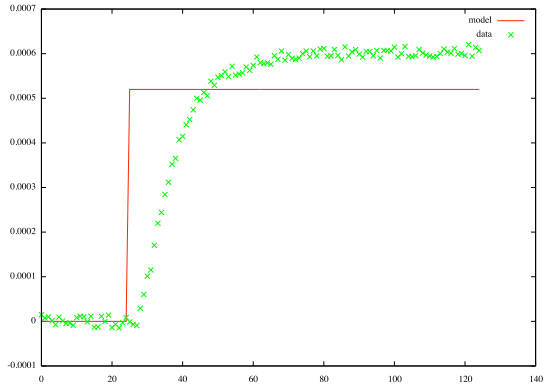


(b) Initial guess of 1.1 for $C_0$ and 0.001 for $D$

Figure 4.4: Inverse problem for determining initial concentration $C_0$ and diffusion coefficient in the room model $D$

are moving through the room. As a consequence we have too little data to be able to trace back the diffusion coefficient in the fiber. The diffusion coefficient in the room is however traceable and the models fit is not too bad after all. After 5 iterations the fit converged with an RMS of $8.816 \times 10^{-6}$. The fitted $D$ was $2.34951 \times 10^{-5}$ with an asymptotic SE of $\pm 0.0145$ or $0.616\%$. Parameter $D_f$ however was fitted as $127.905$ with asymptotic SE of $\pm 1994$ or $1559\%$. The correlation between these parameters is $-0.048$, so it is not responsible for the bad fit. The data fitting can be seen in Fig. 4.5. Fitting can also be done for more than two parameters at a time. For example, it is possible to estimate the

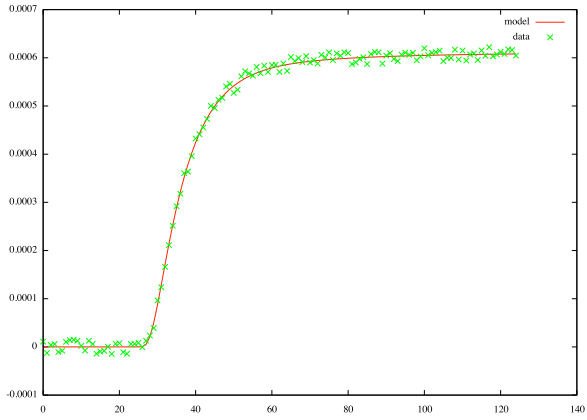


Figure 4.5: Inverse problem for determining diffusion coefficient in the fiber model $D_f$ and diffusion coefficient in the room model $D$

three parameters $C_0$, $v_f$ and $D$. In the forward problem the values used were $1.234$, $1$ and $3.456 \times 10^{-5}$, respectively. Starting from $1.1$, $0.5$ and $1.1 \times 10^{-5}$ it was possible to trace back these values after 5 iterations with an RMS of $9.243 \times 10^{-6}$. The estimated model solving the inverse problem is shown in Fig. 4.6.

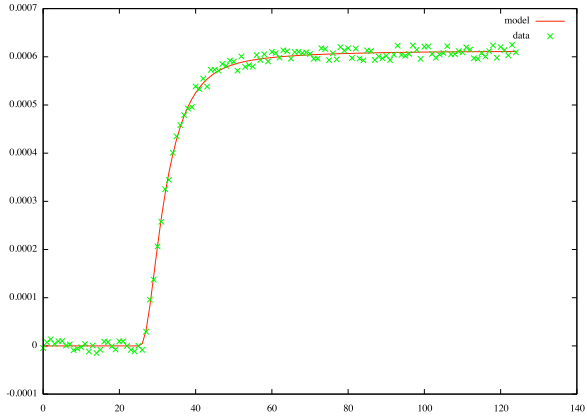


Figure 4.6: Inverse problem with three parameters for determining the initial concentration $C_0$, the evaporation speed $v_f$ and the diffusion coefficient in the room model $D$

### 4.2.5 Conclusion and future work

The characteristic times for the three level diffusion model were calculated and symbolically analyzed. The present coefficients show the dependence between the several diffusion and transport times and we were able to explain them in a physical way. This gives a proof for the correspondence between the calculated values and the visible transition times on the plot of the logarithmic concentration in function of the logarithmic time in [15].
Several inverse problems were solved using the Levenberg-Marquardt algorithm giving a first approach to use the developed model in practice. Based upon these results we have more knowledge of which parameters can be estimated at the same time, and which rather should be tested via chemical experiments. Especially the fiber diffusion coefficient is hard to estimate because of the small time scale where the AI is present in the fiber only. Experimental values now could be used to answer the question of which textile, coating and AI should be used to give the best practical results.

## 4.3 Characteristic times in a three scale model with overlapping domain decomposition

**T. Goessens and D. Constales**

**accepted for publication in Elsevier's Journal of Computational and Applied Mathematics.**

**Abstract** *A three-scale diffusion model for textiles was given in [16]: consisting of a fiber, yarn and room model. To analyze and simplify the model, its characteristic times were investigated in [15, 14]. At these times the fiber and yarn model, and the yarn and room model, respectively, tend to reach a partial equilibrium concentration. Here an addition will be made to the model based upon the previous work. An overlap zone is considered between the yarn and room level. Then the overlapping domain decomposition technique is used to calculate the exchange of active ingredient from one level to another in this zone. The mass balance for the system with the overlap zone is calculated and tested in C-language.*

### 4.3.1 Introduction

We consider textiles wherein the fibers are coated with a polymer solution of an active ingredient (AI), e.g. an insect repellent, a perfume or a healing substance. This substance can easily be replaced by other volatiles that first diffuse to the outer boundary of the textile and from there on evaporate to the surrounding air.
The application in mind has the purpose to track the diffusion of an active component released by the fibers of an open textile structure, like a woven scrim, e.g. a gauze bandage. Models and algorithms for this application were based on [53, 59, 12, 33] and discussed in [16, 18, 17]. The model consists of three levels, starting from the micro level of the fibers. Next the AI is diffusing to the yarn meso-level, considering the concentration build up in a cross-section of a yarn made out of fibers. Afterwards the AI is moving further to the outer boundary of the textile and to the surrounding air represented by the room level. Upscaling from one level to another can be done using volume averaging and/or the overlapping domain decomposition technique.
In [15, 14] the characteristic times were calculated for a model where only volume averaging was used for upscaling. Now an addition is made using an overlap zone where the exchange of AI from one level to another is happening. Solving the standard diffusion equations we know which concentration is coming into this overlap zone at the left boundary, and we want to know how

much is going to the next level after upscaling in the overlap zone. Therefore we will investigate the relation between the Laplacian of both the concentration and the flux at the left and right boundary of the overlap zone. That way we can express the characteristic times, i.e. the moments and cumulants of the system in the overlap zone where concentration is averaged out in one level in function of the other level. This gives an idea of how a perfect exchange of AI would look, or which properties of the textile can influence this movement of substances to go faster or slower. Also it will be possible to implement the relation between the left and right boundary of the overlap zone in the already existing C-code, which is using `lsoda` to solve the system. The original C-code will be extended with the possibility of using domain decomposition for upscaling. For test purposes the conservation of mass is recalculated for the new setting.

We will calculate the relation between the left concentration and flux in function of the concentration and flux at the right boundary. First we will do this for the simple one-dimensional case, afterwards for general dimensions $d_1$ and $d_2$ of the two levels. Furthermore we will calculate these relations for a specific concentration function.

Based upon this, it becomes possible for future research to investigate what will happen if the setting is changing, e.g. a different positioning of the levels and consequently the overlap zone, and what changes if we use the actual concentration instead of the volume average in the overlapping zone equations.

### 4.3.2 One-dimensional overlap zone

The governing system of equations of the complete three-level model is

$$\begin{cases} \dfrac{\partial C_f(\rho,r,t)}{\partial t} = \dfrac{1}{\rho}\dfrac{\partial}{\partial \rho}\left(\rho D_f \dfrac{\partial C_f(\rho,r,t)}{\partial \rho}\right), & \rho \in [\rho_{\min},\rho_{\max}] \quad (4.5a) \\ \dfrac{\partial C_y(r,t)}{\partial t} = \dfrac{1}{r}\dfrac{\partial}{\partial r}\left(r\dfrac{D_y}{\tau_y}\dfrac{\partial C_y(r,t)}{\partial r}\right) + \Gamma_{\text{in}}(r,t), & r \in [0,R_y] \quad (4.5b) \\ \dfrac{\partial C_r(x,t)}{\partial x} = \dfrac{\partial}{\partial x}\left(D\dfrac{\partial C_r(x,t)}{\partial x}\right), & x \in [0,L] \quad (4.5c) \end{cases}$$

with a homogeneous Neumann BC at the left boundaries and an evaporation flux at the right boundaries for the fiber and yarn model (4.5a) and (4.5b):

$$\begin{aligned} &\frac{\partial C_f}{\partial \rho}(0,r,t) = 0, && -D_f\frac{\partial C_f}{\partial \rho}(\rho_{\max},r,t) = v_f(C_f(\rho_{\max},r,t) - C_y(r,t)), \\ &\frac{\partial C_y}{\partial r}(0,t) = 0, && -D_y\frac{\partial C_y}{\partial r}(R_y,t) = v_y(C_y(R_y,t) - C_r(0,t)). \end{aligned}$$

For the room model (4.5c) a homogeneous Neumann BC is present at the right boundary and at the left boundary there exists an evaporation flux coming

from the concentration in the yarn evaporating to the room:

$$D\frac{\partial C_r}{\partial x}(0,t) = \alpha_{yr} v_x (C_r(0,t) - C_y(R_y,t)), \qquad \frac{\partial C_r}{\partial x}(L,t) = 0.$$

In the above system of equations (4.5) the subscripts $f, y$ and $r$ stand for a quantity in the fiber, yarn and room respectively, $C$ represents the concentration of the AI, $D_f, D_y$ and $D$ are the respective diffusion coefficients, which are assumed to be constant, $v_f$ and $v_y$ are the evaporation speeds from fiber to yarn and from yarn to room level resp. $\alpha_{yr}$ is a constant of proportion for the evaporation from yarn to room level. The constant $\tau$ is the tortuosity of the textile used. The term $\Gamma_{\text{in}}$ in (4.5b) is the volume averaged condensation/evaporation rate and is calculated as $\alpha_{fy} v_f (C_f(\rho_{\max}) - C_y(r))$ with $\alpha_{fy}$ the surface/volume ratio of the fiber.

As an upscaling method from fiber level to yarn level, volume averaging is used, the averaged outcome of one model serves as boundary conditions for the other.

As described in [16] we will extend the domain of the yarn model with an overlap zone $\Omega_o$, i.e. a part of the domain of the yarn will coincide with the domain of room model. There the PDE above is adapted with an extra sink-term $\Gamma_{out}(t,\Omega_o)$ which stands for the amount of AI that is removed from the meso-level due to diffusion to the macro-level. Also the BC at the right boundary is changed to a homogeneous Neumann BC.
We are interested in the exchange of AI in this overlap zone, particularly the relation between the AI at the left boundary of $\Omega_o$ and that at its outer right boundary:

$$\begin{pmatrix} \mathcal{L}C_1 \\ \mathcal{L}F_1 \end{pmatrix}_{R_{1\ell}} = \underbrace{\begin{pmatrix} a & b \\ c & d \end{pmatrix}}_{\mathsf{A}} \begin{pmatrix} \mathcal{L}C_2 \\ \mathcal{L}F_2 \end{pmatrix}_{R_{2r}},$$

where we used the Laplace transforms of the concentration of the AI in level 1 and 2, $C_1$ and $C_2$, and the Laplace transformed flux of these concentrations, $F_1$ and $F_2$. We denote the left and right boundary of the overlap zone in the domain of level $i$ by $R_{i\ell}$ and $R_{ir}$. We will work with the Laplace transformation of the quantities to be able to calculate the characteristic times of the model as explained in [14, 15].

For illustrative purpose we will explain the method used in the following sections with the one-dimensional diffusion in one level from $R = 0$ to $R = L$. The relation between the left and right concentration and flux is then given by

$$\begin{pmatrix} \mathcal{L}C \\ \mathcal{L}F \end{pmatrix}_{R=0} = \begin{pmatrix} \cosh(\sqrt{\frac{L^2 s}{D}}) & \frac{1}{\sqrt{sD}} \sinh(\sqrt{\frac{L^2 s}{D}}) \\ \sqrt{sD} \sinh(\sqrt{\frac{L^2 s}{D}}) & \cosh(\sqrt{\frac{L^2 s}{D}}) \end{pmatrix} \begin{pmatrix} \mathcal{L}C \\ \mathcal{L}F \end{pmatrix}_{R=L},$$

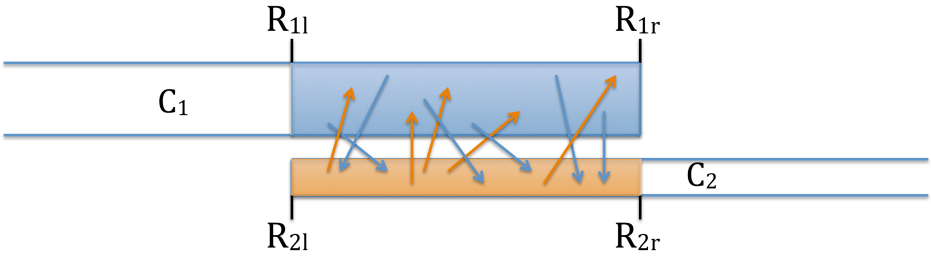


Figure 4.7: Overlap zone of two levels in the model

according to the PDE

$$\frac{\partial C}{\partial t}(x,t) = D\frac{\partial^2 C}{\partial x^2}(x,t), \quad x \in [0,L].$$

To get to this matrix the equation is Laplace transformed

$$s\mathcal{L}C(x,s) = D\frac{\partial^2 \mathcal{L}C(x,s)}{\partial x^2},$$

and solved

$$\mathcal{L}C(x,s) = A\cosh\left(\sqrt{\frac{sx^2}{D}}\right) + B\sinh\left(\sqrt{\frac{sx^2}{D}}\right).$$

Substituting $x = 0$ and $x = L$ in this solution and its derivative with respect to $x$ for the flux gives $4$ equations, and $6$ unknowns. Solving this system to $\mathcal{L}C(0,s)$ and $\mathcal{L}F(0,s)$ in function of $\mathcal{L}C(L,s)$ and $\mathcal{L}F(L,s)$ gives the above matrix. For the more complex systems of equations this exchange matrix A will need further simplification using both Maple and calculations by hand.

We will now introduce the overlap zone equations for two overlapping levels in one dimension as

$$\begin{cases} \dfrac{\partial C_1}{\partial t} = D\dfrac{\partial^2 C_1}{\partial x^2} + k\left(\bar{C}_2 - C_1\right), \\ \dfrac{\partial C_2}{\partial t} = D\dfrac{\partial^2 C_2}{\partial x^2} + k\left(\bar{C}_1 - C_2\right), \end{cases}$$

where $\bar{C}_1$ and $\bar{C}_2$ stand for the mean concentration of AI in domain 1 and 2, resp., $k$ is a constant of proportionality corresponding to the rate of exchange

between both levels.
The boundary conditions are

$$F_1|_{R_{1r}} = 0, \qquad F_2|_{R_{2l}} = 0.$$

Taking the Laplace transform of these equations and solving for $\mathcal{L}C_1$ and $\mathcal{L}C_2$ gives

$$\begin{cases} \mathcal{L}C_1 = A\cosh\left(x\sqrt{\dfrac{(s+k)}{D}}\right) + B\sinh\left(x\sqrt{\dfrac{(s+k)}{D}}\right) + \dfrac{k}{s+k}\mathcal{L}\bar{C}_2, \\ \mathcal{L}C_2 = \tilde{A}\cosh\left(x\sqrt{\dfrac{(s+k)}{D}}\right) + \tilde{B}\sinh\left(x\sqrt{\dfrac{(s+k)}{D}}\right) + \dfrac{k}{s+k}\mathcal{L}\bar{C}_1, \end{cases}$$

and makes it possible to look at the left and right boundaries of both domains. We will denote $\mathcal{L}C_i$ and $\mathcal{L}F_i$ at the left boundary of domain $i$ as $\mathcal{L}C_{i\ell}$ and $\mathcal{L}F_{i\ell}$. This leads to ten equations each giving an expression for the ten unknowns $\mathcal{L}C_{1\ell}$, $\mathcal{L}F_{1\ell}$, $\mathcal{L}C_{2\ell}$, $\mathcal{L}F_{2\ell}$, $\mathcal{L}C_{1r}$, $\mathcal{L}F_{1r}$, $\mathcal{L}C_{2r}$, $\mathcal{L}F_{2r}$, $\mathcal{L}\bar{C}_1$ and $\mathcal{L}\bar{C}_2$. However according to the BC's we put $\mathcal{L}F_{1r} = \mathcal{L}F_{2\ell} = 0$. Furthermore we have the unknowns $A, B, \tilde{A}$ and $\tilde{B}$. In total we end up with 10 equations for 12 unknowns, which leads to a solution with two degrees of freedom. Solving this system for all unknowns except for $\mathcal{L}C_{2r}$ and $\mathcal{L}F_{2r}$ leads to a solution in function of the latter two. In particular we are interested in the solutions for $\mathcal{L}C_{1\ell}$ and $\mathcal{L}F_{1\ell}$, in order to be able to calculate the matrix of interest A,

$$\mathsf{A} = \begin{pmatrix} \dfrac{(2k+s)s}{k(k+s)}T + \dfrac{k}{k+s} & \dfrac{(2k+s)s}{Lk(k+s)^2}T^2 + \dfrac{2k}{L(k+s)^2}T - \dfrac{k}{L(k+s)^2} \\ \dfrac{(2k+s)sL}{k} & \dfrac{(2k+s)s}{k(k+s)}T + \dfrac{k}{k+s} \end{pmatrix},$$

where $T = \coth\left(\dfrac{\sqrt{k+s}\,L}{\sqrt{D}}\right)\dfrac{\sqrt{k+s}\,L}{\sqrt{D}}$. The diagonal entries are equal which means both concentration and flux of the AI at the left boundary of domain 1 have the same dependence on concentration and flux respectively at the right boundary of domain 2. If there was a perfect exchange between the two overlap zones this matrix becomes ($\lim_{k\to\infty}$)

$$\mathsf{A} = \begin{pmatrix} 1 & 0 \\ 2Ls & 1 \end{pmatrix},$$

where we see that the Laplace transformed concentration in both levels is the same at both boundaries and the flux changes linearly with this concentration.

The system thus acts as if there was only one level with double length. If we should want to calculate the first moment of the system i.e. the mean position in time when a particle passes a certain position in space, we are interested in the above matrix with $s$ equal to zero

$$\mathsf{A} = \begin{pmatrix} 1 & \frac{2T(0)-1}{kL} \\ 0 & 1 \end{pmatrix},$$

where we notice that the first moment and consequently also the residence time of the first level is the same as that of the second system.

In a more general setting the diffusion coefficients of the two levels are not equal, and the exchange rate decreases with the length of the overlap zone, which also doesn't need to be equal in a more general case,

$$\begin{cases} \dfrac{\partial C_1}{\partial t} = D_1 \dfrac{\partial^2 C_1}{\partial x^2} + \dfrac{k}{L_1}\left(\bar{C}_2 - C_1\right), \\ \dfrac{\partial C_2}{\partial t} = D_2 \dfrac{\partial^2 C_2}{\partial x^2} + \dfrac{k}{L_2}\left(\bar{C}_1 - C_2\right). \end{cases}$$

Following the same technique as above the needed matrix then becomes

$$\mathsf{A} = \begin{pmatrix} \frac{(L_1(k+L_2s)+L_2k)s}{(k+L_1s)k} T_1 + \dfrac{k}{k+L_1s} & \frac{(L_1(k+L_2s)+L_2k)s}{(k+L_1s)(k+L_2s)k} T_1 T_2 \\ & + \frac{k}{(k+L_1s)(k+L_2s)}(T_1+T_2-1) \\ \dfrac{(L_1(k+L_2s)+L_2k)\,s}{k} & \frac{(L_1(k+L_2s)+L_2k)s}{(k+L_2s)k} T_2 + \dfrac{k}{k+L_2s} \end{pmatrix}.$$

Here $D_i$ and $L_i$ are the diffusion coefficient and length of the overlap zone in the domain of level $i$ and $T_i = \coth\left(\dfrac{\sqrt{L_i s + k}}{\sqrt{D_i}}\sqrt{L_i}\right)\dfrac{\sqrt{L_i s + k}}{\sqrt{D_i}}\sqrt{L_i}$.

### 4.3.3 Two-dimensional cylindrical and one-dimensional cartesian diffusion

The application in mind is described using three levels of diffusion, eq. (1). The overlap zone is situated between the last two levels, i.e. the yarn level which is described by a two-dimensional cylindrical equation and the room level which is described by a one-dimensional cartesian equation. In this overlap zone the

governing equations of eq. (1) are adapted to

$$\begin{cases} \dfrac{\partial C_1}{\partial t} = \dfrac{D_1}{r}\dfrac{\partial}{\partial r}\left(r\dfrac{\partial C_1}{\partial r}\right) + \dfrac{q}{\pi\left(R_2^2 - R_1^2\right)h}\left(\bar{C_2} - C_1\right), \\ \dfrac{\partial C_2}{\partial t} = D_2\dfrac{\partial^2 C_2}{\partial x^2} + \dfrac{q}{AL}\left(\bar{C_1} - C_2\right), \end{cases}$$

where $R_1$ and $R_2$ are the outer left and outer right boundary of the overlap zone of the yarn cylinder, $h$ is the height of a yarn cylinder, $A$ is the area of the room's wall perpendicular to the dimension, $L$ is the length of the overlap zone of the room in the direction of the dimension, $D_1$ and the $D_2$ are the respective diffusion coefficients. The proportionality constant $q$ stands for the discharge of the concentration in $\frac{\mathrm{m}^3}{\mathrm{s}}$. The Laplace transformed system reads

$$\begin{cases} -\left(s + \dfrac{q}{\pi\left(R_2^2 - R_1^2\right)h}\right)\mathcal{L}C_1 + \dfrac{D_1}{r}\dfrac{\partial}{\partial r}\left(r\dfrac{\partial \mathcal{L}C_1}{\partial r}\right) = -\dfrac{q}{\pi\left(R_2^2 - R_1^2\right)h}\mathcal{L}\bar{C_2}, \\ -\left(s + \dfrac{q}{AL}\right)\mathcal{L}C_2 + D_2\dfrac{\partial^2}{\partial x^2}\left(\mathcal{L}C_2\right) = -\dfrac{q}{AL}\mathcal{L}\bar{C_1}, \end{cases}$$

with its solution

$$\begin{cases} \mathcal{L}_1(r) = A_1\, \mathcal{I}_0\left(\sqrt{\dfrac{V_1 s + q}{V_1 D_1}}r\right) + B_1\, \mathcal{K}_0\left(\sqrt{\dfrac{V_1 s + q}{V_1 D_1}}r\right) + \dfrac{q}{V_1 s + q}\mathcal{L}_{2m}, \\ \mathcal{L}_2(x) = A_2 \cosh\left(\sqrt{\dfrac{ALs + q}{ALD_2}}x\right) + B_2 \sinh\left(\sqrt{\dfrac{ALs + q}{ALD_2}}x\right) + \dfrac{q}{ALs + q}\mathcal{L}_{1m}, \end{cases}$$

where $V_1 = \pi\left(R_2^2 - R_1^2\right)h$, $\mathcal{L}_i$ denotes $\mathcal{L}C_i$ and $\mathcal{L}_{im}$ stands for $\mathcal{L}\bar{C_i}$, $i = 1{,}2$, $\mathcal{I}_0$ and $\mathcal{K}_0$ are the modified Bessel functions of the first and second kind of order zero.

Using the boundary conditions for the flux $-D_1\ \frac{\partial \mathcal{L}_1}{\partial r}\big|_{r=R2} = 0$ and $-D_2\ \frac{\partial \mathcal{L}_2}{\partial x}\big|_{x=0} = 0$ we are able to rewrite these solutions and eliminate two unknowns:

$$\begin{cases} \mathcal{L}_1(r) = \tilde{A_1}\mathcal{B}_{0,1}(r, R_2, \dfrac{V_1 s + q}{V_1 D_1}) + \dfrac{q}{V_1 s + q}\mathcal{L}_{2m}, \\ \mathcal{L}_2(x) = A_2 \cosh\left(\sqrt{\dfrac{ALs + q}{ALD_2}}x\right) + \dfrac{q}{ALs + q}\mathcal{L}_{1m}, \end{cases}$$

with

$$\mathcal{B}_{n,m}(r_1, r_2, C) = (-1)^{|n-m|+1}\frac{\mathcal{I}_n\left(\sqrt{C}r_1\right)}{\mathcal{I}_m\left(\sqrt{C}r_2\right)} + \frac{\mathcal{K}_n\left(\sqrt{C}r_1\right)}{\mathcal{K}_m\left(\sqrt{C}r_2\right)},$$

a combination of $\mathcal{I}_n$ and $\mathcal{K}_n$, i.e. the modified Bessel functions of first and second kind of order $n$.

Then for $s = 0$ the aimed matrix is

$$\mathsf{A} = \begin{pmatrix} 1 & \frac{\sqrt{AL}}{\sqrt{D_2 q}} \dfrac{1}{\tanh\left(\sqrt{\frac{qL}{AD_2}}\right)} - \dfrac{A}{q} \\ & + \frac{A\sqrt{V_1}}{\sqrt{qD_1}R_1 h} \dfrac{\mathcal{B}_{0,1}(R_1, R_2, \frac{q}{V_1 D_1})}{\mathcal{B}_{1,1}(R_1, R_2, \frac{q}{V_1 D_1})} \\ \left.\dfrac{s\left(ALV_1 s + ALq + V_1 q\right)}{hR_1 q}\right|_{s=0} = 0 & \dfrac{A}{hR_1} \end{pmatrix}.$$

It is clear that the law of conservation of mass is satisfied since we get that $hR_1 \mathcal{L}F_{1\ell} = A\mathcal{L}F_{2r}$.
For the limit $q$ to infinity, i.e. the perfect exchange of material as if there were no two separate levels, the matrix is

$$\mathsf{A} = \begin{pmatrix} 1 & 0 \\ \dfrac{s\left(AL + V_1\right)}{hR_1} & \dfrac{A}{hR_1} \end{pmatrix}.$$

### 4.3.4 Multidimensional diffusion in both levels

We now will investigate the most general setting possible, where both the yarn and room level have different given dimensions $d_1$ and $d_2$ and different diffusion coefficients $D_1$ and $D_2$. We suppose that both overlap zones are oriented as in Fig. 4.7.
The governing equations for the two overlapping levels are

$$\begin{cases} \dfrac{\partial C_1}{\partial t} = \dfrac{D_1}{r^{d_1-1}} \dfrac{\partial}{\partial r}\left(r^{d_1-1} \dfrac{\partial C_1}{\partial r}\right) + \dfrac{q}{V_{d_1} W_{d_1} (\Delta r^{d_1})} \left(\bar{C}_2 - C_1\right), \\ \dfrac{\partial C_2}{\partial t} = \dfrac{D_2}{r^{d_2-1}} \dfrac{\partial}{\partial r}\left(r^{d_2-1} \dfrac{\partial C_2}{\partial r}\right) + \dfrac{q}{V_{d_2} W_{d_2} (\Delta r^{d_2})} \left(\bar{C}_1 - C_2\right), \end{cases}$$

where $V_{d_i}$ is the volume of the overlap zone, $W_{d_i}$ is the codimension such that the total volume is that of the unit ball, $q$ is the exchange rate of AI from one level to another. In this setting the volume averages are calculated as

$$\bar{C}_i = \frac{d_i}{\Delta r^{d_i}} \int_{R_{\min}}^{R_{\max}} C_i r^{d_i - 1} \, \mathrm{d}r, \qquad i = 1, 2, 3.$$

This system of equations is Laplace transformed and solved as

$$\begin{cases} \mathcal{L}_1(r,s) = \dfrac{A_1}{r^{\frac{d_1}{2}-1}}\,\mathcal{I}_{\frac{d_1}{2}-1}\left(\sqrt{\dfrac{s+q_1}{D_1}}r\right) + \dfrac{B_1}{r^{\frac{d_1}{2}-1}}\,\mathcal{K}_{\frac{d_1}{2}-1}\left(\sqrt{\dfrac{s+q_1}{D_1}}r\right) \\ \qquad\qquad + \dfrac{q_1}{s+q_1}\mathcal{L}_{2m}(s), \\ \mathcal{L}_2(r,s) = \dfrac{A_2}{r^{\frac{d_2}{2}-1}}\,\mathcal{I}_{\frac{d_2}{2}-1}\left(\sqrt{\dfrac{s+q_2}{D_2}}r\right) + \dfrac{B_2}{r^{\frac{d_2}{2}-1}}\,\mathcal{K}_{\frac{d_2}{2}-1}\left(\sqrt{\dfrac{s+q_2}{D_2}}r\right) \\ \qquad\qquad + \dfrac{q_2}{s+q_2}\mathcal{L}_{1m}(s), \end{cases}$$

where $q_i = \dfrac{q}{V_{d_i} W_{d_i}(\Delta r^{d_i})}$, $\mathcal{L}_i$ denotes $\mathcal{L}C_i$ and $\mathcal{L}_{im}$ stands for $\mathcal{L}\bar{C}_i$, $R_{i\ell} < r < R_{ir}$, the functions $\mathcal{I}_{\frac{d_i}{2}-1}$ and $\mathcal{K}_{\frac{d_i}{2}-1}$ are the Bessel functions of first and second kind of order $\frac{d_i}{2}-1$, $i = 1,2$. The matrix A again uses the combination of Bessel functions $\mathcal{B}_{n,m}$ for $s = 0$,

$$\mathsf{A} = \begin{pmatrix} 1 & \dfrac{R_{2r}^{d_2-1}}{R_{1\ell}^{d_1-1}}\dfrac{d_2}{d_1 q_2}\dfrac{\sqrt{q_1}}{\sqrt{D_1}}\dfrac{\left(\Delta r^{d_1}\right)}{\left(\Delta r^{d2}\right)}\dfrac{\mathcal{B}_{\frac{d_1}{2}+1,\frac{d_1}{2}}(R_{1\ell},R_{1r},\frac{q_1}{D_1})}{\mathcal{B}_{\frac{d_1}{2},\frac{d_1}{2}}(R_{1\ell},R_{1r},\frac{q_1}{D_1})} \\ & \quad + \dfrac{d_2}{q_2 R_{2r}}\left(1+\left(\dfrac{R_{1r}}{R_{1\ell}}\right)^{d_1}\dfrac{R_{2r}^{d_2}}{\left(\Delta r^{d_2}\right)}\right) - \dfrac{1}{\sqrt{q_2 D_2}}\dfrac{\mathcal{B}_{\frac{d_2}{2}+1,\frac{d_2}{2}}(R_{2r},R_{2\ell},\frac{q_2}{D_2})}{\mathcal{B}_{\frac{d_2}{2},\frac{d_2}{2}}(R_{2r},R_{2\ell},\frac{q_2}{D_2})} \\ 0 & \dfrac{V_{d_2} W_{d_2} d_2 R_{2r}^{d_2-1}}{V_{d_1} W_{d_1} d_1 R_{1\ell}^{d_1-1}} \end{pmatrix}.$$

The limit situation for perfect exchange of the active ingredient corresponds to the matrix

$$\mathsf{A} = \begin{pmatrix} 1 & 0 \\ \dfrac{sR_{1\ell}}{d_1}\left(\dfrac{\left(\Delta r^{d_2}\right)V_{d_2}W_{d_2}}{R_{1\ell}V_{d_1}W_{d_1}} + \left(\dfrac{R_{1r}}{R_{1l}}\right)^{d_1} - 1\right) & \dfrac{V_{d_2} W_{d_2} d_2 R_{2r}^{d_2-1}}{V_{d_1} W_{d_1} d_1 R_{1\ell}^{d_1-1}} \end{pmatrix}.$$

Both mentioned matrices for general dimensions are according with the above results for more specific dimensions.

### 4.3.5 Application

With the above matrices it is possible to calculate the exchange of concentration of the active ingredient for specific fluxes and functions at the left boundary of the overlap zone of one of the domains. For example if we take the Dirac-function for the concentration or the flux at one of the boundaries, respectively

we can easily calculate the unknown concentration and/or flux at the other boundary, see Table 4.2. Each of these values can be helpful in the determination of the characteristic times of the system. We are particularly interested in the Area Under Curve (AUC), i.e. the concentration at $s = 0$, the first moment, i.e. the mean flux and the first cumulant, i.e. the residence time.

Table 4.2: Dirac-concentration or Dirac-flux at one of the boundaries

| Case | Setting | Result | |
|---|---|---|---|
| 1 | $C_{1\ell} = \delta, F_{2r} = 0$ | $\mathcal{L}C_{2r} = \frac{1}{\mathsf{A}_{11}}$ | $\mathcal{L}F_{1\ell} = \frac{\mathsf{A}_{21}}{\mathsf{A}_{11}}$ |
| 2 | $F_{1\ell} = \delta, C_{2r} = 0$ | $\mathcal{L}F_{2r} = \frac{1}{\mathsf{A}_{22}}$ | $\mathcal{L}C_{1\ell} = \frac{\mathsf{A}_{12}}{\mathsf{A}_{22}}$ |
| 3 | $C_{2r} = \delta, F_{1\ell} = 0$ | $\mathcal{L}C_{1\ell} = \frac{1}{\mathsf{A}_{11}^{-1}}$ | $\mathcal{L}F_{2r} = -\frac{\mathsf{A}_{21}}{\mathsf{A}_{22}}$ |
| 4 | $F_{2r} = \delta, C_{1\ell} = 0$ | $\mathcal{L}F_{1\ell} = \frac{1}{\mathsf{A}_{22}^{-1}}$ | $\mathcal{L}C_{2r} = -\frac{\mathsf{A}_{12}}{\mathsf{A}_{11}}$ |

For the first setting $s = 0$ in $\frac{1}{\mathsf{A}_{11}}$ gives the Laplace transform of the concentration at the right boundary of the second domain, i.e. the AUC for this domain, which is the Dirac-function itself. Since at the left boundary of the first domain there is a peak of concentration and the system is isolated at the right boundary of the second domain, a concentration build up happens until everything stabilizes to the equilibrium concentration at the right boundary, equaling the initial concentration $C_{1\ell}$. The second case lets us calculate the mean flux and the residence time if the concentration of AI is taken away immediately at the right boundary of the second domain. The mean flux, i.e. the first moment, equals $\frac{V_{d_1} W_{d_1} d_1 R_{1\ell}^{d_1-1}}{V_{d_2} W_{d_2} d_2 R_{2r}^{d_2-1}}$, the residence time is

$$\frac{q_1+q_2}{q_1 q_2}\left(\left(\frac{R_{2\ell}}{R_{2r}}\right)^{d_2} - \frac{R_{2r}}{d_2}\sqrt{\frac{q_2}{D_2}}\frac{\mathcal{B}_{\frac{d_2}{2}+1,\frac{d_2}{2}}(R_{2r},R_{2\ell},\frac{q_2}{D_2})}{\mathcal{B}_{\frac{d_2}{2},\frac{d_2}{2}}(R_{2r},R_{2\ell},\frac{q_2}{D_2})}\left[\left(\frac{R_{2\ell}}{R_{2r}}\right)^{d_2} - 1\right]\right) - \frac{1}{q_1}.$$

The third case gives the AUC for the first domain. This again is equal to the Dirac-function. The fourth case also can be used to calculate the first moment and cumulant of the system with a similar result as above but with indices 1 and 2 interchanged. Once the dimensions and other parameters of the system are known, we can numerically calculate the characteristic times using these formulas.

### 4.3.6 Adaptation of C-code and mass balance in time domain

The system of equations (4.5) was programmed in C code and solved using `lsoda` and `fortran77`. Using the input of Table 4.3 for the variables the plot in Fig. 4.8 was generated.

Table 4.3: Input variables

| | | | |
|---|---|---|---|
| $t_0$ | $1.0 \times 10^{-8}$ | $\alpha_{fy}$ | 1000 |
| $\Delta t$ | 1.01 | $\alpha_{yr}$ | 100 or 0.0131111 |
| $t_{\max}$ | $1.0 \times 10^{10}$ | $v_f$ | 1 |
| $n_f$ | 20 | $v_y$ | 1 |
| $n_y$ | 60 | $D_f$ | $1 \times 10^{-10}$ |
| $n_r$ | 40 | $D_y$ | $1 \times 10^{-6}$ |
| $n_{y_o}$ | 2 | $D_r$ | $1 \times 10^{-5}$ |
| $n_{r_o}$ | 2 | rel tol | $1 \times 10^{-6}$ |
| $\rho_{\min}$ | 0 | abs tol | $1 \times 10^{-13}$ |
| $\rho_{\max}$ | 0.0001 | $h_{\max}$ | 10000 |
| $R_y$ | 0.001 | $h$ | 2.0 |
| $L$ | 5 | $A$ | 10.0 |
| $C_f(\rho, r, 0)$ | 1 | $k$ | 1 or 10000 |

To solve this system numerically the $\rho$-domain was divided into $n_f$ intervals, the $r$-domain into $n_y$ intervals and the $x$-domain into $n_r$ intervals. The time domain was divided in varying intervals using $\delta_t$ as default value, but these intervals are adjusted during calculations by the `lsoda`-solver according to the given relative and absolute tolerances. The variable $h_{\max}$ is the maximal stepsize for this solver. The mass balance was calculated as an extra control system on the solution and is displayed as the constant orange line. Also the average fiber, yarn and room concentration are displayed. First the fiber and yarn concentration coincide to an equilibrium concentration at approximately $10^2$ s, afterwards at approximately $10^6$ s that concentration reaches the equilibrium concentration. In this case no overlap zone is used, but volume averaging is used as an upscaling method assuming perfectly smooth exchange between the different levels.

The complete model with overlapping domain decomposition is the ad-

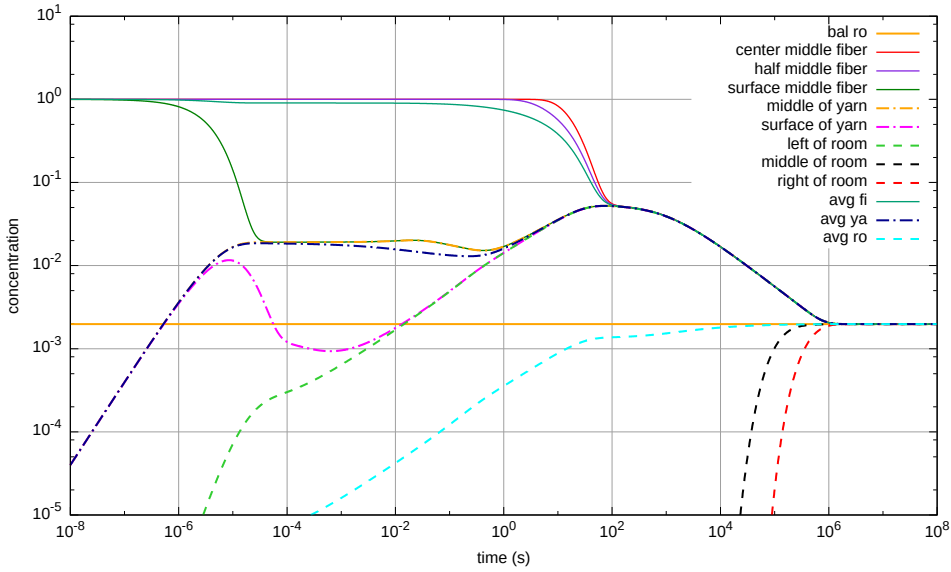


Figure 4.8: Solution without overlapping domain decomposition, but with volume averaging as upscaling between the three levels

justed version of (4.5) in the overlap zone:

$$\begin{cases} \dfrac{\partial C_f(\rho,r,t)}{\partial t} = \dfrac{1}{\rho}\dfrac{\partial}{\partial \rho}\left(\rho D_f \dfrac{\partial C_f(\rho,r,t)}{\partial \rho}\right), & \rho \in [\rho_{\min},\rho_{\max}] \quad (4.6a) \\ \dfrac{\partial C_y(r,t)}{\partial t} = \dfrac{1}{r}\dfrac{\partial}{\partial r}\left(r\dfrac{D_y}{\tau_y}\dfrac{\partial C_y(r,t)}{\partial r}\right) + \alpha_{fy} v_f \left(C_f(\rho_{\max},r,t) - C_y(r,t)\right) \\ \qquad\qquad +k\left(\overline{C_r} - C_y(r,t)\right), & r \in [R_{y_o},R_y] \quad (4.6b) \\ \dfrac{\partial C_r(x,t)}{\partial x} = \dfrac{\partial}{\partial x}\left(D\dfrac{\partial C_r(x,t)}{\partial x}\right) \\ \qquad\qquad +k\alpha_{yr}\left(\overline{C_y} - C_r(x,t)\right), & x \in [0,L_o] \quad (4.6c) \end{cases}$$

and (4.5) in the rest of the domain. The boundary conditions of (4.5) are changed to

$$\begin{aligned} &\frac{\partial C_f}{\partial \rho}(0,r,t) = 0, && -D_f\frac{\partial C_f}{\partial \rho}(\rho_{\max},r,t) = v_f(C_f(\rho_{\max},t) - C_y(r,t)), \\ &\frac{\partial C_y}{\partial r}(0,t) = 0, && \frac{\partial C_y}{\partial r}(R_y,t) = 0, \\ &\frac{\partial C_r}{\partial x}(0,t) = 0, && \frac{\partial C_r}{\partial x}(L,t) = 0, \end{aligned}$$

where $\overline{C_y}$ and $\overline{C_r}$ denote the average concentrations in the overlap zone of the yarn and room level and $R_{y_o}$ is the radius in the yarn corresponding to the beginning of the overlap zone. The factor $k$ is the factor $\frac{q}{\pi(R_y^2 - {R_{y_o}}^2)h}$ we used previously for mass balance purposes. Since it is easier for programming and notation we also used this $k$ in the room model, adjusted with the constant of proportion $\alpha_{yr}$ which as a result slightly changes in physical meaning and thus in size. That is also the reason why there is a second number for $\alpha_{yr}$ in Table 4.3. With the second number the same mass balance concentration is reached and the physical behavior is mimicked. There is also a second number in Tabel 4.3 for the constant $k$ where it becomes relatively big. With this large $k$ it is possible to mimic the kinetical behavior of the problem as seen in the case of only volume averaging as an upscaling method. In the above derivation of the exchange matrix A it became clear that for big $k$ or $q$ a perfect smooth exchange is seen and the exchange matrix can be simplified as if there was no overlap zone. This is also visible in Fig. 4.10.

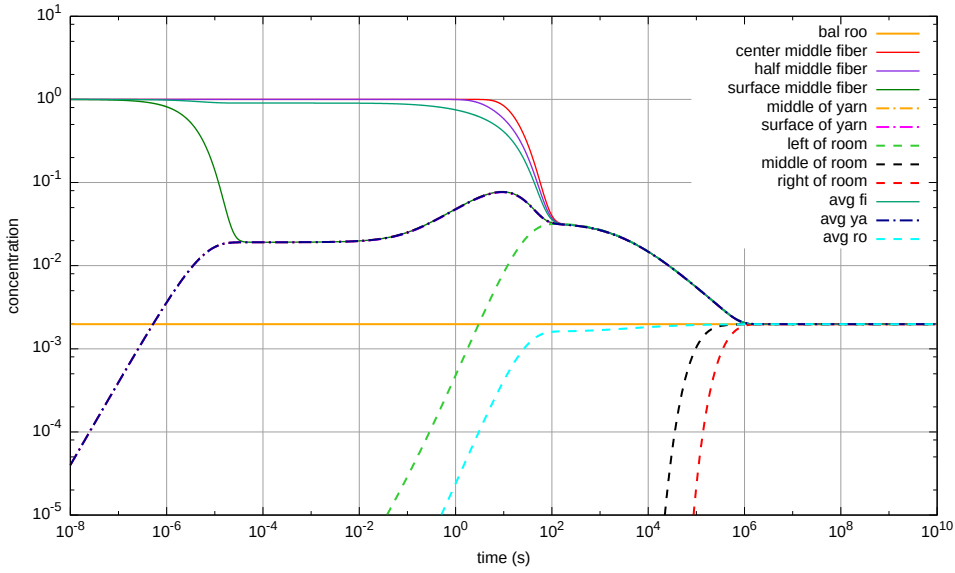


Figure 4.9: Solution with overlapping domain decomposition as upscaling between the yarn and room level

The original code was adjusted with using a part of the $r$-domain as the

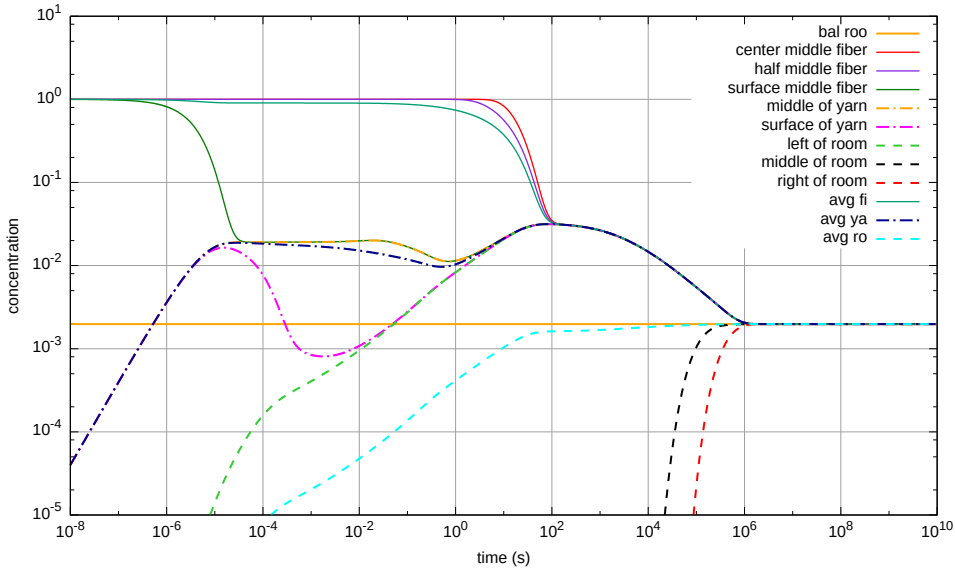


Figure 4.10: Solution with overlapping domain decomposition as upscaling between the yarn and room level, with big $k$, mimicking the kinetical behavior as seen in Fig. 4.8

overlap zone of the yarn, and a part of the $x$-domain for the room overlap zone, each divided in smaller intervals, $n_{y_o}$ and $n_{r_o}$ resp., for numerical calculation purposes. The fluxes were adapted and the extra source and sink terms were added to the concentration array in each space interval. The adjusted number of equations was calculated in order to be able to allocate the memory needed by the band matrix produced by the solver. The solution is visible in Fig. 4.9. Here the equilibrium concentration where the fiber and yarn level solution coincide also seems to be reached at approximately $10^2$ s which is according with what one would expect, since the upscaling method between the fiber and yarn level has not been adapted. The concentration is, however, getting in to the room at a later time but at a higher pace. Before the fiber and yarn concentration are getting to there equilibrium concentration there is a build-up in the yarn concentration which is still behaving separately from the room concentration. This can be explained by the used proportionality constant $\alpha_{yr}$ which regulates how quick the concentration of AI is getting into the room, and is obviously acting as an inhibitor in this system.
Again the mass balance is calculated and displayed as the constant yellow line.

For this mass conservation the three averages of each level, which are each displayed in the solution plot, are calculated as

$$\overline{\overline{C_f}} = \frac{\displaystyle\int_0^{R_y} r\,\mathrm{d}r \int_{\rho_{\min}}^{\rho_{\max}} C_f \rho\,\mathrm{d}\rho}{\displaystyle\int_0^{R_y} r\,\mathrm{d}r \int_{\rho_{\min}}^{\rho_{\max}} \rho\,\mathrm{d}\rho},$$

$$\overline{\overline{C_y}} = \frac{\displaystyle\int_0^{R_y} C_y r\,\mathrm{d}r}{\displaystyle\int_0^{R_y} r\,\mathrm{d}r}, \qquad \overline{\overline{C_r}} = \frac{\displaystyle\int_0^{L} C_r\,\mathrm{d}x}{\displaystyle\int_0^{L} \mathrm{d}x}.$$

Taking the correct integrals of equations (4.6) gives the change in time of the averages over the complete domain $\overline{\overline{C_i}}$, $i = f,y,r$, which should sum up to zero for mass conservation. Using the BC's and carrying out some basic calculations leads to the mass balance equation:

$$\overline{\overline{C_r}} + \frac{L_o}{L} \frac{1}{1 - \left(\frac{R_{y_o}}{R_y}\right)^2} \alpha_{yr} \left( \overline{\overline{C_y}} + \frac{\alpha_{fy}}{\rho_{\max}} \frac{\rho_{\max}^2 - \rho_{\min}^2}{2} \overline{\overline{C_f}} \right) = \mathcal{C},$$

where $\mathcal{C}$ is the mass balance constant visible in Fig. 4.9 and 4.10.

### 4.3.7 Conclusion and future work

A three-scale diffusion model for textiles consisting of a fiber, yarn and room model was further analyzed. Its characteristic times, the first moment and cumulant, were calculated symbolically in an overlap zone. Between the different levels this overlap zone is considered in an overlapping domain decomposition technique for upscaling the exchanged concentration of AI. The original C-code was adjusted, results were interpreted and the mass balance was calculated. Later on we will investigate what will happen if the setting is changing, e.g. a different positioning of the levels and consequently the overlap zone, and what changes if we use the actual concentration instead of the volume average in the overlapping zone equations.

# References


[1] Ali, A., Cantrell, C. L., Bernier, U. R., Duke, S. O., Schneider, J. C., Agramonte, N. M., and Khan, I. Aedes aegypti (diptera: Culicidae) biting deterrence: Structure-activity relationship of saturated and unsaturated fatty acids. *J. Med. Entomol. 49*, 6 (2012), 1370–1378.

[2] Cai, X. Overlapping domain decomposition methods. In *Advanced Topics in Computational Partial Differential Equations*, H. Langtangen and A. Tveito, Eds., vol. 33 of *Lecture Notes in Computational Science and Engineering*. Springer Berlin Heidelberg, 2003, pp. 57–95.

[3] Churchill, S. W., and Bernstein, M. A correlating equation for forced convection from gases and liquids to a circular cylinder in crossflow. *Journal of Heat Transfer 99*, 2 (1977), 300–306.

[4] `http://www.epa.gov/apti/bces/module2/concentrate/concentrate.htm`.

[5] Crank, J. *The Mathematics of Diffusion*. Clarendon Press Oxford, 1979.

[6] Davis, E., and Bowen, M. Sensory physiology basis for attraction in mosquitoes. *J. Am. Mosq. Control Assoc. 10* (1994), 316–325.

[7] Denny, M., and American Society of Zoologists (Meeting). *Air and Water: The Biology and Physics of Life's Media*. Princeton University Press, 1993.

[8] Dethier, V., Browne, B., and Smith, C. The designation of chemicals in terms of the responsesthey elicit from insects. *J. Econ. Entomol. 53* (1960), 134–136.

[9] Ditzen, M., Pellegrino, M., and Vosshall, L. B. Insect odorant receptors are molecular targets of the insect repellent deet. *Science 319*, 5871 (2008), 1838–1842.

[10] Division, E. S. Air emissions models for waste and wastewater epa-453/r-94-080a. Tech. rep., U.S. Environmental Protection Agency, 1994.

[11] Dogan, E. B., Ayres, J. W., and Rossignol, P. A. Behavioral mode of action of deet: inhibition of lactic acid attraction. *Med. Vet. Entomol. 13* (1999), 97–100.

[12] Fan, J., Luo, Z., and Li, Y. Heat and moisture transfer with sorption and condensation in porous clothing assemblies and numerical simulation. *International Journal of Heat and Mass Transfer 43*, 16 (2000), 2989–3000.

[13] Fan, J., Luo, Z., and Li, Y. Heat and moisture transfer with sorption and condensation in porous clothing assemblies and numerical simulation. *International Journal of Heat and Mass Transfer 43*, 16 (2000), 2989 – 3000.

[14] Goessens, T., De Staelen, R. H., and Constales, D. Characteristic times and inverse problems for diffusion in coated textiles. *Applied Mathematics and Information Sciences 9*, 2L (2015), 349–355.

[15] Goessens, T., De Staelen, R. H., and Constales, D. Characteristic times for multiscale diffusion of active ingredients in coated textiles. *Journal of Computational and Applied Mathematics 289* (2015), 426–432.

[16] Goessens, T., Malengier, B., Constales, D., and De Staelen, R. H. A volume averaging and overlapping domain decomposition technique to model mass transfer in textiles. *Journal of Computational and Applied Mathematics 275* (2015), 456 – 464.

[17] Goessens, T., Malengier, B., and Langenhove, L. V. Modeling Textile Fabric used in Pest Control with a 3 Scale Domain Decomposition Method. In *Lecture Notes in Computer Science (LNCS)* (2015), vol. 9045, Springer, pp. 194–201.

[18] Goessens, T., Malengier, B., Li, P., and De Staelen, R. H. Diffusion of active ingredients in textiles. *Journal of Mathematical Modelling and Algorithms* (2012), 1–12.

[19] Grishanov, S., Lomov, S., Cassidy, T., and Harwood, R. The simulation of the geometry of a two-component yarn part ii: Fibre distribution in the yarn cross- section. *Journal of the Textile Institute 88*, 4 (1997), 352–372.

[20] Grishanov, S., Siewe, F., and Cassidy, T. An application of queuing theory to modelling of melange yarns. part ii: A method of estimating the fibre migration probabilities and a yarn structure simulation algorithm. *Textile Research Journal 81*, 8 (may 2011), 798–818.

[21] Guyer, J. E., Wheeler, D., and Warren, J. A. FiPy: Partial differential equations with Python. *Computing in Science & Engineering 11*, 3 (2009), 6–15.

[22] Henry, P. S. H. The diffusion of moisture and heat through textiles. *Discuss. Faraday Soc. 3* (1948), 243–257.

[23] Hoffmann, E. J., and Miller, J. R. Reduction of mosquito (diptera: Culicidae) attacks on a human subject by combination of wind and vapor-phase deet repellent. *Journal of Medical Entomology 39*, 6 (2002), 935–938.

[24] Huang, H., Ye, C., and Sun, W. Moisture transport in fibrous clothing assemblies. *Journal of Engineering Mathematics 61*, 1 (2008), 35–54.

[25] Johnson, N., and Russell, I. *Advances in Wool Technology*. Woodhead Publishing Series in Textiles. Elsevier Science, 2008.

[26] Karr, J. I., Speaker, T. J., and Kasting, G. B. A novel encapsulation of n,n-diethyl-3-methylbenzamide (DEET) favorably modifies skin absorption while maintaining effective evaporation rates. *Journal of Controlled Release 160*, 3 (2012), 502 – 508.

[27] Klun, J. A., and Debboun, M. A new module for quantitative evaluation of repellent efficacy using human subjects. *J. Med. Entomol. 37* (2000), 177–181.

[28] Klun, J. A., Kramer, M., and Debboun, M. A new in vitro bioassay system for discovery of novel human-use mosquito repellents. *Journal of the American Mosquito Control Association 21* (2005), 64–70.

[29] Korycki., R. Method of thickness optimization of textile structures during coupled heat and mass transport. *Fibres & textiles in Eastern Europe 17*, 1 (72) (January/March 2009), 33–38.

[30] `http://ocw.mit.edu/courses/mathematics/18-366-random-walks-and-diffusion-fall-2006/lecture-notes/`.

[31] Li, Y., and Luo, Z. An improved mathematical simulation of the coupled diffusion of moisture and heat in wool fabric. *Textile Research Journal 69*, 10 (1999), 760–768.

[32] Li, Y., and Luo, Z. X. Physical mechanisms of moisture diffusion into hygroscopic fabrics during humidity transients. *Journal of the Textile Institute 91*, 2 (2000), 302–316.

[33] Li, Y., and Zhu, Q. Simultaneous heat and moisture transfer with moisture sorption, condensation, and capillary liquid diffusion in porous textiles. *Textile Research Journal 73*, 6 (2003), 515–524.

[34] Masetti, A., and Maini, S. Arm in cage tests to compare skin repellents against bites of aedes albopictus. *Bulletin of Insectology 59*, 2 (2006), 157–160.

[35] Mathew, T. *Domain Decomposition Methods for the Numerical Solution of Partial Differential Equations (Lecture Notes in Computational Science and Engineering)*, 1 ed. Springer Publishing Company, Incorporated, 2008.

[36] Morton, W. E., Hearle, J. W. S., and Textile Institute (Manchester, England). *Physical properties of textile fibres*, 2nd ed ed. London : Heinemann [for] the Textile Institute, 1975. Previous ed.: 1962.

[37] N'Guessan, R., Knols, B. G., Pennetier, C., and Rowland, M. {DEET} microencapsulation: a slow-release formulation enhancing the residual efficacy of bed nets against malaria vectors. *Transactions of the Royal Society of Tropical Medicine and Hygiene 102*, 3 (2008), 259 – 262.

[38] Nordon, P., and David, H. Coupled diffusion of moisture and heat in hygroscopic textile materials. *International Journal of Heat and Mass Transfer 10*, 7 (1967), 853 – 866.

[39] Petzold, L. Automatic selection of methods for solving stiff and nonstiff systems of ordinary differential equations. *SIAM Journal on Scientific and Statistical Computing 4*, 1 (1983), 136–148.

[40] Polyanin, A. *Handbook of Linear Partial Differential Equations for Engineers and Scientists*. Chapman & Hall/CRC, 2002.

[41] Santhanam, A., Miller, M. A., and Kasting, G. B. Absorption and evaporation of N,N-diethyl-m-toluamide from human skin in vitro. *Toxicology and Applied Pharmacology 204*, 1 (2005), 81 – 90.

[42] Siewe, F., Grishanov, S., Cassidy, T., and Banyard, G. An Application of Queuing Theory to Modeling of Melange Yarns Part I: A Queuing Model of Melange Yarn Structure. *Textile Research Journal 79*, 16 (nov 2009), 1467–1485.

[43] Smith, B., Bjorstad, P., and Gropp, W. *Domain decomposition: parallel multilevel methods for elliptic partial differential equations*. Cambridge University Press, 1996.

[44] Sriprateep, K., and Bohez, E. Computer aided modeling of fiber assemblies. *Computer Aided Design & Applications 3*, 1-4 (2006), 367–376.

[45] Sriprateep, K., and Bohez, E. A new computer geometric modelling approach of yarn structures for the conventional ring spinning process. *Journal of the Textile Institute 100*, 3 (2009), 223–236.

[46] Stroeven, P., He, H., Guo, Z., and Stroeven, M. Particle packing in a model concrete at different levels of the microstructure: Evidence of an intrinsic patchy nature. *Materials Characterization 60*, 10 (2009), 1088–1092.

[47] Syed, Z., and Leal, W. S. Mosquitoes smell and avoid the insect repellent deet. *Proceedings of the National Academy of Sciences* (2008).

[48] Tice, R., and Brevard, B. N,n-diethyl-m-toluamide (deet), review of toxicological literature. Tech. rep., Integrated Laboratory Systems, 1999.

[49] Toselli, A., and Widlund, O. B. *Domain Decomposition Methods - Algorithms and Theory*, vol. 34 of *Springer Series in Computational Mathematics*. Springer Berlin Heidelberg, 2005.

[50] `http://ntp.niehs.nih.gov/ntp/htdocs/Chem_Background/ExSumPdf/DEET_508.pdf`.

[51] `http://www.epa.gov/apti/bces/module4/vaporpres/vaporpres.htm`.

[52] Vassiliadis, S., Kallivretaki, A., Domvoglou, D., and Provatidis, C. Mechanical analysis of woven fabrics: The state of the art. In *Advances in Modern Woven Fabrics Technology*. InTech, 2011.

[53] Wang, Z. *Heat and moisture transfer and clothing thermal comfort*. PhD thesis, Hong Kong Polytechnic University, 2002.

[54] Weast, R. *C.R.C. Handbook of Chemistry and Physics, A ready-reference book of chemical and physical data*. CRC press inc., 1977.

[55] Whitaker, S. *The Method of Volume Averaging*. Theory and Applications of Transport in Porous Media. Kluwer Academic, 1999.

[56] `https://en.wikipedia.org/`.

[57] Yanniotis, S. Mass transfer by convection. In *Solving Problems in Food Engineering*, Food Engineering Series. Springer New York, 2008, pp. 155–162.

[58] Yao, M., et al. *Science of Textile Materials (2nd Edition) (in Chinese)*. China Textile Press, Beijing, 1996.

[59] Ye, C., Huang, H., Fan, J., and Sun., W. Numerical study of heat and moisture transfer in textile materials by a finite volume method. *Communications in Computational Physics 4*, 4 (2008), 929–948.

[60] Zhang, Q., and Sun, W. A numerical study of air-vapor-heat transport through textile materials with a moving interface. *Journal of Computational and Applied Mathematics 236*, 5 (2011), 819–833.

[61] Zhu, Q., and Li, Y. Numerical simulation of the transient heat and liquid moisture transfer through porous textiles with consideration of electric double layer. *International Journal of Heat and Mass Transfer 53*, 7-8 (2010), 1417–1425.